Propriétés physiques et Dynamique des objets sans atmosphère du système solaire

Mirel Birlan

▶ **To cite this version:**

Mirel Birlan. Propriétés physiques et Dynamique des objets sans atmosphère du système solaire. Astrophysique [astro-ph]. Université Paris-Diderot - Paris VII, 2005. tel-00547554

HAL Id: tel-00547554
https://theses.hal.science/tel-00547554

Submitted on 16 Dec 2010

HAL is a multi-disciplinary open access archive for the deposit and dissemination of scientific research documents, whether they are published or not. The documents may come from teaching and research institutions in France or abroad, or from public or private research centers.

L'archive ouverte pluridisciplinaire **HAL**, est destinée au dépôt et à la diffusion de documents scientifiques de niveau recherche, publiés ou non, émanant des établissements d'enseignement et de recherche français ou étrangers, des laboratoires publics ou privés.

Université Paris 7 « Denis Diderot »

Propriétés physiques et Dynamique des objets sans atmosphère du système solaire

Habilitation à diriger des recherches

Présentée par

Mirel BIRLAN

Institut de Mécanique Céleste et de Calculs des Ephémérides
Observatoire de Paris

Jury:

Professeur ***Marcello FULCHIGNONI***	**Président**
Astronome ***Alberto CELLINO***	**Rapporteur**
Professeur ***Guy MOREELS***	**Rapporteur**
Astronome ***Antonella BARUCCI***	**Examinateur**
DR CNRS ***Jean-Eudes ARLOT***	**Examinateur**
Professeur ***Richard BINZEL***	**Examinateur**
Astronome ***William THUILLOT***	**Examinateur**
Astronome ***Jean SOUCHAY***	**Examinateur**

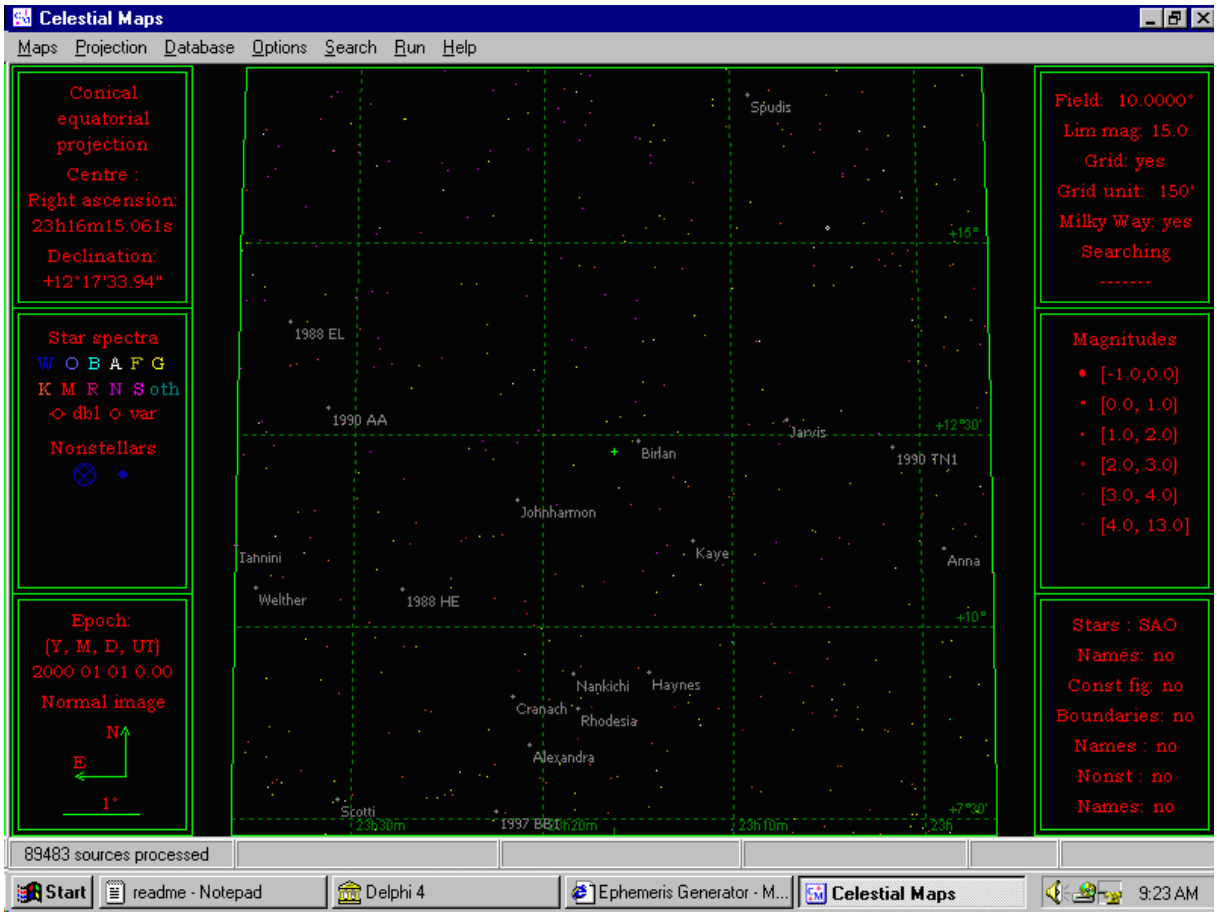
Celestial Maps
Maps Projection Database Options Search Run Help
Conical equatorial projection
Centre :
Right ascension:
23h16m15.061s
Declination:
+12°17'33.94"
Star spectra
W O B A F G
K M R N S oth
db1 o var
Nonstellars
Epoch:
[Y, M, D, UT]
2000 01 01 0.00
Normal image
N
E
1°
Field: 10.0000°
Lim mag: 15.0
Grid: yes
Grid unit: 150'
Milky Way: yes
Searching
Magnitudes
[-1.0,0.0]
[0.0, 1.0]
[1.0, 2.0]
[2.0, 3.0]
[3.0, 4.0]
[4.0, 13.0]
Stars : SAO
Names: no
Const fig: no
Boundaries: no
Names : no
Nonst : no
Names: no
Spudis
1988 EL
1990 AA
Birlan
Jarvis
1990 TN1
Johnhiarmon
Kaye
Anna
Iannini
Welther
1988 HE
Nankichi
Haynes
Cranach
Rhodesia
Alexandra
Scotti
1997 BB1
+15°
+12°30'
+10°
+7°30'
23h30m
23h20m
23h10m
89483 sources processed
Start
readme - Notepad
Delphi 4
Ephemeris Generator - M...
Celestial Maps
9:23 AM

Motto : **Sapere Aude**
Pense par toi-même

A Mariana

et à nos enfants

Diana, Mirela, Daniel et Florian

Peut-être parmi ceux qui écoutent y a-t-il un être jeune; quelqu'un qui se méfie de ses capacités, qui est écrasé par la pensée de sa propre médiocrité, prêt à se donner en aveugle comme beaucoup l'ont fait avant lui. Permettez-moi de lui parler. Je lui dirai: "Mon ami, tu n'es pas un médiocre ou, si tu l'es, cela ne compte pas. Ne pense pas à ce que, choses dignes ou horribles, les autres ont fait avant toi. Pense seulement que, à sa façon, ta vie est une occasion unique. Si au début je t'ai demandé ce que tu penses de toi-même ce n'est pas pour obtenir la réponse : j'en pense du bien ou du mal ! Mais pour que tu te souviennes qu'il faut te battre davantage avec toi-même ; qu'à l'intérieur de toi, quelqu'un d'autre est en train de dormir; une personne plus intéressante que tu n'imagines, un chrétien meilleur que tu ne le montres, peut-être un héros; avant tout un être brave, tout simplement. Prend en soin, ne le laisse pas trop dormir ! "

Constantin NOICA

Qu'est ce qu'est, que peut l'être, l'homme médiocre

Interventions Radiophoniques, Bucarest, 1936

Avant-propos

Par objet sans atmosphère nous considérons tout objet qui gravite autour du Soleil, de dimension inférieure à 2000 km de diamètre, qui ne peut développer ni garder une atmosphère. Du fait de leur nombre, cette définition englobe essentiellement les astéroïdes (ou les petits corps), les objets trans-neptuniens, les comètes, et certains satellites des planètes.

L'intérêt pour les études des petits corps réside principalement dans son apport essentiel à la cosmogonie du Système Solaire. Les deux dernières décennies nous ont permis d'accéder à une connaissance jamais encore atteinte concernant notre système solaire en général et plus particulièrement le domaine des corps de taille réduite (diamètre inférieur à 1000 km). L'image actuelle des petits corps dans le système solaire nous montre une variété de familles et de populations, aussi bien d'objets situés à l'intérieur de l'orbite de la Terre qu' au-delà du système Pluton-Charon. En fonction des orbites des objets sans atmosphère, on parle d'astéroïdes géocroiseurs, de Mars croiseurs, d'astéroïdes de la ceinture principale, d'astéroïdes situés dans des points de stabilité Lagrange, de Centaures, de trans-neptuniens, de comètes à courte ou à longue période.

Plusieurs questions fondamentales ont jalonnées les acquis scientifiques concernant les petits corps. Voici celles que l'on peut citer parmi les plus importantes:

- Pourquoi n'y a-t-il pas une planète massive entre les orbites de Mars et de Jupiter plutôt que des milliers de planétésimaux ?
- Quel est le lien entre les différents catégories de petits corps (astéroïdes, comètes et météors) ?
- Quelle est leur masse volumique ? Que sait-on de leur composition minéralogique ?
- S'agit-il de corps massifs ou de « tas de gravas » maintenus par un faible champ gravitationnel ?
- Peuvent-ils nous fournir la clé permettant de déchiffrer la composition de la nébuleuse planétaire précédant le système planétaire actuel ?
- Comment s'effectue et se répartit le transfert de moment cinétique entre la nébuleuse primordiale, le Soleil et les planètes ?
- Comment leur influence a-t-elle marqué l'histoire du système planétaire en général et celle de la Terre en particulier ? Quels sont les moments les plus importants de notre civilisations marqués par leur présence ?

Chacune de ces questions est génératrice d'un domaine scientifique distinct, en particulier en cosmogonie du système solaire. Plus concrètement, connaître la nature de la surface des astéroïdes et leur minéralogie, étudier les phénomènes de transfert radiatif dans les cas d'objets sans atmosphère, déterminer leur période de rotation propre (synodique), leur forme, le sens de rotation propre ainsi que la position de l'axe ou des axes de rotation, observer les astéroïdes « in situ » dans plusieurs longueurs d'onde grâce aux sondes spatiales, analyser les mécanismes de résonance ainsi que les processus de collisions mutuelles, font partie de ces « détails » qui permettent de mieux connaître la population astéroïdale et finalement de construire des modèles physiques plus fiables.

L'intérêt pour la population de petits corps du système solaire s'est accru aussi grâce à l'important nombre de missions spatiales ayant comme objectif leur étude « in situ ». Le succès des sondes spatiales Galileo, NEAR, a marqué la fin de la dernière décennie du XX^{ème} siècle. Pour la première fois, les images et des paramètres physiques obtenus ont permis l'obtention des formes d'astéroïdes, l'analyse de leur surface et de leur « relief », la présence d'un possible champ magnétique ainsi que leur environnement proche.

De par son grand nombre, la population astéroïdale représente un « champ d'expérimentation » aussi bien pour des mécanismes dynamiques (résonances, mécanismes de transfert et évolution chaotique des orbites) que pour des modèles physiques. L'analyse poussée des observations de haute qualité obtenues aussi bien « in situ » que par les grands télescopes au sol nous montre une population d'objets d'une grande variété, considérés quelques décennies auparavant simplement comme hypothèses de travail « peu probables ». Les scientifiques se sont rendus à l'évidence de la présence de systèmes doubles parmi les astéroïdes, ils ont accepté également l'astéroïde comme agglomération de petits cailloux maintenus ensemble par un faible champ gravitationnel afin d'expliquer leur faible masse volumique. Les astéroïdes survolés par des sondes spatiales nous ont montré des surfaces criblées de cratères, signe que les collisions dans le système solaire est un phénomène qui a eu une grande importance dans l'état actuel du système solaire. La séparation du noyau de la comète SL9 en plus de 20 parts sous l'effet de marée du champ gravitationnel de Jupiter nous a permis pour la première fois l'observation d'une prévision théorique (la limite Roche) et la mise en évidence de l'aspect « fragile » d'un noyau cométaire, confirmant en partie le modèle de « neige(glace) sale » de Fred Whipple.

La recherche scientifique présentée s'inscrit dans l'effort quotidien des scientifiques pour l'exploitation de nouvelles données fournies par des instruments au sol, en utilisant de nouvelles techniques. Cette activité vise également l'obtention de résultats issus de nouveaux

intervalles de longueur d'onde (comme celui de l'infrarouge proche dans le cas d'objets sans atmosphère du système solaire) mais également l'amélioration des techniques d'observations et d'optimisation des processus de réduction des données. Plusieurs des ces travaux ont été faits dans le cadre des recherches au sol liées aux missions spatiales en cours (ROSETTA) et futurs (DAWN et VENUS EXPRESS).

J'ai employé plusieurs techniques d'observation afin de mieux comprendre les propriétés physiques et dynamiques des corps sans atmosphère de notre système solaire : observations photographiques, photoélectriques ainsi qu'imagerie et spectroscopie par l'intermédiaire des cameras CCD. Les images astronomiques m'ont permis l'étude de leur rotation propres ainsi que leur couleurs (chapitre I.2.). La spectroscopie à la longueur d'onde du visible et du proche infrarouge (chapitre I.3.) ont permis l'analyse plus détaillée de la composition de la surface des objets, la connaissance plus précise de la composition minéralogique et la mise en valeur de la diversité des spectres. La dynamique des petit corps a été abordée également sur plusieurs aspects (chapitre I.4.).

L'analyse des spectres des petits corps en proche infrarouge m'a permis d'approfondir davantage les connaissances sur les différents techniques d'observations (chapitre I.1). Ainsi, j'ai pu démarré un projet de création d'un Centre d'Observation à Distance en Astronomie à Meudon, alternative aux campagnes d'observations, sans effectuer la mission au télescope (souvent nécessaires et peu pratiques).

Un autre volet dans mes préoccupations scientifiques a été aussi l'exploitation des résultats issus des observations. L'analyse des couleurs et des albédos m'a permis des études statistiques sur des échantillons significatifs d'astéroïdes de la ceinture principale, mais également sur la population des objets trans-neptuniens(chapitre II.1). J'ai pu affiner les taxonomies modernes ainsi que les méthodes d'analyse statistique. Pour la première fois, notre équipe de recherche a effectué des études statistiques sur des couleurs d'objets trans-neptuniens avec des résultats notables, références pour la caractérisation de cette population mais également pour les scénarios de formation du système solaire.

Observations de petits corps ; Préparation au sol des missions spatiales

I.1. Méthodes et outils liés aux observations ; la télé-observation

I.2. Photométrie des petits corps ;

I.3. Spectroscopie visible et infrarouge proche des objets du système solaire

I.4. Astrométrie et systèmes de références.

De nos jours l'observation des objets du système solaire, dans le domaine spectral du visible et de l'infrarouge proche, est faite par des détecteurs CCD[1]. L'analyse d'un objet sans atmosphère réside essentiellement dans l'interprétation du rayonnement électromagnétique réfléchi par l'objet. L'étape d'observation est donc essentielle pour l'obtention de résultats scientifiquement viables. Plusieurs composants liés à l'observation peuvent être conceptuellement différenciés : la conception des instruments adéquats pour un domaine particulier de l'astronomie, l'établissement d'une technique d'observation, l'établissement

[1] CCD – abbreviation de Charge Coupled Device (Detecteur avec transferts de charge electrique)

d'un protocole optimal d'obtention des observations, la réalisation d'une méthode de réduction des données d'observations,…

Les observations astronomiques suivent les acquis technologiques actuels, la spécialisation au sein même de l'activité d'observation astronomique devient une composante indispensable à la vie d'un astronome. De plus, les observations au sol s'imposent par un volet d'activités (par exemple l'interférométrie de haute résolution) qui actuellement sont difficilement envisageables dans l'espace extra-atmosphérique. Des données obtenues par de nouvelles générations de télescopes (Keck, VLT, Gemini,…) dotés de nouveaux types d'instruments et détecteurs concurrencent les données obtenues par les missions spatiales. Cette compétition fait que les deux volets d'obtention de données (les observations « in situ » délivrées par les missions spatiales et les observations au sol) permettent actuellement une complémentarité de certains aspects scientifiques. Nous assistons également à un transfert des connaissances techniques et technologiques (comme celles de planification automatique des tâches ordinaires d'instruments, de transfert des données, de commande à distance des instruments,…) entre les techniques astronomiques au sol et celles embarquées sur des sondes spatiales.

Ce chapitre traite des observations faites par le biais de mon expérience en matière de télé-observations ainsi que les techniques d'observation et réduction.

I.1 Méthodes et outils liés aux observations ; la télé-observation

Des efforts d'optimisation des observations astronomiques, de flexibilité et d'ergonomie des programmes sont effectués par toutes les équipes d'astronomes autour du globe. Les jalons sont les suivants :

- Une nouvelle génération de grands télescopes dont les plus représentatifs sont les géants VLT et Keck, permet actuellement l'obtention de résultats scientifiques à la mesure de leurs dimensions. Les télescopes avec des ouvertures de 2-4 mètres deviennent ainsi accessibles à des projets fondamentaux pour lesquels les mots-clefs « mission spatiale dans les trois prochaines années » peuvent être remplacés par « intérêt pour des projets spatiaux à long terme ». Ils permettent aussi des projets pilotes d'instrumentations de nouvelle génération.
- Les télescopes à ouverture de 2-4 mètres sont l'objet d'une forte pression sur le temps d'observation. Souvent les temps accordés sont des courtes périodes (1-2 jours). Cela impose un effort important de la part des initiateurs des programmes (les voyages + le temps d'observation + le temps de ré-adaptation = 7-9 jours au total pour une mission de 2 jours), et implique une augmentation inutile des « temps morts ».
- Depuis peu, certains télescopes d'ouvertures de 2-4 m offrent la possibilité de faire des observations à distance (remote observing). Afin d'encourager ce type d'observations, le temps consacré aux observations à distance, peut être, un critère de sélection important s'ajoutant à la pertinence scientifique du projet d'observations.
- L'implication des institutions scientifiques (dans le cas concret l'Observatoire de Paris) dans plusieurs projets instrumentaux et technologiques de pointe entraîne également une stratégie concernant les nouvelles technologies. Par

exemple, les observations à distance (remote observing) sur les instruments propriété du LESIA montés sur des télescopes au sol permettent de faire un usage optimal des moyens techniques et vont à terme réduire les besoins en mission.

Les premiers essais de télé-observations à l'Observatoire de Paris ont démarré au mois de décembre 2001 entre Meudon et Mauna Kea –Hawaii, par le pilotage du télescope IRTF (InfraRed Telescope Facility) de 3 m de diamètre situé au Mauna Kea, Hawaii. Ultérieurement cette activité a été formalisée dans le projet intitulé **Centre d'Observation à Distance en Astronomie à Meudon (CODAM)**.

Le but du projet CODAM est de fédérer les scientifiques de l'Observatoire de Paris afin de répondre à leur besoin d'exécuter des programmes d'observation à distance à partir de Meudon, sans qu'il soit nécessaire d'effectuer la mission sur le site du télescope. Loin d'être un substitut des programmes d'observation classiques, le projet est conçu pour offrir plus de flexibilité dans le programme scientifique des chercheurs, en contournant les problèmes liés à la fatigue du trajet (voyage + décalages horaires), les difficultés physiologiques liées à l'altitude à laquelle les télescopes sont installés. Enfin, ce projet offre la possibilité d'importantes économies financières pour le laboratoire, les sommes d'argent (déboursées au sein du budget de missions d'observations) pouvant ainsi être allouées à d'autres projets.

L'organisation d'un centre de contrôle à distance repose sur le concept d'infrastructure informatique unique afin de répondre aux besoins concrets des différentes manipulations astronomiques (technologies informatiques diverses, flux des données variable, temps de latence différents, architectures informatiques hétérogènes, politiques sécuritaires hétérogènes). L'activité courante consiste non seulement en une infrastructure matérielle, mais également une concentration des compétences techniques et scientifiques. L'expérience acquise dans les quatre dernières années montre qu'une mission de télé-observation est réussie quand plusieurs conditions sont remplies : une bonne connaissance du télescope et du détecteur, une bonne relation de travail entre l'équipe technique au sommet et celle de la salle de contrôle à distance, une bonne liaison Internet, un climat de confiance et de collaboration entre les institutions. Un autre volet des activités au sein du centre de contrôle est la veille technologique nécessaire pour toute mise à jour des instruments et télescopes avec capacités de télé-observations. Enfin, un dernier volet des activités consiste en l'identification des instruments propices à l'implémentation de cette activité.

Une première étape du projet, intitulée CODAM/IRTF, a été faite pour l'utilisation du spectrographe SpeX, qui couvre l'intervalle spectral 0.8-5 microns. L'infrastructure informatique pour cet instrument comporte :

- deux stations de travail sous Linux, permettant la gestion du spectrographe et du télescope à travers des liens sécurisés (tunnels ssh)
- un PC doté d'une webcam et un microphone, permettant une liaison audio-vidéo permanente avec le personnel technique de l'IRTF, au sommet de Mauna Kea, Hawaii ;
- trois connexions Internet ordinaires
- une liaison téléphonique utilisée en cas d'urgence et de panne de la liaison audio-vidéo

Des nos jours, plus de 40 nuits d'observations ont été effectuées avec SpeX-IRTF. Les données scientifiques obtenues ont été le sujet de plusieurs articles, communications et conférences. L'activité d'observation est comparable avec celle effectuée par une mission sur place. De plus, l'observateur ne subit pas les désagréments d'un longue voyage (souvent sur plusieurs fuseaux horaires) et les caprices de la météo lors des observations. Le décalage horaire entre Meudon et Hawaii (11 h) est idéale en ce qui concerne les télé-observations, l'observateur peut ainsi observer pendant son programme normal de recherche.

Le second développement sous l'intitulé CODAM est celui du combinateur interférométrique FLUOR qui travaille actuellement comme instrument invité sur le système CHARA situé au Mont Wilson en Californie. L'instrument FLUOR est la propriété du LESIA de l'Observatoire de Paris qui dispose de 20% de temps d'observation garanti sur le complexe des quatre télescopes (de 1 m de diamètre) qui représentent le système CHARA.

La mise en œuvre des activités de télé-observations nécessite une nouvelle technologie de transmission d'informations par l'informatique (celle des réseaux virtuels privés) ainsi qu'une liaison vidéo pour la surveillance à distance des télescopes et des conditions météo.

Références

M. Birlan, M.A. Barucci, W. Thuillot – *Solar system observations by remote observing technique : useful experience for robotic telescope strategies.* **Astronomische Nachricthen** No. **6-8**, 571-573, 2004.

A. Merand, **M. Birlan,** T. ten Brummelaar, V. Coudé du Foresto, R. Lelu de Brach - *Remote observations with FLUOR and the CHARA Array***, SPIE**, (in press), 2004

M. Birlan, R. Binzel – *Paris Observatory Remote Observing January-May 2002: Sharing the Experience to Educational Astronomy,* Global Hands-On Universe Conference Proceedings, Paris, July, 2002

S. J. Bus, A. J. Denault, J. T. Rayner, R. P. Binzel, **M. Birlan -** *Remote observing at the NASA Infrared Telescope Facility (IRTF)***,- SPIE** Conference**,** Advanced Global Communications Technologies for Astronomy II, Hawaii, August, 2002

Astron. Nachr./AN **325** (2004) 6/7, xxx–xxx

Solar system observations by remote observing technique : useful experience for robotic telescope strategies.

M. BIRLAN[1,2,⋆], A. BARUCCI[3], and W. THUILLOT[1]

[1] IMCEE, Observatoire de Paris, 77 avenue Denfert-Rochereau, 75014 Paris Cedex, France
[2] Astronomical Institute of the Romanian Academy, Cutitul de Argint - 5, 040557 Bucharest, Romania
[3] LESIA, Observatoire de Paris-Meudon, 5 Place Jules Janssen, 92195 Meudon Cedex, France

Received; accepted; published online

Abstract. Remote observations between Paris Observatory and Mauna Kea - Hawaii have been started two years ago. Nowadays ten runs have been already conducted from the remote observing center located in Meudon. The main topics of our investigations were devoted to physical studies of minor planets (Binzel et al. 2004, Birlan et al. 2004) and to spectral investigations of planetary atmospheres. Our experience attained its maturity and the acquired feed-backs allow us to discern between the advantages and difficulties of this observing technique. The main purpose of this paper is to share the remote observing experience and to valorize it in the frame of robotic telescope concept.

Key words: remote observing, spectroscopy, minor planets

©0000 WILEY-VCH Verlag GmbH & Co. KGaA, Weinheim

1. Introduction

One of the strategies of modern groundbased observational astronomy is to perform the observations in remote mode. In the astronomy vocabulary this denomination was introduced for the groundbased telescopes in the eight decade of the XX-th century. Until then several derived notion were implemented in the vocabulary. We talk about remote observing, passive and active remote observing, distribute remote observing or remote observing center (Zijlstra et al. 1997). All these definitions are in connection to the degree of implementation of the control of instrument and telescope from the distant observer.

Remote operation allows the observer to reside in a location that may be more comfortable than a high altitude summit and may reduce observer fatigue if no travel is required from her/his home institution. Such observations could be an answer to the service mode (or queuing mode) proposed by the staff of some large telescopes. The observer will be entirely responsible for the strategy adopted during the observations and the requirements of his scientific program (exposure time, signal-to-noise ratio, photometric or spectroscopic standards necessary for data reduction, airmass requirements,...) could be better accomplished.

⋆ Mirel.Birlan@imcce.fr

The remote observing must not be seen as the technique which could entirely replace ordinary missions to the telescope. The successful remote observing observations are the result of several factors: qualification of the observers for the science obtained through the program, difficulty of program in the frame of the routine work, degree of knowledge of the instrument and detector by the observer, knowledge and training with new procedures implemented in new versions of software for the telescope and the detector, coordination between the remote observer and the technical staff located near the telescope (array of telescopes).

2. CODAM - The Remote Observing Center at Meudon

The main principle of the remote observing center is to use the same technical infrastructure, for implementing several telescopes and instruments. For this purpose, we conceived the informatics and the logistic to the centre in order to be able of a quick switch between different types of astronomic observations.

First tests of observations starts on January 2002 in Meudon Observatory. The remote observing tests were conducted from Meudon during several runs, and the idea of

©0000 WILEY-VCH Verlag GmbH & Co. KGaA, Weinheim

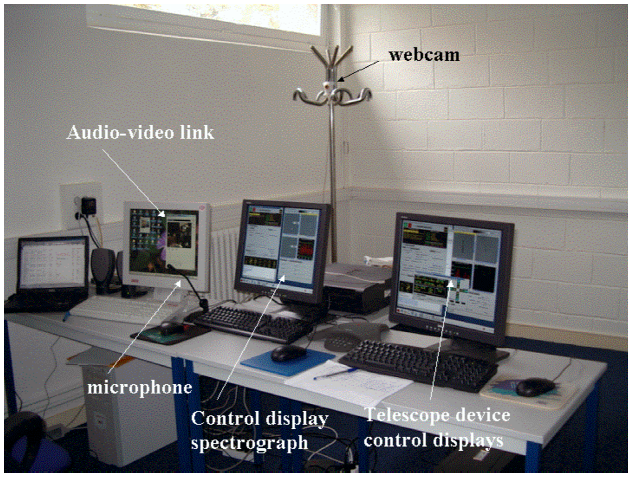

Fig. 1. Remote observing center at Meudon. This image was taken during its inauguration, on November 4, 2003

the Remote observing Center crystallized after six month. Our successful experiment was realized using IRTF 3 m telescope located in Mauna Kea, more than 12,000 km away from Meudon. The concept of remote observing center was imposed by the identification of several telescopes and instruments who are used by the researcher from Paris Observatory. Nowadays, the remote observing technique is perceived like an alternative to the classical observing mission, a service which allow a more flexible schedule for the scientist. The experience acquired with SpeX/IRTF attained its maturity; in parallel the remote observing tests have been started in interferometry, with CHARA system, located on Mount Wilson, in California. Investigations concerning other telescopes and instruments are also foreseen.

2.1. Remote observing with SpeX/IRTF

For the first run of Jannuary 2002, several tests and training sessions were organized beforehand. During these tests compatible computers for guiding and image acquisition were selected, and the strategy of the audio/video link was chosen. For the observers in Meudon, the observing hours occurred during relatively normal working daylight hours. Observation sessions began at 5 a.m. local time and finished at 5 p.m. local time.

The observations are realized through an ordinary network link, without the service quality warranty. Thus, the passband for our link was variable, in function of the traffic between Hawaii and Meudon.

The telescope and the instrument X environment control panels were exported to Meudon via two secure links (ssh tunnels). Two PC's under Linux operating system are devoted to the instrument and telescope control (Fig. 1). In order to have a permanent audio/video link, we use the IP link as it was the most compatible with IRTF operations. Thus, our audio/video link was established with a Polycom professional video-conference system (on Mauna Kea), and webcam / NetMeeting software (at Meudon). In our strategy we can dispose of a telephonic line with an audio-conference system for the unusual case of a completely broken audio/video link.

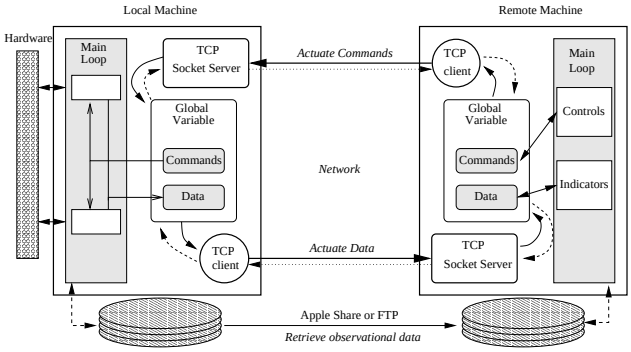

Fig. 2. Design of the client/server architecture for FLUOR/CHARA. The software and queries are written in Labview environment (Merand et al, 2004)

The SpeX instrument (IR spectrograph) was utilized for different scientific purposes.SpeX could be used in several scientific modes (low-resolution or high resolution spectroscopy) in the spectral interval 0.8-5.3 micron.

Nowadays more ten runs summing more than thirty night of observations were done by remote observing. During these runs a wide variety of procedures were commanded remotely: the focus of the telescope, setup of the guiding procedure, manual tracking, setup of the spectrometer and a preliminary analysis of the observations. The mean delay between the image acquisition in Mauna Kea and the refresh on the Meudon displays was 1.5-2 seconds approximately and it was quite stable independently of the internet traffic (our runs were done during the working days as well as during the weekends, as scheduled to IRTF). For all procedures, except for manual guiding on faint objects, such delays did not impede the efficient performance of the observing process. Thus, we estimate the efficiency of our observations very close of these obtained by a classic mission to the telescope.

2.2. Remote observing with FLUOR/CHARA

FLUOR is the acronym of Fiber Linked Unit for Recombination, an interferometric beam combiner developed by researchers and engineers of LESIA, Paris Observatory (Coude du Foresto et al. 2003). FLUOR was installed was installed to the Center for High Angular Resolution Astronomy (CHARA) Array, located at Mount Willson, California, in 2002.

The peculiar status of this instrument inside CHARA as well as the scientific interest for its results, allow of the strategy of remote observing from Meudon. The implementation of remote technique followed several steps such as: tests of physical link from Meudon to CHARA through a VPN technology, design of the client software for FLUOR instrument and the tests of this client in emulation mode, new facilities implementations in the remote observing center - video-projection system for scientific data.

On June 18, 2004, the tests were conducted with real data. From CODAM, we command for the first time the telescopes

and the beam combiner CHARA classic. The fringes of interference for the star HD 138852 were recorded for the first time remotely.

This success of our test was possible only by the close collaborations between the FLUOR and CHARA teams. The next step of our schedule will be the test of client software with real FLUOR data (Fig. 2).

3. Scientific results

During more than ten remote observing runs between CODAM and IRTF/SpeX, several scientific programs of planetology have been scheduled. The main programs were devoted to the solar system objects, mainly as support for the groundbased science in support to futures space missions. In this frame, we can cite the observations of asteroids candidates for Rosetta mission fly-by, and the high resolution spectroscopy of the deeper atmosphere of Venus for preparing the future Venus Express mission of the European Space Agency. Several runs were also devoted of near-infrared spectroscopy of Near-Earth Asteroids (Binzel et al. 2004) and the asteroids from the Main Belt.

The near-IR spectroscopy obtained by remote observations at IRTF was very important for the choice of the asteroids 21 Lutetia and 2867 Steins as targets to the Rosetta fly-bys. The IR observations (Fig. 3) of 21 Lutetia show a flat, featureless spectra, with a small positive slope. The comparaison of several meteorite spectra could conclude to the similarity of the asteroid spectrum with the chondritic materials (Vigarano meteorite from the CV3 carbonaceous chondrite group and Sevrukovo meteorite from the L6 ordinary chondrite group). For the Rosetta mission scientific objectives (finding clues of the formation and the evolution of the Solar System), 21 Lutetia is a very good candidate for 'in-situ' investigations.

4. Conclusion

The remote observing experience acquired during the last four years allow us to conclude the importance this observing mode. Remote observing technique can be considered a powerful interactive tool, with a good efficiency concerning the scientific results. All these assertions are relative to a good informatics infrastructure, for relatively high traffic rates, and the good compatibility of network materials. The quality of remote observations are highly dependent of the knowledge of the instrument and the telescope. Thus, the remote observers must be informed about the changes of the software and the implementation of new routines for the telescope and instrument.In the same time, the team of the telescope must inform the observers (through an e-mail list, web-page updates,...) concerning these modifications. For a efficiency estimated as 90% of that obtained by ordinary missions, we estimate the remote as a good alternative solution of observations, especially during the short runs. The facility of remote observing with instruments ideally located at 11-12 hours of difference offers the possibility to observe during the daylight

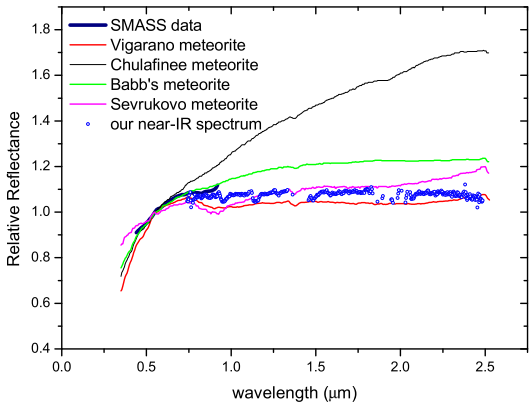

Fig. 3. The composite spectrum of the asteroid 21 Lutetia (the visible data from the SMASS program and the IRTF near-IR spectrum) was compared with several spectra of meteorites representative for some meteoritic groups. The near-IR spectrum of the asteroid is flat and featureless and can be noted the relative resemblance of it with those of chondritic meteorites (e.g. Vigarano and Sevrukovo). The figure contains also the spectra of two meteorites with high content of metallic atoms (Babb's Mill and Chulafinee) in order to mark the discrepancy of spectra. The meteorite spectra were published by Gaffey in 1976.

and increase the performance of observers by eliminating the fatigue of long distance travels.

Another important aspect of the remote observing is the access of the students to time on medium and large aperture telescopes. Students have the potential to be involved in the scientific proposals as a way of learning how to propose their own ideas. Remote observing could allow a strong background in observational techniques as well as experience with the telescope and the instruments.

The flexibility and the interactivity offered by remote observing should be considered in designing of robotic telescope strategies. The wide range of astronomical observations are function of the scientific goals, and it will be difficult to implement all type of observations for same robotic telescope. The choice of observation routines and scientific purposes could deserve also a reflection concerning the implementation of interactive routines which operate remotely.

References

Binzel, R.P.B., Birlan, M., Bus, S.J., et al.: 2004, PSS, 52(4), 291
Birlan, M., Barucci, M.A., Vernazza, P. et al. : 2004, NewAst 9(5), 333
Coude du Foresto, V., Borde, P., Merand, A., et al.: 2003, SPIE 4838, 280
Merand, A., Birlan, M., et al.:2004, SPIE Glasgow(in press)
Zijlstra, A.A., Wallander, A., Kaper, L., Rodriguez, J.A.: 1997, ASP 109, 1256

Remote observations with FLUOR and the CHARA Array

Antoine Mérand[a], Mirel Birlan[a], Rémi Lelu de Brach[a] and Vincent Coudé du Foresto[a]

[a] LESIA, UMR8109 Paris Observatory 5, place Jules Janssen 92295 Meudon CEDEX, (FRANCE)

ABSTRACT

Two years ago, the FLUOR interferometric beam combiner moved from IOTA (Infrared Optical Telescopes Array, Mount Hopkins, AZ) to the Center for High Angular Resolution Astronomy (CHARA) Array (Mount Wilson, CA). Apart from offering the largest baselines in the northern hemisphere, this array can be fully operated remotely to allow observations from a distant place. We present here the automations added to the FLUOR hardware, as well as software modifications made in order to allow us to observe from Paris Observatory. We required the remote service to be as reactive as local observations, implying frequent communications between the instrument and the remote observer. We took particular attention to the available bandwidth and reactivity imposed by the secured connection (Virtual Private Network). The first tests are presented.

1. INTRODUCTION

Remote observation tends to widespread in astronomy. For astronomers living far from the observing site, it may save traveling money and time. Moreover, some programs are not well adapted to few short runs a year: synoptic programs, like the survey of a slowly time-variable object, require a small amount of observing time every month or so.

1.1. The CHARA Array

The CHARA Array is an Optical stellar interferometer consisting in 6 telescopes, six delay lines (to equalize the path differences between telescopes aiming at the same star) and a Light Combination Laboratory (ten Brummelaar et al. 2003[1]). The all instrument is installed atop Mount Wilson, CA. This array can be operated from the remote operations center for Georgia State University's CHARA in the campus in Atlanta GA. The Cleon C. Arrington Remote Operations Center was designed to allow secure connection with the Mount Wilson site without cutting down the end-to-end latency.

1.2. FLUOR

The Fiber Linked Unit for Optical Recombination (FLUOR) is an interferometric combiner using single mode fiber as spatial filters and fiber coupler to combine the light from two telescopes in the infrared K band (mean wavelength, $\lambda = 2.2\,\mu m$). In 2002, FLUOR moved from the Infrared Optical Telescope Array (IOTA, Mount Hopkins, AZ) to the CHARA Array. (for a full description of FLUOR, see Foresto et al. 2003[2]).

2. CONTROL ARCHITECTURE

Existing publications describe the control software implemented to operate the CHARA Array (e.g. Fallon et al. 2003[3]). The FLUOR control software only handles correction to the CHARA optical path difference (OPD) active system (a pair of active delay lines) and specific hardware for FLUOR, thanks to different I/O boards, including:

- A fast scanning mirror that modulates the OPD between the two incoming beams in order to record the interferometric fringes,
- A near infrared detector,
- Step motors used to automatically and finely tune the alignment of the star on the inputs fibers

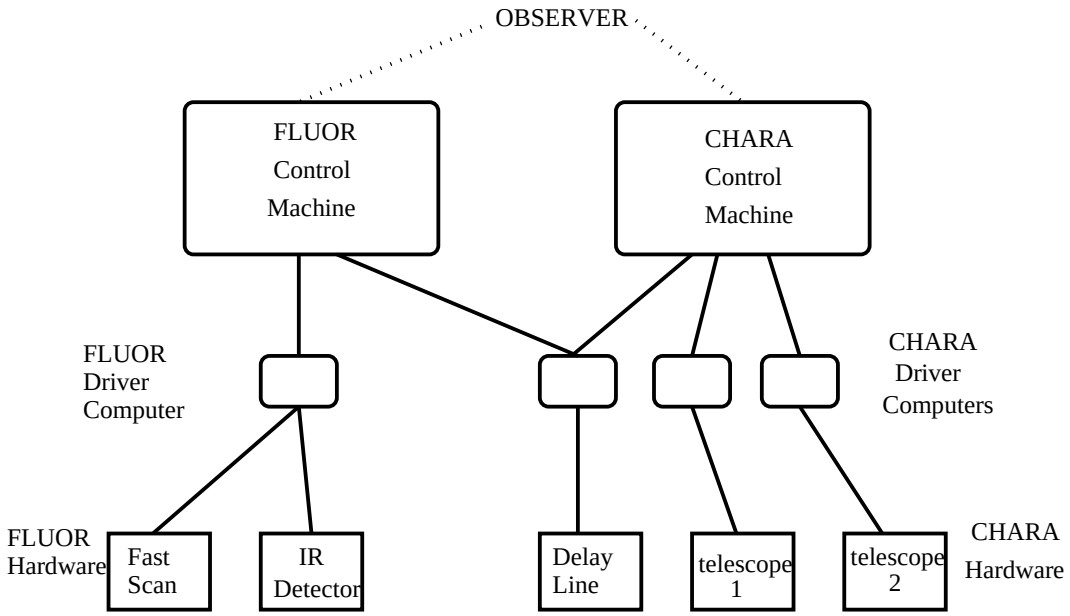

Figure 1. Control of FLUOR/CHARA. on the left, the CHARA control machine runs a single program that controls the whole array via intermediate computers dedicated to a single task and/or hardware device. The FLUOR side follows the same scheme: a Control Machine sequences the observations and access the FLUOR hardware via a dedicated computer.

The FLUOR Software is written in LabVIEW and runs on PowerMac computers under Mac OS X. On IOTA, The software was running on a single machine. On CHARA, a machine, sitting next to the optical table, is dedicated to the hardware low-level control. Another machine, in a comfortable control room, sits next to the CHARA computer that runs the master control software (see Fig.1). The FLUOR control machine runs the FLUOR Master software that sequences the observation and computes the corrections sent to CHARA active delay lines in order to correct from low frequency atmospheric perturbation of the OPD, as well as small drifts in the astrometric model that runs the delay lines. While observing with FLUOR, all CHARA sub-systems (telescopes, delay lines, shutters etc.) are controlled by the CHARA master program.

2.1. Observation cycle

Observing a target (science target or calibration star) with FLUOR/CHARA takes between 15 and 20 minutes. This cycle includes:

1. Aiming the two telescopes at the star (including locking the tip-tilt servo), positioning the delay lines.
2. Once the beams are stabilized (thanks to the tip-tilt system), optimizing the injection to the entrance fibers. This is done by rasterizing the focal plane with step motors moving a flat mirror (Fig. 2) while recording the flux in the photometric outputs. Optimizing consists in going back to the optimum position.
3. Looking for fringes. Usually, the observer has to scan a few millimeters around the delay lines supposed zero OPD position. FLUOR makes a scan (see next item) and then sends a given step to the active delay line if fringes are not found.
4. Recording scans. FLUOR, thanks to its Fast-Scan mirror, modulates the OPD with respect to time (over about 180 microns, 7 times the fringe packet length — 25 microns —). By the same time, the intensity is recorded out of the four output fibers: two photometric channels for further processing and two interferometric channels. Fringes are detected by a simple algorithm, the centroid of the fringe packet is computed and a correction is sent to the delay line.

Send correspondance to A. Mérand, E-mail: antoine.merand@obspm.fr

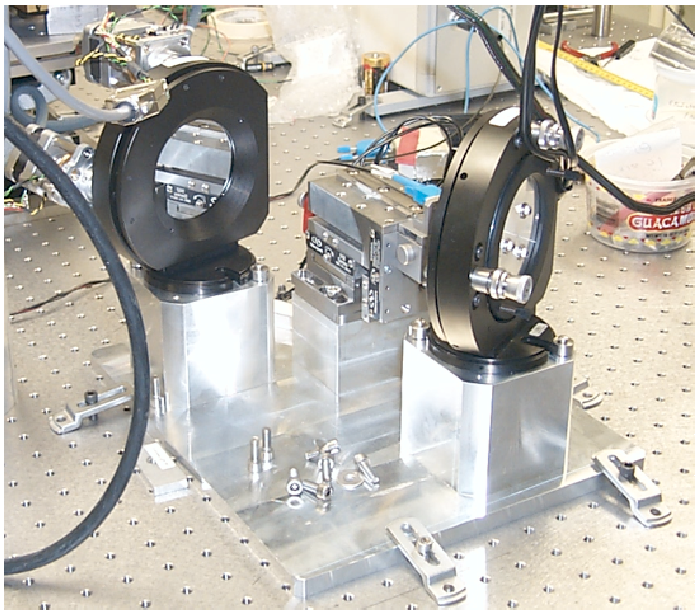

Figure 2. Input stage used to optimize the injection. The plan mirror (left) collects the beam from the telescope and sends it the off-axis parabola (right, behind the mount) in order to focus on the single-mode fiber. The plan mirror mount can be tilted in order to change the star position on the focal plan and thus optimize the injection in the fiber. This process, fully automated, increases the efficiency of the remote mode.

5. All shutter closed, dark frames are recorded. Usually, this time is used to aim at the next target (first item).
6. Checking visually the Data thanks to a synthetic display.

2.2. Latency requirements

Observing remotely usually does not offer the same reactivity because of end-to-end latency. In that section, requirements will be described using the same structure used to describe the observation cycle (previous section):

1. **Aiming the telescopes.** This part is made using CHARA control software and remote control interface (see Fallon et al. 2003[3]), we rely on their implementation.
2. **Optimizing injection.** This process, as described previously, is fairly automatic. Fist, the observer sends a starting signal and then waits for the rasterized focal image. The observer can follow the process but latency is not an issue here.
3. **Looking for fringes.** This process is highly demanding on latency. Recording a single scan (a fringe packet) takes fairly one second. Every second, the remote observer has to receive the fringe packet. Once again, FLUOR control software is mainly automated: an algorithm is used to detect the fringes in the scan. If so, the software stops sending constant steps to the delay lines and starts recording data on the current delay line position. A single false detection thus stops the searching process, the observer can decide to resume it. In that process, it is crucial for the remote observer to get every single scan.
4. **Recording data.** Once fringes are found, the FLUOR software compensates for slow drifts easily: while observing on site, we usually send the fringe signal to a loud-speaker in order to "keep an ear" on the system. If fringes are lost, the searching process (previous item) should resume. This steps requires also quality monitoring: signal to noise ratios, raw visibility estimation etc. have to be send for every scans. This is the most demanding part, in term of latency, of the observing.

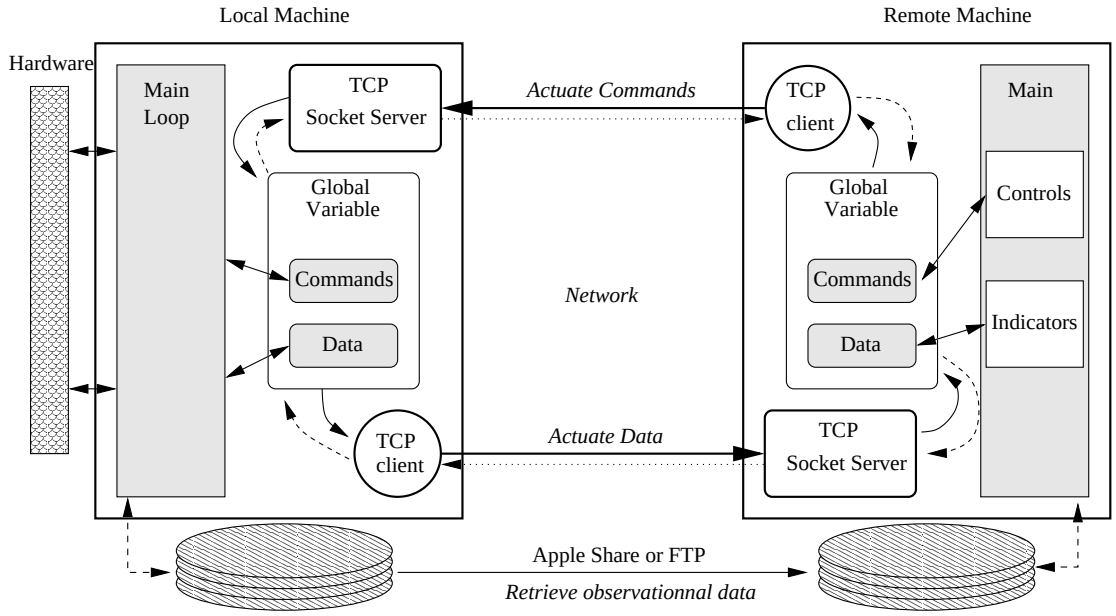

Figure 3. Implementation of the remote computer (right) with respect to the current FLUOR control computer (called local machine, left). The local machine is the same represented in Fig. 1, upper left. This machine is on Mount Wilson site, connected on the local network. Each machine runs a TCP server, allowing to receive text-based messages. The remote machine uses simple text commands while the local machine sends a status report, as well as a very small of data, quick looks essentially (thick lines between clients and servers). Acknowledge messages are sent back when a server receives commands or data (dotted lines).

5. **Dark Frames.** Nothing has to be done here. The observer only wants to have progress status.
6. **Checking Data quality.** This is done based on the actual file. Remote latency is not an issue: data are recorded on site and then downloaded on the remote computer thanks to a FTP (file transfer protocol) server.

It appears that a few tasks only are demanding regarding end-to-end latency, especially items number 3 and 4 (if the FLUOR software fails to keep the fringes in the scanned OPD range, which happens rarely).

2.3. REMOTE CONTROL ARCHITECTURE FOR THE FLUOR SOFTWARE

Considering that the observing cycle is fairly automated and that latency is only an issue for a small number of task, we decided to leave the FLUOR Software running on a computer located on Mount Wilson. Doing so, we protect ourselves against long latency events that can occur during a few seconds or even longer: the FLUOR control remains autonomous and only accepts commands. It sends for each scan a status report (a few tens of ASCII characters) and a quick look signal. We did not modify the software much, we only added a TCP client/server module to the LabVIEW software. Text-based control commands are sent to a dedicated TCP port, while the FLUOR control software can send data (mainly quick-look data) to a server (a listener) running on the remote machine (Fig. 3). The actual data are recorded on site and then retrieved by the remote observer. The two computers are connected to the same local network via a Virtual Private Network (VPN) protocol. This solution is used also to control the CHARA Array other the Internet (see Fallon et al. 2003[3]).

3. FIRST TESTS AND PROSPECTS

Using an emulation mode, we undertook observations using only FLUOR software (CHARA was not involved) from Paris/Meudon Observatory in December 2003. This emulation mode reproduces all steps of the observing

cycle, generates data. Without increasing the duration of a scan (which lasts roughly one second) by waiting for TCP transactions, it has been possible to receive the status string and quick-look data every single scans. Moreover, even operated from the other side of the Atlantic Ocean, the FLUOR control software remained reactive.

In the future, FLUOR/CHARA remote observations will take place in a dedicated room, the "Centre d'Observations à Distance pour l'Astronomie de Meudon" (CODAM) in Paris/Meudon Observatory. Located on the Meudon Campus, this room is also equipped for video conference. Observations were already made from this room using the NASA Infrared Telescope Facility on Mauna Kea with the SpeX instrument (see Birlan et al. 2004[4] for latest results).

4. CONCLUSION

An analysis of the requirements for a remote observing mode was made for the FLUOR interferometric beam combiner, installed on the CHARA Interferometric Array. We presented the actual implementation, consisting in adding a TCP client and server modules to the FLUOR control Software, another computer, running symmetric servers and client is used to send text-based commands and receive quick-look and status informations thru the Internet, the connection being secured by a Virtual Private Network (VPN) protocol. First tests were successfully undertaken, though using an emulation mode, showing promising results.

REFERENCES

1. T. A. ten Brummelaar, H. A. McAlister, S. T. Ridgway, N. H. Turner, L. Sturmann, J. Sturmann, W. G. Bagnuolo, and M. A. Shure, "An Update of the CHARA Array," in *Interferometry for Optical Astronomy II. Edited by Wesley A. Traub. Proceedings of the SPIE, Volume 4838.*, pp. 69–78, Feb. 2003.
2. V. Coude du Foresto, P. J. Borde, A. Merand, C. Baudouin, A. Remond, G. S. Perrin, S. T. Ridgway, T. A. ten Brummelaar, and H. A. McAlister, "FLUOR fibered beam combiner at the CHARA array," in *Interferometry for Optical Astronomy II. Edited by Wesley A. Traub. Proceedings of the SPIE, Volume 4838.*, pp. 280–285, Feb. 2003.
3. T. Fallon, H. A. McAlister, and T. A. ten Brummelaar, "Remote operation of the CHARA array via the Internet," in *Interferometry for Optical Astronomy II. Edited by Wesley A. Traub . Proceedings of the SPIE, Volume 4838.*, pp. 1193–1200, Feb. 2003.
4. M. Birlan, M. A. Barucci, P. Vernazza, M. Fulchignoni, R. P. Binzel, S. J. Bus, I. Belskaya, and S. Fornasier, "Near-IR spectroscopy of asteroids 21 Lutetia, 89 Julia, 140 Siwa, 2181 Fogelin and 5480 (1989YK8), potential targets for the Rosetta mission; remote observations campaign on IRTF," *New Astronomy* **9**, pp. 343–351, June 2004.

Paris Observatory Remote Observing January-May 2002; Sharing the Experience to Educational Astronomy [1]

Mirel BIRLAN[1], Richard BINZEL[1,2]
[1]Observatoire de Paris-Meudon, LESIA, 5 - Place Jules Janssen, 92195 Meudon CEDEX, France,
e-mail : *Mirel.Birlan@obspm.fr*
[2] Department of Earth, Atmospheric, and Planetary Sciences, Massachusetts Institute of Technology, Cambridge, MA 02139 USA
e-mail: *rpb@mit.edu*

Abstract: This paper describes the accomplishments and difficulties of the remote observing campaign between Meudon and the NASA Infrared Telescope Facility on Mauna Kea. The experiment is a three institutions initiative: IRTF team (Dr. S.J. Bus), MIT (Professor R. Binzel), and Paris Observatory (Dr. Mirel Birlan). During 4 observing runs between January and May 2002 we used the SpeX instrument to measure spectra in the range 0.9 - 2.5 microns for a spectroscopic study of near-Earth asteroids and the observation of 4979 Otawara, a flyby-target of the Rosetta mission. All target acquisition and data acquisition procedures were successfully commanded from Meudon with minimal delays in system response. The efficiency of the observing program was virtually the same as if the observers had been on location.

Our successful experiment could be applied for astronomy students. The students will be able to observe and will stimulate theirs initiative in astronomy science. The "live" observations is suggestive for students and will complete the whole teaching sequence, from doing their own observations, through data-reduction techniques, and finally, deducing science results.

One strategy of modern groundbased observational astronomy is to perform observations in a remote mode. Remote operation allows the observer to reside in a location that may be more comfortable than a high altitude summit and may reduce observer fatigue if no travel is required from her/his home institution.

Several weeks of effort were devoted in order to determine the best conditions for the success of the experiment we describe here. Our goals for remote science operation included having control of the instrument and the target acquisition/guider system. Equally important was the good communication between the Principal Investigator and the telescope operator on Mauna Kea. High speed and real time command and response for the instrument, telescope, data, and human communication links were essential to the success. Careful preparation and testing of hardware options showed that all objectives could be achieved during the period of the observing run.

This experiment was completed through an ordinary network link, without the service quality warranty. Thus, the bandwidth for our link was variable, and was a function of the traffic between Hawaii and Meudon.

For this experiment, several tests and training sessions were organized beforehand. During these tests compatible computers for guiding and image acquisition were selected, and the strategy of the audio/video link was chosen. During the pre-observing period, several workstations and terminals were tested. The main conclusion was that the X-windows export through Meudon is highly dependent on the machines we use: the export windows tests were

[1] Presented to *Global Hands-On Universe*, 24-29 July 2002, Paris, France

unsatisfactory for COMPAQ workstations and terminals, as well as for one of the SUN workstations. Finally, two Sparc workstations (with the operating systems 5.7 and 5.8 respectively) were found to be very well suited for the experiment (Figure 1).

The incompatibility of both video conference systems (through a phone line in Meudon, and the IP link in Mauna Kea), constrained us to choose either an IP link or a phone link. Our decision was to use the IP link as it was the most compatible with IRTF operations. Thus, our audio/video link was established with a Polycom professional video-conference system (on Mauna Kea), and webcam / NetMeeting software (at Meudon).

Figure 1 (Left side) Remote control room in Meudon Observatory. In this image the audio/video link is located on the left screen, the SpeX control and the guiding windows on the center and right screen respectively. (Center) SpeX instrument control window. Observing modes and data acquisition are controlled by the window on the left. Spectral images and their preliminary analysis are displayed and controlled on the right. Upper right window of the display shows the spectrum of the asteroid 2002AA in both A and B positions of the slit, after a preliminary treatment. (Right Side) Audio/video link as it was seen from Meudon.

For this collaborative experiment between MIT, IRTF, and Meudon, targets were chosen according to the scientific interests of the investigators at each institution. Priority was given to the science program for which the time was allocated: the compositional investigation of near-Earth asteroids. Supplementary targets included 4979 Otawara, a flyby target for the Rosetta mission planned by the European Space Agency.

The apparent V magnitudes of the measured asteroids were typically in the interval 15-17. The guiding for each object was performed using automatic mode for all but the faintest targets. For the latter, manual tracking was used. For data calibration, the solar analogs Landolt 93-101, Hyades 64, and Landolt 102-1081 were also observed during the course of the night (Binzel et al, submitted 2002).

All software was re-started at the beginning of each night. During the three nights, the audio/video link was very stable and useful for our remote experiment. This link dropped for small intervals during the runs, most likely the result of limits imposed by network security protocols. The telescope/guider control links and SpeX instrument control links remained fully linked and stable throughout all the nights.

All the observations were saved on the Mauna Kea computer system, and subsequently transferred to Meudon after the experiment using ftp.

The spectrum of the asteroid 4979 Otawara (on the top of the figure) illustrates the science. The infrared spectrum of the asteroid 4979 Otawara allows us to classify it as an S-type asteroid (silicate materials, where the 1 micron and 2 microns broad absorption features are characteristics of olivine and pyroxene). The S-type asteroids may be the parent bodies of the ordinary chodrite (OC) meteorites (Fornasier et al submitted 2002)

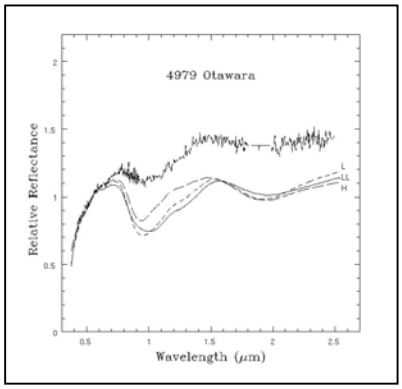

Conclusion:

Our successful experiment demonstrates a new teaching tool for students studying in astronomy. The students will be able to observe and have the observations stimulate their initiative in astronomy science. The "live" observation perception is different from a classical training exercise of astronomy in a class room and is a far more attractive opportunity for students. Within a small budget, a student can be able to complete the whole teaching sequence in practical astronomy, from doing their own observations, learning about the data-reduction technique, and obtaining the final scientific products.

Another important aspect of this experiment is the access of the students to time on medium and large aperture telescopes. Through remote observing participation a student gains a strong background in observational techniques as well as experience with the telescope and instruments. Students also have the potential to be involved in the scientific proposal process as a way of learning how to propose their own ideas.

Since our last run, two remote centre have been decided: one in Meudon Observatory, and the other one in Massachusetts Institute of Technology. Système d'Observations à Distance Astronomique (SODA) is the name of the remote system from Meudon Observatory, and the program was started in July 2002. MIT Remote Command Center became operational in September 2002 while Meudon Remote Command Center will become operational in February 2003.

Reference:

1. Binzel, R.P., Birlan, M., Bus, S.J., Harris, A., Rivkin, A.S., Fornasier, S.– *Spectral Observations for Near-Earth Objects Including Potential Target 4660 Nereus: Results From Meudon Observations at the NASA Infrared Telescope Facility (IRTF)*, **Planetary & Space Science** (submitted August 2002)
2. Fornasier, S., Barucci, M.A., Binzel, R.P., Birlan, M**.**, Fulchignoni, M., Barbieri, C., Bus, S.J., Harris, A.W., Rivkin, A.S., Lazzarin, M., Dotto, E., Erikson, A., Doressoundiram, A., Bertini, I., Peixinho, N., - *A portrait of 4979 Otawara, target of the Rosetta space mission*, **Astronomy & Astrophysics** (submitted April 2002)S.,

Remote observing at the NASA Infrared Telescope Facility

Schelte J. Bus[a], Anthony J. Denault[a], John T. Rayner[b], Richard P. Binzel[c], and Mirel Birlan[d]

[a]Institute for Astronomy, Univ. of Hawaii, Hilo, HI 96720
[b]Institute for Astronomy, Univ. of Hawaii, Honolulu, HI 96822
[c]Massachusetts Institute of Technology, Cambridge, MA 02139
[d]Observatoire de Paris, Meudon Cedex 92195, France

ABSTRACT

The NASA Infrared Telescope Facility (IRTF) on Mauna Kea now offers observers the opportunity to carry out their observations remotely. They can choose to work from the mid-level station at Hale Pohaku, from a dedicated remote observing room at the Institute for Astronomy in Hilo, or from their home institution. As a test of our remote capabilities, observations have been successfully obtained by observers from an office at the Observatoire de Paris in Meudon, France. Their observing program utilized SpeX, the IRTF's low- to medium-resolution near-IR spectrograph and imager, to measure the 0.8-2.5 micron reflectance spectra of fast moving, near-Earth asteroids. All target acquisition, guiding, and instrument control was commanded from Meudon. We describe this observing campaign, and provide details about the techniques we have developed for remote observing.

Keywords: remote observing

1. INTRODUCTION

The NASA Infrared Telescope Facility (IRTF) is a 3.0-m telescope located at an altitude of 4160 m, near the summit of Mauna Kea on the Big Island of Hawaii. The IRTF was established by NASA in 1979 to provide ground-based observations in support of spacecraft missions and basic solar system research. While half of the observing time on the IRTF is reserved for studies of solar system objects, observing proposals are accepted from the entire astronomical community. The IRTF receives observing proposals from astronomers across the US and from many foreign countries.

To best meet the needs of its observers while making the most efficient use of telescope time, the IRTF provides considerable flexibility in its scheduling of observing time. This scheduling puts high priority on approved programs that require time-critical observations. In addition, long-term synoptic or survey programs may be allocated several short slots of time spread over an observing season. To further enhance this flexibility in scheduling and to help relieve observers of some of the burdens (both time and cost) of traveling to Hawaii, members of the IRTF staff have been working to develop the tools and techniques required for remote observing.

When using either SpeX or NSFCAM (two of the facility instruments currently supported at the IRTF), observers now have the opportunity of carrying out their observations remotely. If they should choose to travel to Hawaii, but want to avoid the difficulties of working at the summit, observers have the option of observing from the mid-level station at Hale Pohaku (at an elevation of 2900 m on the slope of Mauna Kea), or from a dedicated remote observing room at the Institute for Astronomy in Hilo. The Hilo remote room is similar in concept to that used by other observatories on Mauna Kea[1]. Observers also have the option of working from their home institution by logging in via the Internet. To make use of this option, observers need access to a minimum level of computing power to provide sufficient connectivity to the IRTF instrument control computers: a workstation (UNIX workstation, PC with Linux, or Windows with X-terminal emulation software are acceptable platforms), dual X-windows monitors supporting 1280 x 1024 resolution in either 8-bit pseudo color or 24/32-bit true color graphics mode, a web camera with video-conferencing software, and fast (Ethernet) connection to the Internet (preferably with an average transfer rate of 100 kb/s or better). For researchers living many time zones from Hawaii, working from their home institution has the added benefit of requiring a smaller shift in sleep schedule in order to carry out nighttime observations in Hawaii.

2. ELEMENTS OF REMOTE OBSERVING

There are a number of different elements that make remote observing successful at the IRTF. The main element is the high-speed bandwidth between both our telescope and base facility, and on the Internet. Having a high-speed (>10MB Ethernet) connection between our telescope and base facility has fueled our desires to implement remote capabilities in the design and construction of instrumentation. As the Internet bandwidth and reliability has increased, it has prompted us to extend our remote observing capabilities further and further.

2.1 Remote capabilities for instrument software

Our previous generation of instrument software (used for the instruments NSFCAM and CSHELL) was developed in the early 1990s. At that time, remote observing was not considered a viable mode of operation for the IRTF. However, client-server separation and network-based communication greatly influenced our design strategy, as seen in Figure 1. The instrumentation software was separated into 3 major applications:

1. The instrument control software (IC). The IC software provides control of all instrument hardware. There are various processes for data acquisition, a command-line interpreter, motor control, temperature control, and control of other miscellaneous hardware.

2. X Windows-based User Interface (commonly referred to as the XUI). The XUI provides an easy to use interface to the IC. Command and status information is transmitted using TCP sockets. The XUI also receives data from the IC to be saved on the local workstation.

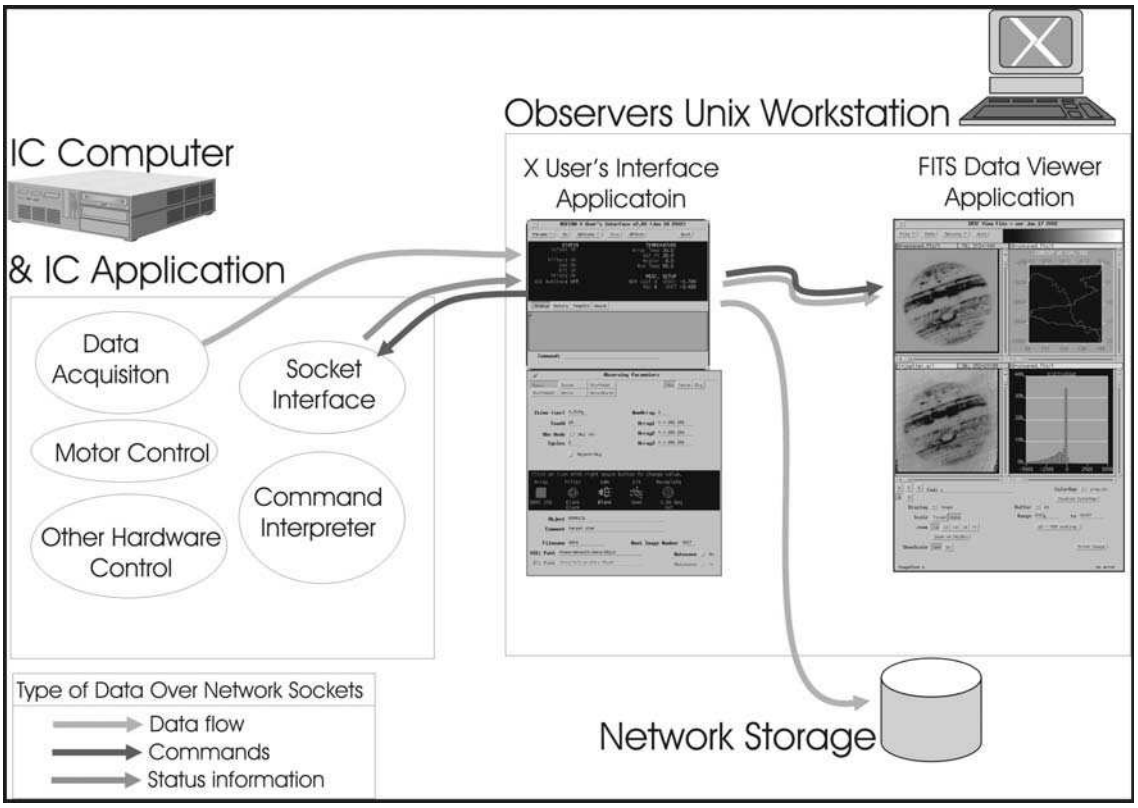

Figure 1. NSFCAM / CSHELL software model

3. A FITS Image Viewer (VF) is a stand-alone FITS data viewer with some image manipulation and graphing functions. It is able to accept commands and FITS data using TCP sockets.

These applications were designed to run on separate computers. The IC software runs in the IC computer located near the instrument, while the XUI and the data viewer run on a Unix workstation located in our observer work area. These applications exchange commands, status, and data using TCP sockets.

Although not initially designed for remote observing, as the Internet bandwidth increased, we began experimenting with running the instruments between Mauna Kea and the IfA campus in Manoa (island of Oahu), and then eventually to the mainland (continental U.S.). Observers at Lowell Observatory in Flagstaff, Arizona were the first to routinely use NSFCAM in this remote mode. By using preset macros to carry out many of the instrument operations, the real-time interaction by the observer was kept to a minimum during these earliest attempts at remote observing.

In 1998, the IRTF started building SpeX. SpeX is a medium-resolution 0.8-5.4 micron spectrograph that utilizes a 1024 x 1024 InSb array. SpeX also contains a 512 x 512 InSb array camera that can be used in imaging mode and as a slit-viewing guider[2]. When it came time to develop the SpeX software, a fundamental consideration was to include remote capabilities that would provide for both remote support and remote observing.

The software design treats SpeX as two separate instruments, a spectrograph and an imager, with each having an independent but almost identical set of software. Our basic software applications are still the Instrument Control (IC), X-User's Interface (XUI), and FITS data viewer (now renamed as DV).

Some slight design changes were implemented to allow for remote observing, depicted in Figure 2.

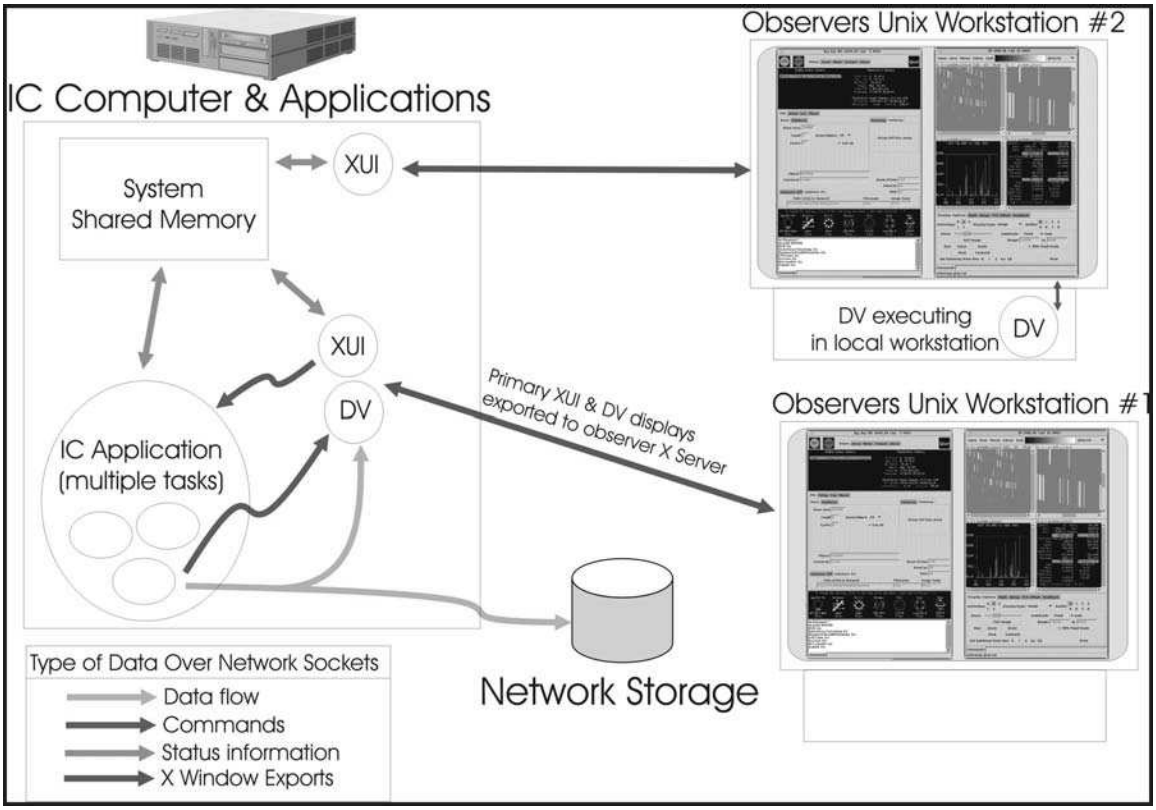

Figure 2. Illustration of the SpeX software design.

The key decisions in the design were:

1. The IC computer should be able to run the IC, XUI, and DV application. For our instrument computer, we selected a VME-based SPARC single-board computer. Our array image acquisition is controlled from VME DSP co-processor boards. Thus, our SPARC host can function as both the IC computer and XUI computer, and all our software applications can run from a single host. The IC application still handles all instrument control. The IC saves its data as FITS files and can write FITS images to sockets. The IC can be configured to send data to up to two DV data ports (TCP sockets). These data ports can be located on the local host or a remote host.

2. The IC and XUI now must run in the same computer. A shared memory area is used to hold all instrumentation parameters. The IC has read and write access, while the XUI has only read access. Commands are generated via the XUI and passed to an IC message queue. The XUI display is normally exported to the observer's workstation. For the purpose of trouble-shooting and observer support, multiple instances of the XUI can now be exported to different hosts.

3. Multiple instances of the data viewer are now possible within the same computer, or DV can be executed on a remote host. This provides the option of exporting the DV X-display from our instrument host or running DV on the observer's workstation.

2.2 Video conferencing

The IRTF is equipped with the following video conferencing system:

1. A Polycom ViewStation FX H.232 unit and 27" TV monitor at the telescope. This monitor and camera can be positioned at different locations within the warm room area occupied by the telescope operator and observer. The field of view and camera angle can be controlled either locally or by an observer working in the dedicated remote room in Hilo.

2. A Polycom ViewStation FX H.232 unit and 27" TV monitor in the Hilo remote observing room, shown in Figure 3. Field of view and camera angle can be remotely controlled from the summit.

Figure 3. Picture of the IRTF Hilo Remote Observing Room. Close up of Polycom unit communicating with telescope operator (left) and observer (right) on the summit.

The remote observers have the option of communicating with the telescope operators or other observing personnel (local observers) via these Polycom units. The remote site must have compatible equipment at their end. However, H.232 is a widely supported audio/video-over-IP protocol that is supported by many video conferencing products. The simplest client can be a PC with a video camera running Microsoft NetMeeting. While the Polycom ViewStation is an example of specialized equipment with higher quality and more advanced options than are available on common web cameras, we have found that remote observers can connect in using NetMeeting, usually with quite good results.

2.3 TCS1 status window

Operation of the IRTF still relies on the original Telescope Control System (TCS) that was built in the 1970s. It is not surprising, therefore, that the TCS is incapable of providing any type of remote services. However, we have developed a simple TCS status window tool that provides some telescope control similar to that of a hardware hand paddle. This window is shown in Figure 4.

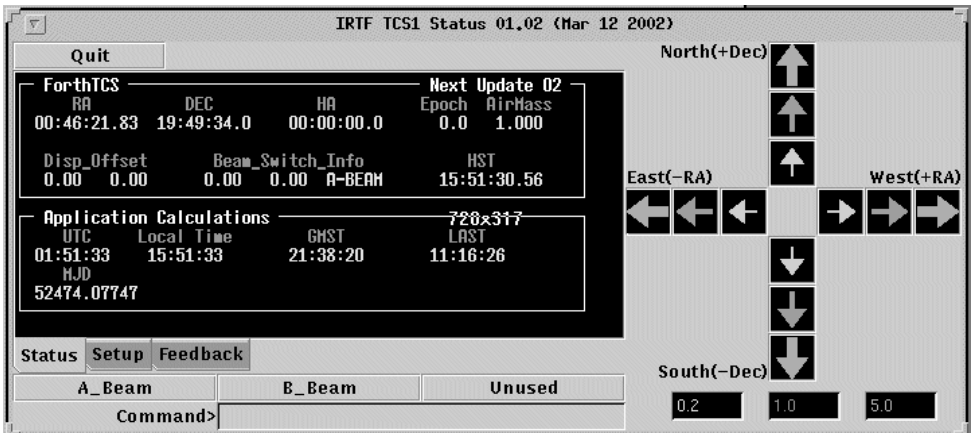

Figure 4. TCS status window.

The TCS1 status window provides a display of the current telescope position, time, and corresponding pointing parameters. Below the status display are buttons that allow the user to execute beam switches and input simple telescope control commands. To the right of the display are multi-colored arrow buttons for offsetting the telescope, a kind of virtual hand paddle. The multiple guide buttons were included to provide different step sizes (in arcseconds) that can be defined by the user.

3. EXPERIMENT IN REMOTE OBSERVING

A significant test of our remote observing capabilities came in January 2002 when observations were successfully obtained by Binzel and Birlan from an office at the Observatoire de Paris in Meudon, France, 11 time zones (about 12,070 km) from Mauna Kea. Their observing program used SpeX in its low-resolution prism mode to measure the 0.8 – 2.5 micron reflectance spectra of faint near-Earth asteroids. All aspects of target acquisition, guiding and instrument control were successfully commanded from Meudon for 2.5 nights. As the support astronomer and scientific collaborator on this project, Bus was present at the telescope throughout this run, but did little to intervene in the observations once all pieces of the remote observing system were up and running. His presence at the telescope was to accompany the telescope operator (thus fulfilling the Mauna Kea mandatory 2-person rule at the summit), and as a precaution in case there was a loss in Internet connectivity. As it turned out, the connection to Meudon was virtually flawless for the entire run.

The observatory at Meudon has a 6 Mb/s Ethernet link into the Internet, and currently experiences average transfer rates of 50-60 kb/s. The equipment used consisted of two SPARC workstations and a PC with a web camera. The workstations were used to display the XUI and DV windows exported by both the spectrograph and imager/guider ICs for SpeX. The TCS1_Status window was also used to monitor the pointing status of the telescope and to allow guiding corrections as necessary. An additional X-term window was used to command focus changes on the telescope. Audio/video conferencing was achieved using Microsoft NetMeeting that was installed on a PC located near the workstations. A measure of the time delay for the echo heard over the Polycom at the telescope revealed that the round-trip audio signal takes about 0.5 seconds, but the video transmission tended to be much slower. The video component would also freeze, often for several seconds before refreshing. This regular loss of video signal had no significant impact on the overall operation of either the telescope (operated from the summit) or the instrument (operated from Meudon), and did not effect the level of scientific output.

Due to their close proximity to Earth, the asteroids that were observed during this run had large non-sidereal motions. While the telescope drive rates were adjusted to compensate for much of this motion, small guiding corrections needed to be regularly applied. For the brighter asteroids, this was accomplished automatically by the auto-guiding software that is part of the SpeX imager. For the faintest targets, however, guide corrections needed to be made by hand using the software guide paddle in the TCS1_Status window. Since the integration times used for the guider images (typically 5 s or longer) were significantly longer than the image transmission time to Meudon (~ 1 s), there was no loss in guiding resolution by making these corrections from Meudon. Binzel and Birlan were able to guide the telescope just as if they were present on the summit.

Images of the spectral data were also transmitted to Meudon in real time via the DV window, while the FITS images (each measuring about 4 Mb) were stored on a local disk at the telescope. This data was archived at the IRTF and transferred to Meudon via ftp for analysis at the end of the observing run.

Three additional IRTF observing runs have been carried out remotely from Meudon by Binzel and Birlan with results comparable to their first attempt. Minor difficulties were encountered, especially in the ability to carry out video conferencing, due to the addition of a secure firewall at the IRTF and modifications to the firewall in Meudon. These changes in security meant that connections needed to be tested and troubleshot prior to each observing run.

The four successful runs carried out from Meudon provided a valuable learning experience and have helped us refine many aspects of our remote observing strategy. We realize that the most significant factor related to our capabilities for remote observing is the bandwidth and reliability of the Internet. The results we have achieved thus far are very encouraging and should only improve over time as the Internet grows. We anticipate that within a couple of years, the majority of observers using the IRTF will be making their observations remotely, in many cases without traveling any farther than to their office.

4. REFERENCES

1. R. I. Kibrick, S. L. Allen, and A. Conrad, “Remote observing with the Keck Telescope from U.S. mainland”, *Proc. SPIE* **4011**, pp. 84-92, 2000.
2. J. T. Rayner, D. W. Toomey, P. M. Onaka, A. J. Denault, W. E. Stahlberger, D. Y. Watanabe, and S.-I. Wang, “SpeX: a medium-resolution IR spectrograph for IRTF”, *Proc. SPIE* **3354**, pp. 468-479, 1998.

I.2. Photométrie des petits corps

Pendant mes recherches, j'ai employé plusieurs type de détecteurs, notamment la camera CCD et le photomètre photoélectrique, pour les problèmes liés à la photométrie.

Dans le cas des objets sans atmosphère, la technique de photométrie d'ouverture, dans le cas d'un photomètre à un seul détecteur, comporte une certaine séquence (observation de l'objet, du fond du ciel à coté de l'objet, suivie par une observation de l'étoile de comparaison), qui introduit des erreurs dues aux variations de l'atmosphère, durant cette courte période. Pour avoir une bonne précision, il faut alterner le plus rapidement possible les observations de l'astéroïde et de l'étoile de comparaison. L'équipement photoélectrique est capable de détecter des variations de luminosité nettement plus petites que celles obtenues avec la photométrie photographique. Cette technique est cependant de moins en moins utilisée dans les observations actuelles en raison d'une manipulation un peu difficile en comparaison de celles nécessitées par les technique nouvelles (photométrie CCD).

Les CCD constituent une famille de récepteurs à semi-conducteurs basés sur l'effet photoélectrique. De nos jours, les CCD ont quasiment remplacés (dans leur intervalle de longueur d'onde) les autres types de détecteurs sur des télescopes de grande, moyenne et petite taille et permettent de faire des observations d'objets sans atmosphère du système solaire, peu lumineux. Un autre avantage notable de l'utilisation des caméras CCD est la possibilité (voir nécessité) d'un post-traitement des images obtenues. Plusieurs techniques de traitement/réduction en chaîne (pipe-lines) se sont développées afin d'obtenir les résultats finaux.

En première instance, les observations photométriques nous permettent d'en déduire la magnitude des objets, ainsi que leur couleurs. La variation temporelle de la magnitude nous mène à la courbe de lumière de l'objet avec, en première approche, l'obtention de la période de rotation propre de l'objet. L'observation de l'une ou de plusieurs courbes de lumières du

même objet, à différentes oppositions et géométries, permet d'en déduire la position du pôle de l'objet et d'obtenir des informations sur la morphologie et la forme de l'objet. D'autre part, les différentes couleurs obtenues pour des objets distincts permettent une conclusion provisoire concernant les propriétés physiques de leur surfaces.

Les observations photométriques effectuées pendant mes recherches se sont inscrites sur trois programmes distincts :

- la photométrie des astéroïdes cibles de la mission spatiale Rosetta ;
- la photométrie des astéroïdes de petite taille (diamètre inférieur à 50 km) de la ceinture principale ;
- la photométrie des astéroïdes de période de rotation propre très longue ;

Au total j'ai observé 55 courbes de lumière, pour 21 astéroïdes dont 19 sont des astéroïdes de petite taille (Birlan et al, PSS, 1996, Florczack et al, 1997). J'ai pu obtenir environ 4% de l'ensemble des périodes de rotation déterminées jusqu'à maintenant, pour les astéroïdes de petite taille. C'est la première fois que l'on estime la période de ces astéroïdes. La plage des périodes de rotation propre obtenues est très large, entre 2.4 heures et 35 heures. Dans le cas des astéroïdes à période de rotation courtes, j'ai employé une nouvelle technique, avec un échantillonnage des images plus rapide. Les courbes de lumière présentent des amplitudes dans l'intervalle 0.2-1.0 magnitudes. Les observations ont permis de résoudre la courbe de lumière des deux astéroïdes censés avoir une longue période.

L'étude statistique des périodes de rotation sur l'ensemble des astéroïdes de petite taille montre que la distribution expérimentale/observée peut être reproduite par une combinaison des trois distributions de type Maxwell.

Parmi les astéroïdes observés, sept astéroïdes ont été des candidats au survol par la mission spatiale ROSETTA (Doressoundiram et al, A&A, 1999). Ces observations font partie du programme de préparation au sol de la mission, afin d'avoir une meilleure connaissance de la physique des candidats. Même si ces candidats ne sont pas retenus, les résultats obtenus sont importants pour la population astéroïdale dans son ensemble, permettant ainsi de mieux préciser les conditions de formation du Système Solaire.

Les couleurs et les spectres obtenus pour 4979 Otawara, astéroïde cible de ROSETTA, et 9969 Braille, astéroïde cible de la mission DEEP SPACE 1 (Lazzarin et al, A&A, 2001) ont permis de les classer dans les classes taxonomiques des astéroïdes avec une évolution thermique importante (types taxonomiques S, V, Q)

L'imagerie CCD de comètes représente un volet particulier des activités d'observations. Ainsi, les observations de la comète Hyakutake ont permis l'obtention de paramètres tels que la configuration de l'environnement au voisinage du noyau et l'orientation de la queue.

Références :

Birlan M., Barucci M.A., Angeli C., Doressoundiram A., DeSanctis M.C. - *Rotational properties of asteroids: CCD observations of nine small asteroids* **Planetary and Space Science** vol. **44**, n. **6**, 555-558, 1996.
Florczak M., Dotto E., Barucci M.A., **Birlan M.**, Erikson A., Fulchignoni M., Nathues A., Perret L., Thebault P. - *Rotational properties of main belt asteroids: Photoelectric and CCD observations of 15 objects* **Planetary and Space Science** vol. **45**, n. **11**, 1423-1435, 1997.
Doressoundiram A., Weissman P.R., Fulchignoni M., Barucci M.A., LeBras A., Colas F., Lecacheux J., **Birlan M.**, Lazzarin M., Fornasier S., Dotto E., Barbieri C., Sykes M.V., Larson S., Hergenrother C. - *4979 Otawara: Flyby target of the Rosetta mission* **Astronomy & Astrophysics** , vol **352**, n. **2**, 697-702, 1999.
Lazzarin M., Fornasier S., Barucci M.A., **Birlan M.** - *Groundbased investigation of asteroid 9969 Braille, target of the spacecraft mission Deep Space 1* **Astronomy and Astrophysics**, n. **375**, 281-284, 2001.
Vaduvescu 0., Stefanescu G., **Birlan M.** - *CCD and photographic observations of the comet C/1996B2 (Hyakutake)* **Romanian Astronomical Journal**, vol. **8**, 43-51, 1998.

Pergamon
Planet. Space Sci., Vol. 44, No. 6, pp. 553–558, 1996
Copyright © 1996 Elsevier Science Ltd
Printed in Great Britain. All rights reserved
0032–0633/96 $15.00+0.00

PII: S0032–0633(96)00019–0

Rotational properties of asteroids: CCD observations of nine small asteroids

M. Birlan,[1,2] M. A. Barucci,[2] C. A. Angeli,[2] A. Doressoundiram[2] and M. C. De Sanctis[3]

[1]Astronomical Institute of the Romanian Academy, str Cutitul de Argint-5, Bucharest 28, Romania
[2]Observatoire de Paris, 92195 Meudon Principal Cedex, France
[3]Univ. of Rome, Istituto Astronomico, Via Lancisi 29, 00161 Rome, Italy

Received 24 November 1995; revised 30 January 1996; accepted 30 January 1996

Abstract. The observational programme on small asteroids (diameter less than about 50 km) is continued to enlarge the available dataset of small asteroids. The results are presented of CCD observations of nine small asteroids ($D \leq 23$ km), performed in France with the 1.2 m telescope at Haute Provence Observatory and with the 2 m telescope at Pic du Midi Observatory. A total of 27 single night lightcurves for nine asteroids were obtained. All the objects were observed for the first time and rotational periods have been determined for all of the observed asteroids: 1992 Galvarino ($P_{syn} = 7^h.004$), 2419 Moldavia ($P_{syn} = 2^h.412$), 2921 Sophocles ($P_{syn} = 4^h.778$), 3247 Di Martino ($P_{syn} = 5^h.445$), 3623 Chaplin ($P_{syn} = 8^h.361$), 3986 Rozhkovskij ($P_{syn} = 4^h.26$), 4436 1983 EX ($P_{syn} = 6^h.656$), 5046 1981 DQ ($P_{syn} = 6^h.050$) and 1992 YG3 ($P_{syn} = 8^h.91$). Copyright © 1996 Elsevier Science Ltd

Introduction

The study of asteroid spin rates may provide information on the collisional evolution of main belt asteroids. Fulchignoni *et al.* (1995) have performed a statistical analysis of asteroid rotational periods and reanalysed the rotational rate distribution of a whole "high quality" sample of 516 asteroids. They found that the small object population ($D \leq 50$ km) can be represented by a linear combination of three Maxwellian functions which have been interpreted in terms of collisional evolution of the asteroid population. However, the present sample of asteroid rotations is still poor in the small diameter range and some bias exists. For this reason, we continue our observational campaigns aiming to determine the rotational properties of small asteroids.

In this paper, the results of CCD observations of nine small asteroids ($D \leq 23$ km), carried out in France at Haute Provence Observatory and Pic du Midi Observatory, using respectively the 1.2 and 2 m telescopes, are presented. The aspect data are listed in Table 1, where in the last column we have reported the mean magnitude level $V(1,\alpha)$, which corresponds to the zero level on the composite lightcurve plots. In Table 2 we summarize the values found for the synodic rotational period, the amplitude of the lightcurve, and the diameters (Tholen, 1992). The reported observations are not corrected for the light-time.

Observations and data reduction

Observations have been carried out in the V band, with the 2 m telescope (Pic du Midi Observatory) in January 1993, for the asteroid 1992 YG3, and with the 1.2 m telescope (Haute Provence Observatory) between April and October 1995 for the other objects. The transformation to the V magnitude has been carried out observing groups of standard stars (Landolt, 1983). When the conditions of the sky were not photometric, the data were reduced only taking into account the differential extinction between the asteroid and the comparison star.

For the nine observed asteroids we determined the synodic rotational period, and the corresponding uncertainty, by applying Fourier analysis as described in Harris *et al.* (1989). The composite lightcurves of the observed asteroids are presented in Figs 1–9.

Results

1992 Galvarino, considered by ESA as one of the alternative candidates of the Rosetta mission, was observed

Correspondence to: A. Barucci

Table 1.

Date 0 UT	R.A. 2000.0 h m s	Decl. 2000.0 ° ′	Long 2000.0	Lat. 2000.0	r AU	Δ AU	Phase deg	$V(1,\alpha)$ mag
1992 Galvarino								
1995 09 26	03 28 29.5	+10 37.8	52.4	−8.0	3.058	2.320	14.63	10.35
1995 09 27	03 28 21.4	+10 32.9	52.4	−8.0	3.058	2.310	14.41	10.35
1995 09 28	03 28 12.0	+10 27.8	52.3	−8.1	3.059	2.300	14.18	—
1995 09 29	03 28 01.2	+10 22.7	52.2	−8.2	3.059	2.290	13.94	—
2419 Moldavia								
1995 09 26	01 17 05.9	+03 09.5	18.9	−4.6	2.168	1.190	7.81	11.50
1995 09 27	01 16 22.4	+03 00.4	18.7	−4.6	2.168	1.186	7.30	11.49
1995 10 02	01 12 30.1	+02 14.1	17.5	−5.0	2.163	1.171	4.81	—
2921 Sophocles								
1995 10 01	00 15 52.8	+00 17.2	3.7	−1.3	2.773	1.773	1.40	11.17
1995 10 02	00 15 10.2	+00 12.2	3.5	−1.3	2.774	1.775	1.80	—
3247 Di Martino								
1995 09 28	01 15 04.5	+04 21.8	18.9	−3.3	2.680	1.698	5.50	—
1995 09 29	01 14 10.9	+04 17.2	18.7	−3.3	2.679	1.695	5.07	—
1995 09 30	01 13 16.5	+04 12.6	18.5	−3.2	2.679	1.693	4.64	10.96
3623 Chaplin								
1995 10 01	23 12 23.0	−09 25.5	345.3	−3.9	2.615	1.661	8.37	10.43
1995 10 02	23 11 45.9	−09 29.3	345.2	−3.9	2.615	1.667	8.77	—
3986 Rozhkovskij								
1995 09 26	22 46 25.0	+01 05.7	343.4	+8.2	2.231	1.265	9.13	10.93
1995 09 27	22 45 35.9	+01 00.0	343.2	+8.2	2.230	1.268	9.60	10.93
4436 1983 EX								
1995 04 26	13 58 37.8	+11 44.5	203.1	+22.2	3.292	2.354	7.49	11.93
1995 04 27	13 57 51.7	+11 45.3	202.9	+22.2	3.293	2.357	7.64	11.94
1995 04 28	13 57 05.9	+11 45.9	202.7	+22.1	3.293	2.360	7.79	11.97
5046 1981 DQ								
1995 09 28	22 47 47.9	+10 03.2	347.3	+16.3	2.478	1.527	9.28	—
1995 09 29	22 47 12.7	+09 52.6	347.1	+16.2	2.478	1.530	9.57	—
1995 09 30	22 46 38.6	+09 41.9	346.9	+16.1	2.477	1.533	9.88	11.35
1992 YG3								
1993 01 17	07 57 55.6	+20 19.8	117.4	−0.3	2.701	1.717	0.22	—
1993 01 19	07 56 10.7	+20 26.1	117.0	−0.3	2.699	1.716	0.72	—
1993 01 20	07 55 18.2	+20 29.2	116.8	−0.3	2.699	1.716	1.16	—
1993 01 21	07 54 25.8	+20 32.3	116.6	−0.2	2.698	1.716	1.61	—
1993 01 22	07 53 33.6	+20 35.4	116.4	−0.2	2.698	1.717	2.05	—

Table 2.

Asteroid	Rot. period (h)	Amplitude (mag)	D (km)
1992 Galvarino	7.004±0.003	≥0.59	10.50
2419 Moldavia	2.412±0.003	0.14±0.03	7.28
2921 Sophocles	4.778±0.005	0.16±0.04	8.35
3247 Di Martino	5.445±0.006	0.51±0.05	17.70
3623 Chaplin	8.361±0.005	0.97±0.02	13.80
3986 Rozhkovskij	4.26±0.03	0.26±0.05	10.50
4436 1983 EX	6.656±0.006	0.40±0.05	23.00
5046 1981 DQ	6.050±0.003	0.21±0.03	11.50
1992 YG3	8.91±0.03	0.36±0.05	15.10

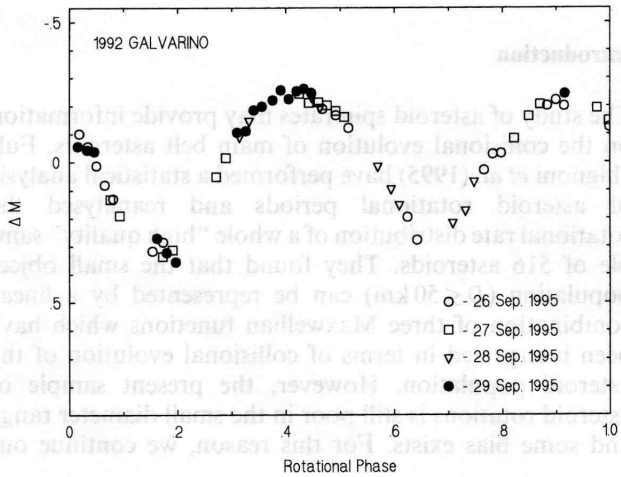

Fig. 1. Composite lightcurve of the asteroid 1992 Galvarino in rotational phase. 0 phase corresponds to UT 1995 Sep. 26, $3^h.012$

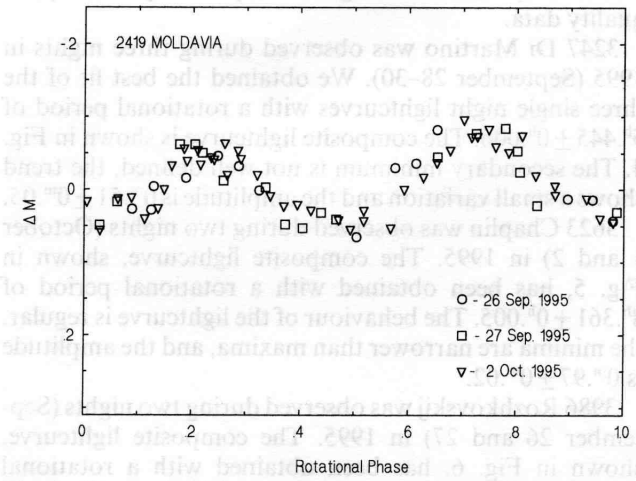

Fig. 2. Composite lightcurve of the asteroid 2419 Moldavia in rotational phase. 0 phase corresponds to UT 1995 Oct. 2, $0^h.205$

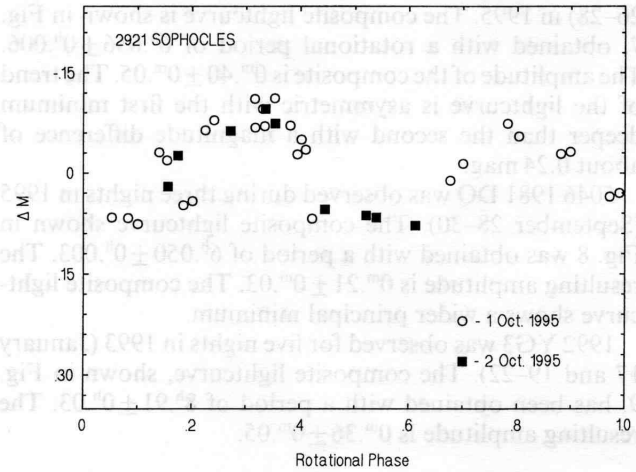

Fig. 3. Composite lightcurve of the asteroid 2921 Sophocles in rotational phase. 0 phase corresponds to UT 1995 Oct. 1, $0^h.279$

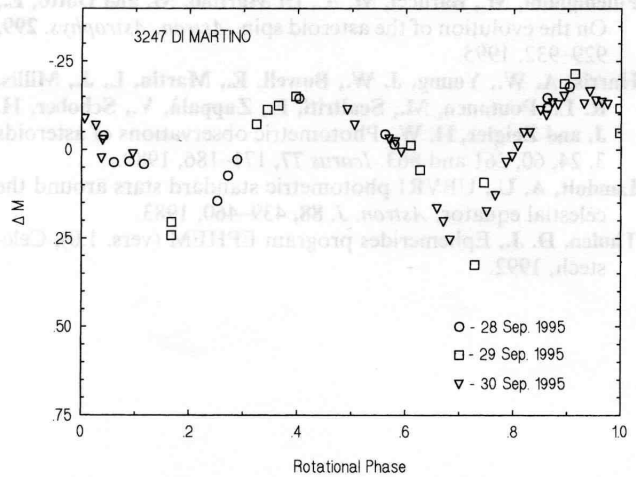

Fig. 4. Composite lightcurve of the asteroid 3247 Di Martino in rotational phase. 0 phase corresponds to UT 1995 Sep. 28, $2^h.239$

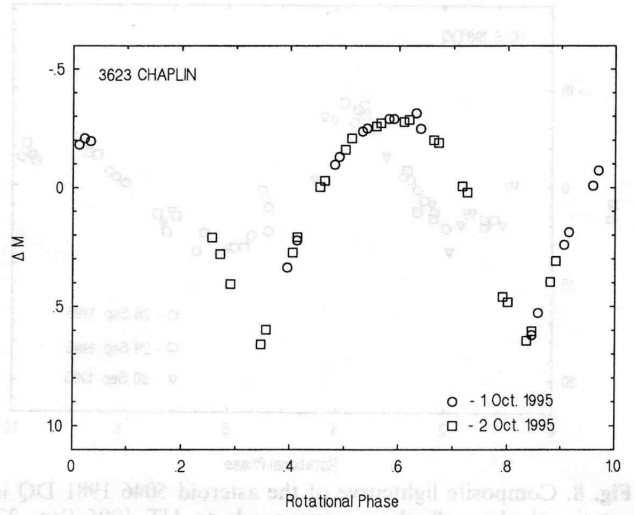

Fig. 5. Composite lightcurve of the asteroid 3623 Chaplin in rotational phase. 0 phase corresponds to UT 1995 Oct. 1, $0^h.185$

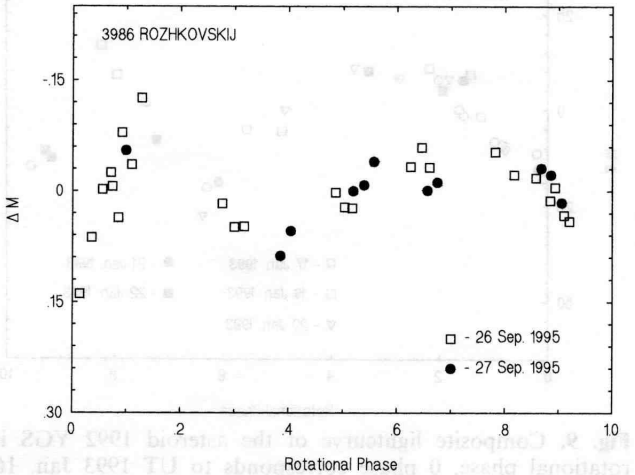

Fig. 6. Composite lightcurve of the asteroid 3986 Rozhkovskij in rotational phase. 0 phase corresponds to UT 1995 Sep. 26, $19^h.743$

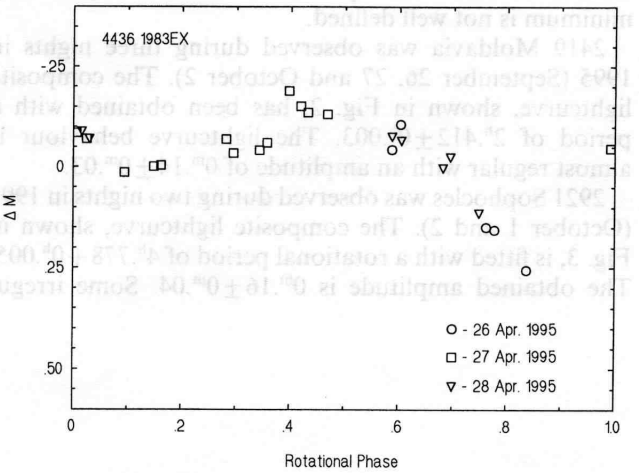

Fig. 7. Composite lightcurve of the asteroid 4436 1983 EX in rotational phase. 0 phase corresponds to UT 1995 Apr. 25, $21^h.366$

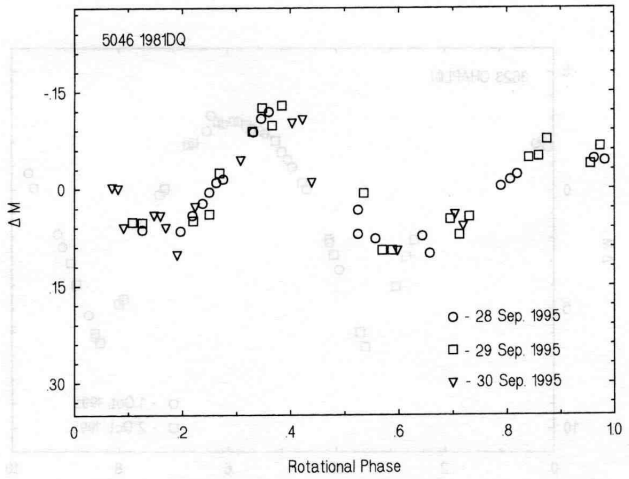

Fig. 8. Composite lightcurve of the asteroid 5046 1981 DQ in rotational phase. 0 phase corresponds to UT 1995 Sep. 27, $23^h.611$

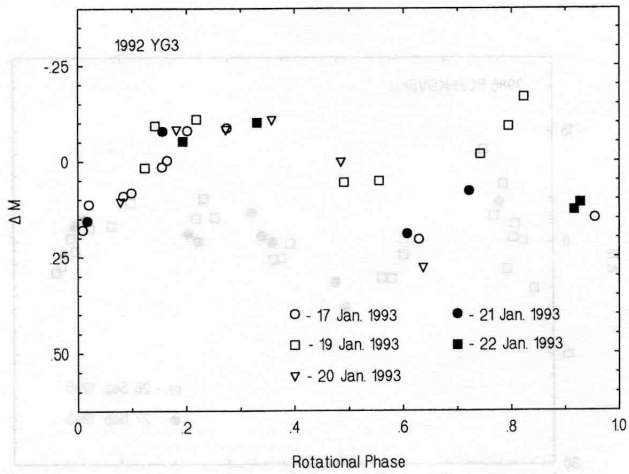

Fig. 9. Composite lightcurve of the asteroid 1992 YGS in rotational phase. 0 phase corresponds to UT 1993 Jan. 16, $17^h.784$

during four nights in 1995 (September 26–29). The composite lightcurve, fitted with a period of $7^h.004 \pm 0^h.003$, is shown in Fig. 1. The lightcurve amplitude can be larger than $0^m.59$ and seems symmetric even if the secondary minimum is not well defined.

2419 Moldavia was observed during three nights in 1995 (September 26, 27 and October 2). The composite lightcurve, shown in Fig. 2, has been obtained with a period of $2^h.412 \pm 0^h.003$. The lightcurve behaviour is almost regular with an amplitude of $0^m.14 \pm 0^m.03$.

2921 Sophocles was observed during two nights in 1995 (October 1 and 2). The composite lightcurve, shown in Fig. 3, is fitted with a rotational period of $4^h.778 + 0^h.005$. The obtained amplitude is $0^m.16 \pm 0^m.04$. Some irregularities are present in the lightcurve, probably due to poor quality data.

3247 Di Martino was observed during three nights in 1995 (September 28–30). We obtained the best fit of the three single night lightcurves with a rotational period of $5^h.445 \pm 0^h.006$. The composite lightcurve is shown in Fig. 4. The secondary minimum is not well defined, the trend shows a small variation and the amplitude is $0^m.51 \pm 0^m.05$.

3623 Chaplin was observed during two nights (October 1 and 2) in 1995. The composite lightcurve, shown in Fig. 5, has been obtained with a rotational period of $8^h.361 \pm 0^h.005$. The behaviour of the lightcurve is regular, the minima are narrower than maxima, and the amplitude is $0^m.97 \pm 0^m.02$.

3986 Rozhkovskij was observed during two nights (September 26 and 27) in 1995. The composite lightcurve, shown in Fig. 6, has been obtained with a rotational period of $4^h.26 \pm 0^h.03$. The computed lightcurve shows an amplitude of $0^m.26 \pm 0^m.05$ and an irregular trend with fluctuations probably due to poor quality data. Other possible periods cannot be excluded.

4436 1983 EX was observed during three nights (April 26–28) in 1995. The composite lightcurve is shown in Fig. 7, obtained with a rotational period of $6^h.656 \pm 0^h.006$. The amplitude of the composite is $0^m.40 \pm 0^m.05$. The trend of the lightcurve is asymmetric with the first minimum deeper than the second with a magnitude difference of about 0.24 mag.

5046 1981 DQ was observed during three nights in 1995 (September 28–30). The composite lightcurve shown in Fig. 8 was obtained with a period of $6^h.050 \pm 0^h.003$. The resulting amplitude is $0^m.21 \pm 0^m.03$. The composite lightcurve shows a wider principal minimum.

1992 YG3 was observed for five nights in 1993 (January 17 and 19–22). The composite lightcurve, shown in Fig. 9, has been obtained with a period of $8^h.91 \pm 0^h.03$. The resulting amplitude is $0^m.36 \pm 0^m.05$.

Acknowledgements. We are grateful to Dr François Colas for his assistance with the image processing ASTROL software.

References

Fulchignoni, M., Barucci, M. A., Di Martino, M. and Dotto, E., On the evolution of the asteroid spin. *Astron. Astrophys.* **299,** 929–932, 1995.

Harris, A. W., Young, J. W., Bowell, E., Martin, L. J., Millis, R. L., Poutanen, M., Scaltriti, F., Zappalà, V., Schober, H. J. and Zeigler, H. W., Photometric observations of asteroids 3, 24, 60, 261 and 863. *Icarus* **77,** 171–186, 1989.

Landolt, A. U., UBVRI photometric standard stars around the celestial equator. *Astron. J.* **88,** 439–460, 1983.

Tholen, D. J., Ephemerides program EPHEM (vers. 1.0), Celestech, 1992.

Pergamon PII: S0032-0633(97)00121-9

Planet. Space Sci., Vol. 45, No. 11, pp. 1423–1435, 1997
© 1997 Elsevier Science Ltd.
All rights reserved. Printed in Great Britain
0032-0633/97 $17.00+0.00

Rotational properties of main belt asteroids: photoelectric and CCD observations of 15 objects*

M. Florczak,[1,2,3] E. Dotto,[3,4] M. A. Barucci,[3] M. Birlan,[5] A. Erikson,[6] M. Fulchignoni,[3,7] A. Nathues,[6] L. Perret[3] and P. Thebault[3]

[1]ON/CNPq, Dep. Astrofísica, 20921 Rio de Janeiro, Brazil
[2]CEFET, Dep. Física, 80000 Curitiba, Brazil
[3]Observatoire de Paris, 92195 Meudon Principal Cedex, France
[4]Università di Padova, Dip. di Fisica, V. Marzolo 8, 35131 Padova, Italy
[5]Astronomical Institute of the Romanian Academy, str. Cutitul de Argint 5, Bucharest 28, Romania
[6]DLR, Institute of Planetary Exploration, Rudower Chausse 5, D-12489 Berlin, Germany
[7]Université Paris 7, Paris, France

Received 19 March 1997; accepted 20 May 1997

Abstract. In this paper we present the results of several observational campaigns carried out during 1996 at the 1.2 m telescope of the Haute Provence Observatory (France) and at the 1.5 m Danish, 0.9 m Dutch, 0.6 m Bochum and 0.5 m telescopes of the European Southern Observatory (ESO, La Silla, Chile), in order to enlarge the available sample of know asteroid rotational periods.

A total of 64 single night lightcurves for 15 asteroids were obtained. The rotational periods have been determined for 12 objects, with different quality code: 424 Gratia (P_{syn} = 19.47 h), 440 Theodora (P_{syn} = 4.828 h), 446 Aeternitas (P_{syn} = 15.85 h), 491 Carina (P_{syn} = 14.87 h), 727 Nipponia (P_{syn} = 4.6 h), 732 Tjilaki (P_{syn} = 12.34 h), 783 Nora (P_{syn} = 34.4 h), 888 Parysatis (P_{syn} = 5.49 h), 1626 Sadeya (P_{syn} = 3.438 h), 2209 Tianjin (P_{syn} = 9.47 h), 2446 Lunacharsky (P_{syn} = 3.613 h) and 3776 Vartiovuori (P_{syn} = 7.7 h). For 1246 Chaka, 1507 Vaasa and 1994 Shane the complete rotational phase was not covered and for two of them it was possible to find only an indication of the rotational period. © 1997 Elsevier Science Ltd. All rights reserved

Introduction

The knowledge of the asteroid spin rate is an important tool to gain information on the collisional evolution state of the asteroid population. Binzel *et al.* (1989) showed that the intermediate size range is important in terms of collisional evolution: the limit between 100 km and 125 km is considered as very representative because it seems to be the transition region between the larger primordial asteroids and the population of the smaller objects which are supposed to be the fragments, results of collisional events. Fulchignoni *et al.* (1995), analysing the rotational rate distribution for a sample of 516 main belt asteroids, found, for small objects ($D \leq 50$ km), the superimposition of three sub-populations: the more populated (similar to the distribution of larger objects) and the slow and the rapid rotator ones. Harris (1996), analyzing the rotational spin of asteroids with mean diameter $D \leq 10$ km, pointed out an absence of very rapid rotators, and an excess of slow rotators: the first characteristic (cut-off for period of less than 2.25 h) seems to imply a "rubble pile" structure, while the excess of slow rotators can be due to a state of non-principal axis rotation, or "tumbling" (Harris, 1994).

In order to enlarge the available data set of asteroid spins, we are carrying out a long-term observing program.

In this paper we present 64 lightcurves of 15 asteroids, obtained during 1996 by CCD observations at the 1.2 m telescope of the Haute Provence Observatory (France) and at 0.9 m Dutch, 1.5 m Danish and 0.6 m Bochum telescopes of the European Southern Observatory (ESO, La Silla, Chile) and by photoelectric observations carried out with the 0.5 m telescope at ESO. For all the objects, with the exception of 783 Nora, lightcurves were measured for the first time. The survey has been carried out on small asteroids: 13 out of the 15 observed objects have a diameter $D < 50$ km, while the remaining objects have a diameter of about 90 km.

Two of the observed asteroids (732 Tjilaki and 2446

*Based on observations carried out at the European Southern Observatory (ESO), La Silla, Chile.

Correspondence to: M. A. Barucci. E-mail: BARUCCI@obspm.fr.

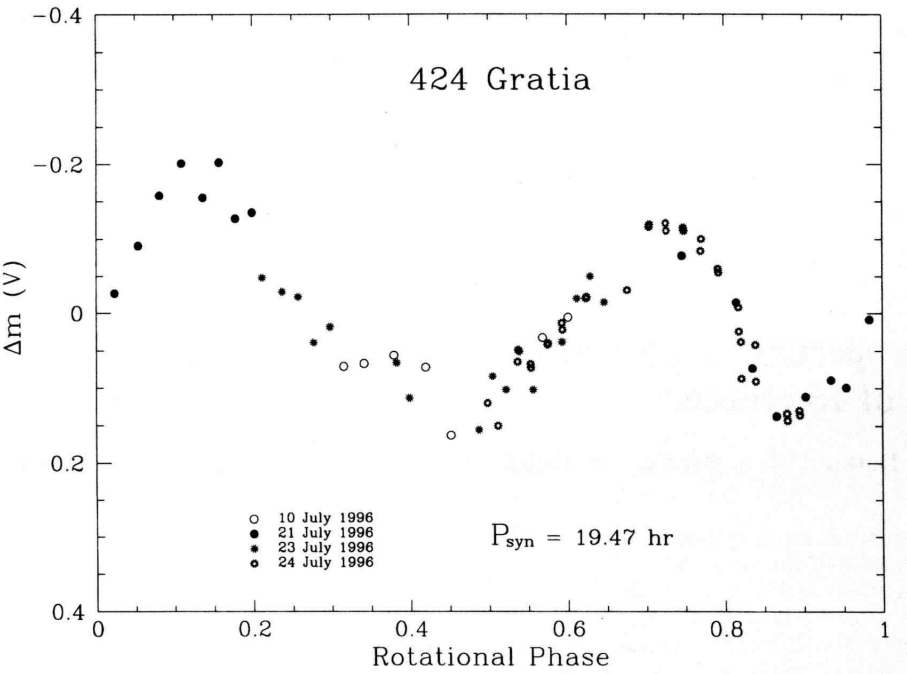

Fig. 1. Composite lightcurve of the asteroid 424 Gratia in rotational phase. Zero phase corresponds to U.T. 1996 July 22.0

Lunacharsky) are possible candidates for the Rosetta mission : 732 Tjilaki is an alternative candidate for the mission to comet P/Wirtanen, while 2446 Lunacharsky is a candidate for other Rosetta comet rendezvous opportunities (ESA, SCI(93)7).

Observations and data reduction

All the observations reported here have been obtained in the V-band. The transformation to the standard system has been carried out observing groups of standard stars, taken from the Harvard E-regions (Graham, 1982), Landolt (1983) and Guide Star Photometric Catalog (Lasker *et al.*, 1988). The data reduction procedure has been carried out using the standard method described by Hardie (1962). The photoelectric observations have been reduced using the ESO photometric reduction package RANBO2. The CCD observations have been reduced with either the software package IRAF or ASTPHOT, a synthetic aperture photometric package developed at DLR. When the conditions of the sky were not photometric, the data have been reduced only taking into account the differential extinction between the asteroid and the comparison star. The aspect data, calculated using the Ephemerides Program Ephem (version 1.1, Tholen, 1996) and the telescope used are listed in Table 1 : the mean magnitude level $V(1,\alpha)$, reported in the ninth column, corresponds to the zero level of the respective composite lightcurve. We determined the synodic rotational period, and the corresponding uncertainty for 12 asteroids, by applying Fourier analysis as described in Harris *et al.* (1989). The composite or single lightcurves of the observed asteroids, corrected for the lightime, are presented in Figs 1–15.

Results

The main results are listed in Table 2: the synodic rotational period (when determined), the corresponding reliability code (according to Harris and Young, 1983), the amplitude of the lightcurve and the diameter of each object. The observations of individual objects are discussed below.

424 *Gratia*

This asteroid was observed at the ESO during four nights (10, 21, 23, 24 July 1996) for a total of more then 30 h. The composite lightcurve, shown in Fig. 1, has been obtained with a period of 19.47 ± 0.01 h. The lightcurve is quite regular with an amplitude of 0.32 ± 0.02 mag.

440 *Theodora*

We observed this asteroid at the 0.9 m Dutch telescope of the ESO during two nights (24 and 25 July 1996) for a total of about 18 h. The composite lightcurve, shown in Fig. 2, is quite symmetric with well defined maxima and minima. The computed rotational period is 4.828 ± 0.004 h and the maximum amplitude of the light variation is 0.43 ± 0.03 mag.

446 *Aeternitas*

This asteroid was observed at the 0.5 m ESO telescope during three nights (8–10 July 1996) for a total of about

Table 1. Aspect data of the observed asteroids

Date (0 UT)	R.A. (2000)	Decl (2000)	Longi-tude (2000)	Lati-tude (2000)	r (AU)	Δ (AU)	Phase	V (mag)	Observed
424 Gratia									
96/07/10	19 34 13	−24 02 37	290.7	−2.3	2.996	1.981	1.39	—	0.5m ESO
96/07/21	19 24 11	−24 48 49	288.3	−2.7	2.988	1.982	3.35	—	0.5m ESO
96/07/23	19 22 24	−24 56 32	287.9	−2.8	2.986	1.985	4.11	—	0.5m ESO
96/07/24	19 21 31	−25 00 17	287.7	−2.8	2.985	1.988	4.49	—	0.9m Dutch ESO
440 Theodora									
96/07/24	20 08 49	−19 44 45	299.4	+0.3	2.444	1.428	0.57	—	0.9m Dutch ESO
96/07/25	20 07 43	−19 47 24	299.1	+0.4	2.444	1.428	1.07	—	0.9m Dutch ESO
446 Aeternitas									
96/07/08	19 13 18	−38 25 31	284.1	−15.9	2.484	1.491	6.47	—	0.5m ESO
96/07/09	19 12 16	−38 29 16	283.9	−15.9	2.483	1.491	6.54	—	0.5m ESO
96/07/10	19 11 13	−38 32 48	283.7	−15.9	2.483	1.491	6.64	—	0.5m ESO
91 Carina									
96/02/09	09 18 51	−00 57 21	141.7	−15.8	3.133	2.174	5.00	—	1.5m Danish ESO
96/02/10	09 18 08	−00 49 38	141.5	−15.7	3.134	2.173	4.93	—	1.5m Danish ESO
96/02/11	09 17 24	−00 41 47	141.3	−15.6	3.135	2.174	4.88	—	1.5m Danish ESO
96/02/22	09 09 50	+00 50 59	138.9	−14.7	3.145	2.195	6.07	9.6	0.6m Bochum ESO
96/02/23	09 09 12	+00 59 50	138.7	−14.7	3.145	2.199	6.29	9.6	0.6m Bochum ESO
96/02/24	09 08 35	+01 08 44	138.5	−14.6	3.146	2.203	6.52	9.6	0.9m Dutch ESO
96/02/25	09 07 58	+01 17 40	138.3	−14.5	3.147	2.208	6.76	9.6	0.9m Dutch ESO
96/02/26	09 07 22	+01 26 37	138.1	−14.4	3.148	2.212	7.00	9.6	0.9m Dutch ESO
96/02/27	09 06 47	+01 35 36	137.9	−14.3	3.149	2.217	7.26	9.6	0.9m Dutch ESO
727 Nipponia									
96/07/23	19 32 20	−14 08 50	291.8	+7.5	2.646	1.641	4.16	—	0.5m ESO
96/07/24	19 31 26	−14 16 47	291.6	+7.4	2.645	1.642	4.48	—	0.9m Dutch ESO
732 Tjilaki									
96/02/09	07 21 16	+08 27 30	109.9	−13.5	2.501	1.607	11.94	—	0.9m Dutch ESO
96/02/11	07 20 02	+08 41 53	109.6	−13.3	2.500	1.619	12.65	—	0.9m Dutch ESO
96/02/13	07 18 54	+08 56 21	109.3	−13.1	2.499	1.631	13.35	—	0.9m Dutch ESO
96/02/17	07 16 57	+09 25 20	108.7	−12.7	2.498	1.658	14.71	11.4	0.6m Bochum ESO
96/02/18	07 16 32	+09 32 34	108.6	−12.6	2.497	1.666	15.04	11.4	0.6m Bochum ESO
96/02/19	07 16 09	+09 39 47	108.5	−12.5	2.497	1.673	15.36	11.4	0.6m Bochum ESO
96/02/20	07 15 48	+09 46 58	108.4	−12.4	2.497	1.681	15.68	11.5	0.6m Bochum ESO
96/02/21	07 15 29	+09 54 07	108.3	−12.3	2.496	1.689	15.99	11.5	0.6m Bochum ESO
96/02/22	07 15 11	+10 01 15	108.2	−12.1	2.496	1.697	16.30	11.5	0.6m Bochum ESO
96/02/23	07 14 55	+10 08 21	108.1	−12.0	2.495	1.706	16.60	11.5	0.6m Bochum ESO
783 Nora									
96/02/09	09 35 16	+13 57 39	140.8	−0.3	2.805	1.819	0.71	—	0.9m Dutch ESO
96/02/10	09 34 17	+14 05 23	140.5	−0.3	2.803	1.817	0.28	—	0.9m Dutch ESO
96/02/11	09 33 19	+14 13 07	140.3	−0.2	2.802	1.816	0.22	—	0.9m Dutch ESO
96/02/17	09 27 27	+14 59 13	138.7	−0.0	2.796	1.814	2.89	11.4	0.6m Bochum ESO
96/02/18	09 26 29	+15 06 47	138.4	+0.0	2.794	1.815	3.34	11.4	0.6m Bochum ESO
96/02/19	09 25 32	+15 14 18	138.2	+0.0	2.793	1.816	3.79	11.5	0.6m Bochum ESO
96/02/20	09 24 34	+15 21 45	137.9	+0.1	2.792	1.817	4.23	11.5	0.6m Bochum ESO
96/02/21	09 23 38	+15 29 08	137.7	+0.1	2.791	1.819	4.67	11.6	0.6m Bochum ESO
96/02/22	09 22 41	+15 36 27	137.4	+0.2	2.790	1.821	5.11	11.6	0.6m Bochum ESO
96/02/23	09 21 46	+15 43 42	137.2	+0.2	2.788	1.823	5.54	11.6	0.6m Bochum ESO
96/02/24	09 20 51	+15 50 51	136.9	+0.3	2.787	1.826	5.98	11.6	0.9m Dutch ESO
96/02/25	09 19 57	+15 57 55	136.7	+0.3	2.786	1.829	6.41	11.6	0.9m Dutch ESO
96/02/26	09 19 03	+16 04 54	136.4	+0.4	2.785	1.832	6.83	11.6	0.9m Dutch ESO
96/02/28	09 17 19	+16 18 34	136.0	+0.5	2.782	1.839	7.67	11.6	0.9m Dutch ESO
888 Parysatis									
96/07/21	19 20 49	−17 42 45	288.5	+4.3	2.977	1.971	3.49	—	0.5m ESO
96/07/24	19 18 10	−18 00 21	287.9	+4.1	2.927	1.975	4 57	—	0.9m Dutch ESO
1246 Chaka									
96/10/03	00 20 14	+37 50 37	20.6	+32.3	1.882	0.968	17.32	—	1.2m OHP
96/10/04	00 19 20	+37 47 30	20.4	+32.3	1.884	0.969	17.16	—	1.2m OHP

Table 1—*Continued.*

Date (0 UT)	R.A. (2000)	Decl (2000)	Longi-tude (2000)	Lati-tude (2000)	r (AU)	Δ (AU)	Phase	V (mag)	Observed
1507 Vaasa									
96/10/05	00 35 19	+25 35 30	17.8	+19.9	1.814	0.845	11.35	—	1.2m OHP
96/10/06	00 34 24	+25 30 58	17.6	+19.9	1.816	0.846	11.18	—	1.2m OHP
1626 Sadeya									
96/02/09	07 07 14	+01 27 53	107.3	−20.9	1.903	1.021	18.29	—	1.5m Danish ESO
96/02/10	07 06 35	+01 20 09	107.1	−21.0	1.905	1.030	18.71	—	1.5m Danish ESO
96/02/11	07 05 59	+01 12 46	107.0	−21.2	1.908	1.039	19.11	—	1.5m Danish ESO
96/02/12	07 05 25	+01 05 42	106.8	−21.3	1.911	1.048	19.51	—	1.5m Danish ESO
96/02/22	07 02 13	+00 10 58	106.1	−22.3	1.939	1.148	22.96	12.5	0.6m Bochum ESO
96/02/23	07 02 08	+00 06 52	106.1	−22.4	1.942	1.159	23.26	12.5	0.6m Bochum ESO
1994 Shane									
96/10/03	00 07 31	+17 42 59	8.2	+15.4	2.198	1.217	6.99	—	1.2m OHP
96/10/04	00 06 48	+17 33 29	8.0	+15.3	2.199	1.219	7.02	—	1.2m OHP
2209 Tianjin									
96/07/25	18 12 45	−20 34 02	272.2	+2.8	2.959	2.033	9.74	—	0.9m Dutch ESO
96/07/26	18 12 08	−20 35 16	271.1	+2.8	2.959	2.039	10.07	—	0.9m Dutch ESO
2446 Lunacharsky									
96/07/12	22 03 02	−18 05 56	325.7	−5.7	2.031	1.124	17.48	—	0.9m Dutch ESO
96/07/13	22 02 42	−18 09 52	325.6	−5.7	2.032	1.117	17.04	—	0.9m Dutch ESO
3776 Vartiovuori									
96/07/12	18 07 18	−57 10 18	270.4	−33.7	3.128	2.265	11.56	—	0.9m Dutch ESO
96/07/13	18 06 05	−57 10 04	270.2	−33.7	3.129	2.269	11.69	—	0.9m Dutch ESO

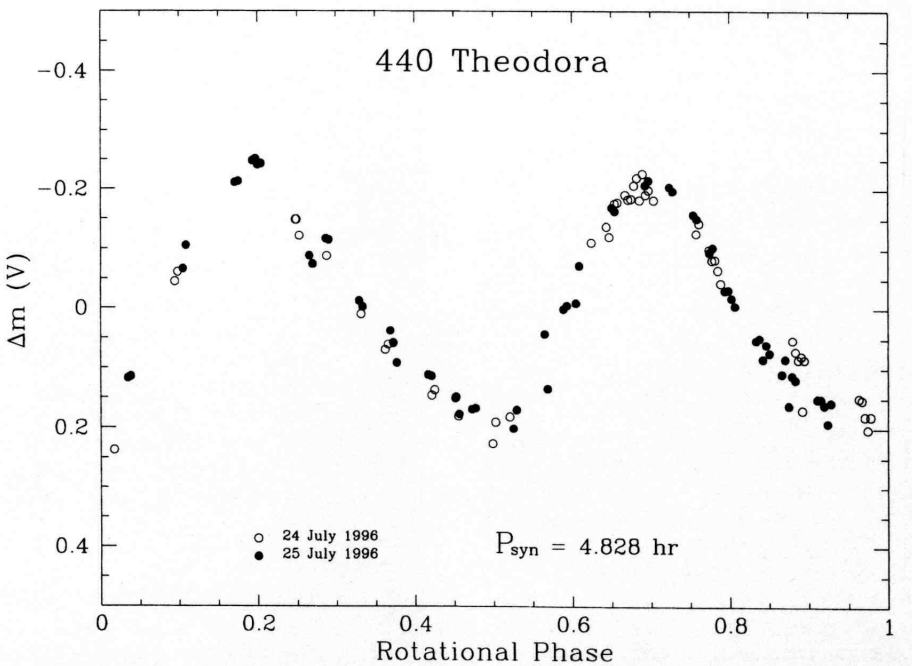

Fig. 2. Composite lightcurve of the asteroid 440 Theodora in rotational phase. Zero phase corresponds to U.T. 1996 July 25.0

Table 2. Physical parameters of the observed asteroids

Asteroid	Rotational Period (hr)	Reliability Code[a]	Amplitude (mag)	D (km)
424 Gratia	19.47±0.01	3	0.32±0.02	87[b]
440 Theodora	4.828±0.004	3	0.43±0.03	19[c]
446 Aeternitas	15.85±0.01	2	>0.33	45[b]
491 Carina	14.87±0.01	3	0.12±0.02	97[b]
727 Nipponia	4.6±0.1	1	0.14±0.02	32[b]
732 Tjilaki	12.34±0.01	3	0.19±0.03	38[b]
783 Nora	34.4±0.5	2	0.08±0.02	40[b]
888 Parysatis	5.49±0.01	3	0.23±0.02	44[b]
1246 Chaka	>20	1	—	18[b]
1507 Vaasa	>14	1	—	10[c]
1626 Sadeya	3.438±0.009	3	0.22±0.02	30[c]
1994 Shane	—	—	—	26[c]
2209 Tianjin	9.47±0.01	3	0.42±0.02	16[b]
2446 Lunacharsky	3.613±0.004	3	0.41±0.02	10[c]
3776 Vartiovuori	7.7±0.1	2	0.12±0.02	24[b]

[a]Meaning of the reliability codes:
1: the result is based on fragmentary lightcurves, may be completely wrong;
2: the result is based on less than full coverage, so that the period may be wrong by 30% or so;
3: sure result with no ambiguity and full lightcurve coverage.
[b]by IRAS (Tedesco *et al.*, 1992)
[c]estimation by Tholen (1996), based on the values of the magnitude and the location on the Solar System.

17 h. Figure 3 shows the composite lightcurve obtained with a rotational period of 15.85±0.01 h with an amplitude larger than 0.33 mag. The rotational phase is not well covered, only two minima and one maximum are defined, and therefore the period is given with a quality code 2.

491 *Carina*

We observed this object at ESO for 9 nights during 1996 for about 35 h. The composite lightcurve shown in Fig. 4 has been obtained fitting the data with a synodical period of 14.87±0.01 h. The lightcurve amplitude is 0.12±0.02 mag.

727 *Nipponia*

This asteroid was observed at the 0.5 m and 0.9 m Dutch telescopes of the ESO during two nights (23–24 July 1996). More than 11 h of observations are available, but because the poor quality of the data, only a tentative solution for the rotational period can be given. Figure 5 shows the composite lightcurve obtained with $P_{syn} = 4.6 \pm 0.1$ h and a quality code 1.

732 *Tjilaki*

This asteroid has been considered as an asteroid target in the Phase A study of the Rosetta mission for an alternative (non baseline) mission to comet P/Wirtanen. We observed this asteroid at ESO for 10 nights during February 1996 for about 35 h and the best fitting rotational period is 12.34±0.01 h. The composite light-curve obtained, shown in Fig. 6, is very asymmetric with a difference between

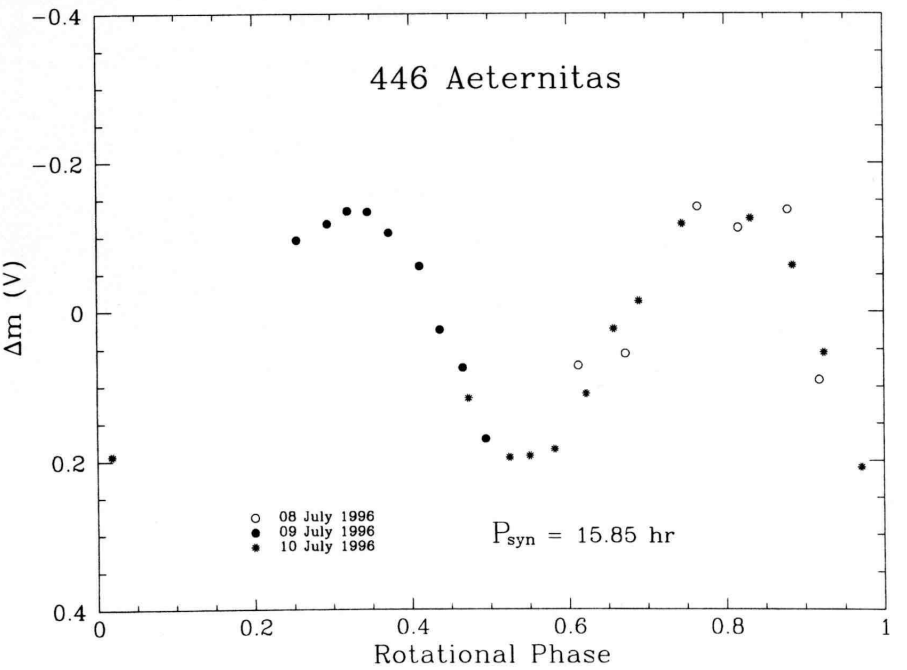

Fig. 3. Composite lightcurve of the asteroid 446 Aeternitas in rotational phase. Zero phase corresponds to U.T. 1996 July 9.0

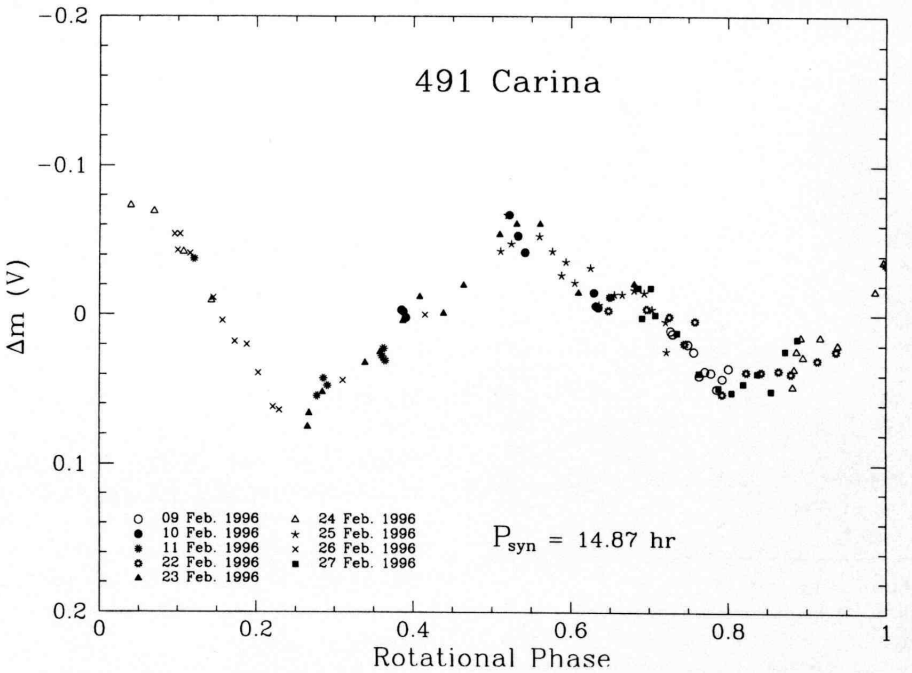

Fig. 4. Composite lightcurve of the asteroid 491 Carina in rotational phase. Zero phase corresponds to U.T. 1996 February 21.0

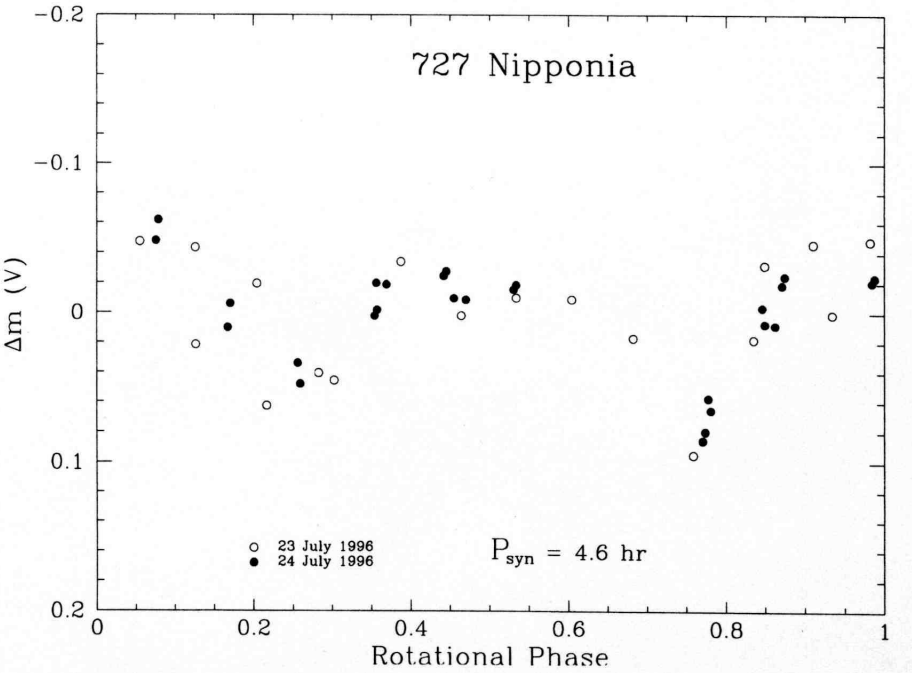

Fig. 5. Composite lightcurve of the asteroid 727 Nipponia in rotational phase. Zero phase corresponds to U.T. 1996 July 24.0

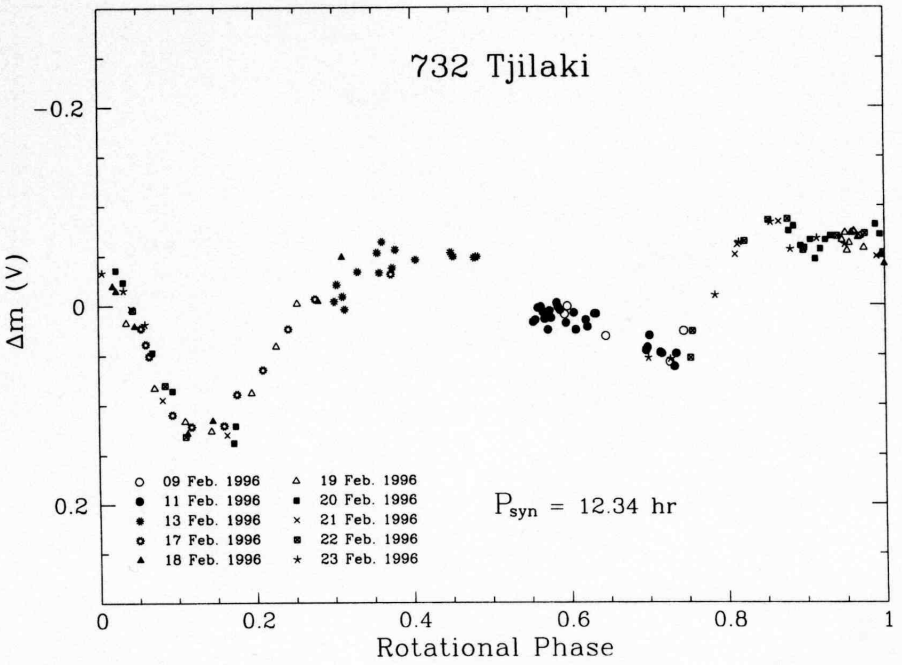

Fig. 6. Composite lightcurve of the asteroid 732 Tjilaki in rotational phase. Zero phase corresponds to U.T. 1996 February 17.0

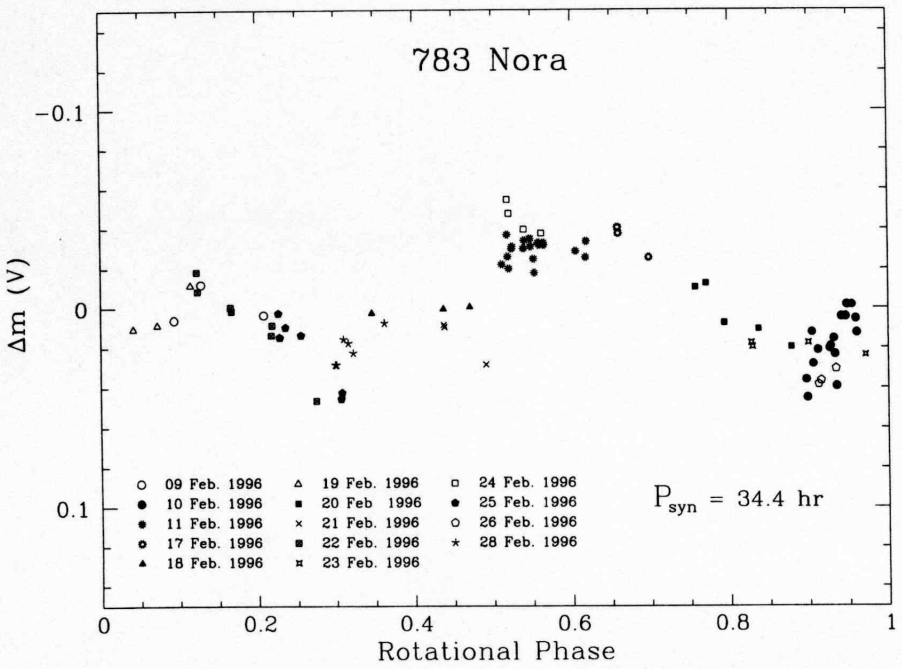

Fig. 7. Composite lightcurve of the asteroid 783 Nora in rotational phase. Zero phase corresponds to U.T. 1996 February 19.0

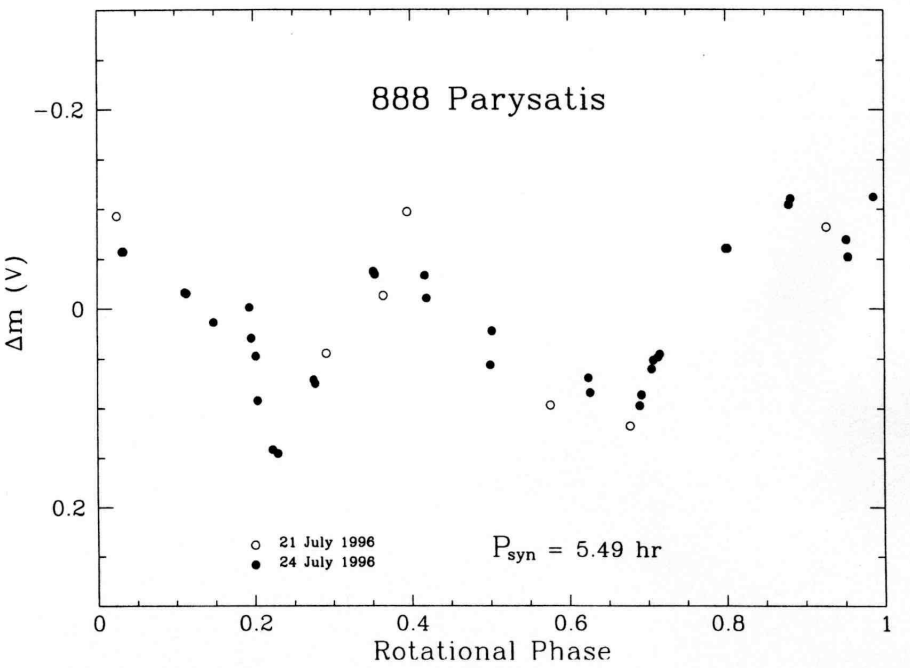

Fig. 8. Composite lightcurve of the asteroid 888 Parysatis in rotational phase. Zero phase corresponds to U.T. 1996 July 24.0

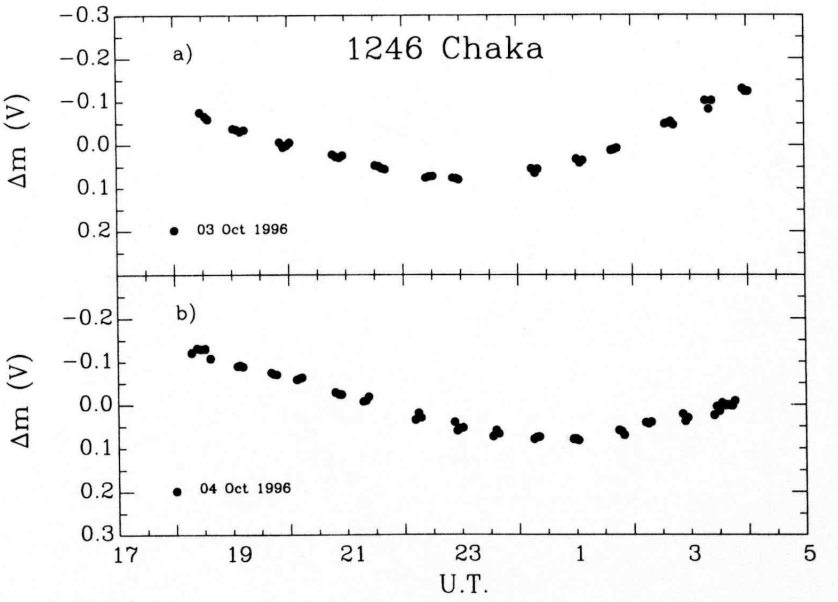

Fig. 9. Single night lightcurves of the asteroid 1246 Chaka for the nights (a) 1996, October 3 and (b) 1996, October 4

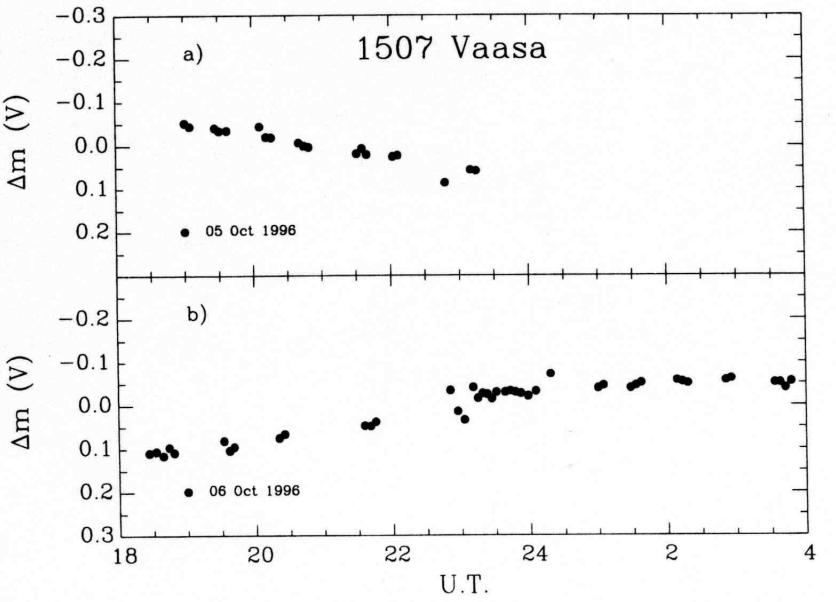

Fig. 10. Single night lightcurves of the asteroid 1507 Vaasa for the nights (a) 1996, October 5 and (b) 1996, October 6

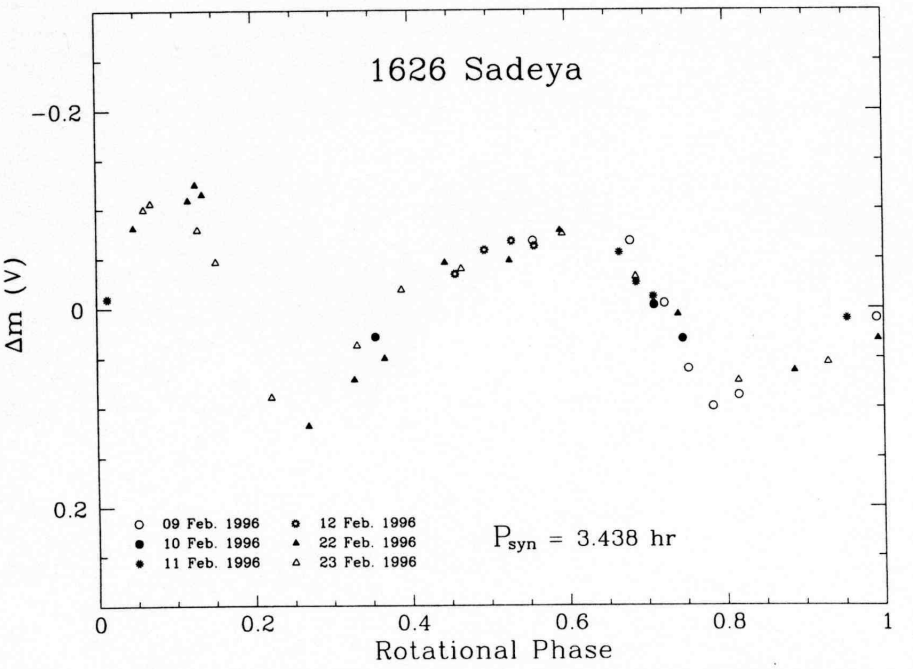

Fig. 11. Composite lightcurve of the asteroid 1626 Sadeya in rotational phase. Zero phase corresponds to U.T. 1996 February 17.0

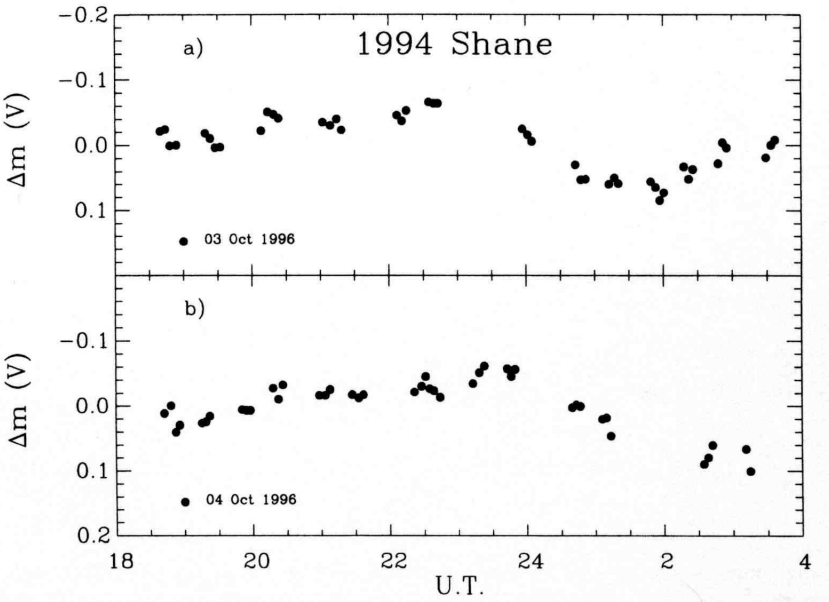

Fig. 12. Single night lightcurves of the asteroid 1994 Shane for the nights (a) 1996, October 3 and (b) 1996, October 4

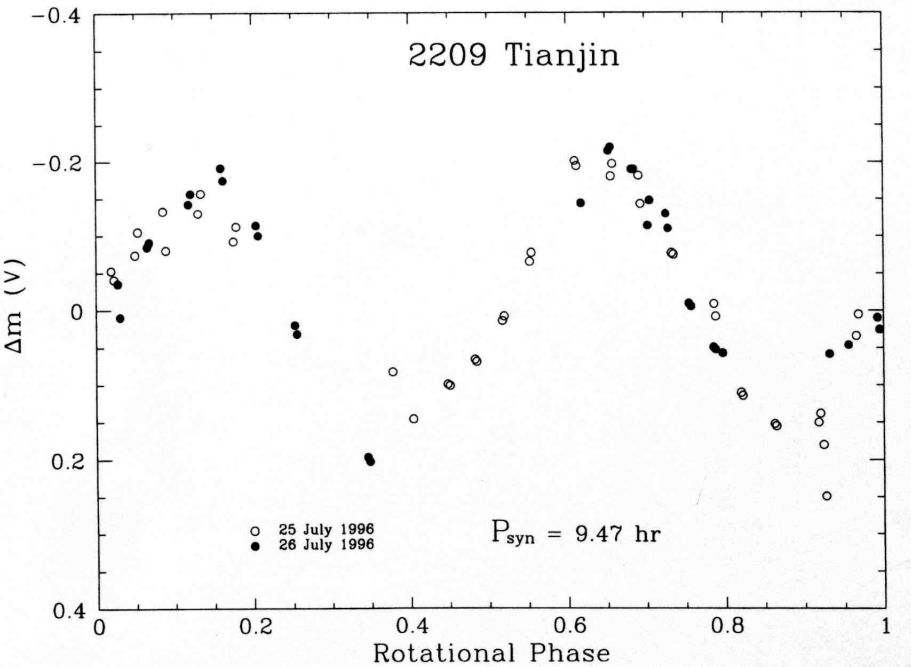

Fig. 13. Composite lightcurve of the asteroid 2209 Tianjin in rotational phase. Zero phase corresponds to U.T. 1996 July 26.0

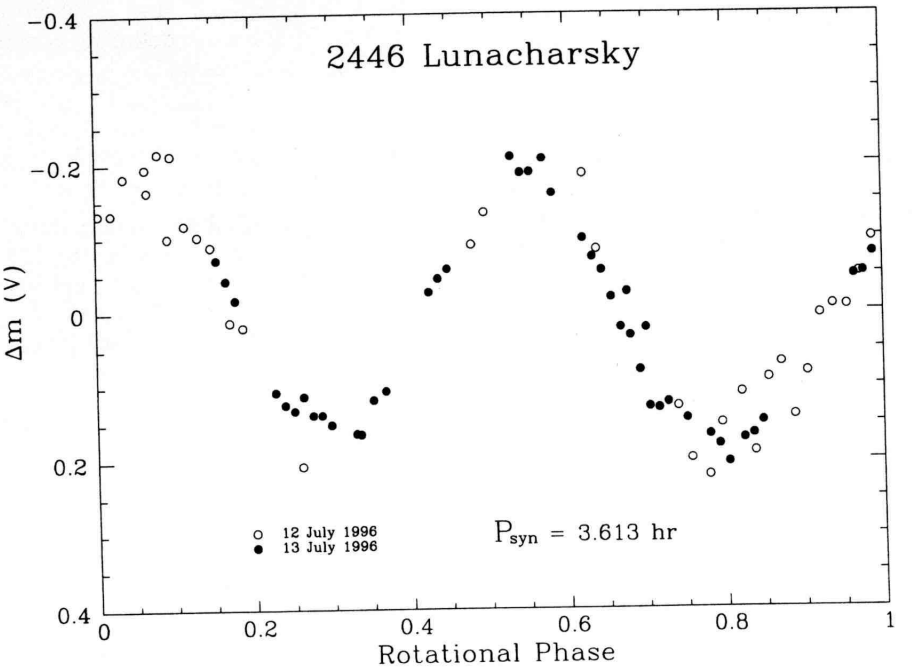

Fig. 14. Composite lightcurve of the asteroid 2446 Lunacharsky in rotational phase. Zero phase corresponds to U.T. 1996 July 13.0

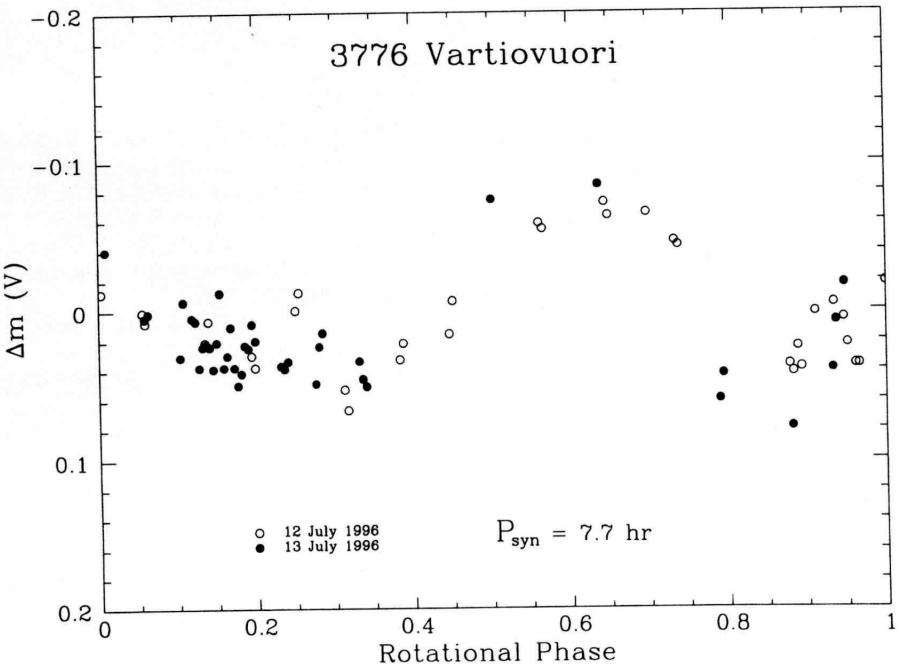

Fig. 15. Composite lightcurve of the asteroid 3776 Vartiovuori in rotational phase. Zero phase corresponds to U.T. 1996 July 13.0

the principal and secondary minima of 0.07 mag. The lightcurve amplitude is 0.19 ± 0.03 mag.

783 *Nora*

This object was observed for one night during the 1990 apparition (Lagerkvist *et al.*, 1992) and the lightcurve obtained suggested a long rotational period. During the 1996 apparition we reobserved 783 Nora during 14 nights. The obtained data are very close to the opposition, phase angles ranging between 0.2 and 8°. Figure 7 shows the composite lightcurve with a rotational period of 34.4 ± 0.5 h. However, owing to the long rotational period, the large dispersion and the small amplitude (0.08 ± 0.02 mag), alternative rotational periods cannot be completely excluded.

888 *Parysatis*

We observed 888 Parysatis at ESO during two nights (21–24 July 1996) for a total of about 15 h. The composite lightcurve, shown in Fig. 8, has been obtained by fitting the single night lightcurves with a rotational period of 5.49 ± 0.01 h. The obtained amplitude is 0.23 ± 0.02 mag.

1246 *Chaka*

1246 Chaka was observed at the 1.2 m telescope of the OHP during 2 nights (3–4 October) for a total of about 20 h. The two single night lightcurves (Fig. 9) display two different wide minima suggesting a period longer than 20 h.

1507 *Vaasa*

We observed 1507 Vaasa during two nights (5 and 6 October) in 1996 at the 1.2 m telescope of the OHP for about 14 h. The available single night lightcurves, shown in Fig. 10, did not allow us to determine an unique rotational period. From the available data it seems longer then 14 h.

1626 *Sadeya*

1626 Sadeya was observed during 1996 for 6 nights 9, 10, 11, 12, 22, 23 February) at ESO for more than 13 h. The composite lightcurve, shown in Fig. 11, is very asymmetric with a principal maximum wider and brighter than the secondary one. The computed rotational period is 3.438 ± 0.009 h and the amplitude obtained is $0.22 + 0.02$ mag.

1994 *Shane*

This object has been observed at the 1.2 m telescope of the OHP during two nights (3 and 4 October 1996). The individual lightcurves are shown in Fig. 12 and seem to cover the same maximum. This constrains the rotational period to be either 12 h or a longer multiple of 6 h (such as 18 or 24 h) but no definitive conclusion can be drawn from the available data.

2209 *Tianjin*

2209 Tianjin was observed with the 0.9 m Dutch telescope at ESO during two nights in 1996 (25–26 July) for a total of about 16 h. The composite lightcurve, obtained with a rotational period of 9.47 ± 0.01 h, is shown in Fig. 13 with a maximum amplitude of 0.42 ± 0.02 mag.

2446 *Lunacharsky*

We observed this object in 1996 at the 0.9 m Dutch telescope at ESO (12–13 July) for more than 9 h. Figure 14 shows the composite lightcurve, obtained fitting the observed data with a rotational period of 3.613 ± 0.004 h. The lightcurve is quite asymmetric with an amplitude of 0.41 ± 0.02 mag.

3776 *Vartiovuori*

3776 Vartiovuori was observed at the 0.9 m Dutch telescope of the ESO for more than 15 h (12–13 July 1996). The composite lightcurve, shown in Fig. 15, has been obtained fitting the single night lightcurves with a rotational period of 7.7 ± 0.1 h. However, a somewhat longer rotational period (11.5 h) cannot be completely excluded with the available data.

Acknowledgements. E. Dotto and M. Florczak thank ESA and CNPq, respectively, for the financial support during the present research.

References

Binzel, R., Farinella, P., Zappalà, V., Cellino V. (1989) Asteroid rotation rates: distributions and statistics. In *Asteroids II*, eds. R. Binzel, T. Gehrels, and M. S. Matthews, pp. 416–441. University of Arizona Press, Tucson, AZ.

Fulchignoni, M., Barucci, M. A., Di Martino, M. and Dotto, E. (1995) On the evolution of the asteroid spin. *Astron. Astrophys.* **299,** 929–932.

Graham, J. A. (1982) UBVRI standard stars in the E-regions. *P.A.S.P.* **94,** 244–265.

Hardie, R. H. (1962) Photoelectric reductions. In *Astronomical techniques*, Vol. II. *Stars and Stellar Systems*, ed. A. W. Hintler, pp. 178–208. The University of Chicago Press, Chicago and London.

Harris, A. W. (1994) Tumbling asteroids. *Icarus* **107,** 209–211.

Harris, A. W. (1996) The rotation rates of very small asteroids: evidence for "rubble-pile" structure. *Lunar Planet. Sci.* **XXVII,** 493–494.

Harris, A. W. and Young, J. W. (1983) Asteroid rotation—IV. 1979 observations. *Icarus* **54,** 59–109.

Harris, A. W., Young, J. W., Bowell, E., Martin, L. J., Millis, R. L., Poutanen, M., Scaltriti, F., Zappalà, V., Schober, H. J. and Zeigler, H. W. (1989) Photometric observations of asteroids 3, 24, 60, 261 and 863. *Icarus* **77,** 171–186.

Lagerkvist, C.-I., Magnusson, R., Debehogne, H., Hoffmann, M., Erikson, A., De Campos, A. and Cutispoto, G. (1992) Physical studies of asteroids—XXV Photoelectric photometry of asteroids obtained at ESO and Hoher List Observatory. *Astron. Astrophys. Supl. Ser.* **95,** 461–470.

Landolt, A. U. (1983) UBVRI photometric standard stars around the celestial equator. *Astron. J.* **88,** 439–460.

Lasker, B. M., Sturch, C. R., Lopez, C., Mallamas, A. D., McLaughlin, S. F., Russell, J. L., Wisniewski, W. Z., Gillespie, B. A., Jenkner, H., Siciliano, E. D., Kenny, D., Baumert, J. H., Goldberg, A. M., Henry, G. W., Kemper, E. and Siegel, M. J. (1988) The guide star photometric catalog. *Astroph. J. Suppl. Ser.* **68,** 1–90.

Tedesco, E. F., Veeder, G. J., Fowler, J.W, and Chillemi, J. R. (1992) The Iras Minor Planet Survey PL-TR-92-2049.

Tholen, D. J. (1996) Ephemerides Program Ephem version 1.1, Celestech.

Astron. Astrophys. 352, 697–702 (1999)
ASTRONOMY AND ASTROPHYSICS

4979 Otawara: flyby target of the Rosetta mission⋆

A. Doressoundiram[1,2], P. R. Weissman[1], M. Fulchignoni[2,3], M.A. Barucci[2], A. Le Bras[2], F. Colas[4], J. Lecacheux[2], M. Birlan[2], M. Lazzarin[5], S. Fornasier[5], E. Dotto[2,8], C. Barbieri[5], M.V. Sykes[6], S. Larson[7], and C. Hergenrother[7]

[1] Jet Propulsion Laboratory, 4800 Oak Grove Drive, Pasadena, CA 91109, USA
[2] Observatoire de Paris, DESPA, 5, Place Jules Janssens, 92190 Meudon, France
[3] Université de Paris VII, Paris, France
[4] IMCCE, 77 avenue Denfert-Rochereau, 75014 Paris, France
[5] Osservatorio Astronomico di Padova, vicolo dell'Osservatorio, 5, 35122 Padova, Italy
[6] Steward Observatory, University of Arizona, Tucson, AZ 85719, USA
[7] Lunar and Planetary Laboratory, University of Arizona, Tucson, AZ 85719, USA
[8] Osservatorio Astronomico di Torino, 10025 Pino Torinese, Italy

Received 20 September 1999 / Accepted 2 November 1999

Abstract. An international observing campaign was organized to determine the physical and chemical characteristics of asteroid 4979 Otawara, which is the first target of the Rosetta mission (flyby on July 10, 2006). Knowledge of the physical parameters of the flyby targets is required for both refinement of the design of the spacecraft and the instrument payload, and optimization of the mission trajectory and scenarios. We present the results of observations obtained from December, 1998 through March, 1999. The spectral classification of 4979 Otawara could be either a pyroxene and/or olivine-rich S-type asteroid or a V-type asteroid, a member of the Vesta dynamical family. Further observations are needed in order to discriminate between the two spectral types. The synodic rotation period of Otawara is $P_{syn} = 2.707 \pm 0.005$ hr. The lower limit for the axial ratio of the enveloping ellipsoid is $a/b \geq 1.3$. The circular effective radius is 2.0 or 1.3 km in the case of an S-type or a V-type asteroid, respectively. A lower limit on its density is obtained: $\rho_{min} \geq 1.9\,\mathrm{g\,cm^{-3}}$ if we assume that Otawara is an aggregate or rubble pile object. However, if Otawara is a single solid body, no constraint can be set on its density. 4979 Otawara is a small, fast rotating asteroid (FRA) and hence, will be a particularly interesting target to be studied from a spacecraft, since no fast rotator has been visited yet.

Key words: minor planets, asteroids – planets and satellites: individual: 4979 Otawa

1. Introduction

The International Rosetta Mission is the planetary cornerstone mission of the European Space Agency. The mission is devoted to the study of the nature of primitive small bodies in the solar system. The baseline mission includes two asteroid flybys: 4979 Otawara on July 10, 2006 and 140 Siwa on July 23, 2008, and the exploration of comet 46P/Wirtanen. The Rosetta spacecraft will rendezvous with the comet in March 2012 at 4.2 AU from the Sun. The spacecraft will be put into an orbit around the comet nucleus and an instrumented probe will land on the nucleus surface.

Several other spacecraft missions to comets and asteroids are now either on their way, under development, or in the planning stages. These include NEAR, Deep Space 1, Stardust, Contour and Muses C. Knowledge of the physical parameters of the target bodies is required for both refinement of the designs of the spacecraft and their instrument payloads and optimization of the mission trajectories and scenarios.

An international observing campaign was organized to determine the physical and chemical characteristics of the Rosetta asteroid targets. Results for 140 Siwa have been published by Schober & Stanzel (1979), Harris & Young (1980), Lagerkvist et al. (1992) and Barucci et al. (1998). This paper deals with the first results obtained for 4979 Otawara.

2. Observations and data reduction

We observed 4979 Otawara during seven runs from December, 1998 to March, 1999. The purpose of these observations was to obtain lightcurve photometry, color photometry and spectroscopy. The specifics of the observations, including observing conditions and orbital geometry for the asteroid are shown in Table 1.

2.1. Observations

Steward Observatory (SO): Two nights of data were obtained on December, 13–14, 1998 with the 2.3 m telescope of Steward Observatory on Kitt Peak (Arizona). The telescope was equiped with the facility 2k×2k CCD imaging system at the cassegrain

Send offprint requests to: A. Doressoundiram (alain.doressoundiram@obspm.fr)

⋆ partly based on observations carried out at the European Southern Observatory (ESO) of La Silla, Chile, and at Steward Observatory, University of Arizona, Tucson, AZ USA.

Table 1. Observational circumstances

UT date	r (AU)	δ (AU)	α (deg.)	Telescope	Filter or $\delta\lambda$
1998 Dec 13	2.463	1.714	17.9	Steward Obs. 2.3m	R
1998 Dec 14	2.462	1.704	17.6	Steward Obs. 2.3m	R
1998 Dec 16	2.462	1.686	17.1	Pic du Midi Obs. 1.0 m	R
1998 Dec 17	2.461	1.676	16.8	Pic du Midi Obs. 1.0 m	R
1998 Dec 18	2.460	1.666	16.5	Pic du Midi Obs. 1.0 m	R
1999 Jan 08	2.248	1.503	8.1	Haute-Provence Obs. 1.2 m	V
1999 Jan 12	2.245	1.483	6.2	Haute-Provence Obs. 1.2 m	V
1999 Jan 20	2.439	1.457	2.1	Pic du Midi Obs. 1.0 m	R
1999 Jan 23	2.437	1.453	0.6	Pic du Midi Obs. 1.0 m	R
1999 Jan 24	2.436	1.452	0.5	Pic du Midi Obs. 1.0 m	R
1999 Jan 23	2.437	1.453	0.6	Table Mountain Obs. 0.6m	R
1999 Feb 14	2.418	1.497	10.7	European Southern Obs. NTT 3.6m	BVRI
1999 Feb 15	2.417	1.502	11.2	European Southern Obs. NTT 3.6m	BVRI
1999 Feb 16	2.416	1.507	11.6	European Southern Obs. NTT 3.6m	BVRI
1999 Mar 15	2.389	1.722	20.9	European Southern Obs. 1.5m	4500–9000 Å
1999 Mar 16	2.388	1.732	21.2	European Southern Obs. 1.5m	4500–9000 Å

focus. The CCD was binned 2×2 for data taking, giving an image scale of 0.32 arcsec per pixel. The data were taken with the Harris R filter (λ=0.63 microns). Both nights were photometric with seeing of 1.5–3 arcsec. Integration times were 400 to 600 sec. The telescope was guided at the asteroid rate.

Pic du Midi Observatory (PDM): 4979 Otawara was observed with the Pic du Midi Observatory (France), 1 m telescope during two runs: in December, 1998 (16, 17 and 18) and January 1999 (20, 23 and 24). The telescope was equiped with a Thomson CCD imaging system (388×284). A F/D=6 focal reducer was used giving an image scale of 0.75 arcsec per pixel. The data were taken with the Cousins R filter (λ=0.60 microns). The nights were photometric with an average seeing of 1.8–2.2 arsec. Integration times were 180 to 300 sec. guided at sidereal rate.

Haute Provence Observatory (OHP): 4979 Otawara was observed during the nights of January 8 and 12, 1999 with the 1.2 m telescope of Haute-Provence Observatory, France. The CCD was a TK 1024×1024, and the pixel-scale was 0.69 arcsec. The data were obtained with the Cousins V filter (λ=0.53 microns), and the exposure times ranged from 60 to 420 sec. The nights were not photometric, with a seeing of 2.4–3 arcsec. Thus, only relative photometry between the asteroid and the comparison stars was possible for this run.

Table Mountain Observatory (TMO): 4979 Otawara was observed on January 23, 1999 at Table Mountain Observatory (California). A Photometrics CCD (1024×1024) was used at the cassegrain focus of the 0.6 m telescope. The image scale was 0.52 arcsec per pixel. Digital images were recorded through a Bessel R filter with central wavelength of 0.64 microns. The night was photometric and the seeing ranged between 1 and 3 arcsec. The exposure time was 720 sec. The telescope was guided at the asteroid rate.

European Southern Observatory, NTT: Broadband color observations were obtained on February 14–16, 1999 using the SuSI2 CCD camera of the 3.6 m ESO New Technology Telescope (NTT) on La Silla, Chile. The image scale was 0.16 arcsec per pixel. Digital images were recorded through Bessel B, V, R, and I filters with central wavelengths at 0.421, 0.544, 0.642 and 0.795 microns, respectively. The nights were photometric with an average seeing of 1.2–1.8 arsec. The integration times were 60 to 90 sec.

European Southern Observatory, 1.5 m: Spectroscopic observations of 4979 Otawara were obtained in March, 1999 at the European Southern Observatory on La Silla (Chile). The 1.5 m telescope was equipped with a Boller & Chivens spectrograph and a Loral Lesser CCD detector (2048×2048 pixels). The grating used had 225 gr/mm, with a dispersion of 331 Å/mm in the first order. The CCD has 15 μm square pixels, giving a dispersion of about 5 Å/pixel in the wavelength direction. The spectral range is about $0.48 < \lambda < 0.88$ μm with a FWHM of about 10 Å. The spectra were recorded through a slit oriented in the east–west direction. The slit was opened to about 8 arcsec in order to reduce effects due to differential refraction and the possibility of losing signal due to guiding errors of the telescope.

The spectroscopic observations of 4979 Otawara were performed on two different nights: the first on 15 March 1999, at 01 31 27 UT, with a 1 hour exposure, the second on 16 March 1999, at 01 11 58 UT, with 1 hour and 10 minutes of exposure time. During the observations, Otawara had a visual magnitude of about 18.4 and was at an airmass of about 1.6.

2.2. Data reduction

Photometry: The CCD images obtained were reduced and calibrated in a standard manner using aperture photometry (PHOT task in IRAF Digiphot package, MAGNITUDE/CIRCLE in MIDAS, and ASTROL software developped by Francois Colas from IMCCE). First, an average bias frame was subtracted from each science image. Pixel-to-pixel variations in the CCD sensitivity were removed by dividing the frames by a median of several images (flats) of the twilight sky. The instrumental magnitudes were measured using aperture photometry. The radius of

the aperture used was typically about twice the average seeing. This was deemed optimum since it is large enough to include most of the point spread function, yet small enough to minimize background sky noise. Sky subtraction was performed using a 7–12 pixels wide annulus around the asteroid or reference star. Finally, for magnitude calibration purposes, observations of standard stars (Landolt, 1992) were obtained over a wide range of airmasses and stellar types. The zero point, extinction and colour terms obtained from the Landolt fields were then used to convert instrumental magnitudes to apparent magnitudes. The errors quoted take into account both the instrumental error given by photon statistics alone and the calibration error. The latter error came from the scatter in the field star photometry. When the sky conditions were not photometric, as on the nights of 8 and 12 January 1999, the data have been reduced taking into account the differential extinction between the asteroid and the comparison stars.

Spectroscopy: During each night, we also recorded bias, flat–field, calibration lamp, spectrophotometric standard and solar analog stars (Hardorp, 1978) spectra at different intervals throughout the night. The solar analog stars (we observed Hyades64, HD44594, HD89010, HR6060, HD144585, HD76151) are necessary to remove the solar contribution from the spectra of the asteroid and to obtain the asteroidal reflectivity versus wavelengh. The spectral behaviour of the stars was very similar during each night. Moreover, to obtain Otawara's reflectivity, we used the solar analog with the closest airmass to that of the asteroid, that is HD 44594 for the first observation, and Hyades 64 for the second.

The spectra were reduced using standard data reduction procedures with the software packages Midas and IDL. The spectra are normalized to unity at 5500 Å and have been smoothed with a median filter technique.

3. Reflectance Properties

3.1. Colors

BVRI band images were obtained at the NTT (ESO) on February 14 to 16, 1999. The B - V, V - R and V - I colors are presented in Table 2. These colors fall within the S spectral type region (Schevchenko & Lupishko, 1998). However information at longer wavelength is necessary to distinguish between other close spectral types such as the types M or V. The BVRI data will be compared and discussed along with the spectroscopic results presented below.

3.2. Spectrum

The spectra obtained on the two nights in March (Fig. 1) appear very similar. The reflectance slope measured in the spectral range 5000–8000 Å, is $8.2 \pm 0.1\%/10^3$ Å, for the night of 15 March 1999 and $7.1 \pm 0.2\%/10^3$ Å, for the night of 16 March 1999. Small differences are associated with noise and also with the presence of spurious characteristics due to a non-perfect subtraction of sky absorption bands. Both spectra show a strong absorption feature longwards of 8000 Å. This feature is the well known 0.9 μm band associated with silicate minerals (pyroxene and olivine). Its position and depth is related to the presence and abundance of both silicates (Gaffey et al. 1993).

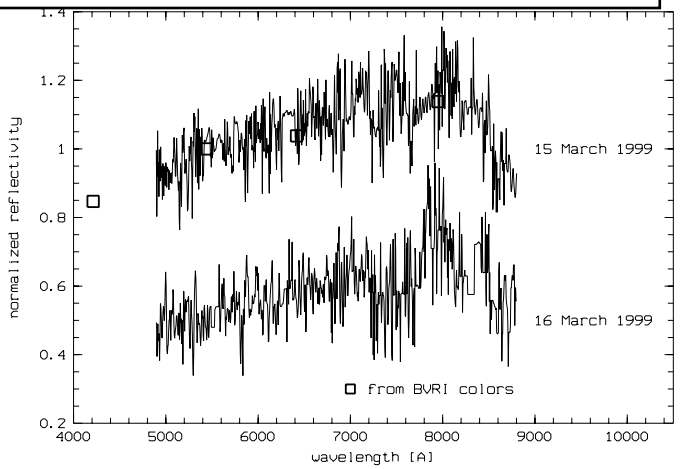

Fig. 1. Reflectance spectra of 4979 Otawara obtained on March 15 (top) and 16 (bottom), 1999. The spectra are normalized to unity at 5500 Å and have been vertically offset for clarity. Broadband color data from the ESO NTT on February 14–16, 1999 are also plotted (squares) on the top spectrum.

Table 2. Colors of 4979 Otawara

UT date	B-V	V-R	V-I
1999 Feb 14	0.87 ± 0.02	0.37 ± 0.01	0.84 ± 0.02
1999 Feb 15	0.86 ± 0.02	0.46 ± 0.02	0.83 ± 0.02
1999 Feb 16	0.82 ± 0.03	0.38 ± 0.02	0.82 ± 0.03
weighted mean	0.86 ± 0.01	0.40 ± 0.01	0.83 ± 0.01

The relative reflectances obtained from the BVRI color photometry are also plotted in Fig. 1. The reflectivity has been computed using solar colors. It can be seen that the broadband colors agree quite well with the spectroscopic measurements.

In order to characterize the spectral type of Otawara, we used the G-mode analysis applied to asteroids by Barucci et al. (1987) and Birlan et al. (1996). We found that the spectral types V and SV are most likely to match the spectrum of Otawara in Fig. 2. Extended spectral coverage (especially beyond 1 μm) and knowledge of the albedo would allow us to discriminate between the two spectral types. The V-type is associated with the asteroid 4 Vesta and HED meteorites (Binzel & Xu 1993).

The SV type is somewhat intermediate between the V and S-types. The appearance of the strong 0.9 μm band is suggestive that Otawara is a pyroxene and/or olivine-rich S-type asteroid

The possible association with the V-type is surprising and exciting. Indeed, all the known V-type asteroids are either members of the Vesta dynamical family (Zappala et al. 1995, Binzel & Xu 1993) or are near-Earth asteroids (Cruikshank et al. 1991). Asteroid 4979 Otawara is a main belt asteroid and does not belong to either of these populations. However, according to Migliorini et al. (1997) the Vesta family is much more extended than previously determined and extends close to the ν_6 and 3:1

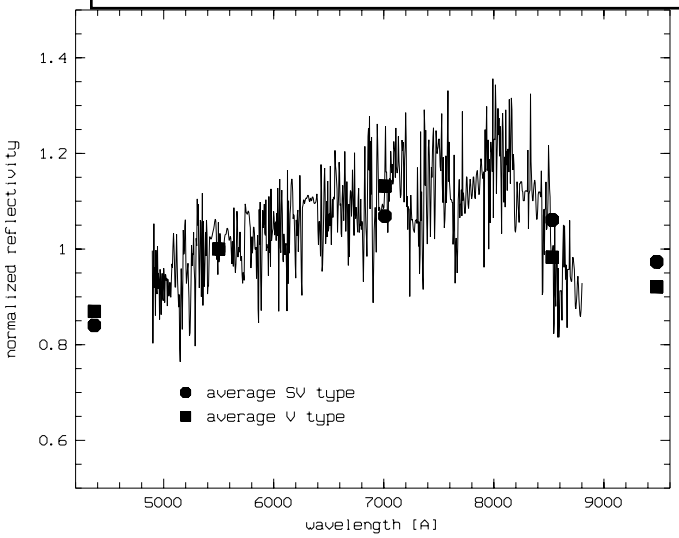

Fig. 2. Spectrum of 4979 Otawara compared with the mean spectrum of SV and V spectral type asteroids (Birlan et al., 1996).

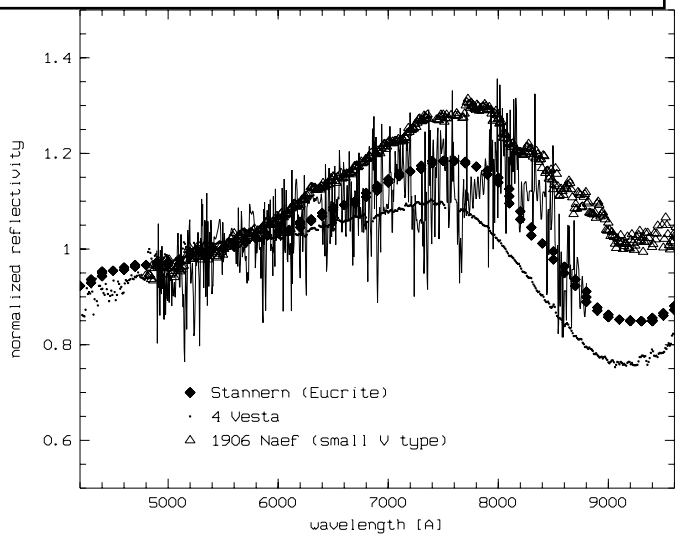

Fig. 3. A good match is obtained between the spectrum of 4979 Otawara and the spectrum of a eucrite (filled diamonds). The spectra of 4 Vesta (dotted line) and 1906 Naef (open triangles) are plotted for comparison. Eucrite spectrum is from Gaffey (1976) and spectra of Vesta and Naef are from SMASS (Xu et al. 1995).

resonances (a $\approx$ 2.15 and a $\approx$ 2.5 respectively). The position of Otawara in proper elements space is a = 2.168AU, e = 0.117 and sin i = 0.0071. Therefore, 4979 Otawara, which lies close to the ν_6 resonance, may in fact be a Vesta family member.

We also found a good match for the spectrum of Otawara with the spectrum of a eucrite meteorite, (Gaffey et al., 1976) suggesting once again a V-type classification (Fig. 3). The spectra of two Vesta family members: 4 Vesta and 1906 Naef are also plotted in Fig. 3. The latter one is a small asteroid (d = 6 km) like 4979 Otawara (see next section). It can be seen that Otawara' spectrum is comparable and certainly lies in the spectral range of the Vesta family.

4. Photometry

4.1. Rotation period

Because different filters were used in the observations and the observations were made over a wide range of phase angles, we analysed the three sets of photometric data independently in order to search for the asteroid's rotation period: 1) the data obtained in December, 1998 with the R filter ($16.5 < \alpha < 17.9$ degrees where α is the phase angle), 2) the data obtained in January 1999 with the R filter when the asteroid was very close to opposition ($0.5 < \alpha < 2.1$ degrees) and 3) the data obtained with the V filter in January 1999 ($6.2 < \alpha < 8.1$ degrees). We determined the synodic rotation period and the corresponding uncertainty by assuming a double-peaked lightcurve and by applying a Fourier analysis as described in Harris et al. (1989). We found rotation period of 2.707 $\pm$ 0.005, 2.707 $\pm$ 0.005 and 2.63 $\pm$ 0.01 hours for the three data sets, respectively. The disagreement in the third data set is likely the results of the fact that these data were taken under non-photometric conditions. Combining all three data sets, we found the best rotation period for Otawara

$$\mathrm{P_{syn}} = 2.707 \pm 0.005\,\mathrm{hr}.$$

The composite lightcurves, shown in Figs. 4, 5 and 6, are consistent and have symmetric double-peaks, typical of a ellipsoidal shape-dominated lightcurve. The peak-to-peak amplitude is 0.25 $\pm$ 0.04 mag for the December R data, 0.29 $\pm$ 0.05 mag for the January R data and 0.27 $\pm$ 0.03 mag for the January observations in the V filter.

4.2. Shape

The highest peak-to-peak amplitude is Δm = 0.29. If we assume that the brightness variation of Otawara is purely shape-induced, with no albedo features, we can model the asteroid as a tri-axial ellipsoid with semi-axes a, b and c where $a > b > c$. We, then can estimate a lower limit for the axial ratio:

$$\frac{a}{b} \geq 10^{0.4\Delta m} \quad (1)$$

The lightcurve amplitude of 4979 Otawara thus implies an axis ratio of $a/b \geq 1.3$. This corresponds to an elongation of at least 30%.

4.3. Size

We attempted to fit the data using the standard H, G magnitude system. Due to insufficient data, poor coverage down to sub-degree phase angles and possibly the use of different R filters, we could not obtain reliable absolute magnitude and slope parameters. Thus we choose to compute the absolute magnitude assuming G = 0.24 (S-type) and 0.49 (V-type). These latter values are the mean values of the parameter G for the respective compositional types, calculated from a sample containing 98 objects (Schevchenko & Lupishko, 1998).

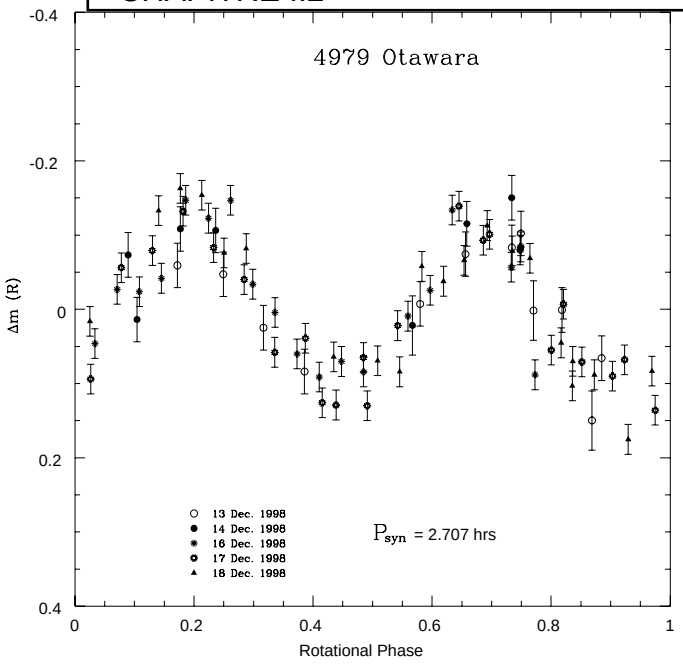

Fig. 4. Composite lightcurve of 4979 Otawara in rotational phase obtained in December 1998 in the R filter.

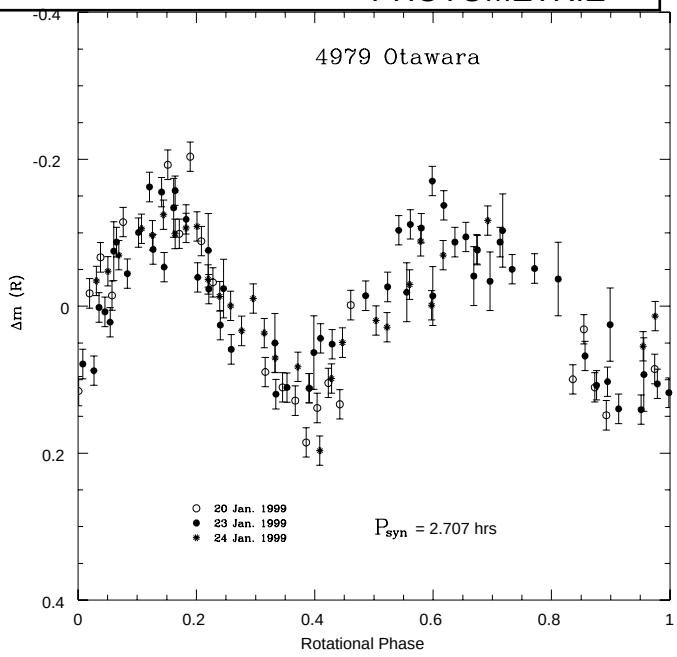

Fig. 5. Composite lightcurve of 4979 Otawara in rotational phase obtained in January 1999 in the R filter.

The absolute magnitude H_R is computed following Bowell et al. (1989). The mean absolute magnitude for all the nights in the R filter is:

$\mathrm{H_R} = 14.08 \pm 0.04$ assuming an S-type,
$\mathrm{H_R} = 14.23 \pm 0.04$ assuming an V-type.

If we assume an albedo of 0.19 or 0.38 as typical respectively for S and V-type asteroids (Tedesco et al. 1989), these correspond to a circular effective radius of 2.0 or 1.3 km, for S and V-types respectively. Knowing its axial ratio, (assuming $b = c$) we can then infer that 4979 Otawara is an elongated body having semi-axes $a = 2.4$ km and $b = 1.9$ km for a typical S-type albedo, and $a = 1.6$ km and $b = 1.2$ km for a V-type albedo.

5. Internal properties

Given its small size and its rotation period, 4979 Otawara belongs to a group of special interest, the small and fast rotating asteroids (FRAs). Typically observed lightcurve amplitudes of FRAs like Otawara are much smaller than those of slower rotators, indicating that the FRAs are less elongated, rather spheroidal bodies. For instance, for NEAs with $P > 4$ hr, the mean amplitude is 0.69 $\pm$ 0.05 mag, whereas for $P < 4$ hr, the mean amplitude is 0.21 $\pm$ 0.03 mag (Pravec, 1999). Observational and theoretical studies of small, fast rotating asteroids show that they have distinct properties that bring important information to our understanding of the collisional evolution of the asteroid population (see Pravec, 1999 for the latest review of this subject). In particular, FRAs, unlike asteroids with longer periods, are near the rotational break-up limit for aggregates

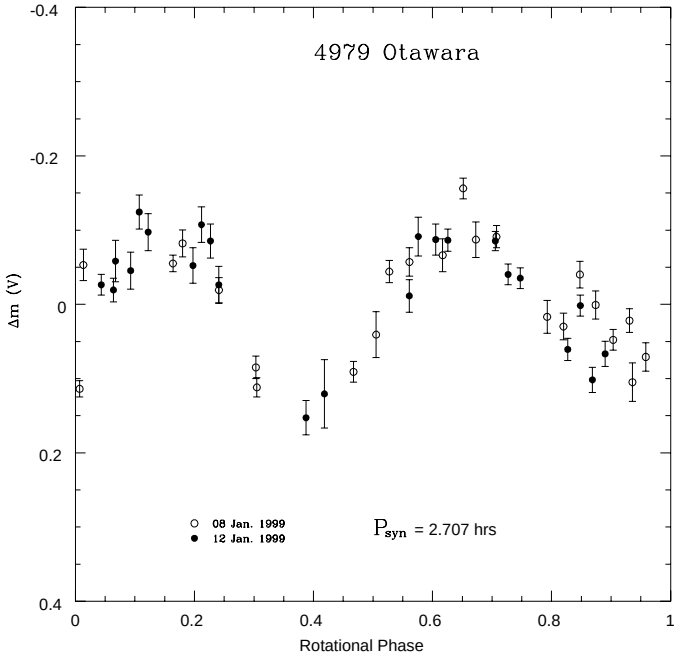

Fig. 6. Composite lightcurve of 4979 Otawara in rotational phase obtained in January 1999 in the V filter.

with no tensile strength, assuming plausible bulk densities for asteroids.

If Otawara is an aggregate or "rubble pile" object we can constrain its density knowing its rotation period and shape. If a body has no tensile strengh, a minimum density is required in order to resist centrifugal disruption. This is obtained by simply equating the centrifugal acceleration with the gravitation acceleration for the elongated body. Thus the minimum density ρ_{min}

for a body with axis ratio a/b and rotation period P is (Harris, 1996)

$$\rho_{min} \approx \left(\frac{3.3^h}{P}\right)^2 \frac{a}{b} \quad (2)$$

Applying this formula to 4979 Otawara, we find:

$\rho_{min} \geq 1.9.$

This density rules out densities as low as that of the C type asteroid 253 Mathilde ($\approx 1.3 \pm 0.4$ g cm^{-3}) found by the NEAR spacecraft team (Veverka et al. 1997) but allows densities comparable to that of 243 Ida (2.6 ± 0.5 g cm^{-3}) found by the Galileo imaging team (Belton et al. 1995). Hovewer, if 4979 Otawara is a single, consolidated body, then the fast rotation period gives us little information about its density.

6. Conclusion and discussion

Asteroid 4979 Otawara was observed on seven occasions from December 1998 through March, 1999. The main results of these observations are the following:

- Otawara exhibits a solar reflected spectrum indicating either a pyroxene and/or olivine-rich S-type asteroid, or a V-type asteroid, a member of the Vesta dynamical family. Further observations, in particular at near-infrared wavelenghs are needed in order to discriminate between the two spectral types.
- The synodic rotation period of Otawara is $P_{\rm syn} = 2.707 \pm 0.005$ hr.
- The lower limit for the axial ratio of the enveloping ellipsoid is $a/b \geq 1.3$.
- The circular effective radius is 2.0 or 1.3 km in the case of an S-type or a V-type asteroid, respectively.
- 4979 Otawara is a small, fast rotating asteroid (FRA). A lower limit on its density is obtained, $\rho_{min} \geq 1.9$, if we assume that Otawara is an aggregate or "rubble pile" object.

Asteroid 4979 Otawara will be a particularly interesting target to be studied from a spacecraft, since no fast rotator asteroid has been visited yet. The fast rotation of Otawara will allow the onboard Rosetta remote sensing instruments to image and measure the asteroid surface characteristics during one complete rotation of the asteroid at the highest possible resolution.

Further CCD photometric observations near opposition, occuring at different celestial latitudes, are necessary in order to determine the rotation pole direction of this asteroid. Also, additional spectroscopic observations are needed, in particular observations in the near infrared. Spectra taken at different rotational phases (Doressoundiram et al., 1997) will give a better estimate of the surface composition and its homogeneity/heterogeneity.

Acknowledgements. The authors thanks P. Pravec and A.W. Harris for helpful discussions. This work was supported in part by the NASA Planetary Astronomy Program. It was performed in part at the Jet Propulsion Laboratory under a contract with the National Aeronautics and Space Administration.

References

Barucci M.A., Capria M.T., Coradini A., Fulchignoni M., 1987, Icarus 72, 304
Barucci M.A., Doressoundiram A., Fulchignoni M., et al., 1998, Planet. Space Sci. 46, 75
Belton M., Chapman C., Thomas P., et al., 1995, Nature 374, 785
Binzel R.P., Xu S., 1993, Science 260, 186
Birlan M., Fulchignoni M., Barucci M.A., 1996, Icarus. 124, 352
Bowell E., Hapke B., Domingue D., et al., 1989, In Asteroids II (R.P. Binzel, T. Gehrels, M.S. Matthews, Eds.), pp. 524 Univ. of Arizona Press, Tucson
Cruikshank D.P., Tholen D.J., Hartmann W.K., Bell J.F., Brown R.H., 1991, Icarus 89, 1
Doressoundiram A., Barucci M.A., Fulchignoni M., 1997, A&A 325, L9-L11
Gaffey M.J., 1976, J. Geophys. Res. 81, 905
Gaffey M.J., Bell J.F., Brown R.H., et al., 1993, Icarus 106, 573
Gradie J.C., Chapman C.R., Tedesco E.F., 1989, In Asteroids II (R.P. Binzel, T. Gehrels, M.S. Matthews, Eds.), pp. 316 Univ. of Arizona Press, Tucson
Hardorp J., 1978, A&A 63, 383
Harris A.W., Young J.W., 1980, Icarus 43, 20
Harris A.W., Young J.W., Bowell E., et al., 1989, Icarus 77, 171
Harris A.W., 1996, Lunar and Planetary Science 27, 493
Harris A.W., Harris A.W., 1997, Icarus 126, 450
Lagerkvist C.-I., Magnusson P., Debehogne H., et al., 1992, A&AS 95, 461
Landolt A.U., 1992, Icarus 72, 304
Migliorini F., Morbidelli A., Zappala V., et al., 1997, Meteor. & Planet. Sci. 32, 903
Pravec P., 1999, Icarus in press
Schober H.J., Stanzel R., 1979 A&AS 38, 265
Shevchenko V. G., Lupishko, D. F., 1998 AJ 97, 580
Tedesco E. F., Williams J. G., Matson D.L., et al., 1989 Solar System Research 32, 220
Veverka J., Thomas P., Harch A., et al., 1997, Science 278, 2109
Xu S., Binzel R.P., Burbine T.H., Bus S.J., 1995, Icarus 115, 1
Zappala V., Bendjoya P., Cellino A., Farinella P., Froeschle C., 1995, Icarus 116, 291

A&A 375, 281–284 (2001)
DOI: 10.1051/0004-6361:20010789
© ESO 2001

Astronomy & Astrophysics

Research Note

Groundbased investigation of asteroid 9969 Braille, target of the spacecraft mission Deep Space 1⋆

M. Lazzarin[1], S. Fornasier[1], M. A. Barucci[2], and M. Birlan[2]

[1] Dip. di Astronomia, Vic. Osservatorio 5, 35122 Padova, Italy
[2] Obs. de Paris, 92195 Meudon Principal Cedex, France

Received 19 December 2000 / Accepted 24 May 2001

Abstract. Asteroid 9969 Braille (1992 KD) was encountered on July 29, 1999 by the Deep Space 1 mission, the first of NASA's New Millennium Program, launched on October 24 1998. The data obtained by the space mission seem to indicate a composition of the object similar to that of Vesta. To complete the information obtained in the infrared region by the Deep Space 1 mission we have performed a visible spectroscopic and photometric investigation of the asteroid respectively with the 1.5 m telescope and the NTT of ESO, La Silla. The spectrum was obtained in the spectral range 4500–8200 Å and, for the photometry, *BVRI* filters were used. In this paper we report the results of the analysis of the data obtained indicating that, on the basis of our visible data, the composition of the asteroid may range from V-type to Q-type, but we observe also a strong similarity to the H-type ordinary chondrites.

Key words. solar system: general – minor planets – asteroids

1. Introduction

In the last years, the number of space missions devoted to the investigation of comets and asteroids has increased due to the importance of studying these small bodies for the understanding of the origin and evolution of our Solar System. In fact, comets and asteroids are believed to be the most primitive objects in the Solar System and they hold many clues about the physical, thermal and compositional conditions present during the formation of the Solar System. In particular, the investigation of the composition of these bodies can give fundamental information on these subjects. In this context, we have made a spectroscopic and photometric study of the asteroid 9969 Braille (1992 KD), a target of the Deep Space 1 mission.

The Deep Space 1 is the first of a series of technology demonstration probes being developed by NASA's New Millennium Program to test new technologies for future space and Earth-observing missions. The spacecraft made a fly-by with the asteroid 9969 Braille (formerly known as 1992 KD) on 29 July 1999. Just after the encounter with Braille, NASA decided to extend the DS1 mission to fly-by the dormant comet Wilson-Harrington in January 2001 and comet Borrelly in September 2001.

Along with the technology demonstrations, the probe carries the Miniature Integrated Camera-Spectrometer (MICAS), an instrument combining two visible imaging channels with UV and IR spectrometers. MICAS was used to study the chemical composition, geomorphology, size, spin-state, and atmosphere of 9969 Braille (Soderblom et al. 1999). DS1 carries also the Plasma Experiment for Planetary Exploration (PEPE), an ion and electron spectrometer which is able to measure the solar wind during cruise, the interaction of the solar wind with the target bodies during encounters, and the composition of the cometary coma.

Deep Space 1 arrived within 26 km of asteroid 9969 Braille at 04:46 UT on July 29, 1999. The asteroid was not successfully imaged during the close flyby due to an on-board target-tracking problem. Two images were obtained 914 and 932 s after the closest approach from about 14 000 km and a dozen infrared spectra were

Send offprint requests to: M. Lazzarin,
e-mail: lazzarin@pd.astro.it

⋆ Based on observations carried out at the European Southern Observatory (ESO) of La Silla, Chile, programs N.62S-0173 and N.62S-0305A.

obtained about 3 minutes later, revealing what is probably a V-type classification of this NEA (Soderblom et al. 1999). The images show that 9969 Braille has an irregular shape, and is approximately 2.2 km along its longest side and 1 km at its shortest.

The study of Braille is also interesting in itself: it was discovered by E. F. Helin in 1992 (Helin et al. 1992) and very little was known about it before the encounter with the spacecraft. It was discovered as an Amor asteroid and a successive more accurate determination of the orbit classified it as a Mars crosser. The study of these objects is important because they represent one of the most peculiar classes of objects in the Solar System and their origin is not well understood yet. This population is very diverse in nature, many having unusual shapes (very elongated or bifurcated); binary systems have been discovered among the population. Some of these objects have a complex, non–principal axis rotation state while some others display very long rotational periods, which are not easily explained by the current dynamical and collisional models.

Their diversity is also reflected by the different taxonomic types present in the population: S, C, V, M, Q and D types have been identified to date (Binzel et al. 1997).

The origin of these bodies also is not well understood. We know that their present orbits are unstable over time scales much shorter than the age of the Solar System, and that over these time scales NEAs are ejected or collide with the Sun or a planet. Because the cratering record on the Moon suggests a fairly constant NEA population during the past 2 billion years, new NEAs must be continuously supplied by some sources in order to maintain the present steady state. Currently, two sources for NEAs have been identified. The first one is the Main Belt, where gravitational perturbations by the major planets cause dynamical resonances which provide escape routes. The second source is represented by extinct comets. A good number of NEAs represent the final evolutionary state of comets, that is, a devolatilized nucleus. An example is the asteroid Apollo 4015, the next target of the DS1 mission, which was the comet Wilson Harrington in 1949. It is not clear, however, what the efficiency of the delivery mechanism is, and what percentage of the NEAs we observe today comes from the one or other source. One way of addressing this problem is to characterize these objects spectroscopically, in order to derive their mineralogy.

Another interpretation of the origin of Braille, theorized by some astronomers, is that it may have been knocked off of Vesta and in effect the data obtained from the DS1 present on the WEB site of the DS1 at JPL would suggest a V-type composition.

Also Hicks et al. (1999) investigated Braille obtaining *BVRI* photometric data: they find colors closer to those of ordinary chondrite and basaltic achondrite meteorites than those of the vast majority of main-belt asteroids.

Binzel et al. (2001) also made a spectrum of Braille in the visible region suggesting a similarity to Q-type asteroids (A. W. Harris, private communication).

We have spectroscopically and photometrically investigated 9969 Braille in order to obtain information on its surface composition and its possible variations and in particular to complete the data obtained in the infrared region by the DS1 mission. A spectrum between about 4500 and 8200 Å and *BVRI* data have been compared; unfortunately, observations planned in the near infrared have not been successfull owing to bad weather conditions.

2. Observations and data reduction

Spectroscopy: we performed a spectroscopic investigation of 9969 Braille on 17 March 1999 at the European Southern Observatory of La Silla (Chile), with the 1.5 m telescope equipped with a Boller & Chivens spectrograph and a Loral Lesser CCD as detector (2048×2048 pixels). The grating used was a 225 gr/mm, with a dispersion of 331 Å/mm in the first order. The CCD has a 15 μm square pixels, giving a dispersion of about 5 Å/pixel in the wavelength direction. The spectral range is about $0.45 < \lambda < 0.82$ μm with a FWHM of about 10 Å.

The spectrum was recorded through a slit oriented in the East–West direction. The slit was opened to about 8 arcsec in order to reduce effects due to differential refraction and the possibility of losing signal due to guiding errors of the telescopes.

9969 Braille was observed on 17 March 1999, at 01:30:58 UT, with an exposure time of 75 min. During the observation, Braille had a visual magnitude of about 18.3, and an airmass of about 1.1.

We also recorded bias, flat–field, calibration lamp spectra, and solar analog stars' spectra at different intervals throughout the same night.

The solar analog stars observed (Hyades64, HD 44594, HD 89010, HR 6060, HD 144585, HD 76151) (Hardorp 1978), are necessary to remove the solar contribution from the spectrum of the asteroid and to obtain the asteroidal reflectivity. The spectral behaviour of the stars was very similar during the night with differences in the reflectivity gradient around $1\%/10^3$ Å. To obtain the asteroid spectrum reflectivity we then divided the spectrum of the asteroid by the spectrum of the solar analog with airmass closest to that of the asteroid (Hyades64).

The spectrum was reduced using ordinary procedures of data reduction (Luu & Jewitt 1990) with the software packages Midas and IDL.

These procedures include: subtraction of the bias from the raw data, division by flat field, cosmic ray removal, background subtraction, collapsing the two dimensional spectra, wavelength calibration, atmospheric extinction correction. Wavelength calibration was made using a lamp with He, Ar, Fe and Ne emission lines. The residuals of the wavelength calibration were $\leq$2 Å. After these procedures, we normalized all the spectra, both of asteroids and solar analog stars, at 1 around 5500 Å.

The spectrum was then smoothed with a median filter technique. Some spurious, easily recognizable, features

Table 1. Color indices with relative errors of Braille. Two obervations were performed during the 13–14 night: at 1:36 UT and 5.51 UT.

Date	$B-V$	$V-R$	$V-I$
13–14 Feb.	0.791 ± 0.030	0.411 ± 0.013	0.708 ± 0.018
13–14 Feb.	0.813 ± 0.032	0.441 ± 0.010	0.708 ± 0.015
14–15 Feb.	0.817 ± 0.045	0.468 ± 0.011	0.728 ± 0.020

due to an incomplete removal of sky lines (in particular of the water telluric bands around 7200 Å and of the O_2A band around 7600 Å) are present on the asteroid spectrum. The spectrum of Braille is reported in Fig. 1.

Photometry: the broadband color data were obtained at NTT of ESO on two nights (February 14–15, 1999). The SUSI2 CCD camera (55×55) at the f/11 Nasmyth focus of the 3.5 m New Technology Telescope (NTT) was used to obtain direct images. The EEV camera (ESO No. 46) was selected for our observations with the Bessel B, V, R, and I filters (central wavelength at 0.421, 0.544, 0.642 and 0.795 μm respectively). The observations were carried out in 2×2 binning mode, yielding a pixel scale of 0.16 arcsec/pixel. The seeing throughout the run was in the range 0.6–1.5 arcsec. The exposure time was 90 s.

The CCD images were reduced and calibrated with a standard method using aperture photometry (MAGNITUDE/CIRCLE in MIDAS). First, bias and flat-field corrections were performed. The instrumental magnitudes were measured using aperture photometry. The radius of the aperture used was typically about twice the average seeing. This was deemed optimum since it is large enough to include most of the point spread function, yet small enough to minimize background sky noise. Sky subtraction was performed using a 7–12 pixels wide annulus around the asteroid or reference star. Finally, for magnitude calibration, observations of standard stars were obtained over a wide range of airmasses and stellar types (three fields PG0942, SA107, and SA95 were used, Landolt 1992). The zero point, extinction and colour terms obtained from the Landolt fields were then used to convert instrumental magnitudes to apparent magnitudes. The errors quoted take into account both the instrumental errors given by photon statistics alone and the calibration error. The latter error came from the scatter in the field star photometry.

3. Results and discussion

BVRI band images were obtained at NTT on February 14 to 15, 1999. The $B-V$, $V-R$ and $V-I$ colors are reported in Table 1.

Little variation on the photometric data could be attributed to surface composition variations of the object.

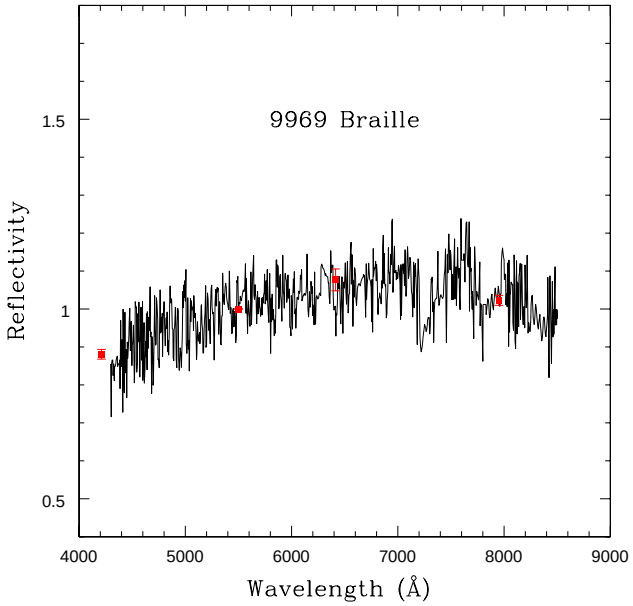

Fig. 1. Reflectance spectrum of 9969 Braille obtained on 17 March 1999 at ESO-La Silla. The spectrum is normalized at 1 around 5500 Å. The average broadband color data with the relative errors are also reported (squares) on the spectrum.

The spectrum of 9969 Braille (Fig. 1) has a reflectance slope of $(7.13 \pm 0.29)\%/10^3$ Å computed in the spectral range of 4300–7200 Å. It also presents some spurious features due to an imperfect subtraction of sky absorption bands (for example the water telluric band around 7200 Å).

The average relative reflectance obtained from the *BVRI* color photometry is also plotted in Fig. 1. The reflectivity from the photometric data was computed using solar colors. We adopted the maximum semi-dispersion as the error bar. The broadband colors agree quite well with the spectroscopic data.

In order to characterize the spectral type of 9969 Braille we used the extension of the G-mode multivariate method (Fulchignoni et al. 2000). The taxonomic classes proposed by Birlan et al. (1996) were taken into account. The results of our analysis reveal that 9969 Braille could be a V or SV asteroid. However, the spectrum of Braille does not cover the whole spectral interval of the defined classification; our analysis underlines the affinity of the asteroid to a given taxonomic class.

In Fig. 2 we compare the spectrum of Braille with that of Vesta and the result is a good match.

However, we also tried a comparison with the spectrum of a Q-type asteroid (1862 Apollo), with the average spectrum of V-type and S-type asteroids (Bus 1999) and with the spectra of several H, L and LL ordinary chondrites. What results is that in effect Braille is similar to Vesta, and compatible, within the errors, with the average of V-type asteroids, but also with the Q-type spectrum (Fig. 2). Moreover, the comparison with ordinary

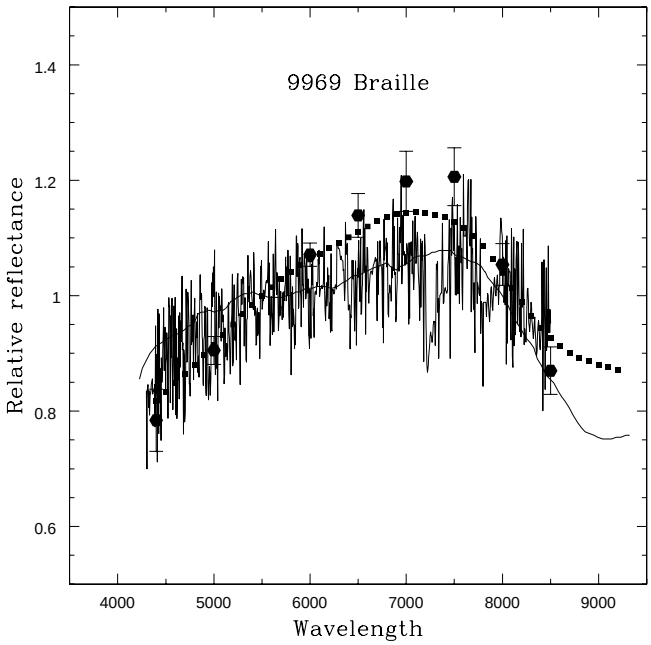

Fig. 2. Spectrum of 9969 Braille superimposed on the spectrum of asteroid Vesta (continuum) (Binzel et al. 1993), the average spectrum of V-type (hexagons) and the spectrum of the Q-type asteroid 1862 Apollo (squares) (Bus 1999).

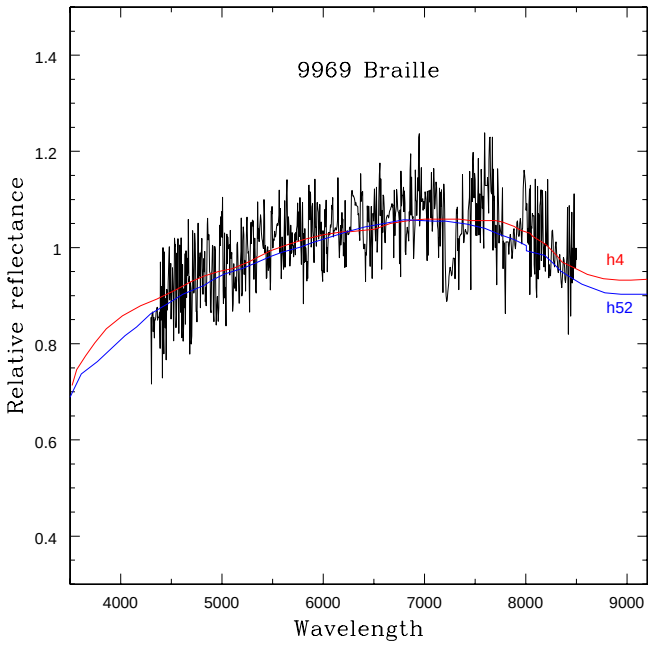

Fig. 3. Spectrum of 9969 Braille superimposed on the spectra of ordinary chodrites H4 and H52.

chondrites has revealed that the spectrum of Braille is pratically indistinguishable from that of H4 and H52 ordinary chondrites (Fig. 3). Instead, our spectrum is incompatible with that of the average spectrum of S-type asteroids (redder than the spectrum of Braille).

So, from our data we might confirm the data obtained in the infrared region by the Camera-Spectrometer MICAS of the Deep Space 1 during its fly-by with Braille on 29 July 1999 and reported by Soderblom et al. (1999). However, on the basis of our visible spectrum of Braille other interpretations of its composition are also possible: in fact it ranges between the Q-type and V-type and it shows a strong similarity with the ordinary chondrites H4 and H52 (Fig. 3).

4. Conclusion

Asteroid 9969 Braille was spectroscopically and photometrically observed during two observational runs at ESO with the 1.5 m telescope and the NTT respectively. From the data obtained here a clear conclusion on the composition of Braille is not easy to draw as the spectrum is compatible with that of Vesta, but also with the Q-types. A strong similarity is in particular evident with the ordinary chondrites. So we think that further observations, in particular in the near infrared, would help to define the surface composition of Braille.

References

Binzel, R. P., Harris, A. W., Bus, S. J., & Burbine, T. H. 2001, Icarus, in press
Binzel, R. P., Bus, S. J., & Burbine, T. H. 1997, Am. Astron. Soc., DPS Meeting, BAAS, 29, 05.01
Binzel, R. P., & Xu, S. 1993, Science, 260, 186
Birlan, M., Fulchignoni, M., & Barucci, M. A. 1996, Icarus, 124, 352
Bus, S. J. 1999, Ph.D. Thesis
Fulchignoni, M., Birlan, M., & Barucci, M. A. 2000, Icarus, 146, 204
Hardorp, J. 1978, A&A, 63, 383
Helin, E. F., Lawrence, K., Rose, P., Alu, J., & Williams, G. V. 1992, IAUC 5531
Hicks, M. D., Buratti, B. J., Rabinowitz, D. L., et al. 1999, 30th Annual Lunar and Planetary Science Conference, Houston, TX, abstract, No. 1719
Landolt, A. U. 1992, Icarus, 72, 304
Luu, J. X., & Jewitt, D. C. 1990, AJ, 99, 1985
Soderblom, L., Boice, D., Britt, D., et al. 1999, Am. Astron. Soc., DPS Meeting, BAAS, 31, 34.03

CCD AND PHOTOGRAPHIC OBSERVATIONS OF THE COMET C/1996 B2 (HYAKUTAKE)

OVIDIU VĂDUVESCU, GABRIEL ŞTEFĂNESCU, MIREL BÎRLAN

Astronomical Institute of the Romanian Academy
Str. Cuţitul de Argint 5, 75212 Bucharest 28, Romania

Abstract: About 200 CCD images of the comet C/1996 B2 - HYAKUTAKE were obtained and reduced, using four approaches by PPM stars and one by a GSC star, in March 20, 24, 25 and April 1-st, 1996, in Bucharest. Also, three photographically plates were reduced using PPM stars. The O-C analysis of the astrometric data allowed testing the accuracy of both the observational technique and the reduction method. The variation of the orientation of the comet's tail was also computed.

Key words: comet, appulse, astrometry, CCD

1. INTRODUCTION

Comets, together with asteroids, play an essential role in the knowledge of the origin and evolution of the Solar System. The spectacular and rare visible naked-eye apparitions of a comet in the inner Solar System become a major event for the astronomical community.

C/1996 B2 (Hyakutake) was announced at the end of January 1996, and became one of the "comets of the century" at the end of this century. The close approach opportunities from the Earth allowed favorable conditions of ground-based observations, even for the modest instruments.

More than 400 comets were observed photographically at Bucharest Observatory (Vass, 1994). The double refractor Prin-Merz of the Astronomical Institute in Bucharest has an F = 6m/D = 38cm and works as an astrograph, both photographically and CCD. The plates have a field by 2°×2° and ensure a limiting magnitude 12 (at maximum 30 min exposure time). The CCD has 768×512 pixels, "sees" a 4'×2.5' field and a limiting magnitude 15 (at 15 seconds time of integration). It is used in binning mode 2, 1pixel = 0.62".

2. ASTROMETRICAL OBSERVATIONS

In two cloudless nights we obtained three photographically positions of Hyakutake (March 20-th and 24-th), which were measured using an

Rom. Astron. J., Vol. 8, No. 1, p. 43–51, Bucharest, 1998

ASCORECORD machine, and were reduced with a classical least-squares method, using five-PPM stars. The results are given in Table 1.

Table 1

Photographic positions of the comet C/1996 B2

Date	Topocentric positions		Geocentric positions	
	α_{2000}	δ_{2000}	α_{2000}	δ_{2000}
$1996^{y}3^{m}20^{d}.930716$	$14^{h}\ 52^{m}\ 21^{s}.956$	4° 40' 13".04	$14^{h}\ 52^{m}\ 20^{s}.330$	4° 40' 47".93
1996 3 20 .950107	14 52 20 .179	4 47 27 .77	14 52 18 .776	4 48 02 .66
1996 3 24 .951746	14 35 33 .646	53 04 50 .37	14 35 30 .493	53 06 30 .85

Since the equipping of the mentioned instrument with the CCD, although various sources have been observed (the Saturnian satellites, asteroid appulses, globular clusters), C/1996 B2 is the first cometary object observed by CCD in Bucharest. His spectacular passing near the Earth in March 1996 offered the opportunity to test this new astrometrical technique on the comet observations.

March 24/25 was the most fruitful night of observation, because of the minimum distance of the comet from the Earth, which produced the greatest proper motion at that time 1'/min (Marsden, 1996), and due to the good meteorological conditions.

The possibility to make astrometrical observations using a CCD was discussed previously (Văduvescu & Vass,1995). Comparing with the photographical observations, the main problem of the CCD consists in the small field of the receptor ($10.4016'^{2}$), and consequently in the small density of the catalogue stars in the field (0.025 PPM stars/CCD field). Nevertheless, there are two important advantages of the CCD: the very short integration time (and accordingly a lot of exposures), and the procedure of the measurement of the source's position (such as the Gauss distribution of the light intensities). This method gives good results mainly to diffuse sources (as the nucleus of the comets), comparing to the visual method at the measuring machine for astrometric positions.

In order to plot the path of the comet through the stars, graphical software, *Celestial Maps v.4.5* was used (Văduvescu & Bîrlan, 1996). Both the program and the ephemeris certified the accuracy of the predictions. Thus, in March 24/25 the comet approached four-PPM stars (PPM34602 at $22^{h}0^{m}$, PPM34601 at $22^{h}34^{m}$, PPM34595 at $0^{h}36^{m}$, and PPM34582 at $1^{h}39^{m}$, all in UT). At these moments, 15, 22, 20 and respectively 26 CCD exposures were made using 5-s times of integration (the stars has V_{ph} = 11.1, 10.1, 10.3 and 8.0 respectively).

The method of reduction uses the *one-star* reference systems (Văduvescu & Vass, 1995), and the orientation of the CCD was solved using *two - PPM stars* in the vicinity of the comet. All the 83 positions of the nucleus were reduced and reported to the Central Bureau for Astronomical Telegrams.

The reduced positions of the comet are presented in Figure 1. We can observe the good agreement between the results obtained by the two methods.

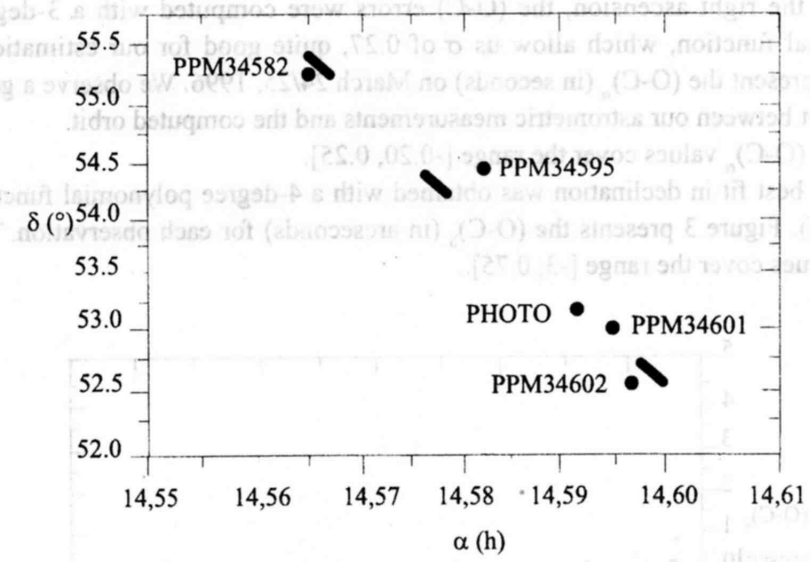

Fig. 1. – Reduced photographic and CCD positions of the comet C/1996 B2

We estimated the possibility to make astrometry using a single reference catalogue star. For this purpose, the (O-C) estimation is a good indicator. We used the comparison of our observations with the computed positions of Smithsonian (B. Marsden, private correspondence). Then, we used a polynomial fit.

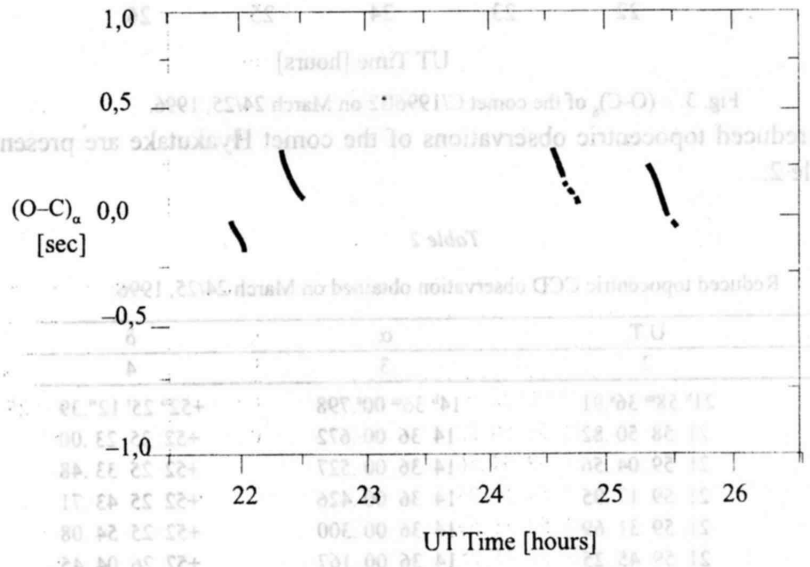

Fig. 2. – $(O-C)_\alpha$ of the comet C/1996B2 on March, 24/25, 1996.

For the right ascension, the (O-C) errors were computed with a 3-degree polynomial function, which allow us σ of 0.27, quite good for our estimations. Figure 2 present the $(O-C)_\alpha$ (in seconds) on March 24/25, 1996. We observe a good agreement between our astrometric measurements and the computed orbit.

The $(O-C)_\alpha$ values cover the range [-0.20, 0.25].

The best fit in declination was obtained with a 4-degree polynomial function ($\sigma = 0.05$). Figure 3 presents the $(O-C)_\delta$ (in arcseconds) for each observation. The (O-C) values cover the range [-3, 0.75].

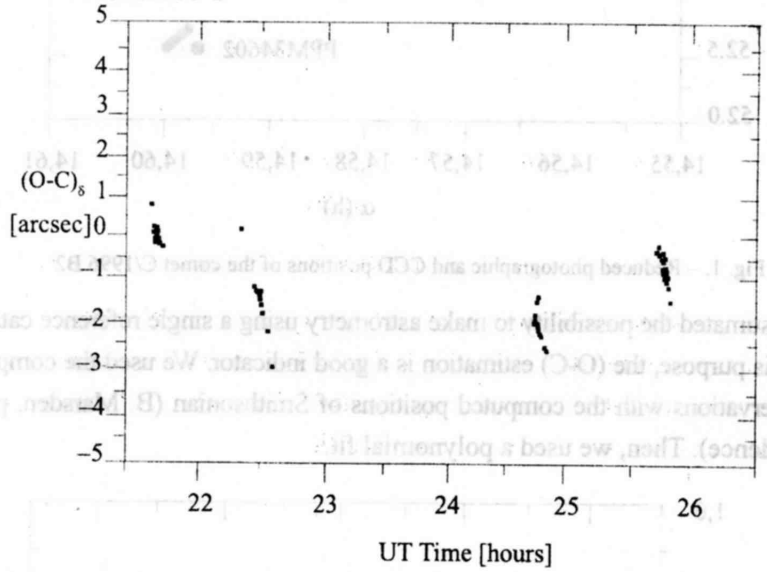

Fig. 3. – $(O-C)_\delta$ of the comet C/1996B2 on March 24/25, 1996.

The reduced topocentric observations of the comet Hyakutake are presented in the Table 2.

Table 2

Reduced topocentric CCD observation obtained on March 24/25, 1996.

N.	U.T.	α	δ
1	2	3	4
1	$21^h\ 58^m\ 36^s.91$	$14^h\ 36^m\ 00^s.798$	+52° 25' 12".39
2	21 58 50 .82	14 36 00 .672	+52 25 23 .00
3	21 59 04 .56	14 36 00 .527	+52 25 33 .48
4	21 59 17 .95	14 36 00 .426	+52 25 43 .71
5	21 59 31 .69	14 36 00 .300	+52 25 54 .08
6	21 59 45 .25	14 36 00 .167	+52 26 04 .45
7	22 00 12 .38	14 35 59 .899	+52 26 26 .06

Table 2 (continued)

1	2	3	4
8	22 00 25 .95	14 35 59 .805	+52 26 35 .62
9	22 00 39 .69	14 35 59 .683	+52 26 45 .80
10	22 00 53 .16	14 35 59 .556	+52 26 56 .21
11	22 01 06 .82	14 35 59 .432	+52 27 06 .75
12	22 01 20 .38	14 35 59 .312	+52 27 16 .95
13	22 01 33 .95	14 35 59 .188	+52 27 27 .43
14	22 01 47 .60	14 35 59 .059	+52 27 37 .84
15	22 02 01 .16	14 35 58 .926	+52 27 48 .14
16	22 31 15 .08	14 35 43 .992	+52 50 07 .53
17	22 31 29 .16	14 35 43 .870	+52 50 18 .15
18	22 31 42 .82	14 35 43 .738	+52 50 28 .62
19	22 31 56 .38	14 35 43 .610	+52 50 38 .95
20	22 32 09 .95	14 35 43 .478	+52 50 49 .40
21	22 32 23 .60	14 35 43 .359	+52 50 59 .71
22	22 32 37 .25	14 35 43 .224	+52 51 10 .07
23	22 32 50 .81	14 35 43 .106	+52 51 20 .54
24	22 32 50 .81	14 35 43 .104	+52 51 20 .54
25	22 33 04 .38	14 35 42 .980	+52 51 30 .85
26	22 33 18 .12	14 35 42 .849	+52 51 41 .32
27	22 33 31 .68	14 35 42 .719	+52 51 51 .69
28	22 33 45 .24	14 35 42 .599	+52 52 02 .10
29	22 33 58 .81	14 35 42 .480	+52 52 13 .99
30	22 34 12 .46	14 35 42 .342	+52 52 21 .45
31	22 34 39 .59	14 35 42 .091	+52 52 43 .53
32	22 34 53 .33	14 35 41 .963	+52 52 54 .01
33	22 35 06 .81	14 35 41 .830	+52 53 04 .36
34	22 35 20 .46	14 35 41 .696	+52 53 14 .18
35	22 35 34 .11	14 35 41 .586	+52 53 24 .97
36	22 36 14 .03	14 35 41 .208	+52 53 55 .45
37	22 36 41 .07	14 35 40 .952	+52 54 16 .16
38	22 36 54 .63	14 35 40 .828	+52 54 26 .44
39	24 34 34 .20	14 34 35 .624	+54 24 29 .19
40	24 34 48 .03	14 34 35 .478	+54 24 39 .69
41	24 35 01 .68	14 34 35 .342	+54 24 50 .11
42	24 35 15 .33	14 34 35 .195	+54 25 00 .50
43	24 35 28 .81	14 34 35 .059	+54 25 10 .94
44	24 35 42 .55	14 34 34 .911	+54 25 21 .26
45	24 35 56 .11	14 34 34 .779	+54 25 31 .75
46	24 36 09 .68	14 34 34 .643	+54 25 42 .12
47	24 36 23 .33	14 34 34 .513	+54 25 52 .49
48	24 36 36 .89	14 34 34 .360	+54 26 02 .96
49	24 36 50 .54	14 34 34 .226	+54 26 13 .34
50	24 37 04 .11	14 34 34 .097	+54 26 23 .73
51	24 37 17 .76	14 34 33 .940	+54 26 34 .27
52	24 37 31 .32	14 34 33 .808	+54 26 44 .49
53	24 39 06 .45	14 34 32 .828	+54 27 58 .36

Table 2 (continued)

1	2	3	4
54	24 39 20 .10	14 34 32 .710	+54 28 08 .91
55	24 39 33 .75	14 34 32 .552	+54 28 18 .10
56	24 39 47 .23	14 34 32 .423	+54 28 28 .47
57	24 40 00 .97	14 34 32 .279	+54 28 38 .89
58	24 40 14 .45	14 34 32 .147	+54 28 49 .23
59	25 36 22 .23	14 33 59 .208	+55 11 53 .19
60	25 36 35 .97	14 33 59 .070	+55 12 03 .50
61	25 36 49 .45	14 33 58 .928	+55 12 13 .89
62	25 37 03 .10	14 33 58 .779	+55 12 24 .31
63	25 37 16 .67	14 33 58 .636	+55 12 35 .06
64	25 37 30 .32	14 33 58 .493	+55 12 45 .22
65	25 37 43 .88	14 33 58 .348	+55 12 55 .40
66	25 37 57 .53	14 33 58 .212	+55 13 06 .19
67	25 38 11 .18	14 33 58 .071	+55 13 16 .39
68	25 38 24 .66	14 33 57 .921	+55 13 27 .04
69	25 38 38 .40	14 33 57 .772	+55 13 37 .48
70	25 38 51 .88	14 33 57 .636	+55 13 47 .80
71	25 39 05 .53	14 33 57 .487	+55 13 58 .21
72	25 39 19 .18	14 33 57 .343	+55 14 08 .52
73	25 39 32 .75	14 33 57 .197	+55 14 18 .88
74	25 39 46 .40	14 33 57 .055	+55 14 29 .34
75	25 39 59 .96	14 33 56 .902	+55 14 39 .78
76	25 40 13 .53	14 33 56 .769	+55 14 50 .19
77	25 40 40 .66	14 33 56 .477	+55 15 11 .06
78	25 40 54 .31	14 33 56 .342	+55 15 20 .17
79	25 41 07 .87	14 33 56 .198	+55 15 31 .83
80	25 41 21 .52	14 33 56 .046	+55 15 42 .17
81	25 41 35 .09	14 33 55 .911	+55 15 52 .67
82	25 41 48 .74	14 33 55 .773	+55 16 03 .04
83	25 42 02 .30	14 33 55 .607	+55 16 13 .58

Those observations are very useful in certain cases, such as the objects weakly observed. Thus, we tested for the first time such a method and we make the evaluation of the measurements with our CCD camera.

3. ORIENTATION OF THE TAIL

Figures 4 and 5 present two images of the comet, taken in March 24-th and April 1-st, and viewing in isophotes.

We made measurements of the position angle of the comet's tail using five images for each approach to the PPM stars on March 24/25. First, the position of the nucleus was measured using the centering method described above. After that, using a double representation of the images (in false colors and isophotes), we measured ten position in the tail direction on each image. These absolute coordinates on the images were reduced using linear regression. We obtained in the

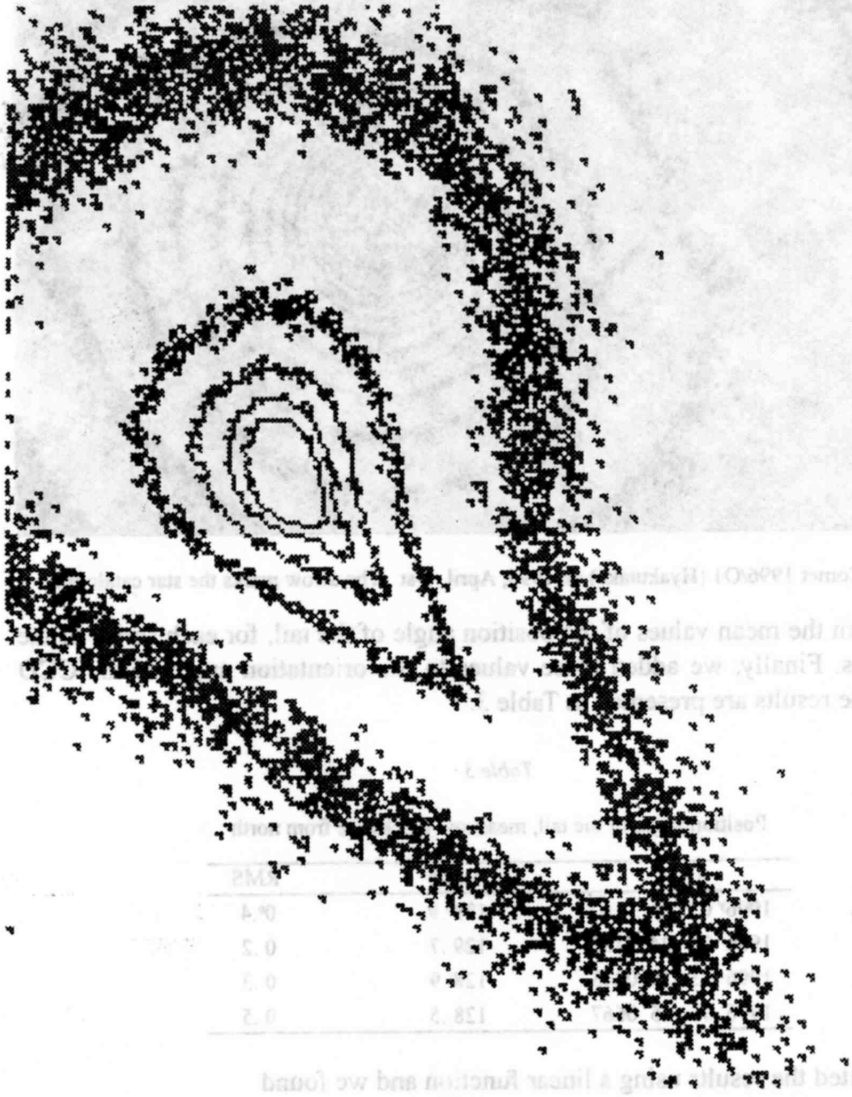

Fig. 4. – Comet C/1996B2 (Hyakutake) in 1996, March, 24-th.

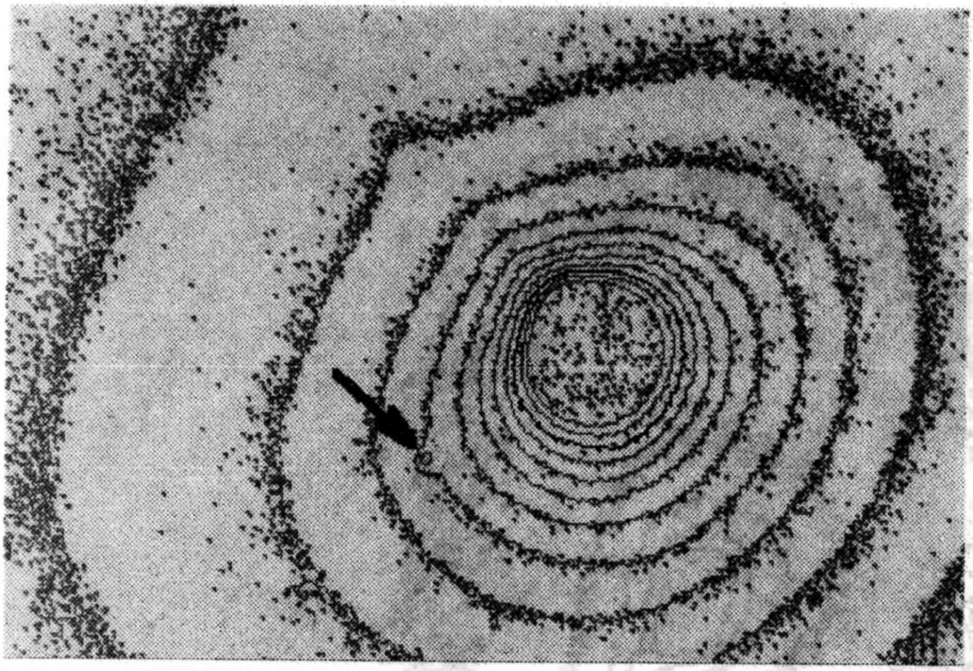

Fig. 5. – Comet 1996/O1 (Hyakutake) on 1996, April, 1-st . The arrow marks the star catalogue.

CCD system the mean values of the position angle of the tail, for each series of the five images. Finally, we added these values to the orientation angle of the CCD camera. The results are presented in Table 3.

Table 3

Position angle of the tail, measured clockwise from north

Date	Angle	RMS
$1996^{y}\ 03^{m}\ 24^{d}.9167$	$129^{o}.9$	$0^{o}.4$
1996 03 24 .9382	129 .7	0 .2
1996 03 25 .0243	128 .9	0 .3
1996 03 25 .0667	128 .5	0 .5

We fitted the results using a linear function and we found

$$\theta = -0.3886\ t + 138.45\ ,$$

where θ represents the orientation angle, and t is the time, given in hours.

Acknowledgements: We would like to thanks Dr. B. Marsden for promptly taking into consideration our astrometrical requests related to the comet. Special thanks Mrs. A. Alexiu for the "know-how" on the ASCORECORD measuring machine.

REFERENCES

Marsden, B.: 1996, *M.P.E.C.1996-F03.*
Vass, Gh.: 1994, *Rom. Astron. J.*, **2**, 183.
Văduvescu, O., Vass, Gh.: 1995, *Position of Asteroids from CCD Observations,* Communication at The Academic Days of Cluj, 1995 October, Cluj-Napoca.
Văduvescu, O., Bîrlan, M.: 1996, *Rom. Astron. J.* **6**, 97.

Received on 14 January 1998

I.3. Spectroscopie visible et infrarouge proche des objets du système solaire

Le spectroscopie est une méthode nouvelle d'observation pour les objets sans atmosphère, les développements notables datent des deux dernières décennies. La difficulté majeure est en grande partie due au fait que nous rencontrons plusieurs minéraux assez différents par leurs éléments constituants pouvant donner une signature spectrale assez semblable. De plus, les mêmes composants minéralogiques, suivant leur processus de cristallisation, peuvent donner différentes signatures. Contrairement au gaz, les signatures des minéraux se caractérisent (suivant le cas) dans de larges bandes d'absorption de différents profondeurs.

Dans l'intervalle spectral 0,4-3,00 μm (domaine du visible et de l'infrarouge proche) les photons incidents sont absorbés et d'autres photons sont émis aux fréquences correspondant à celles de vibrations des molécules présentes à la surface du corps sans atmosphère.

Dans l'intervalle spectral considéré, l'émission thermique de leur surface est négligeable et les absorptions sont produites par des vibrations, par les transitions du champ cristallin et par des mécanismes de transfert de charges électriques. La minéralogie de la surface des astéroïdes joue donc un rôle essentiel dans l'explication de chaque spectre.

Y-a-t-il des contraintes concernant le type de minéraux ? A cette question nous pouvons répondre en nous appuyant sur des résultats de la minéralogie des autres corps solides (et sans atmosphère) dont nous avons des échantillons sur Terre : météorites, roches lunaires, roches terrestres. La planétologie comparée, les études en laboratoire des échantillons des minéraux, jouent donc un rôle important dans les considérations faites sur la composition à la surface des objets.

Qu'est ce qui produit les caractéristiques d'un spectre de corps sans atmosphère ? Le rayonnement électromagnétique incident ne peut pas pénétrer à l'intérieur de l'objet. La

surface étant rugueuse et non uniforme, marquée par des grains des minéraux à l'état cristallin (des régolites), les bandes d'absorption sont donc les résultats de l'interaction du rayonnement incident avec la couche superficielle du corps.

L'absorption la plus fréquente de photons incidents est causée par la présence d'atomes de fer ou d'atomes de métaux de transition (nickel, cobalt, cuivre, titanium, etc.) dans les différents réseaux cristallins de la surface de l'astéroïde. Le photon incident est absorbé par un électron qui devient capable d'occuper un niveau d'énergie supérieur. L'énergie de ce niveau est égale à la somme de l'énergie du photon et de l'énergie du niveau qu'il a quitté. Ainsi, on peut identifier les minéraux, établir la présence de tel où tel cation métallique et, éventuellement déterminer l'abondance du métal de transition dans la structure minérale. Voici quelques exemples : $\boldsymbol{Fe^{2+}}$ présent dans l'ortopyroxène est responsable des bandes d'absorption symétriques centrées respectivement sur 1 et 2 µm. Le même $\boldsymbol{Fe^{2+}}$ dans le minéral de feldspath donne une faible bande d'absorption vers 1,25 µm. Le remplacement d'un métal de transition par un autre modifie les transitions du champ cristallin ; par conséquent, les bandes d'absorption seront déplacées par le nouvel atome.

De façon semblable, la présence d'une bande d'adsorption étroite dans la région du visible, autour de 0,49 µm, peut être expliquée par la présence de sulfure de fer ($Fe^{2+}S$) ou de sulfure de calcium (CaS) dans les minéraux comme les troilites ou les oldhamides respectivement.

Les bandes d'absorption dues aux vibrations des molécules sont aussi présentes dans le domaine spectral 0,4-3,0 µm. Les molécules les plus étudiées sont celles trouvées de façon significative à l'intérieur des météorites : l'eau, les minéraux carbonés, les composants hydrocarbonés. Par exemple, la présence de molécules d'eau dans les minéraux est à l'origine d'une forte bande d'absorption centrée sur 3 µm et deux autres bandes moins importantes centrées sur 1,4 et 1,9 µm respectivement. Certains auteurs proposent la présence d'une large bande (de faible profondeur) d'altération aqueuse autour de 0,7 microns pour des astéroïdes de la ceinture principale. L'ion $\boldsymbol{CO_3^{2-}}$ présent dans les composants carbonés donne une bande d'absorption centrée sur 1,6 µm et les composants carbonés contenant des métaux de transition sont à l'origine d'une bande d'absorption centrée sur 1 µm. Aussi, la vibration de la liaison ***C-H*** dans les hydrocarbures donne une bande d'absorption centrée sur environ 3,4 µm.

Quels sont les particularités liées à la spectroscopie au sol ?

Le rayonnement électromagnétique incident des domaines spectraux du visible et de l'infrarouge proche ne bénéficie pas de régimes similaires pendant la traversée de l'atmosphère terrestre. En effet, l'atmosphère terrestre est beaucoup plus fluctuante en

infrarouge proche et ultraviolet, essentiellement par les interactions (excitations) de certaines espèces chimiques de la haute atmosphère avec le rayonnement solaire ultraviolet et X (airglow phenomena = lueur de l'air). La nuit, ces lueurs sont souvent associées à la recombinaison des atomes de la haute atmosphère (80-100 km d'altitude). La technique utilisée pour l'obtention des spectres en infrarouge proche consiste à réaliser de courtes expositions. Par la soustraction des deux images successives, le fond du ciel sera ainsi enlevé. Ensuite, la somme de ces nouvelles images permettra l'obtention du rapport signal-bruit nécessaire. Etant donnée la faible luminosité de la majeure partie des corps sans atmosphère, un spectre en infrarouge proche peut être obtenu en 80-100 minutes d'exposition en moyenne pour un objet de magnitude 18-19, avec un rapport signal sur bruit[1] égale à 100. Le formalisme mathématique est représentée par la relation :

$$I_f = \sum_{i=1,2}^{n} (I_{i+1} - I_i)$$

où *n* représente le nombre d'images individuelles nécessaires pour atteindre le rapport signal-bruit désiré.

Dans les cas des objets sans atmosphère les contraintes liées à la résolution spectrale ne sont pas très importantes. Souvent la conception des instruments prend en compte des résolutions spectrales supérieures aux besoins pour les corps sans atmosphère (leur science nécessite une résolution spectrale entre 100 et 200). Dans la majeure partie des cas, pour une meilleure analyse, les spectres des corps sans atmosphère sont remis à une échelle adéquate, par un re-échantillonnage en longueur d'onde.

La majeure partie de mes activités d'observation et d'analyse des spectres visibles et infra-rouge s'est développée en vue de la préparation au sol de la mission spatiale ROSETTA, mais aussi en vue de la préparation d'autres missions spatiales (la mission spatiale DAWN et une éventuelle mission européenne vers des astéroïdes géocroiseurs).

L'activité d'analyse spectroscopique des astéroïdes cibles potentielles de la mission ROSETTA s'est déroulée pendant des nombreuses années, avec pour but de trouver les objets correspondant le mieux possible aux objectifs scientifiques de cette mission, survols et analyse « in situ » des objets avec une minéralogie gardant les caractéristiques de la formation du système solaire.

Les campagnes d'observations spectroscopiques se sont déroulées sur plusieurs télescopes de taille moyenne (diamètre du miroir primaire entre 2 et 4 m) : InfraRed Telescope Facility (3 m d'aperture) et Canada-France-Hawaii Telescope (3,60m) du Mauna

[1] La magnitude peut être atteinte sur un télescope de classe moyenne (2,5-4 m de diametre)

Kea-Hawaii, Telescopio Nazionale Galileo (3,52 m) des Canaries, New Technology Telescope (3,58 m) de l'ESO-La Silla). Plusieurs spectrographes (SpeX, Dolores, NICS, EMMI, …) ont été utilisés afin d'obtenir des données dans la région du visible et de l'infrarouge proche.

Les astéroïdes cibles potentielles de la mission spatiale ROSETTA ont polarisé une bonne partie des campagnes d'observations. Les changements de dernière minute de la fenêtre de lancement a fait que les astéroïdes candidats au survol ont été choisis après le lancement de la sonde. Les deux astéroïdes désignés sont 21 Lutetia et 2867 Steins, localisés dans la ceinture principale.

L'astéroïde 21 Lutetia est un objet de grande taille (diamètre estimé à 95.5 ± 4.1 km). Le survol de cet objet par la sonde ROSETTA est prévu pour juillet 2010. Les données spectroscopiques obtenues dans l 'infra-rouge proche montrent un spectre plat, neutre, sans bandes d'absorption. Ce type de spectre est souvent associé à des minéraux contenant du carbone, souvent rencontrés dans les météorites chondritiques carbonnées. Ce comportement spectral de l'objet le classe plutôt dans les objets primitifs de la ceinture principale (souvent on le nomme objet de type **C**, d'après la taxonomie des astéroïdes), ce qui complète les résultats publiés déjà, laissant ouvert le débat concernant la composition minéralogique de la surface. Sur la base de la pente du spectre dans la région du visible et de son albédo thermique obtenus par les données du satellite IRAS, 21 Lutetia a été classé auparavant comme étant un objet contenant une quantité importante des métaux (astéroïde de type M, essentiellement associé à des fragments de noyau d'un objet différencié).

Nous avons observé spectroscopiquement pour la première fois 21 Lutetia dans la région 2,9 - 3,8 μm, afin de pouvoir analyser quantitativement l'altération aqueuse publiée par d'autres auteurs (Rivkin et al, Icarus, vol 145, 2000) sur la base des observations photométriques. Nous pensons que le traceur représenté par cette bande peut apporter un argument important pouvant trancher sur le caractère primitif de l'objet. Nos observations ne confirment pas cette bande. Cependant nous ne pouvons pas exclure définitivement sa présence pour plusieurs raisons : la principale étant que la surface de l'hémisphère nord est la seule à réfléchir la lumière (géométrie « pole-on »). Par conséquent, nos mesures ne peuvent pas être comparées directement avec celles de la littérature. Des nouveaux programmes d'observations seront proposés afin d'obtenir des résultats permettant de caractériser l'autre hémisphère de l'astéroïde.

Le second candidat au survol de la mission ROSETTA est 2867 Steins, un astéroïde de petite taille dont toutes les données physiques restent à découvrir avant la rencontre. Les

données spectroscopiques obtenues dans la région du visible et de l'infra-rouge proche montrent un spectre avec une pente positive importante dans la région du visible. Dans la région d'infrarouge proche le spectre ne présente pas de bandes d'absorption mais la pente est toujours positive et moins importante. Le spectre peut être associé à des spectres de météorites différenciés contenant de l'enstatite ($Mg_2Si_2O_4$). La ressemblance avec les spectres de météorites composés d'enstatite est plus marquée par la présence d'une bande a 0,49 microns, dans les spectre du 2867 Steins correspondant aux assemblages des sulfites (Fe-S) ou (Ca-S). Des campagnes soutenues de surveillance seront nécessaires pour caractériser au sol le mieux possible cet objet avant son survol par Rosetta, évènement planifie pour septembre 2008.

Des campagnes d'observations ont eu lieu également afin de mieux caractériser la composition de la surface des astéroïdes 1 Ceres et 4 Vesta, les deux cibles de la mission spatiale DAWN. Les campagnes se poursuivent encore. Ces observations nous ont permis non seulement l'obtention de nouvelles données, mais aussi la possibilité de modélisation de leur spectres en termes minéralogique. Ce volet des activités sera développé dans le chapitre de modélisation.

La structure interne des astéroïdes, est également sujet de débat au sein des scientifiques qui étudient des astéroïdes. Il y a une liaison indéniable entre l'étude des surfaces des astéroïdes et leur composition d'ensemble : en fait, les conclusions des études spectroscopiques sont associées à une évolution thermique des objets. Elle est en partie le réflexe d'un comportement global de l'objet. Souvent, nous caractérisons la minéralogie de l'ensemble de l'objet par les données issues de l'analyse de leur surfaces. Cette hypothèse de travail est-elle vraie ? Des missions de recherche de la structure interne des astéroïdes sont en cours de préparation. Les cibles de ces missions peuvent être les astéroïdes géocroisseurs. Des programmes d'observations ont été initiés dans le cadre des collaborations internationales mais aussi en réponse à des initiatives nationales (par exemple, suite au programme d'Actions Coordonnées Interdisciplinaires initié par le Ministère de l'Education et de la Recherche). Les actions visent une meilleure connaissance de la population ainsi que l'identification de la caractérisation des astéroïdes géocroiseurs pouvant faire l'objet de missions.

Références :

Binzel, R.P., **Birlan, M.**, Bus, S.J., Harris, A., Rivkin, A.S., Fornasier, S.– *Spectral Observations for Near-Earth Objects Including Potential Target 4660 Nereus: Results From Meudon Observations at the NASA Infrared Telescope Facility (IRTF)*, **Planetary & Space Science,** Vol. **52(4)**, 291-296, 2004.

Birlan M., Barucci M.A., Vernazza, P., Fulchignoni M., Binzel R.P., Bus S.J., Fornasier S. *Near-Ir Spectroscopy of asteroids21 Lutetia, 89 Julia, 140 Siwa, 2181 Fogelin, and 5480 (1989YK8), potential targets of the Rosetta mission; remote observations campaign on IRTF,* **New Astronomy,** Vol**. 9 (5),** 343-351, 2004.

Barucci, M.A., Fulchignoni, M., Fornasier, S., Dotto, E., Vernazza, P., **Birlan, M.**, Binzel, R., Carvano, J., Merlin, F., Barbieri, C., Belskaya, I. – *Asteroid target selection for the new Rosetta mission baseline : 21 Lutetia and 2867 Steins* – **Astronomy and Astrophysics** v.430, 313-317, 2005.

M.A. Barucci, M. Fulchignoni, **M. Birlan**, P. Vernazza, E. Dotto, A. Doressoundiram – *Rosetta asteroid candidates* - Highlights of Astronomy, vol. 13, **XXVth General Assembly of the IAU**, Sidney, July 2003

Barucci M.A., Fulchignoni, M., Belskaya, I., Vernazza, P., Dotto, E., **Birlan, M. -** *Rosetta asteroid candidates*, in *The NEW Rosetta targets. Observations, simulations and instrument performances* Astrophysics and Space Science Library (ASSL) Vol. 311, Kluwer (ISBN: 1-4020-2572-6). (Eds. L. Colangeli, E. Mazzotta-Epifani, P. Palumbo)

Birlan M. – *Emission in absobtion lines; results of the SL9 L nucleus impact on Jupiter*, **Romanian Astronomical Journal**, vol **10**, n. **8**, 137-144, 2000.

Available online at www.sciencedirect.com
SCIENCE DIRECT®
Planetary and Space Science 52 (2004) 291–296
Planetary and Space Science
www.elsevier.com/locate/pss

Spectral observations for near-Earth objects including potential target 4660 Nereus : Results from Meudon remote observations at the NASA Infrared Telescope Facility (IRTF)

Richard P. Binzel[a,*], Mirel Birlan[a], Schelte J. Bus[b], Alan W. Harris[c], Andrew S. Rivkin[d], Sonia Fornasier[e]

[a] *Observatoire de Paris–Meudon, 5 Place Jules Janssen, 92195 Meudon Cedex, France*
[b] *Institute for Astronomy, 640 North A'ohoku Place, Hilo, HI 96720, USA*
[c] *Jet Propulsion Laboratory, Pasadena, CA 91109, USA*
[d] *Department of Earth, Atmospheric and Planetary Sciences, Massachusetts Institute of Technology, Cambridge, MA 02139, USA*
[e] *Astronomical Department of Padova, Vicolo dell'Osservatorio 2, 35122 Padova, Italy*

Received 20 September 2002; received in revised form 10 July 2003; accepted 30 October 2003

Abstract

We present visible and near-infrared spectral measurements for the highly accessible spacecraft target 4660 Nereus and three additional near-Earth objects displaying diverse color characteristics. All near-infrared measurements were carried out during the first remote observing operations between the Observatoire de Paris at Meudon and Mauna Kea, Hawaii. From Meudon, we had fine pointing and guiding control of the NASA Infrared Telescope Facility 3.0-m telescope and the near-infrared spectrograph "SpeX" to measure asteroid spectra in the range 0.8–2.4 μm. The efficiency of the observation was virtually the same as if the observers had been on location. We combine our near-infrared results with complementary 0.4–0.9 μm spectral measurements. Nereus is found to be a rare Xe-type asteroid with a composition that may be analogous to very high albedo enstatite achondrite (aubrite) meteorites, leading to a diameter estimate of less than 0.5 km. 1685 Toro displays a classic S-type spectrum while a steeper visible wavelength slope and a less pronounced 1 μm absorption feature for 1943 Anteros places it in the L-class. Also unusual is the apparent olivine-rich spectrum for 4142 Dersu-Uzala, which is classified as an A-type.
© 2003 Elsevier Ltd. All rights reserved.

Keywords: Remote observation; Spectroscopy; Asteroid; Space mission

1. Remote observation setup

Remote observation is becoming increasingly common at telescopes throughout the world as it allows the observer to reside in a location that may be more comfortable than a high-altitude summit and may reduce observer fatigue if no travel is required from her/his home institution. Circumstances that are particularly conducive to successful remote observations include using an instrument and telescope with which the observer is familiar and for which the observing procedures are well practised. Having these circumstances in our favor allowed us to test the remote observing capabilities being established at the NASA Infrared Telescope Facility (IRTF) on Mauna Kea, Hawaii. Such control differs from pre-programmed robotic systems for survey programs, and "service mode" observational programs, in that the observer has complete control to select program targets in real-time in response to conditions, to perform real-time assessment of data quality, and to immediately select new targets of opportunity. Brunswig et al. (2000) and Martin et al. (2000) give examples of previously established remote observation connections. In fact, several telescopes on Mauna Kea, Hawaii (Kibrick et al., 2000) offer the possibility to observe remotely from Hilo and Waimea (sea level and 760 m altitude, respectively). The uniqueness of our experiment consists in conducting remote observations from Meudon, France, more than 12,000 km away from Hawaii. For the observers in Meudon, the observing sessions ideally coincided with relatively normal working daylight hours. Observing sessions

* Corresponding author. Department of Earth, Atmospheric and Planetary Sciences, Massachusetts Institute of Technology, Mail Stop 54-410, Cambridge, MA, 02139, USA.
E-mail address: rpb@mit.edu (R.P. Binzel).

0032-0633/$ - see front matter © 2003 Elsevier Ltd. All rights reserved.
doi:10.1016/j.pss.2003.10.003

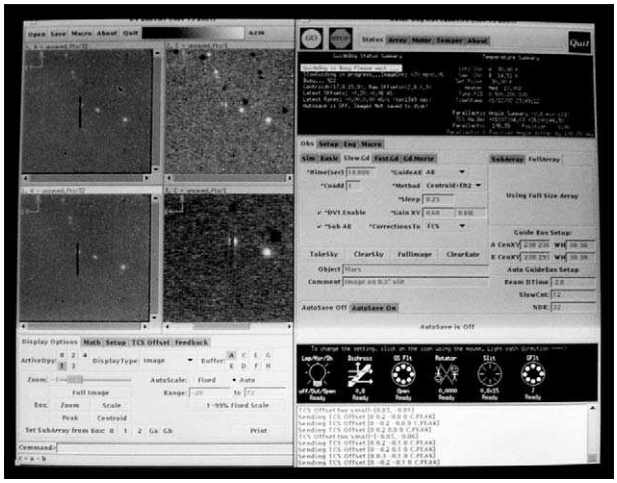

Fig. 1. IRTF control and guider (named "Guidedog") X-windows as seen from Meudon. Images of the spectral slit are seen in the upper left, where the display parameters are controlled immediately below. Control for the guide camera is seen on the right. An overview of the instrument configuration appears at lower right.

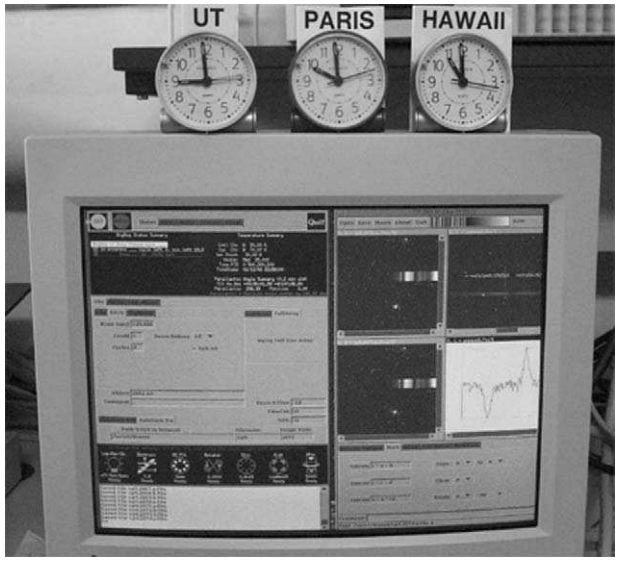

Fig. 2. SpeX instrument control system (named "Bigdog") as seen from Meudon. Observing modes and data acquisition are controlled by the window on the left. Spectral images and their preliminary analysis are displayed and controlled on the right.

began at 5 a.m. local time and finished at 5 p.m. local time.

Our goals for remote science operation included having control of the instrument and the target acquisition/guider system as well as constant audio/visual interaction with the telescope operator. Several weeks of effort were devoted in order to determine the best means for reaching these operational goals using existing equipment. Two Sparc workstations (operating under SunOS versions 5.7 and 5.8) were found to be very well suited for the task of controlling the fine pointing and guiding of the telescope and the instrument via X-windows exported from Mauna Kea to Meudon. In order to have a continuous audio/video link, we started with the idea to set up remote computers within a video-conference room. The incompatibility of both systems (through a phone line in Meudon and an IP link in Mauna Kea), constrained us to choose either an IP link or a phone link. Our decision was to use the IP link as it was most compatible with IRTF operations. Thus, our audio/video link was established with a Polycom ViewStation FX video-conference system (on Mauna Kea), and webcam/NetMeeting software (at Meudon). Figs. 1 and 2 show the displays as seen at Meudon that allowed real-time control of the target centering and guiding and all instrument setup and data acquisition functions of the spectrograph.

This experiment was realized through an ordinary network link, without any service quality warranty. Thus, the bandwidth for our link was variable and was a function of the internet traffic between Hawaii and Meudon. Our remote observing sessions occurred during both weekdays and weekends and we noted very few perturbations due to internet traffic from within the campus of the Meudon Observatory and between Mauna Kea and Meudon. Most communications occurred with a latency of about 0.5 s. The mean delay between the image acquisition in Mauna Kea and the refresh of the Meudon displays was 2 s. Images communicated in real time were for verification purposes only. The full spectral image files (~ 4 Mbytes each) were transferred to Meudon after the completion of the night. For all procedures, except for manual guiding on faint objects, such delays did not impede the efficient performance of the observation process. Overall, we estimate our total efficiency relative to being on-site was about 90 %. Having significant on-site experience with the instrument and typical weather conditions were critical factors in achieving this efficiency and can be considered prerequisites for remote observation success.

2. Science measurements

Our remote observation experiments on the 3.0-m aperture telescope of the IRTF were conducted using SpeX, a medium resolution near-infrared spectrograph employing a 1024×1024 InSb array (Rayner et al., 1998). SpeX was used in its low-resolution prism mode to obtain spectra over the range 0.8–2.5 μm with the resulting measurements binned at 50 Å/ pixel. SpeX observations were calibrated with respect to the solar-like stars Hyades 64 and SA 102-1081 (Landolt, 1973). All observations were made using a 0.8 arcsec slit width with pairs of exposures ("A" and "B") alternated along the 15-arcsec long spatial direction of the slit for the purpose of producing near-simultaneous images for sky subtraction. Residual sky values (after A − B and B − A subtraction) were fit and removed in the spectral extraction.

Table 1
Log of observations

Asteroid	Telescope	Wavelength range (μm)	Date and time (or reference)
1685 Toro	MDM 2.4 m	0.4–0.9	Bus and Binzel (2002a,b)
	IRTF 3 m	0.9–1.6	Burbine and Binzel (2002)
	IRTF 3 m	0.8–2.5	2002 May 08 09:19–09:57 UT
1943 Anteros	Palomar 5 m	0.3–0.9	Binzel et al. (2001a)
	IRTF 3 m	0.8–2.5	2002 January 12 12:25–13:01 UT
4142 Dersu-Uzala	MDM 2.4 m	0.4–0.9	Bus and Binzel (2002a,b)
	IRTF 3 m	0.8–2.5	2002 April 15 09:57–10:54 UT
4660 Nereus	Palomar 5 m	0.3–0.9	2001 October 22 06:40-07:06 UT
	KPNO 4 m	0.5–0.9	2002 February 23 11:19–11:52 UT
	IRTF 3 m	0.8–2.5	2002 March 15 11:18–12:36 UT

We performed Meudon–Mauna Kea remote operations over the course of four observing runs (totaling seven nights) between January and May, 2002. Near-Earth objects were our primary targets as part of a program to explore the diversity of their compositions and the potential relationships between asteroids, comets, and meteorites. (See Binzel et al., 2002 for more details on the motivation of near-Earth object studies.) Near-infrared (0.8–2.5 μm) spectral measurements of near-Earth objects (and asteroids in general) are highly diagnostic of their compositions owing to the existence of spectral signatures (absorption bands) due to pyroxene near 1- and 2 μm and olivine near 1 μm. These are common constituents in the majority of meteorites and thus provide a powerful means for exploring asteroid–meteorite associations. SpeX provides a new capability for near-Earth objects in that objects may be measured down to a limiting magnitude near V18, placing many dozens of these objects within reach at any given time. Remote observation is also quite advantageous to the reconnaissance of near-Earth objects as they typically have very short windows of observability when they make close (and often fast) passages near-the Earth. Thus frequent access to the telescope is necessary—making the capability of remote observation all the more desirable for eliminating frequent travel.

To exemplify the results of our remote observation experiment, we present one object from each run that is representative of the diversity found within the near-Earth object population. (A more complete analysis of the larger sample is forthcoming as observations are continuing.) A primary focus for the science results reported here is our findings for 4660 Nereus: a near-Earth asteroid with a low-inclination Earth-intersecting orbit that makes it among the most easily accessible (in terms of low delta-V trajectories) objects currently known. Table 1 gives a summary log of our reported science measurements. These measurements include complementary visible wavelength spectra obtained at Palomar, Kitt Peak, and Michigan-Dartmouth-MIT (MDM) observatories. At the 5.0-m Hale telescope on Palomar Mountain, California we employed the Double Spectrograph described by Oke and Gunn (1982). This instrument uses a pair of 1024 × 1024 pixel (binned 2 × 2 on readout) CCD cameras to simultaneously record the blue and red halves of a long-slit spectrum. Binzel et al. (2001a) give a description of the techniques we employed with this instrument. Additional supporting visible wavelength measurements were obtained with the 4.0-m Mayall Telescope at Kitt Peak National Observatory, Arizona, using the RCSP spectrograph and Tektronix 2048 × 2048 CCD binned 2 × 2 on readout. A GG495 order sorting filter and 5 arcsec slit width provided 0.5–0.9 μm spectral coverage with a dispersion of 10 Å/pixel and a spectral resolution of about 50 Å. Binzel et al. (2001b) give a description of the techniques we employed with this instrument. For the Mark III CCD spectrograph and similar techniques employed at the MDM 2.4-m Hiltner telescope, we refer the reader to Bus and Binzel (2002a) and Bus et al. (2002).

3. Science results

3.1. 4660 Nereus

A close approach in early 2002 provided the first favorable opportunity for spectral measurements of Nereus since its 1982 discovery. For the IRTF measurements, all target acquisition, guiding, and data acquisition commands were executed and controlled from Meudon. For the final 0.8–2.4 μm near-infrared spectrum, data were binned (4 × 50 Å) in 0.02 μm intervals so as to improve the signal-to-noise. Visible wavelength measurements complementary to our IRTF remote observations were obtained at both Kitt Peak and Palomar Observatories. These separate visible spectra were normalized to unity at 0.55 μm and then combined by a weighted average. Overlapping spectral coverage in the range of 0.8–0.9 μm was used to scale the near-infrared spectrum to match the normalized relative

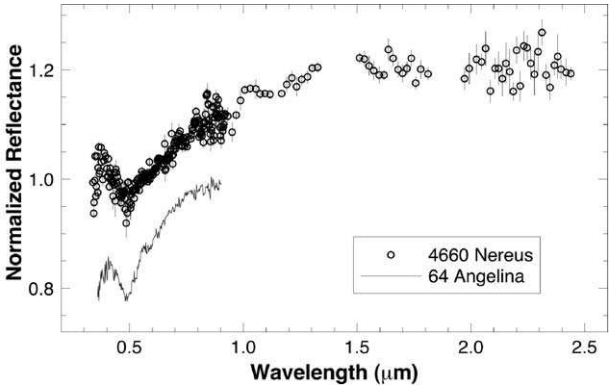

Fig. 3. Relative reflectance spectrum (data points) of near-Earth asteroid 4660 Nereus normalized to unity at 0.55 μm. (Gaps at 1.4 and 1.9 μm as well as the small feature at 0.92 μm are due to the presence of telluric water.) While the near-IR spectrum is featureless, we note the match of the rarely seen 0.49 μm feature to that for the E-type asteroid 64 Angelina (curve, vertically offset for clarity and shown below).

reflectance scale established by the visible measurements. The resulting Nereus spectrum, shown in Fig. 3, has a combined wavelength coverage from 0.34 to 2.44 μm.

Over the range 0.8–2.4 μm, Nereus shows a moderate red slope (increasing reflectance with increasing wavelength) but does not show substantial 1.0- or 2.0 μm absorption bands arising from the presence of Fe^{2+}-bearing pyroxene–olivine mixtures that are most typically seen in the spectra of near-Earth asteroids (Binzel et al., 2001a). The red slope of the Nereus spectrum also is greater than the generally very flat and featureless spectra seen for C-type asteroids. Within the Tholen taxonomy system (Tholen and Barucci, 1989), the moderate red slope and lack of silicate absorption features are consistent with Nereus being either an E-, M,- or P-class asteroid. (Formally, this degeneracy is denoted by the designation "X" pending an albedo measurement to resolve the spectral ambiguity.) Bus (1999) and also Bus and Binzel (2002a,b) present an extension to the Tholen taxonomy that takes advantage of the higher spectral resolution of CCD spectra for identifying features that are diagnostic for recognizing taxonomic classes. Within the feature-based taxonomy system of Bus, the Slope and PC2' scores for Nereus are 0.368 and 0.324, respectively, placing Nereus within the "X-complex".

The key to resolving the likely nature of Nereus' composition is the presence of a strong but relatively narrow absorption feature near 0.49 μm. This feature was first detected in the spectrum of asteroid 64 Angelina (Bus, 1999; Bus and Binzel, 2002a). Within the Bus taxonomy, this feature unambiguously places both Angelina and Nereus within the Xe-class. Angelina is known to have a high albedo (listed as 0.43 within Tedesco, 1989) and is therefore classified as an E-type by Tholen. Independent thermal flux measurements of Nereus (Delbo et al., 2003) confirm a high albedo for Nereus, also making it consistent with the Tholen E-class. For an albedo similar to or likely higher than the value for Angelina (Delbo et al., 2003), an *H* magnitude of 18.2 (IAU Minor Planet Center) yields a diameter estimate not larger than 0.5 km according to the relation of Bowell et al. (1989).

Meteorite associations for E-type asteroids have been extensively investigated (e.g. Gaffey et al., 1992) and the 0.49 μm feature within the Bus Xe-class has been analyzed by Burbine et al. (1998, 2001) with troilite (FeS) and oldhamite (CaS) as possible constituents. Burbine et al. (2002) compared the spectrum of 64 Angelina with oldhamite, aubrites, and troilite and found good agreement between Angelina and oldhamite. Asteroids such as Angelina and Nereus may be analogous to enstatite achondrite meteorites with somewhat higher oldhamite abundances than seen within laboratory samples. Enstatite achondrite meteorites, for which Norton County is a common example, are high albedo samples of chondritic material that has undergone heating and melting sufficient to allow almost complete extraction of NiFe metal and FeS.

Finally, it is interesting to *speculate* on the origin of 4660 Nereus. Gaffey et al. (1992) forged a plausible link for the enstatite achondrites to the Hungaria region of the inner asteroid belt where E-type asteroids are common. Asteroid 3103 Eger, an E-type near-Earth asteroid with a similar high inclination to the Hungaria region, is viewed by Gaffey et al. as a prototype for the connection between Hungarias and enstatite achondrites arriving on Earth. We note that Eger and Nereus have similar semi-major axes (1.40 and 1.48 AU, respectively) and orbital eccentricities (0.35 and 0.36, respectively). However, the significantly lower orbital inclination for Nereus (1.4° compared with 20.9°) makes a connection to Eger and the Hungaria region more problematic. For example, in a planetary encounter, the encounter velocity is generally a conserved quantity making it implausible to change inclination only while leaving the semi-major axis and eccentricity mostly unchanged. Thus any connection between Nereus, Eger, and the Hungarias is both problematic and complex.

3.2. 1685 Toro, 1943 Anteros, 4142 Dersu-Uzala

Similar to our Nereus IRTF measurements, all commands for the target centering, guiding, and near-infrared spectral measurement of the three additional objects presented here were executed and controlled from Meudon. These spectra and their complementary visible wavelength measurements (detailed in Table 1) are presented in Fig. 4. As an ensemble, they display roughly a factor of two range in spectral slope and exemplify the diversity of the inner solar system population of asteroids. We briefly discuss each object in turn.

1685 Toro is a dynamically interesting object that alternates between librations in a 5/8 commensurability with Earth and 5/13 commensurability with Venus (Williams and Wetherill, 1973). Spectrally it falls within the S(IV) spectral class of Gaffey et al. (1993) with a Band I position of

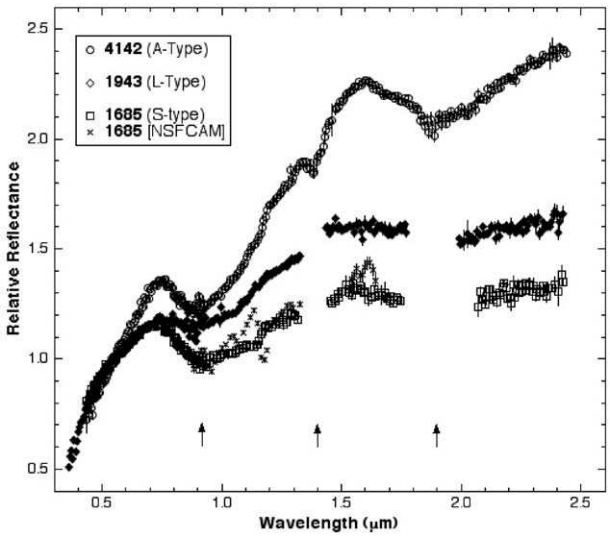

Fig. 4. Combined near-infrared plus visible spectra for (bottom to top) 1685 Toro, 1943 Anteros, and 4142 Dersu-Uzala. (All spectra are normalized to unity at 0.55 μm.) The range of spectral slopes and 1- and 2 μm absorption bands seen among these objects in the inner solar system well represents the diversity seen within the main asteroid belt. The enhanced capability of SpeX relative to the previous generation of near-IR CCD spectroscopy at the IRTF (NSFCAM; Binzel et al., 2001a; Burbine and Binzel, 2002) is shown in comparison for 1685 Toro. Arrows indicate wavelengths dominated by telluric water, which under excellent conditions and with abundant signal-to-noise can be almost be completely removed. For more limiting signal-noise-cases encountered by observing near the magnitude limit of the system, we delete these affected wavelengths and caution against the interpretation of any residual features at these arrowed wavelengths in the spectrum of 4142.

0.94 ± 0.01 μm and a Band II / Band I ratio of 0.48 ± 0.10. (We compute our uncertainties based on results of a wide range of fitting trials to the continuum.) In Fig. 4 we are able to illustrate the evolution of near-infrared spectroscopy at the IRTF by comparing the spectrum of Toro obtained with the NSFCAM "asteroid grism" (Binzel et al., 2001a; Burbine and Binzel, 2002) and that obtained by SpeX. SpeX is able to provide longer wavelength coverage (out to 2.5 μm) and provide higher signal-to-noise measurements.

1943 Anteros displays a similar spectral slope with Toro shortward of 0.7 μm, but then remains relatively flat with a very shallow absorption band in the 1 μm region. These characteristics over the visible wavelength spectrum place it within the L-class of the Bus taxonomy, a subset of the larger range of "S-like" objects that make up what is referred to as the "S-complex" (Bus, 1999; Bus and Binzel, 2002a, b). Extending the spectral coverage for Anteros out to 2.5 μm shows an increase in spectral slope with a weak 2 μm band, a Band I position of 0.96 ± 0.01 μm and a Band II/Band I ratio of 0.40 ± 0.12. With these features 1943 Anteros is placed in the transition region between S(III) and S(IV) spectral class in the Gaffey et al. (1993) classification scheme.

4142 Dersu-Uzala is a Mars-crossing object. Spectrally, it is an end member with a very steep visible wavelength spectrum and deep and broad 1 μm band, placing it within the A-class of the Bus taxonomy. Cruikshank and Hartmann (1984) have shown the connection between the A-class and olivine-rich mineralogies, but we caution that taxonomy is not mineralogy. (Taxonomic classifications such as that of Bus, 1999 are based on visible wavelength data, while mineralogic characterization requires extension into the near-infrared.) Dersu-Uzala displays a 2 μm band that may not be typical for A-class objects such as those presented by Cruikshank and Hartmann (1984), indicating a non-negligible pyroxene component. Burbine and Binzel (2002) noted two groups of A-type objects, based on "deep" or "weaker" features out to 1.6 μm, where 4142 is in the "weaker" group. Further characterization of these objects will show whether this latter group typically displays evidence for a non-negligible pyroxene content. Dersu-Uzala also shows a very steep slope in the 1–1.5 μm region. With a Band I position of 0.97 ± 0.01 μm and a Band II/Band I ratio of 0.75 ± 0.08, this object places outside the S-subtypes regions in the Gaffey et al. (1993) classification scheme.

4. Conclusions

For a well-established program in which the observers are experienced, we find remote observations to be highly successful and efficient. The quality of the link the target acquisition, performance of the scientific measurements, and communication with the operator is the single most important requirement for remote observation success. Our science results reveal very diverse objects in the inner solar system vicinity of Earth. Our enstatite achondrite-like conclusion for Nereus implies its parent body experienced substantial heating early in the solar system. As a completely different class of asteroids than that which has been previously explored, Nereus represents a compelling spacecraft target for both its scientific uniqueness and relatively easy accessibility. The range of spectral characteristics for the additional objects presented here show that the range of olivine–pyroxene mineralogies seen within the main-belt is well represented within the near-Earth population.

Acknowledgements

We thank T. Burbine and M. Gaffey for their reviews that generated important improvements to this paper. The authors are grateful to Tony Denault who answered many questions prior to our IRTF run about the Polycom system and exporting of X-windows for SpeX and the guiding system. We also thank Paul Sears and Bill Golish, the telescope operators during this experiment. This work was supported by NSF Grant AST-9530282 and NASA Grant NAG5-3939 (RPB). Binzel and Birlan had the privilege to be virtual Visiting Astronomers at the Infrared Telescope Facility, which is operated by the University of Hawaii under Cooperative Agreement No. NCC 5-538 with the National Aeronautics and Space Administration, Office of Space Science,

Planetary Astronomy Program. Binzel and Rivkin were real Visiting Astronomers at Kitt Peak National Observatory, National Optical Astronomy Observatory, which is operated by the Association of Universities for Research in Astronomy, Inc. (AURA) under cooperative agreement with the National Science Foundation. Observations obtained at the Hale Telescope, Palomar Observatory are part of a collaboration between the California Institute of Technology, NASA/JPL, and Cornell University.

References

Binzel, R.P., Harris, A.W., Bus, S.J., Burbine, T.H., 2001a. Spectral properties of near-Earth objects: palomar and IRTF results for 48 objects including spacecraft targets (9969) Braille and (10302) 1989 ML. Icarus 151, 139–149.

Binzel, R.P., Bus, S.J., Sunshine, J., Burbine, T.H., 2001b. MUSES-C target asteroid (25143) 1998 SF36: a reddened ordinary chondrite. Meteoritics Planet. Sci. 36, 1167–1172.

Binzel, R.P., Lupishko, D.F., Di Martino, M., Whiteley, R.J., Hahn, G.J., 2002. Physical properties of near-Earth objects. In: Bottke, W.F., Cellino, A., Paolicchi, P., Binzel, R.P. (Eds.), Asteroids III. University of Arizona Press, Tucson, pp. 255–271.

Bowell, E., Hapke, B., Domingue, D., Lumme, K., Peltoniemi, J., Harris, A.W., 1989. Application of photometric models to asteroids. In: Binzel, R.P., Gehrels, T., Matthews, M.S. (Eds.), Asteroids II. University of Arizona Press, Tucson, pp. 524–556.

Brunswig, W., Sievers, A., Thum, C., Wild, W., 2000. Remote observing with the 30-m radiotelescope In: Kibrick, R.I., Wallander, A. (Eds.), Advanced Global Communications Technologies for Astronomy, Proceedings of the SPIE, Vol. 4011, pp. 84–92.

Burbine, T.H., Binzel, R.P., 2002. Small main-belt asteroid spectroscopic survey in the near-infrared. Icarus 159, 468–499.

Burbine, T.H., Cloutis, E., Bus, S.J., Meibom, A., Binzel, R.P., 1998. The detection of Troilite (FeS) on the surfaces of E-class asteroids. Bull. Am. Astron. Soc. 30, 1025.

Burbine, T.H., McCoy, T.J., Binzel, R.P., Bus, S.J., 2001. Spectra of aubrites and their constituent minerals. Meteoritics Planet. Sci. (Suppl.) 36, A31–A32.

Burbine, T.H., McCoy, T.J., Nittler, L.R., Benedix, G.K., Cloutis, E.A., Dickinson, T.L., 2002. Spectra of extremely reduced assemblages: implications for mercury. Meteoritics Planet. Sci. 37, 1233–1244.

Bus, S.J., 1999. Compositional structure in the asteroid belt. Ph. D. Thesis, Massachusetts Institute of Technology, Cambridge, MA.

Bus, S.J., Binzel, R.P., 2002a. Phase II of the small main-belt asteroid spectroscopic survey: the observations. Icarus 158, 106–145.

Bus, S.J., Binzel, R.P., 2002b. Phase II of the small main-belt asteroid spectroscopic survey: a feature-based taxonomy. Icarus 158, 146–177.

Bus, S.J., Vilas, F., Barucci, M.A., 2002. Visible-wavelength spectroscopy of asteroids. In: Bottke, W.F., Cellino, A., Paolicchi, P., Binzel, R.P. (Eds.), Asteroids III. University of Arizona Press, Tucson, pp. 169–182.

Cruikshank, D.P., Hartmann, W.K., 1984. The meteorite–asteroid connection: two olivine-rich asteroids. Science 223, 281–283.

Delbo, M., Harris, A.W., Binzel, R.P., Pravec, P., Davies, J.K., 2003. Keck observations of near-earth asteroids in the thermal infrared. Icarus 166, 116–130.

Gaffey, M.J., Reed, K.L., Kelley, M.S., 1992. Relationship of E-type Apollo asteroid 3103 (1982 BB) to the enstatite achondrite meteorites and the Hungaria asteroids. Icarus 100, 95–109.

Gaffey, M.J., Bell, J.F., Brown, R.H., Burbine, T.H., Piatek, J.L., Reed, K.L., Chaky, D.A., 1993. Mineralogical variations within the S-type asteroid class. Icarus 106, 573–602.

Kibrick, R.I., Allen, S.L., Conrad, A., 2000. Remote observing with the Keck telescopes from US mainland. In: Kibrick, R.I., Wallander, A., (eds.), Advanced Global Communications Technologies for Astronomy. Proceedings of the SPIE, Vol. 4011, pp. 84–92.

Landolt, A.U., 1973. UBV photoelectric sequences in celestial equatorial selected areas 92-115. Astron. J. 78, 959–981.

Martin, R., Johnson, P., Cash, J., 2000. Remote observing capabilities of the Wyoming infraRed observatory. Bull. Am. Astron. Soc. 52, 13.

Oke, J.B., Gunn, J.E., 1982. An efficient low resolution and moderate resolution spectrograph for the Hale telescope. PASP 94, 586–594.

Rayner, J.T., Toomey, D.W., Onaka, P.M., Denault, A.J., Stahlberger, W.E., Watanabe, D.Y., Wang, S., 1998. SpeX: a medium-resolution IR spectrograph for IRTF. Proc. SPIE 3354, 468–479.

Tedesco, E.F., 1989. Asteroid magnitudes, UBV colors, and IRAS albedos and diameters. In: Binzel, R.P., Gehrels, T., Matthews, M.S. (Eds.), Asteroids II. University of Arizona Press, Tucson, pp. 1090–1138.

Tholen, D.J., Barucci, M.A., 1989. Asteroid taxonomy. In: Binzel, R.P., Gehrels, T., Matthews, M.S. (Eds.), Asteroids II. University of Arizona Press, Tucson, pp. 298–315.

Williams, J.G., Wetherill, G., 1973. Long-term orbital evolution of 1685 Toro. Astron. J. 78, 510–515.

Available online at www.sciencedirect.com
SCIENCE DIRECT®
New Astronomy 9 (2004) 343–351
New Astronomy
www.elsevier.com/locate/newast

Near-IR spectroscopy of asteroids 21 Lutetia, 89 Julia, 140 Siwa, 2181 Fogelin and 5480 (1989YK8), potential targets for the Rosetta mission; remote observations campaign on IRTF

Mirel Birlan [a,b,*], Maria Antonietta Barucci [a], Pierre Vernazza [a], Marcello Fulchignoni [a], Richard P. Binzel [c], Schelte J. Bus [d], Irina Belskaya [a,e], Sonia Fornasier [f]

[a] *Observatoire de Paris-Meudon, LESIA, 5 Place Jules Janssen, 92195 Meudon Cedex, CNRS, France*
[b] *Astronomical Institute of the Romanian Academy, Str Cutitul de Argint n 5, Bucharest 28, Romania*
[c] *Department of Earth, Atmospheric and Planetary Sciences, Massachusetts Institute of Technology, Cambridge, MA 02139, USA*
[d] *Institute for Astronomy, 640 North A'ohoku Place, Hilo, HI 96720, USA*
[e] *Astronomical Observatory of Kharkov University, Sumskaya str. 35, Kharkov 310022, Ukraine*
[f] *Astronomical Department of Padova, Vicolo dell'Osservatorio 2, 35122 Padova, Italy*

Received 27 October 2003; received in revised form 5 December 2003; accepted 10 December 2003

Communicated by W.D. Cochran

Abstract

In the frame of the international campaign to observe potential target asteroids for the Rosetta mission, remote observations have been carried out between Observatoire de Paris, in Meudon-France and the NASA Infrared Telescope Facility on Mauna Kea. The SpeX instrument was used in the 0.8–2.5 μm spectral region, for two observing runs in March and June 2003. This paper presents near-IR spectra of the asteroids 21 Lutetia, 89 Julia, 140 Siwa, 2181 Fogelin and 5480 (1989YK8). Near-IR spectra of the asteroids 21 Lutetia and 140 Siwa are flat and featureless. The spectrum of 89 Julia reveals absorption bands around 1 and 2 μm, which may indicate the presence of olivine and olivine-pyroxene mixtures and confirm the S-type designation. The small main-belt asteroids 2181 Fogelin and 5480 (1989YK8) are investigated spectroscopically for the first time. Near-IR spectra of these asteroids also show an absorption feature around 1 μm, which could be and indicator of igneous/metamorphic surface of the objects; new observations in visible as well as thermal albedo data are necessary to draw a reliable conclusion on the surface mineralogy of both asteroids.
© 2003 Elsevier B.V. All rights reserved.

* Corresponding author.
E-mail addresses: mbirlan@despace.obspm.fr, mirel.birlan@obspm.fr (M. Birlan).

1384-1076/$ - see front matter © 2003 Elsevier B.V. All rights reserved.
doi:10.1016/j.newast.2003.12.005

PACS: 95.45.+i; 95.85.Jq; 96.30.Ys

Keywords: Methods: miscellaneous; Techniques: spectroscopic; Minor planets: asteroids; Infrared: solar system

1. Introduction

The observational program presented in this paper is intimately linked to the scientific programme of the space mission Rosetta. The Rosetta mission was approved in 1993 as a Cornerstone Mission within the ESA's Horizons 2000 science programme. The original launch date for the mission was January 2003 and the scientific targets were assigned to be the nucleus of comet 46P/Wirtanen and two main-belt asteroids: 140 Siwa and 4979 Otawara. The main scientific goals of the Rosseta mission are to investigate 'in situ' primitive objects of the solar system and to find answers concerning the chemical composition of the primitive planetary nebula, thought to be 'frozen' in the comet nucleus and the asteroid mineralogical matrix.

Since 1993, several international campaigns of observations have been started in order to obtain a large amount of data for the targets of the Rosetta mission (Fornasier et al., 2003; LeBras et al., 2001; Barucci et al., 1998, etc.). The groundbased knowledge of these objects is essential to optimise the science return as well as the mission trajectory.

In January 2003 the European Space Agency decided to postpone the launch of the Rosetta, with a new launch date set to February 2004. This decision implied a new mission baseline: rendezvous with the comet P/Churyumov-Grasimenko and one or two asteroid fly-bys to be defined after the spacecraft interplanetary orbit insertion manoeuvre, when the total amount of available δv will be known. Several fly-bys scenarios have been studied and several possible asteroid targets have been found. These potential targets are poorly known and for this reason systematic observation are needed in order to significantly improve on our knowledge of the physics and the mineralogy of these objects.

In this paper we present the spectroscopic results obtained for five asteroids [21 Lutetia, 89 Julia, 140 Siwa, 2181 Fogelin and 5480 (1989YK8)], potential targets of the Rosetta mission. The 0.8–2.5 μm wavelength region was investigated using the SpeX instrument on IRTF-Hawaii, in 'remote observing' mode.

2. The observing protocol

The remote observations were conducted from Meudon-France, more than 12,000 km away from Hawaii, using several informational structures and networks. For the observers in Meudon, the observing hours occurred during relatively normal working daylight hours. Observation sessions began at 5 a.m. local time and ended at 5 p.m. local time. This type of observations between Meudon and IRTF/Hawaii was started in 2002 (Birlan and Binzel, 2002); since then, more than twenty nights of observations (in eight runs) were conducted from Meudon. The observations were realized through an ordinary network link, without the service quality warranty. Thus, the passband for our link was variable, a function of the traffic between Hawaii and Meudon.

During the remote observing run, the Observatoire de Paris team had the control of both the instrument/guider system and the spectrograph set-up and spectra acquisition. A permanent and constant audio/video link with the telescope operator is essential in order to administrate possible service interruptions. Two PC's running Linux were devoted to the telescope/spectrograph control. The X environment for the telescope and instrument control was exported from Mauna Kea to Meudon via two secure links (ssh tunnels). A third PC was used to keep the IP audio-video link open (webcam/Netmeeting at Meudon and Polycom ViewStation video-conference system on Mauna Kea). All software was re-initialized at the beginning of each night.

The communication lag was relatively small (approximately 0.5 s), and the image refresh time

was 2 s on the average. Real-time image display was performed mainly for verification purposed and preliminary analysis. At the completion of each run, all files were transferred to Meudon.

The SpeX instrument was utilized in low-resolution mode for this campaign. The observations were made in the 0.8–2.5 μm spectral interval. We used a 0.8 arcsec wide slit, with a 15 arcsec length and oriented North–South, which allowed us simultaneous measurements of the object and sky. The object position on the slit was alternated between two locations referred to as the A and B positions. The seeing varied between 0.7 and 1.8 arcsec during the observing runs and the humidity was in the 25–55% range. The automatic guiding mode of the telescope was used for spectra acquisition.

The asteroids were observed in during two observing runs: 28–30 March 2003 and 5 July 2003. The observed objects are summarized in Table 1. We also observed the standard stars SA 98-978, SA 102-1081, SA 105-56, SA 107-684, SA 113-276, SA 115-271, HD 28099, HD 88618 and 16 CyB. Flat-fields and Argon lamp arc images were taken each night and used for data reduction.

Our strategy was to observe all asteroids as close to the zenith as possible. Thus, we managed to observe with an airmass less then 1.6 for all targets except 2181 Fogelin, which we could only observe with an airmass in the 1.7–1.78 range. Science exposures were alternated with standard stars spectra exposures, the latter taken to cover the 1–1.8 airmass range.

In order to obtain a S/N in the 80–150 range, we needed 20–40 min of exposure time, depending on the asteroid magnitude and counting both the effective exposure and CCD camera readout time. This exposure time is unacceptable for a single near-IR spectrum due to the large variations in the atmospheric conditions (a single near-IR spectral exposure is usually no longer than 120 s). In order to obtain the required S/N, we obtained a number of 6–10 A and B exposure pairs (cycles) for both

Table 1
Potential asteroid targets for the Rosetta mission

Object	Date	a (a.u.)	e	i (deg)	Φ (deg)	V (mag)
21 Lutetia	March 30 2003	2.4347	0.1636	3.0645	14.6	11.32
89 Julia	March 30 2003	2.5519	0.1825	16.1437	13.2	11.39
140 Siwa	March 30 2003	2.7365	0.2153	3.1882	21.2	13.72
2181 Fogelin	July 5 2003	2.5918	0.1177	13.0205	11.2	16.59
5480 1989YK8	March 30 2003	3.1366	0.087	6.6717	12.7	16.25

Observation date, semimajor axis, eccentricity, inclination, phase angle and the apparent magnitude are presented for each asteroid.

Table 2
Exposure data for each asteroid

Object	UT (h m s)	Itime (s)	Cycles	Airmass
21 Lutetia	13 35 46	15	8	1.223
21 Lutetia	11 28 17	20	4	1.329
21 Lutetia	15 01 03	15	9	1.414
21 Lutetia	10 20 21	20	3	1.635
89 Julia	10 44 44	40	6	1.561
140 Siwa	07 06 07	120	8	1.000
140 Siwa	07 46 10	120	6	1.016
2181 Fogelin	12 10 35	2×60	4	1.769
2181 Fogelin	12 31 40	2×60	4	1.744
2181 Fogelin	12 55 17	2×60	4	1.740
5480 1989YK8	12 41 01	120	6	1.151
5480 1989YK8	14 36 01	120	6	1.230

The columns show the mean UT value for each series, the individual time for each spectrum (Itime), the number of cycles and the mean airmass of each series.

the asteroids – science exposures – and the standard stars. This constitutes *one series* of observations for each object. Details the science exposures are given in Table 2.

3. Data reduction and results

The major points of our reduction procedure are classic for the near-IR spectroscopy. We started by combining and normalizing flat-fields for each observing night. The resulting flats were later used for the reduction of spectra of both the asteroids and the standard stars. In order to minimize the atmospheric and telescope influence and to eliminate the influence of electronic bias level and the dark current, we subtracted the B position spectra from the A position spectra for each pair of exposures (cycle), in the assumption of quasi-homogeneous sky background during A plus B exposure pair. The result of the subtraction was flat fielded. For each object, we median combined the result of all cycles in each observing series. This technique produces one positive and one negative spectrum on the same image. Next step was the construction of an accurate spatial profile for the extraction of the spectra. The final step was the wavelength calibration.

The Spextool package (the description of the procedures are presented in Cushing et al., 2003) allowed us to perform following steps for both the asteroids and the standard stars: global flat-field and arc construction, possible non-linearity correction, addition of spectra of the same object, spatial profile determination of the spectrum in the image, aperture location, extraction of the spectrum, wavelength calibration and cleaning the spectra. The results are saved in both FITS and ASCII formats, as used by several image processing packages (like IDL, MIDAS and IRAF), respectively, dedicated plot/graphics software (Easyplot, Origin, Dataplot, etc.).

The next step in the process of data reductions was the calculation of the extinction coefficients. The solar analogs spectra were used to find the correspondent extinction coefficient for each wavelength. A "superstar" was created by summing appropriately weighted contributions of the standard stars. The resulting "superstar", corrected for atmospheric extinction, was used to obtain the spectral reflectance of asteroids at different airmasses. Careful choice of the "superstar", combined with several tests of shift between the spectrum of the asteroid and that of the superstar are very important in order to minimize the influence of the terrestrial atmosphere in the 1.4 and 1.9 μm spectral regions. In order to make more readable our spectra, we choose to eliminate these spectral regions. Moreover, the elimination of these spectral regions does not affect the conclusions of this article.

3.1. 21 Lutetia

With an estimated diameter of 95.5 ± 4.1 km – for an IRAS albedo of 0.221 ± 0.020 (Tedesco and Veeder, 1992) – 21 Lutetia belongs to the large asteroid class (diameter $\geqslant 100$ km). Its synodic period has been computed from several lightcurve analysis and the value is 8.17 ± 0.01 h (Zappala et al., 1984). Color analysis of the ECAS data (Zellner et al., 1985) designates the asteroid 21 Lutetia to be part of the *X* complex. Also, global ECAS and IRAS thermal albedo data analysis assign Lutetia to the M taxonomic type (Barucci et al., 1987; Tholen, 1989). The M type asteroids are considered to be part of the core of differentiated asteroids and the parent bodies of metallic meteorites. On the basis of SMASS II spectroscopic data, Bus and Binzel (2002) proposed the new taxonomic class *Xk* for the asteroid 21 Lutetia.

21 Lutetia was observed on UT 2003 March 29 for the entire night. Four series of exposures resulted in four IR spectra with S/N in the 90–140 range. In order to detect possible surface spectral features variations, our observations covered 65% of the synodic period. These spectra are presented in Fig. 1. However, a check of the physical ephemeris of 21 Lutetia revealed a close pole-on geometry of the asteroid, so our spectra are most probably dominated by the contribution of the same surface features on 21 Lutetia. There are no significant spectral features in the spectral region 0.8–2.5 μm and the slightly increasing slope varies around 0.3%.

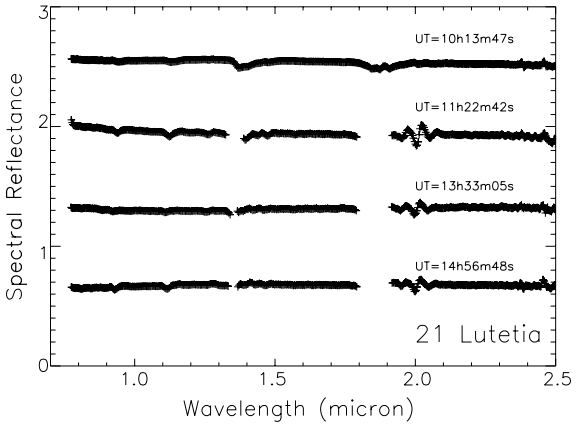

Fig. 1. The spectra of the asteroid 21 Lutetia. The IRTF spectra are offset for clarity and presented in chronological order. The beginning of each series of spectra (UT) was marked on the graph.

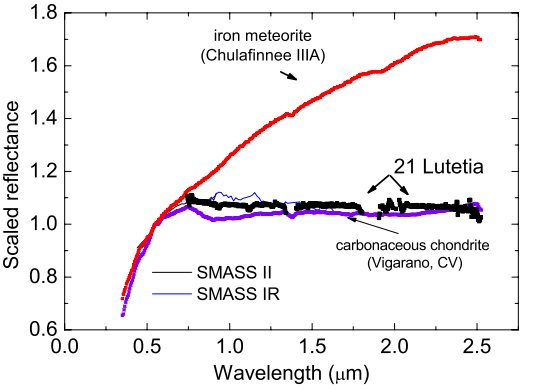

Fig. 2. The average spectrum of the asteroid 21 Lutetia. The SMASS II and SMASS IR data are plotted as solid lines. Our data is in agreement with the SMASSIR data over the 0.75–1.6 μm spectral interval. The comparison with Chulafinnee (iron meteorite) and Vigarano (carbonaceus chondrite) reveal the good match with the IR spectrum associated to carbon rich surfaces.

The lack of features in the spectrum of 21 Lutetia makes its taxonomic and compositional interpretation difficult. While the high IRAS albedo value of 0.221 leads to the previous M-type classification, we note there is an ambiguity in determining the albedo of Lutetia. An alternate low albedo value of 0.09 has been reported by Zellner et al. (1977) from polarimetric measurements and groundbased radiometric measurements.

In Fig. 2 we compare our measurements of Lutetia with others published in the literature. We found a good match with both SMASS IR data (spectral interval 0.8–1.6 μm) and the 52-color asteroid survey (Bell et al., 1988) spectrophotometric data. We also compare in Fig. 2 all of these Lutetia results with reflectance spectra of meteorites from Gaffey (1976). Our goal is to find which meteorites may be most analogous with Lutetia in terms of near-IR spectral properties. We note the spectrum of Lutetia is most qualitatively similar to the spectrum of the Vigarano meteorite, a CV3 carbonaceous chondrite, while being quite a poor match to the class IIIA iron meteorite Chulafinee. The purpose of our comparison is to note the difficulty of making a non-ambiguous interpretation of the composition of 21 Lutetia.

In Fig. 3 we plot the negative polarization depth versus the inversion angle (Belskaya and Lagerkvist, 1996) for both 21 Lutetia and a sample asteroids and meteorites. The asteroid 21 Lutetia has the largest inversion angle ever observed for the asteroids. The same peculiarly large inversion angle were found in the laboratory for the carbonaceous chondrites of the CV3 and CO3 samples. These types of chondrites are characterized by a low carbon content and thus relatively a larger

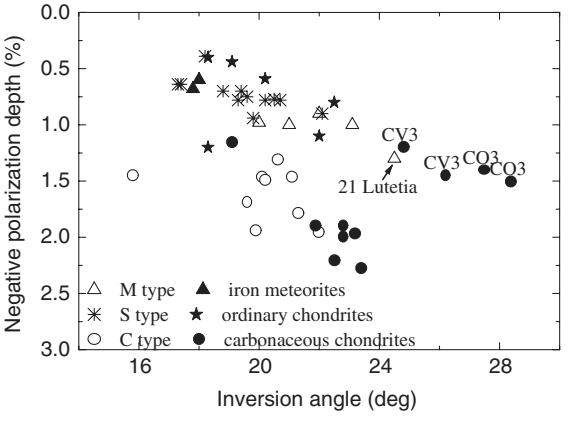

Fig. 3. Diagram of the negative polarization depth and the inversion angle of asteroids and meteorites from Belskaya and Lagerkvist (1996).

albedo when compared to other types (Zellner et al., 1977).

3.2. 89 Julia

The asteroid 89 Julia has an estimated diameter of 151.4 ± 3.1 km, for an IRAS albedo of 0.176 ± 0.007. Photometry of 89 Julia yields a synodic period of 11.387 ± 0.002 h (Schober and Lustig, 1975). Multivariate statistics classified the asteroid as part of the S cluster (Barucci et al., 1987; Tholen, 1989). The mineralogical classification of the S-type asteroids (Gaffey et al., 1993) based on the ECAS data and 52-color spectrophotometric Survey (Bell et al., 1988) data assigns 89 Julia (together with the asteroid 9 Metis) as 'ungrouped' S-asteroids. The main reason of this 'unclassification' is the long wavelength position of the 1 μm feature, which could be the presence of the abundant calcic clinopyroxene component (Gaffey et al., 1993). Based on the SMASS II data, Bus and Binzel (2002) proposed a K cluster membership (derived from the S cluster) for 89 Julia.

The asteroid spectrum was obtained for an effective integration time of 10 min, with a S/N ratio of 90 in both A and B beams. This spectrum presents a significant positive slope in the region 1.1–1.5 μm and a plateau in the 1.7–1.9 μm and 2.2–2.5 μm spectral regions. In Fig. 4 the IR spectrum of Julia was overlapped with the SMASS II spectrum in the 0.78–0.92 μm spectral region. We confirm a broad absorption band at 1 μm, typical of the silicate rich minerals. We also confirm a global trend of the spectral reflectance, which increases in the near-IR. The influence of atmospheric water absorbtion on the spectra is visible around 1.4 and 1.9 μm. The geometry of observations was fairly unfavourable for this asteroid (airmass = 1.56).

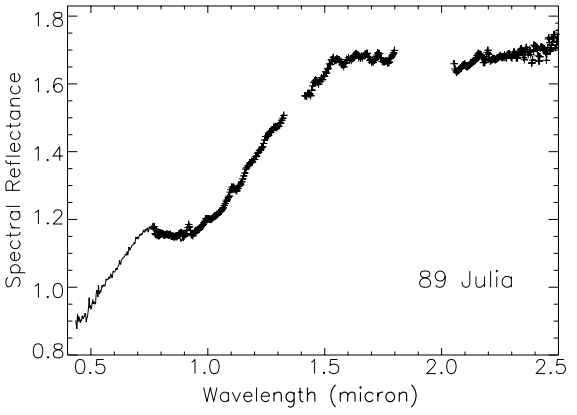

Fig. 4. The spectrum of the asteroid 89 Julia. The IRTF spectrum was overlapped with the SMASS II visible spectrum in the region 0.78–0.92 μm.

In order to calculate the center of 1 μm absorbtion band (designated as Band I in the literature), the continuum was defined between the local maximum of spectral reflectance at 0.76 μm and the small shoulder of the spectrum at 1.27 μm. The spectrum was then continuum subtracted and the result was fitted with an order three polynomial function. We find the center of the feature localized at 1.01 ± 0.06 μm, which is a slightly shorter wavelength than the one found by Gaffey et al. (1993).

3.3. 140 Siwa

140 Siwa is one of the initial targets of the Rosetta mission (departure in January 2003). One of the proposed scenarios (February 2003) suggests keeping this asteroid as a candidate for flyby. This was our motivation to observe it.

An IRAS albedo of 0.068 ± 0.004 for the asteroid 140 Siwa allows the calculation of a diameter of 109.8 ± 3.0 km. Lightcurve analysis for two runs in 2000 (LeBras et al., 2001) reveals a slow-rotator asteroid; the composite lightcurve presents an amplitude of 0.1 magnitudes and its synodic period was estimated at 18.495 ± 0.005 h.

Two series of near-IR spectra were obtained in March 30, 2003, with the ratio S/N of 50 and 70 (obtained in both A and B beams) for the spectrum obtained at airmass 1.001 and 1.018, respectively, (Fig. 5). The IR spectrum of 140 Siwa does not contain deep absorption features corresponding to mafic minerals. The spectrum slope is slightly positive, with a value 1% (0.8% and 0.7%, respectively), which confirms the slope trend of its spectrum (LeBras et al., 2001). We confirm a typical neutral spectrum of consistent with the a C-type asteroid; the IRAS albedo for 140 Siwa also fits very well the average value of C taxonomic

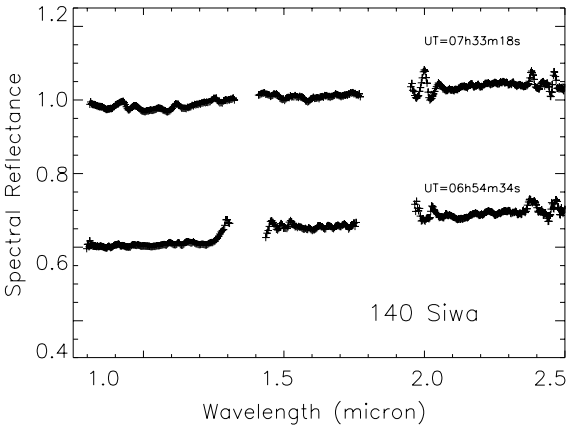

Fig. 5. The spectra of the asteroid 140 Siwa. The spectra were offset for clarity and the UT represents the beginning of each series of exposures.

class. The near-IR slope of our spectra is slightly different of those of a typical C-type asteroid but this alone cannot indicate a different mineralogy of the surface.

Fig. 6 shows the computed a global IRTF spectrum for the asteroid 140 Siwa overlapped with SMASS II data (the overlap is only for the 0.7–0.85 μm region). This composite spectrum was compared to meteorite reflectance spectra from the

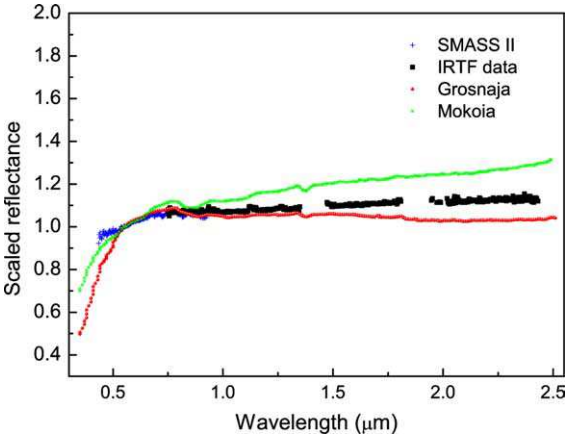

Fig. 6. Cumulated spectral reflectance of the asteroid 140 Siwa obtained during the IRTF run. The spectrum was overlapped with the SMASS II data in the 0.70–0.85 μm spectral region. The spectrum is similar to CV3 meteorites Grosnaja and Mokoia. The surface of 140 Siwa shows similar properties with carbonaceous chondrite meteorites, with a reflectance trend between the curves for the two meteorites.

Gaffey database. There is no meteorite spectrum that fits our spectrum very well. However, the carbonaceous chondrite meteorites spectra are similar to our spectrum and the asteroid spectral reflectance spans a value in the range of CV3 meteorite class. The nearest spectra are those of Grosnaja and Mokoia meteorites.

3.4. 2181 Fogelin

No physical data are available in the literature for the asteroid 2181 Fogelin. Thus, we can only roughly estimate its diameter. Following the asteroid mass distribution proposed by Kresak (1977) and the H magnitude of 2181 Fogelin, the diameter could be in the 12–18 km range. A second estimate can be made using an empirical relationship between the absolute magnitude, diameter and geometric albedo (Fowler and Chillemi, 1992):

$$\log D = 3.1236 - 0.5 \cdot \log p_v - 0.2 \cdot H. \quad (1)$$

Using an IRAS albedo of 0.05–0.25 we find a 12–22 km diameter for the asteroid.

The observations of 2181 Fogelin were carried out in July, 5, 2003, with the ratio S/N of 80 in both A and B beams. The geometry of observation (airmass = 1.7) was unfavourable. However, the final spectrum is the average of 32 individual spectra, which can alleviate the high airmass problem. The IR spectrum presented in Fig. 7 shows the large

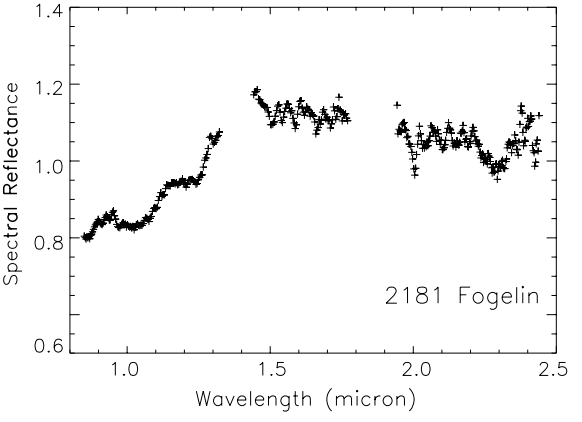

Fig. 7. The spectrum of the asteroid 2181 Fogelin, normalized to 1.275 μm, the maximum of J filter.

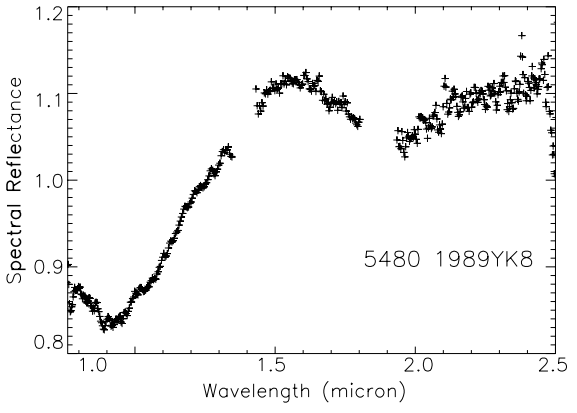

Fig. 8. The spectrum of the asteroid 5480 1989YK8, normalized to 1.275 μm, the maximum of J filter.

broad band absorbtion around 1 μm, typical of mafic minerals. The slightly positive slope in the 1.2–1.5 μm wavelength region doesn't allow us to classify this object as a S-type asteroid. Further observations in the visible region as well as thermal albedo data are necessary to make a taxonomic class assignment for this asteroid.

3.5. 5480 1989 YK8

There are no previous photometric or spectroscopic data available for the asteroid 5480 1989YK8. The same methods used for 2181 Fogelin have been used to compute its theoretical diameter. The diameter spans the 13–20 km range (following Kresak, 1977) and 13–31 km following the diameter empirical formula (1), used with IRAS albedos in the 0.05–0.25 range.

The asteroid was observed on March, 30, 2003 and the final spectrum S/N ratio is around 100 for the A and B positions in the slit. The analysis of the 0.8–2.3 μm region reveals an absorption band around 1 μm (Fig. 8). The global tendency in near-IR could justify a S-type asteroid classification; however, a visible spectrum and thermal albedo data are necessary for a taxonomical assignment.

4. Conclusions

Five asteroids potential targets for the Rosetta mission have been observed in the 0.8–2.5 μm spectral range: 21 Lutetia, 89 Julia, 140 Siwa, 2181 Fogelin and 5480 (1989YK8). We confirm the flat near-IR spectrum of 21 Lutetia. The near-IR spectrum of 89 Julia contains features confirming the initial idea that it belongs to the 'heated' bodies, possible to the S or K taxonomic class. A value 1.01 ± 0.06 μm was found for the center of the Band I. The asteroid 140 Siwa spectrum presents a slightly positive slope and there are no major mineralogical signatures; we confirm the assignment of the asteroid as an 'unheated' asteroid.

The small asteroids 2181 Fogelin and 5480 (1989YK8) were observed spectroscopically for the first time. Our data shows the presence of a large (and weak) absorption band around 1 μm for both asteroids; new observations in visible and infrared are necessary to draw a reliable conclusion concerning their surface mineralogy.

The remote observations between IRTF and Observatoire de Paris-Meudon proved to be a robust and handy observing technique. It offered full access to the command line of the spectrograph and to several telescope controls (focus, tracking, etc.). We consider our observing program entirely accomplished without any discernable difference in the typical amount of spectra obtained in remote observations mode versus the local observing mode.

Acknowledgements

The authors are grateful to Paul Hardersen for useful comments that improved our article. We are indebted to Tony Denault who answered many questions prior to our runs about the Polycom system and exporting of X-windows for SpeX and guiding system, to Miranda Hawarden-Ogata for the administration system support and to Paul Sears and Bill Golish, the telescope operators during the remote observing runs.

References

Barucci, M.A., Doressoundiram, A., Fulchignoni, M., Florczak, M., Lazzarin, M., Angeli, C., 1998. P&SS 46, 75.

Barucci, M.A., Capria, M.T., Coradini, A., Fulchignoni, M., 1987. Icar 72, 304.

Bell, J.F, Hawke, B.R., Owensby P.D, Gaffey, M.J., 1988. The 52-color asteroid survey; final results and interpretation. Lunar Planet. Sci. XIX.

Belskaya, I., Lagerkvist, C.-I., 1996. P&SS 44, 783.

Birlan, M., Binzel, R.P., 2002. Paris Observatory Remote Observing January–May 2002: Sharing the Experience to Educational Astronomy, Global Hands-On Universe Conference Proceedings, Paris, July.

Bus, S.J., Binzel, R.P., 2002. Icar 158, 146.

Cushing, M.C., Vacca, W.D., Rayner, J.T., 2003. Spextool: a spectral extraction package for SpeX, a 0.8–5.5 μm cross-dispersed spectrograph, PASP (in press), http://irtf-web.ifa.hawaii.edu/Facility/spex/.

Fornasier, S., Barucci, M.A., Binzel, R.P., et al., 2003. A&A 398, 327.

Fowler, J.W., Chillemi, J.R., 1992. IRAS asteroid data processing. In: Tedesco, E.F., Veeder, G.J., Fowler, J.W., Chillemi, J.R. (Eds.), The IRAS Minor Planet Survey. Technical Report PL-TR-92-2049, Phillips Laboratory, Hanscom AF Base, MA.

Gaffey, M.J., 1976. JGR 81, 905.

Gaffey, M.J., Burbine, T.H., Piatek, J.L., Reed, K.L., Chaky, D.A., Bell, J.F., Brown, R.H., 1993. Icar 106, 573.

Kresak, L., 1977. BAICz, n. 28, 82.

Le Bras, A., Dotto, E., Fulchignoni, M., Doressoundiram, A., Barucci, M.A., Le Mouelic, S., Forni, O., Quirico, E., 2001. A&A 379, 660.

Schober, H.J., Lustig, G., 1975. Icar 25, 339.

Tedesco, E.F., Veeder, G.J., 1992. IMPS albedos and diameter catalog(FP102). In: Tedesco, E.F., Veeder, G.J., Fowler, J.W., Chillemi, J.R., The IRAS Minor Planet Survey. Technical Report PL-TR-92-2049, Phillips Laboratory, Hanscom AF Base, MA.

Tholen, D., 1989. Asteroid taxonomic classifications. In: Asteroids II. University of Arizona Press, AZ, pp. 1139–1150.

Zappala, V., DiMartino, M., Knezevic, Z., Djurasevic, G., 1984. A&A 130 (1), 208.

Zellner, B., Tholen, D.J., Tedesco, E.F., 1985. Icar 61, 355.

Zellner, B., Leake, M., LeBerte, T., Duseaux, M., Dollfus, A., 1977. The asteroid albedo scale. II. Laboratory polarimetry of meteorites. In: Proceedings of the Lunar Science Conference, 8th ed. Pergamon Press, Oxford, pp. 1091–1110.

A&A 430, 313–317 (2005)
DOI: 10.1051/0004-6361:20041505
© ESO 2005

Astronomy & Astrophysics

Asteroid target selection for the new Rosetta mission baseline

21 Lutetia and 2867 Steins⋆

M. A. Barucci[1], M. Fulchignoni[1], S. Fornasier[2], E. Dotto[3], P. Vernazza[1], M. Birlan[4], R. P. Binzel[5], J. Carvano[1], F. Merlin[1], C. Barbieri[2], and I. Belskaya[6]

[1] LESIA, Observatoire de Paris, 92195 Meudon Principal Cedex, France
e-mail: antonella.barucci@obspm.fr
[2] Astronomy Department, Padova University, Vicolo dell'Osservatorio 2, 35122 Padova, Italy
[3] INAF – Osservatorio Astronomico di Roma, via Frascati 33, 00040 Monte Porzio Catone, Roma, Italy
[4] IMCCE, Observatoire de Paris, 75014 Paris, France
[5] Dep. of Earth, Atmosph. and Planetary Sciences, Massachusetts Institute of Technology, Cambridge, MA 02139, USA
[6] Astronomical Observatory of Kharkiv National University, Ukrania

Received 22 June 2004 / Accepted 18 September 2004

Abstract. The new Rosetta mission baseline to the comet 67P/Churyumov-Gerasimenko includes two asteroid fly-bys. To help in target selection we studied all the candidates of all the possible scenarios. Observations have been carried out at ESO-NTT (La Silla, Chile), TNG (Canaries), and NASA-IRTF (Hawaii) telescopes, in order to determine the taxonomy of all the candidates. The asteroid targets were chosen after the spacecraft interplanetary orbit insertion manoeuvre, when the available total amount of ΔV was known. On the basis of our analysis and the available of ΔV, we recommended to the ESA Science Working Group the asteroids 21 Lutetia and 2867 Steins as targets for the Rosetta mission. The nature of Lutetia is still controversial. Lutetia's spectral properties may be consistent with a composition similar to carbonaceous chondrite meteorites. The spectral properties of Steins suggest a more extensive thermal history. Steins may have a composition similar to relatively rare enstatite chondrite/achondrite meteorites.

Key words. minor planets, asteroids – techniques: spectroscopic

1. Introduction

In 1993, the European Space Agency (ESA) selected the Rosetta mission including a rendezvous with in situ investigation of a comet and at least one (or more probably two) fly-bys of asteroids. The aim of the mission is to investigate the origin of the Solar System through the composition of planetesimals and their origin over the last 4.6 billion years.

In January 2003, ESA decided to postpone the launch of the spacecraft due to problems with the launcher (Barucci et al. 2004). The new baseline mission included a long orbital rendezvous with the 67P/Churyumov-Gerasimenko comet nucleus and one or two asteroid fly-bys. Several single or double fly-by scenarios were designed (Table 1), depending on the total ΔV available after the spacecraft interplanetary orbit insertion manoeuvre. In December 2003, the asteroid 2513 Baetsle was included on the basis of the pre-launch resource budget as baseline target, due to the minimum extra ΔV required to reach it (only 19 m/s).

Table 1. Double and single asteroid mission opportunity with fly-by between 2008 and 2010. The listed ΔV values were estimated before the launch.

Double fly-by	ΔV m/s	Single fly-by	ΔV m/s
Rhodia + Lutetia	159	Lutetia	125
Steins + Lutetia	139	Rhodia	97
Luichewoo + Lutetia	129	Steins	57
Baetsle + Izvekov	73	Sofala	101
Baetsle + Fogelin	79	Fogelin	18
Luichewoo + Izvekov	32	Baetsle	19
Rhodia + Izvekov	112	Luichewoo	32
Rhodia + Fogelin	113	Carrera	102
Steins + Izvekov	77	Izvekov	15
Sofala + Izvekov	146		
Steins + Fogelin	83		
Luichewoo + Fogelin	35		

The mission was launched successfully on March 2nd 2004. The spacecraft started its journey to the comet 67P/Churyumov-Gerasimenko that will be reached on 2014, after three Earth and one Mars gravity assisted swing-bys and

⋆ Based on observations collected at ESO-La Silla, NASA/IRTF and TNG-Canaries.

Table 2. Observational circumstances of asteroid targets for the Rosetta mission.

Object	Night	UT-start (hh:mm)	T_{exp} (s)	Tel.	Instr.	Grism/prism	Slit (arcsec)	airm.
437 Rhodia	25 Jan. 04	15:35	600	IRTF	SpeX	0.8–2.5 μm	0.8	1.30
437 Rhodia	03 Mar. 04	10:07	960	IRTF	SpeX	0.8–2.5 μm	0.8	1.17
1393 Sofala	25 Jan. 04	15:00	720	IRTF	SpeX	0.8–2.5 μm	0.8	1.05
2513 Baetsle	25 Jan. 04	14:21	1320	IRTF	SpeX	0.8–2.5 μm	0.8	1.10
2867 Steins	25 Jan. 04	13:21	1100	IRTF	SpeX	0.8–2.5 μm	0.8	1.02
3050 Carrera	25 Jan. 04	11:00	1200	IRTF	SpeX	0.8–2.5 μm	0.8	1.08
21 Lutetia	26 May 04	10:13	660	NTT	EMMI	GRISM 1 (0.4–0.95 μm)	1.5	1.55
2513 Baetsle	30 Jan. 04	8:40	960	NTT	EMMI	GRISM 1 (0.4–0.95 μm)	1.5	1.13
2867 Steins	29 Jan. 04	7:58	720	NTT	EMMI	GRISM 1 (0.4–0.95 μm)	1.0	1.40
2867 Steins	25 May 04	23:28	1200	NTT	EMMI	GRISM 1 (0.4–0.95 μm)	1.5	1.41
3050 Carrera	30 Jan. 04	6:50	960	NTT	EMMI	GRISM 1 (0.4–0.95 μm)	1.5	1.29
5538 Luichewoo	29 Jan. 04	7:00	1920	NTT	EMMI	GRISM 1 (0.4–0.95 μm)	1.0	1.20
437 Rhodia	29 Feb. 04	02:42	180	TNG	DOLORES	LR-R (0.51–0.95 μm)	1.5	1.28
1393 Sofala	29 Feb. 04	03:46	360	TNG	DOLORES	LR-R (0.51–0.95 μm)	1.5	1.09
2513 Baetsle	29 Feb. 04	04:06	1200	TNG	DOLORES	LR-R (0.51–0.95 μm)	1.5	1.31
3418 Izvekov	29 Feb. 04	02:18	480	TNG	DOLORES	LR-R (0.51–0.95 μm)	1.5	1.07
1393 Sofala	1 Mar. 04	05:08	480	TNG	NICS	AMICI (0.8–2.5 μm)	1.5	1.25
2513 Baetsle	2 Mar. 04	02:44	1920	TNG	NICS	AMICI (0.8–2.5 μm)	1.5	1.19
3418 Izvekov	2 Mar. 04	01:38	1920	TNG	NICS	AMICI (0.8–2.5 μm)	1.5	1.08
5538 Luichewoo	2 Mar. 04	03:51	1920	TNG	NICS	AMICI (0.8–2.5 μm)	1.5	1.32

the asteroid fly-bys. Due to the optimal launch conditions, the available remaining ΔV is enough to fly-by two asteroids. To help in the selection of the best targets for scientific return, we observed all the possible candidates by visible (V) and near-infrared (NIR) spectroscopy. In this paper we report the results of the observational campaign as well as the characterization of the selected targets.

2. Observations and data reduction

Visible and near-infrared spectroscopic observations were performed at the ESO 3.5 m New Technology Telescope (NTT, La Silla, Chile), the 3.5 m Telescopio Nazionale Galileo (TNG, La Palma, Spain), and the 3 m NASA Infrared Telescope Facility (IRTF, Hawaii, USA). The circumstances of these observations are summarized in Table 2. During each observing run we also acquired bias, flat-field, calibration lamp and several solar analog star spectra at different intervals throughout the night.

The observations at IRTF were performed in remote mode from the Observatoire de Paris-Meudon (Binzel et al. 2004; Birlan et al. 2004). The NIR acquisition procedure was the same both for the TNG and IRTF telescopes, consisting of cycle series of 4 images each (ABBA cycle). The images had an exposure time of 120 s each, and were taken in two different positions along the slit, named A and B, offsetting the telescope. This technique obtains near-simultaneous images for sky and bias subtraction. The ABBA cycles were repeated several times for the fainter objects. The total exposure time for each object is indicated in Table 2.

Spectra were reduced using standard data reduction procedures with the software package Midas (e.g. Fornasier & Lazzarin 2001; Fornasier et al. 2003). The asteroid relative reflectance has been obtained by division of the asteroid spectrum with that one of the solar analog star closest in time and airmass to the asteroid. For the IRTF data, the asteroid spectrum has been divided by a "superstar", created by summing appropriately weighted contributions of several observed analog stars, corrected for atmospheric extinction and computed at the same airmass of the asteroids.

3. Data analysis and discussion

We obtained the first V+NIR spectra of seven out of the nine asteroid candidates listed in Table 1 (437 Rhodia, 1393 Sofala, 2513 Baetsle, 2867 Steins, 3050 Carrera, 3418 Izvekov, and 5538 Luichewoo). A visible spectrum of 21 Lutetia has been also obtained and reported in Fig. 2. The NIR spectra of Lutetia and Fogelin have been recently published by our group (Birlan et al. 2004).

All the objects reported in Fig. 1 seem to belong to the S taxonomic class because of well defined 1 and 2 μm silicate bands. Spectra shown in Fig. 2 have flatter behaviors. The presence of the absorption band at 0.9 μm in the spectra of Rhodia together with its high albedo value (0.56, IRAS data: Tedesco et al. 1992) suggests a possible classification as an E-type asteroids; Carrera has a similar spectral behaviour with the presence of the peculiar 0.9 μm band and might also be an E type asteroid, even if the knowledge of its albedo is necessary to make a definitive taxonomic class assignment. Izvekov has a very peculiar flat spectrum, typical of primitive dark objects like B- or C-type. The spectral behaviour of Steins seems to suggest that it belongs to E-type class. Spectra of the same object obtained during different epochs are essentially the same. For Sofala a visible spectrum was

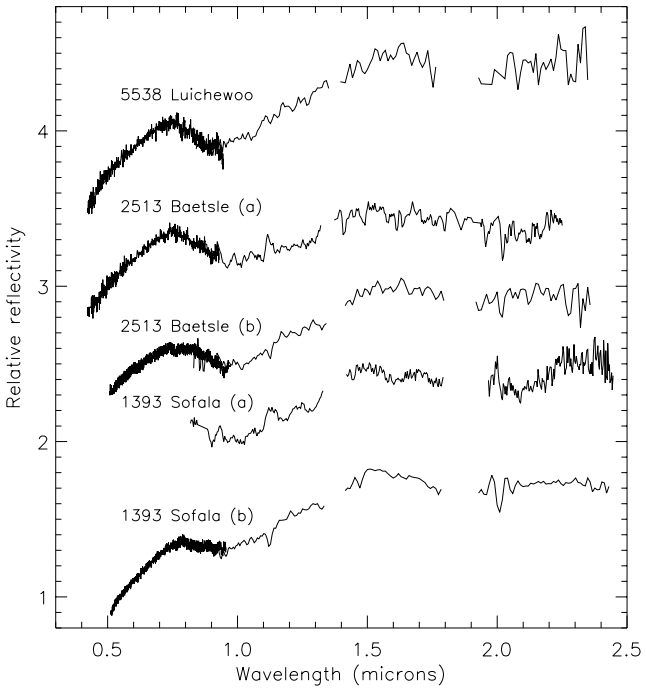

Fig. 1. V and NIR spectra of Luichewoo, Baetsle, and Sofala. For Baetsle and Sofala, the spectra (a) include V data obtained at NTT and NIR spectra obtained at IRTF, while spectra (b) have been obtained at TNG. All the spectra are normalized at 0.55 μm and shifted by 0.7 for clarity. All these objects have been classified as S-type.

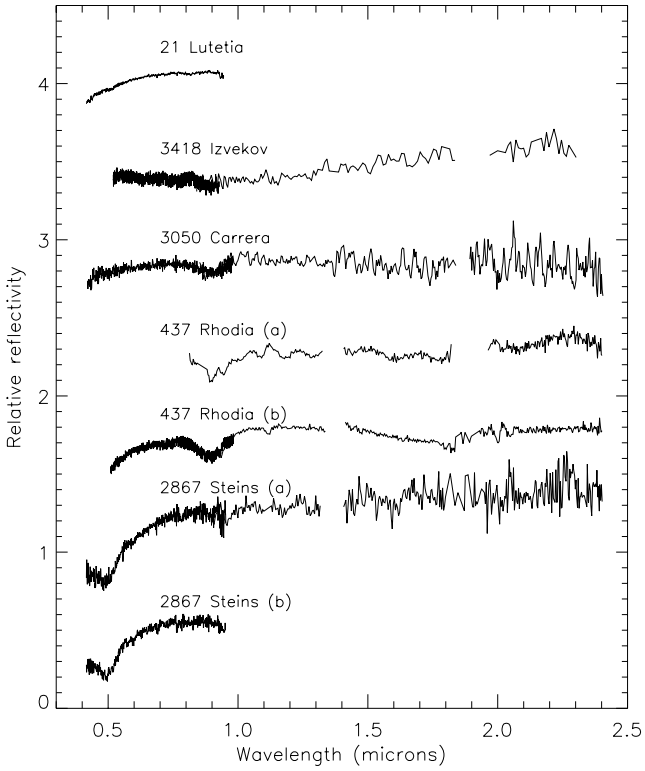

Fig. 2. V spectrum of Lutetia, and V and NIR spectra of Izvekov, Carrera, Rhodia, and Steins. The NIR spectrum (a) of Rhodia has been obtained on January 2004, while the NIR spectrum (b) has been obtained on March 2004. The V spectrum (b) of Steins has been obtained on May 2004. All the spectra are normalized at 0.55 μm and shifted by 0.6 for clarity.

already published by Xu et al. (1995). We confirm their S-type classification.

4. Target selection and characterization

Analyzing the list of possible targets and the relative available data, we strongly recommended the inclusion of asteroid 21 Lutetia in the Rosetta baseline because of its high interest. In fact it is the only object of the list which will allow the radio science experiment to measure the mass, and consequently to deduce the bulk density.

After the insertion manoeuvre of Rosetta into its interplanetary orbit, the available ΔV for the asteroid encounters was enough to allow the selection of any pair of asteroids listed in Table 1 for a double fly-by, except for the Rhodia-Lutetia one. The two remaining pairs which include 21 Lutetia are Steins-Lutetia and Luichewoo-Lutetia. As Luichewoo is a S-type (S class asteroids have already been visited by space missions), we exclude it from the possible baseline.

On the basis of the obtained spectra, we suggested Lutetia and Steins as the best asteroid targets for the Rosetta mission. In fact, these asteroids seem to be peculiar and show spectral behaviors different from the previous asteroid targets of space missions.

21 Lutetia was discovered in 1852 by H. Goldchmidt at the Paris Observatory. The name Lutetia derives from the Roman name of Paris (Lutetia Parisorum) and was given to the asteroid to honour the French capital. 21 Lutetia is the largest asteroid out of the possible candidates (IRAS diameter of 95.8 ± 4.1 km). The main orbital and physical characteristics are listed in Table 3. The rotational period of 8.17 ± 0.01 h has been determined by Zappalá et al. (1984). The spin vector direction of Lutetia has been computed by several authors (see Magri et al. 1999 for details) giving different pole solutions. The prograde rotation state was in agreement with the different methods and determinations. Torppa et al. (2003), analysing all the available lightcurves, computed pole coordinates and a model with sharp and irregular shape (see Table 3).

Because of the high IRAS albedo, Lutetia was previously classified as M-type by Barucci et al. (1987) and Tholen (1989) and was supposed to be a parent body of iron meteorites. Hiroi et al. (1993) found a good fit with the M meteorite Mundrabilla under particular ad hoc conditions. Bus & Binzel (2002) proposed for it a new class X_k. Further observations have shown that its infrared spectrum is unusually flat compared to other M asteroids (Howell et al. 1994; Burbine & Binzel 2000). Moreover the observations obtained at IRTF (Birlan et al. 2004) suggested a similarity with the carbonaceous chondrite spectra which characterize the C-type asteroid. Busarev et al. (2004) and Lazzarin et al. (2004), obtained several V spectra showing rotational phase variation with possible presence of features at 0.44 and 0.67 μm probably associated to hydrated silicates.

Many other characteristics seem to be in agreement with the carbonaceous chondrite analogy: the polarimetric properties (Belskaya & Lagerkvist 1996), lower radar albedo (Magri et al. 1999), and the 3 μm absorption feature diagnostic of water

Table 3. Orbital and physical characteristics of 21 Lutetia.

Semimajor axis (AU)	2.435
Eccentricity	0.164
Inclination (deg)	3.064
Taxonomic type	C (or M)
Synodical rotation period (h)	8.17 ± 0.01
Absolute magnitude	7.294
Slope parameter	0.110
IRAS D (km)	95.5 ± 4.1
IRAS albedo	0.221 ± 0.20
Pole solution from radar observations (Magri et al. 1999):	
$\lambda_1 = 228° \pm 11°$ $\beta_1 = +13° \pm 5°$	$\lambda_2 = 48° \pm 11°$ $\beta_2 = +5° \pm 5°$
Sense of rotation	Prograde
$2a \times 2b \times 2c$	$130 \times 104 \times 74$ km
Pole solution from lightcurve analysis (Torppa et al. 2003):	
$\lambda_1 = 220° \pm 10°$ $\beta_1 = +3° \pm 10°$	$\lambda_2 = 39° \pm 10°$ $\beta_2 = +3° \pm 10°$
$a/b = 1.2$; $b/c = 1.2$	

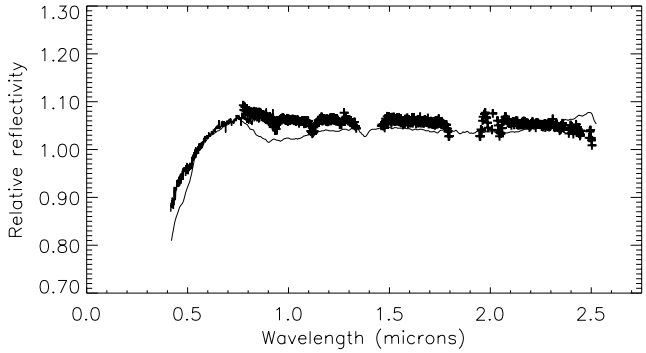

Fig. 3. Comparison of the Lutetia spectra (our V spectrum + the NIR one by Birlan et al. 2004) and the spectra of the CV3 carbonaceous chondrite meteorite Vigarano.

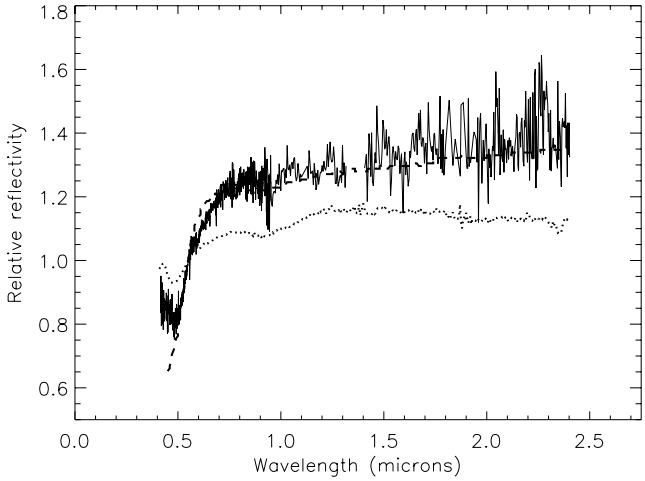

Fig. 4. Comparison of the spectrum of Steins and the spectra of the EL6 enstatite chondrite Atlanta (dashed line), and the enstatite achondrite (aubrite) ALH 78113 (dotted line). All the spectra are normalized at 0.55 μm.

of hydration (Rivkin et al. 2000). All these evidences suggest that Lutetia is an atypical M-type object. In Fig. 3 the NIR spectra of Lutetia by Birlan et al. (2004) with our visible spectrum is reported and compared with the spectrum of the CV3 carbonaceous chondrite Vigarano.

All of the information available for Lutetia are consistent with a primitive composition, except the high IRAS albedo value. New albedo determinations are needed to eliminate the doubts about the taxonomic classification of Lutetia, or to further enhance our view of this unusual object.

2867 Steins, discovered on 1969 by N. Chernykh at Nauchnyj, is a very small object and only few of its properties are known (Table 4). Assuming an albedo in the range 0.04–0.40, a diameter of 17.5–5.5 km can be estimated. Its rotational period of 6.06 ± 0.05 h and a lightcurve amplitude of 0.2 mag has been recently determined by Hicks & Bauer (2004).

The obtained V and NIR spectra (Figs. 2 and 4) show a strong feature at about 0.5 μm, a weaker feature at about 0.96 μm and a flat and featureless behaviour over 1 μm. This spectral behaviour is very similar to E-type asteroids, even if it is necessary that the albedo, still to be determined, would be larger than 0.3 to classify Steins as an E-type.

Table 4. Orbital and physical characteristics of 2867 Steins.

Semimajor axis (AU)	2.364
Eccentricity	0.146
Inclination (deg)	9.944
Taxonomic type	E
Synodical rotation period (h)	6.06 ± 0.05
Absolute magnitude (with slope par. assumed = 0.15)	12.561

E-type objects are thought to be differentiated bodies which experienced significant heating.

Analyzing the 0.5 μm feature observed in the spectra of some E-type asteroids, Burbine (2000) suggested that some kind of sulfides, such as troilite or pyrrhotite, could produce this feature. Troilite is a rare sulfide (FeS), abundant in meteorites. It is a known constituent of the aubrites but it is also a very dark agent not easily compatible with the high albedo of E-type asteroids (Fornasier & Lazzarin 2001). Moreover

the spectra available in literature of meteoritic and synthetic samples of troilite show quite different spectral behaviours. Also the band at about 0.5 μm changes in wavelength position and shape, probably due to the different crystal structure of each samples.

The spectral behaviour of Steins as shown in Figs. 2 and 4 is similar to that of the E-type asteroid 64 Angelina. According to the classification of Gaffey & Kelley (2004) and Clark et al. (2004), Steins would belong to the same group of Angelina, and its surface composition would include silicates and sulfides, like oldhamite (CaS). The presence of oldhamite on the surface of Angelina, has been also suggested by Burbine et al. (2002). Gaffey & Kelley (2004) suggested that this group of objects (also called E[II] subtype) may have surfaces composed of partial melts derived from E-chondrite-like parent bodies.

In order to investigate the surface composition of Steins we compared its V and NIR spectrum with the spectra of many meteorites available in literature. In Fig. 4 the spectrum of Steins is overlain onto with the spectra of an enstatite achondrite, and an enstatite chondrite. The enstatite chondrite Atlanta (EL6) presents a spectrum that fits very well the observed spectral behaviour of Steins with the exception of the feature at about 0.5 μm. The enstatite achondrite ALH 78113 (aubrite) presents spectral features at 0.5 μm and 0.96 similar to those of Steins' spectrum but with a flatter behaviour at $\lambda > 0.6$ μm.

The differences between asteroid spectra and those of meteorites and mineral assemblages could be due to the effects of space weathering (caused to long cosmic ray exposure) and of surface collisional processing (porosity, grain size distribution, aging of materials...).

5. Conclusions

On the basis of i) the results obtained by the spectroscopic observations; and ii) on the analysis of all the known physical properties of the candidates, we recommend target selection of 21 Lutetia and 2867 Steins. The Rosetta Science Working group supported our recommendation and the ESA's Rosetta Project included these asteroids in the new mission baseline. The fly-by with Steins will take place on September 5th, 2008, with a relative velocity of 8.6 km s^{-1} and the one with 21 Lutetia on July 10th 2010 with a relative velocity of 15 km s^{-1}. In particular, for the two selected candidates:

1. Lutetia represents the most interesting candidate, as it is the only one (among the possible targets) which will allow us to obtain, by radio science experiments, mass determination and density estimation. Moreover, if the primitive chondritic character of Lutetia will be confirmed, it will be well within the early Solar system scientific objectives of the mission.
2. After the choice of the first target, following the criteria to be within the available ΔV and to visit an interesting object, leads 2867 Steins as the best candidate for the other fly-by. Steins has relatively unusual spectral properties and may be classified as E-type object. Rosetta will perform the first in-situ exploration of a member of this rare class of objects, giving an answer to the question if its parent body underwent a total differentiation or a partial melting.

Ground-based observations are still needed to better define the physical and mineralogical characteristics of Lutetia and Steins. Further observations, in particular in the thermal infrared, are fundamental to know the albedo of both the objects. More information will allow us to optimize the science operations during the fly-bys.

References

Barucci, M. A., Capria, M. T., Coradini, A., & Fulchignoni, M. 1987, Icarus, 72, 304
Barucci, M. A., Fulchignoni, M., Belskaya, I., et al. 2004, in The new Rosetta targets, ASSL (Kluwer), 69
Belskaya, I. N., & Lagerkvist, C.-I. 1996, PSS, 44, 783
Binzel, R. P., Birlan, M., Bus, S. J., et al. 2004, PSS, 52, 291
Birlan, M., Barucci, M. A., Vernazza, P., et al. 2004, New Astron., 9, 343
Burbine, T. H. 2000, Ph.D. Thesis, MIT
Burbine, T. H., & Binzel, R. P. 2002, Icarus, 159, 468
Burbine, T. H., McCoy, T. J., Nittler, L. R., et al. 2002, Meteo. Planet. Sci., 37, 1233
Bus, B., & Binzel, R. 2002, Icarus 158, 146
Busarev, V., Bochokov, V., Prokof'eva, V., et al. 2004, in The new Rosetta targets, ASSL (Kluwer), in press
Clark, B. E., Bus, S. J., Rivkin, A. S., et al. 2004, J. Geo. Res., 109, 2001
Fornasier, S., & Lazzarin, M. 2001, Icarus, 152, 127
Fornasier, S., Barucci, M. A., Binzel, R. P., et al. 2003, A&A, 398, 327
Gaffey, M. J., & Kelley, M. S. 2004, LPI XXXV, 1812
Hicks, M. D., & Bauer, J. M. 2004, IAUC, 8315
Hiroi, T., Bell, J. F., Takeda, H., et al. 1993, Icarus, 102, 107
Howell, E. S., Merenyi, E., & Lebofsky, L. A. 1994, J. Geo. Res., 99, 10848
Lazzarin, M., Marchi, S., Magrin, S., & Barbieri, C. 2004, A&A, 425, L25
Magri, C., Ostro, S. J., Rosema, D. K., et al. 1999, Icarus, 140, 379
Rivkin, A. S., Howell, E. S., Lebofsky, L. A., et al. 2000, Icarus, 145, 351
Tedesco, E. F., & Veeder, G. F. 1992, in The IRAS Minor planet Survey, Tech. Rep. PL-TR-92-2049, Phillips Laboratory, Hanscom AF Base, MA
Tholen, D. 1989, in Asteroids II (Univ. of Arizona Press), 1139
Torppa, J., Kaasalainen, M., Michalowski, T., et al. 2003, Icarus, 164, 346
Xu, S., Binzel, R. P., Burbine, T. H., et al. 1995, Icarus, 115, 1
Zappalà, V., Di Martino, M., Knezevic, Z., et al. 1984, A&A, 130, 208

Highlights of Astronomy, Vol. 13
International Astronomical Union, 2003
O. Engvold, ed.

Rosetta Asteroid Candidates

M.Antonietta Barucci
LESIA, Observatory of Paris

Marcello Fulchignoni
LESIA, Observatory of Paris

Mirel Birlan
LESIA, Observatory of Paris

Pierre Vernazza
LESIA, Observatory of Paris

Elisabetta Dotto
INAF, Osservatorio Astronomico di Roma

Alain Doressoundiram
LESIA, Observatory of Paris

Abstract. The new scenario of the Rosetta mission to comet 67/P Churyumov-Gerasimenko (launch on February 2004), includes as baseline the fly-by of one or two asteroids. Several asteroids are now possible fly-by candidates (single or double) within the available resources. Other candidates whose fly-bys require a larger Δv can be also considered if the Rosetta interplanetary orbit insertion will cost less Δv.

All the up to date available information on the possible targets are discussed in this report.

The new baseline of the Rosetta mission includes the fly-by of at least an asteroid (2009-2010) which will precede a long orbital rendez-vous with the 67/P Churyumov-Gerasimenko comet nucleus (2014). The selection of the asteroid target(s) depends on the Δv available after the Rosetta probe interplanetary orbit insertion manoever. A few meter/sec Δv are available for the asteroid science in the pre-launch resource budget; but there is the possibility to allocate to the asteroid some of the remnant Δv, now reserved as contingenty for the insertion manoever, as soon as the Rosetta probe will be on its way toward the comet. The idea is to wait the results (in terms of Δv expenses) of the insertion manoever and to consider the new available budget to perform the asteroid fly-by(s). For this reason it is necessary to be ready shortly after the beginning of the Rosetta interplanetary journey: an international observational campaign is

started with the aim to increase at the maximum level the characterization of the possible asteroid targets of the mission.

This paper present the situation concerning the Rosetta asteroid targets choice as it is at the date of the IAU General Assembly in Sidney (July 2003). Ten main belt asteroids have been found allowing the Rosetta probe to have a single or even few double fly-bys whitin a Δv range 10-150 m/s (see table).

21 Lutetia is the largest object between these possible targets. On the basis of its visible spectra and IRAS albedo (Tedesco, 1992), it was classified as M type, but new observations in near-infarered and polarimetric data (Birlan et al. 2003) suggest that it is rather a C-type object similar to carbonaceous chondrite.

No data on *2181 Fogelin* are available in literature. Considering its absolute magnitude the diameter can be estimated in the range 12-22 km. We observed it with the IRTF/NASA on July 2003 and its near-infared spectrum suggest a S type object (Birlan et al. 2003).

Asteroid	Diameter (km)	IRAS albedo	Extra Δv (km)	Fly-by date mm.dd.yy	Rel. Vel. (km/s)
21 Lutetia	96	0.22±0.02	131	07.10.10	14.9
437 Rhodia	13	0.70±0.08	87	09.17.08	11.2
1393 Sofala	–	–	113	09.11.08	6.9
1714 Sy	–	0.11±0.03	11	03.06.08	8.2
2181 Fogelin	–	–	19	05.25.10	13.6
2513 Baethsle	17	0.03±0.01	16	10.05.08	8.6
2867 Steins	–	–	61	09.06.08	8.6
3050 Carrera	–	–	74	07.31.08	11.2
3418 Izvekov	27	0.07±0.01	14	12.04.10	11.3
5538 Luichewoo	–	–	35	04.08.09	5.6

The asteroid *437 Rhodia* is an intriguing object due to its very high IRAS albedo. The synodical period of $\geq$ 56 hours (Binzel, 1987) allow us to consider it within the slow rotator asteroid group.

If we consider the family members having spectra quite homogeneous (Florczak et al, 1998), we can assume that the asteroids *2513 Baethsle* and *5538 Luichewoo* belong to the S type which is characteristic of the members of the Flora family. IRAS albedo of *2513 Baethsle*, very far from the typical S-type, may indicate its "interloper" character and its appurtenance to a more primitive (C or D) asteroid class. The asteroid *3418 Izvekov* belongs to the C-type Themis family, this is in agreement with its IRAS albedo value. The visible spectrum of the asteroid *1393 Sofala* (Xu et al, 1995) indicats a S-type composition.

The final decision on the asteroid candidates will be taken after the launch. Information on all the possible target asteroids is important to be able to contribute to the best choice of the targets and to optimise the mission science return.

21 Lutetia represents one of the most interesting candidate, infact it's the only one which will allow us to obtain mass determination by radio science experiments, and consequently it will be possible to determine its density. Moreover,

if the chondritic character of this object will be confirmed, it will cope with the scientific objectives of the mission: the exploration of the primitive bodies of the planetary system.

If Lutetia cannot be selected due to the lack of available Δv, the asteroid candidate choice has to be done favouring the objects characterized by: 1) the more primitive compositional types (C, P, D); 2) the slower fly-by relative velocity; and 3) the larger diameter.

To obtain all these information we urge the observer community to participate to the observational campaign of these objects during their 2004 opposition.

1. References

Binzel, R. P. 1987, Icarus, 72, 135.
Birlan, M., Barucci, M.A., Vernazza, V., Fulchignoni, M., Binzel, R.P., Bus, S.J., Belskaia, I. & Fonasier, S. 2003, New Astronomy, in press.
Florczak, M., Barucci, M.A., Doressoundiram, A., Lazzaro, D., Angeli, C. & Dotto, E. Icarus, 133, 233.
Xu, S., Binzel, R.P., Burbine, T.H. & Bus, S.J. 1995, Icarus, 115, 1.
Tedesco, E.F. 1992, PL-TR-92-2049.

ROSETTA ASTEROID CANDIDATES

M.A. Barucci
LESIA, Observatoire de Paris, France

M. Fulchignoni
LESIA, Observatoire de Paris, France

I. Belskaya
Astronomical Observatory of Kharkiv National University, Ukraine

P. Vernazza
LESIA, Observatoire de Paris, France

E. Dotto
INAF-Osservatorio Astronomico di Roma, Monte Porzio Catone, Italy

M. Birlan
IMCCE, Observatoire de Paris, France

Abstract

The new scenario of the Rosetta mission to comet 67/P Churyumov-Gerasimenko (launch on February 2004), includes as baseline the fly-by of the asteroid 2513 Baetsle. Several other asteroids are possible fly-by candidates (single or double) within the available resources. Other candidates whose fly-bys require a larger Δv can be considered if the execution of the Rosetta interplanetary orbit insertion maneuver will allow the Rosetta Project to make available, for the asteroid fly-by, a fraction or the totality of the contingency Δv.

This paper present the history of Rosetta asteroid target selection as well as the situation concerning the Rosetta asteroid targets choice as it is at January 2003. A particular attention is devoted to the asteroid 21 Lutetia which represents the most interesting candidate.

2

1. Introduction

In late 1993 the European Space Agency (ESA) selected the mission Rosetta as the Planetary Cornerstone of its "Horizon 2000" program. The mission baseline included a rendez-vous with in situ investigations of a comet and fly-bys with two asteroids. The mission was named from the Rosetta Stone, due to the importance it had for the archeologists, allowing them to decipher the Egyptian hieroglyphics. In fact the knowledge of the nature of the primordial material (composing comets and asteroids) is considered by the planetologists of fundamental importance for the understanding of the origin and evolution of our solar system. The aim of the mission is to investigate the formation, the composition of planetesimals and their evolution over the last 4.5 billion years. The mission was scheduled to be launched by ESA using European technology and infrastructure. Considering a dedicated Ariane V launch followed by two or three gravity-assist swing-bys with the Earth, Venus and/or Mars, the ESA science team identified a number of mission scenarios which include different possible targets.

2. History of the asteroid target selection

On the Rosetta phase A Report (ESA SCI(93)7), ESOC listed many possible asteroid fly-bys both for rendezvous with the comet P/ Wirtanen and for some others comets rendezvous opportunities.

To select the most primitive targets and to complete the scenario of the asteroid already visited by space missions, an international workshop was organized at Max-Planck Institute (Katlenbur-Lindau) in May 1994. The scientific community underline the necessity to observe all the asteroid candidates suggested by ESA. Asteroids represent a vast heterogeneous population of small bodies with a wide range of orbital, physical and compositional characteristics. Although some asteroids can be differentiated and they can have experienced a collisional evolution, most of them have undergone relatively little thermal and geological evolution since their formation. A considerable amount of information regarding some of the primordial processes which governed the evolution of the whole solar system, immediately after the collapse of the protoplanetary nebula and before the formation of the planets is "frozen" in the asteroid population. The asteroid belonging to the taxonomic class of C (carbonaceous chondrite-like material) and D (volatile-rich ultracarbonaceous material) are considered quasi-unaltered, volatile-rich objects and for these reason the scientific community recommended to include in the mission the fly-by of these primitive objects.

Among various targets, the comet P/Wirtanen was selected as baseline with two fly-bys to the asteroids 3840 Mimistrobel and 2530 Shipka on the basis of the minimum Δv expenses criterium. The announcement of Opportunity published by ESA on March 1995 established the launch date in January 22, 2003.

Barucci and Lazzarin (1995) observed the two targets spectroscopically at CFHT (Mauna Kea observatory) deducing that Mimistrobel and Shipka revealed to belong to S and B classes respectively. As for each selected comet, several asteroid fly-bys were possible, Barucci and Lazzarin suggested to find other targets less evolved.

In 1996, refining the spacecraft trajectory, ESA redefined the mission baseline, changing the second target (Shipka) to 2703 Rodari, selected by the Rosetta Project always on the basis of the minimum Δv cost criterium. Barucci et al. (1998) observed the new target together with all the other possible candidates. The conclusion of their work was that Rodari was again another S type asteroid, as 951 Gaspra and 243 Ida already visited by Galileo mission and 433 Eros target of the NEAR mission. On the basis of their spectral analysis they concluded that 140 Siwa was the best target. The obtained data indicated that Siwa is a more primitive object, belonging to the C taxonomic class. Due to the spectral type and its large dimention (110 km), 140 Siwa was strongly pushed to be the primary asteroid target of the mission. After Barucci et al. (1998) study and suggestion, ESA selected in early 1999, 140 Siwa and 4979 Otawara as the asteroid targets in the new baseline for the Rosetta mission. The asteroid Otawara was added for the small increase of the total Δv. During its cruise to 46P/Wirtanen (rendez-vous), the Rosetta spacecraft was supposed to encounter Otawara on 11 July 2006 (heliocentric distance of 1.86 AU, minimum encounter distance of 2200 km and a relative velocity of 10.63 km s^{-1}) and Siwa on 24 July 2008 (at 2.75 AU from the Sun, at a minimum distance of 3500 km, and a relative velocity of 17.04 km s^{-1}).

3. 140 Siwa and 4979 Otawara

Many international observational campaigns followed to characterize the nature of Otawara and Siwa in order to optimize both the mission trajectory and the science operations. Doressoundiram et al. (1999) determined the synodic rotational period of 2.707 $\pm$ 0.005 hr for Otawara. On the basis of visual spectrum a possible taxonomic class S or V was associated at the object. Le Bras et al. (2001) observed the two candidates obtaining a precise determination of the synodic rotational period of Siwa (18.495 $\pm$ 0.005 hr) and confirming the previous determination of that of Otawara. The phase functions allowed them to determine the H and G parameters for both asteroids. The near-IR spectrum of Siwa confirmed the C/P type nature of Siwa. Just few months before the

4

programmed Rosetta launch, Fornasier et al. (2003) gave a complete portrait of Otawara. The spin vector is presented with a retrograde sense of rotation and the axial ratio a/b=1.21 $\pm$ 0.05. The visible and the near-IR spectra allow them to classify Otawara as S type asteroid and more specifically, on the basis of the analysis of band depths and slopes, in the S(IV) subgroup, suggesting a similarity to ordinary chondrite meteorites.

4. New baseline

In January 2003 the European Space Agency decided to postpone the launch of the spacecraft due to problems with Arianne V launcher, the new launch date has been fixed at the end on February 2004. A new baseline of the Rosetta mission including a long orbital rendez-vous with the 67/P Churyumov-Gerasimenko comet nucleus (in 2014) and one or two asteroids flybys (in the time span 2008-2010). The selection of the asteroid target(s) depends on the Δv available after the Rosetta probe interplanetary orbit insertion manoever. A few meter/sec Δv are available for the asteroid science in the pre-launch resource budget; but there is the possibility to allocate to the asteroid some of the remnant Δv, now reserved as contingency for the insertion maneuver, as soon as the Rosetta probe will be on its way toward the comet.

On December 2003 at ESTEC, the asteroid 2513 Baetsle has been selected as target of the baseline mission. In fact a minimum extra Δv of 19 m/s is necessary to allow the spacecraft to flyby this asteroid on August 8, 2010 with a relative velocity of 8.6 km/s. 2513 Baetsle is a very small asteroid with an IRAS albedo of 0.028 and an estimated diameter of 16.7 km. The asteroid, on the basis of its orbital parameters, has been assigned to the Flora family, which members have spectra characteristic of S type. This fact is in contrast with its low albedo, typical of a C or D type objects, and for this reason it could be an interloper of the Flora family.

Many other possible targets have been individuated for the mission. In table I the single fly by and in table II the double fly-bys opportunities are listed. On December 2003 at ESTEC a priority has been given also for the double fly-bys within a Δv range 30–160 m/s. The first priority has been given to 437 Rhodia and 21 Lutetia and as the second one to 5538 Luichewoo and 21 Lutetia. The scientific community has strongly pushed to include Lutetia as asteroid target.

The idea is to wait the insertion maneuver and to consider the new available budget (in terms of Δv) to perform the asteroid fly-by(s). For this reason an international observational campaign is started with the aim to increase at the maximum level the characterization of the possible asteroid targets of the mission (Birlan et al. 2004).

Following the scientific objective of the mission, *21 Lutetia* represents one of the most interesting candidate.

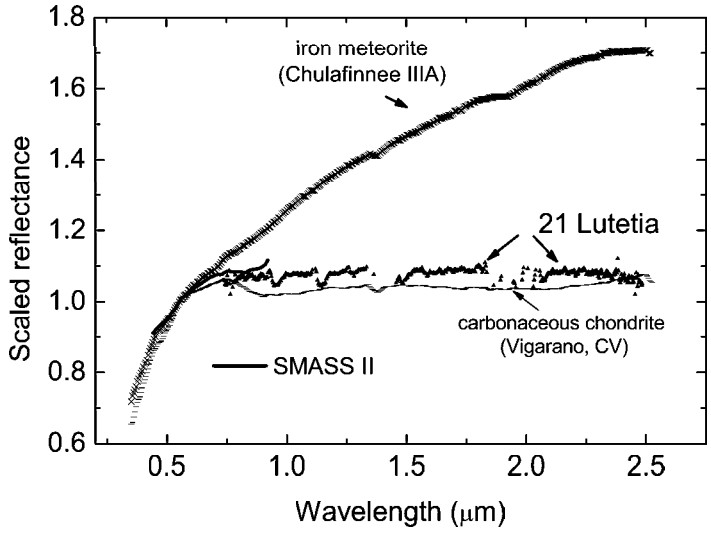

Figure 1. Spectra of Lutetia obtained by Birlan et al. (2004). The comparison with iron meteorite and carbonaceous chondrite reveals the similarity of the asteroid to C class objects.

Table 1. Single fly-by asteroid with the main physical characteristics and encounter data

Asteroid	Diameter (km)	IRAS albedo	Tax. type	Extra Δv m/s	Fly-by date dd.mm.yy	Rel. Vel. (km/s)
21 Lutetia	96	0.221±0.020	C	125	10.07.10	14.9
437 Rhodia	13	0.703±0.084	E?	97	17.09.08	11.2
1393 Sofala	–	–	?	111	11.09.08	6.9
2181 Fogelin	–	–	S	18	25.05.10	13.6
2513 Baetsle	17	0.028±0.007	C-D?	19	10.05.08	8.6
2867 Steins	–	–	?	57	07.09.08	8.6
3050 Carrera	–	–	?	102	30.07.08	11.3
3418 Izvekov	27	0.066±0.013	?	15	05.12.10	11.2
5538 Luichewoo	–	–	S?	32	08.04.09	5.6

5. 21 Lutetia: the best possible choice

21 Lutetia is the largest asteroid available in the list of the possible candidates. On the basis of IRAS observations, the estimated diameter is 95.8 ± 4.1 km with an albedo of 0.221 ± 0.020 (Tedesco and Veeder, 1992). Its synodic period is of 8.17 ± 0.01 hr (Zappala et al. 1984). Previously classified as M type (Barucci et al., 1987 and Tholen 1989), Lutetia was supposed to

6

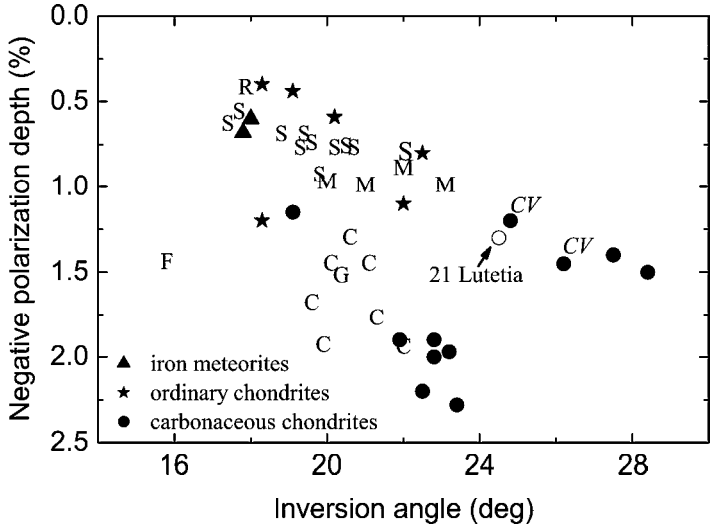

Figure 2. Diagram of the negative polarization depth versus the inversion angle of asteroids and meteorites.

be a parent body of iron meteorites. Further observations have shown that 21 Lutetia is atypical for the M taxonomic class. Its infrared spectrum is unusually flat as compared to other M-asteroids (Howell et al., 1994; Burbine and Binzel, 2002). New observations in near-infrared (Birlan et al. 2004) suggest a similarity with the carbonaceous chondrite spectra classifying this objects as a C-type asteroid (Fig 1). Its polarimetric properties are also better interpreted by a carbonaceous chondrite composition (Belskaya and Lagerkvist, 1996). The asteroid 21 Lutetia presents the largest inversion angle ever observed for asteroids and very similar to those found in laboratory for the carbonaceous chondrites of the CV type (Fig. 2). According to radar observations (Magri et al., 1998) Lutetia has the lowest radar albedo of any other M-asteroids which excludes metallic surface composition. Rivkin et al.(2000) reported the detection of the water-of-hydration absorption feature at 3 micron in its spectrum. All mentioned properties of 21 Lutetia are consistent with a carbonaceous chondrite composition of this asteroid though the high IRAS albedo leads some controversy. A lower albedo of 0.09 has been reported by Zellner et al. (1977) from both polarimetry and radiometry measurements. New measurements of Lutetia's albedo is very important for solving the controversy.

Table 2. Double asteroid fly-bys with relative extra Δv

1st encounter between Earth and Earth	2nd encounter between Earth and comet	extra Δv m/s
437 Rhodia	21 Lutetia	159
5538 Luichewoo	21 Lutetia	129
2867 Steins	21 Lutetia	139
437 Rhodia	2181 Fogelin	113
2513 Baetsle	2181 Fogelin	79
2867 Steins	2181 Fogelin	83
5538 Luichewoo	2181 Fogelin	35
437 Rhodia	3419 Izvekov	112
1393 Sofala	3419 Izvekov	146
2513 Baetsle	3419 Izvekov	73
2867 Steins	3419 Izvekov	77
5538 Luichewoo	3418 Izvekov	32

21 Lutetia represents one of the most interesting candidate, infact it's the only one which will allow us to obtain mass determination by radio science experiments, and consequently it will be possible to determine its density. Moreover, if the chondritic character of this object will be confirmed, it will cope with the scientific objectives of the mission: the exploration of the primitive bodies of the planetary system.

6. Possible double fly-by

After the Rosetta probe interplanetary orbit insertion maneuver, the final Δv available will be known and only at that time we will know if a double fly-bys will be possible. In table 2, a list with double asteroid fly-bys is presented. The first three represent the order of scientific interest priority. The asteroid *437 Rhodia* is an intriguing object due to its very high IRAS albedo 0.70 ± 0.08 (Tedesco and Veeder, 1992) which is the largest one ever observed for asteroids. The synodical period of $\geq$ 56 hours (Binzel, 1987) allow us to consider it within the slow rotator asteroid group which can imply a binary possibility for the object. There is any available spectral observations of the asteroid. However the measured B-V color of Rhodia (Binzel, 1987) together with high albedo are consistent with the E-type composition (Fig. 3).

All the other candidates are in general very small with an unknown taxonomic type. If we consider the family members having spectra quite homogeneous (Florczak et al, 1998), we can assume that the asteroid *5538 Luichewoo* belong to the S type which is characteristic of the members of the Flora family.

8

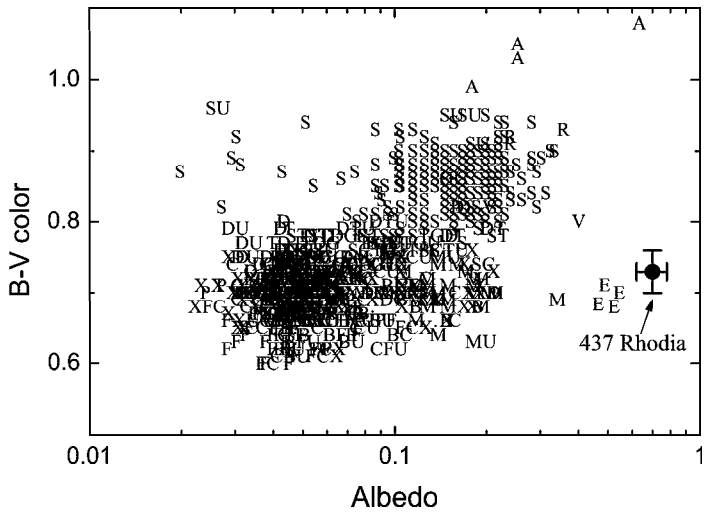

Figure 3. The diagram of the B-V colors versus albedo for asteroids of different types.

7. Conclusion

The asteroid fly-bys were part of the science definition of the Rosetta mission. The scientific community requires to have one or two asteroid visited by Rosetta during the cruise to the comet.

The final decision on the asteroid candidates will be taken after the launch when the remnant Δv will be known. Information on all the possible target asteroids is important to be able to contribute to the best choice of the targets and to optimise the mission science return.

21 Lutetia represents one of the most interesting candidate, infact it's the only one which will allow us to obtain mass determination by radio science experiments, and consequently it will be possible to determine its density. Moreover, if the chondritic character of this object will be confirmed, it will cope with the scientific objectives of the mission: the exploration of the more primitive bodies of the planetary system.

If Lutetia cannot be selected due to the lack of available Δv, the asteroid candidate choice has to be done favouring the objects characterized by: 1) the more primitive compositional types (C, P, D); 2) the slower fly-by relative velocity; and 3) the larger diameter.

8. Acknowledgement

I.Belskaya is grateful to the European Space Agency who granted her fellowship to spend a year at LESIA, Observatoire de Paris, as visiting scientist.

References

Barucci, M. A., Capria, M. T., Coradini, A., and Fulchignoni, M. (1987). Classification of asteroids using G-mode analysis. *Icarus*, 72:304–324.

Barucci, M.A., and Lazzarin, M. (1995). Visible Spectroscopy of the Rosetta Asteroid Targets: 3840 Mimistrobel and 2530 Shipka. *Icarus* 118: 216–218.

Barucci, M.A., Doressoundiram, A., Fulchignoni, M., Florzac, M., Lazzarin, M., and Angeli C. (1998) Composition type characterization of Rosetta asteroid targets. *Planet Space Sci.* 46: 75–82.

Belskaya, I. N., and Lagerkvist, C.-I. (1996). Physical properties of M-class asteroids. *Planet. Space Sci.*, 44:783–794.

Binzel, R. P. (1987). A photoelectric survey of 130 asteroids. *Icarus*, 72:135–208.

Birlan, M., Barucci, M. A., Vernazza, P., Fulchignoni, M., Binzel, R. P., Bus, S. J., Belskaya, I., and, Fornasier, S. (2004). Near-IR spectroscopy of asteroids 21 Lutetia, 89 Julia, 140 Siwa, 2181 Fogelin and 5480 (1989 YK8), potential targets for the Rosetta mission; remote observations campaign. *New Astronomy*, in press.

Burbine, T. H., and Binzel, R. P. (2002). Small main-belt asteroid spectroscopic survey in the near-infrared. *Icarus*, 159:468–499.

Doressoundiram, A., Weissman, P.R., Fulchignoni, M. Barucci, M.A., Le Bras, A., Colas,F., Lecacheux, J., Birlan, M., Lazzarin, M., Fornasier, S., Dotto, E., Barbieri, C., Sykes, M.V., Larson, S., Hergenrother, C.(1999) 4979 Otawara: fly-by target of the Rosetta mission. *Astron. Astrophy.* 352: 697-702.

Florczak, M., Barucci M.A., Doressoundiram A., Lazzaro D., Angeli C.A., and Dotto, E. (1998). A visible spectroscopic survey of the Flora clan. *Icarus* 133: 233–246.

Fornasier, S., Barucci M.A., Binzel R.P., Birlan M., Fulchignoni M., Barbieri, C., Bus, S.J., Harris, A.W., Rivkin, A.S., Lazzarin,M., Dotto,E., Michalowski, T., Doressoundiram, A., Bertini, I., and Peixinho, N (2003). A portrait of 4979 Otawara, target of the Rosetta space mission. *Astron. Astroph.* 398: 327–333.

Howell, E. S., Merenyi, E., and Lebovsky, L. A. (1994). Classification of asteroid spectra using a neural network. *J. Geophys. Res.*, 99:10848–10865.

Le Bras, A., Dotto, E., Fulchignoni, M., Doressoundiram, A., Barucci, M.A., Le Mouelic, S., Forni, O., and Quirico, E. (2001). The 2000 Rosetta asteroid targets observational campaign: 140 Siwa and 4979 Otawara. *Astron. Astroph* 379: 660–663.

Magri, C., Ostro, S. J., Rosema, K. D., Thomas, M. L., Mitchell, D. L., Campbell, D. B., Chandler, J. F., Shapiro, I. I., Giorgini, J. D., and Yeomans, D. K. (1999). Mainbelt asteroids: results of Arecibo and Goldstone radar observations of 37 objects during 1980–1995. *Icarus*, 140:379–407.

Rivkin, A. S., Howell, E. S., Lebofsky, L. A., Clark, B. E., and Britt, D. T. (2000). The nature of M–class asteroids from 3 μm observations. *Icarus*, 145:351–368.

Tedesco, E. F., and Veeder, G. F. (1992). IMPS albedos and diameter catalog. In Tedesco, E. F., Veeder, G. F., Fowler, J. W., and Chillemi, J. R., editors, *The IRAS Minor Planet Survey*, Tech. Rep. PL–TR–92–2049. Phillips Laboratory, Hanscom AF Base, MA.

10

Tholen, D. (1989). Asteroid taxonomic classifications. In: Binzel, R.P., Gehrels T., and Matthews, M.S., editors, *Asteroids II*, Univ. of Arizona Press, Tucson:1139–1150.

Zappala, V., Di Martino, M., Knezevic, Z., and Djurasevic, G. (1984). New evidence for the effect of phase angle on asteroid lightcurve shape - 21 Lutetia. *Astron. Astroph* 130: 208–210.

Zellner, B., Leake, M., LeBerte, T., Duseaux, M., and Dollfus, A. (1977). The asteroid albedo scale. II. Laboratory polarimetry of meteorites. In *Proc. Lunar Sci. Conf.*, 8th:1091–1110. Pergamon Press, Oxford.

EMISSION IN ABSORBTION LINES: RESULTS OF THE SL9 L NUCLEUS IMPACT WITH JUPITER

MIREL BÎRLAN [1,2]

[1] *Observatoire de Paris-Meudon, DESPA*
F-92195 Meudon Cedex, France
E-mail: Mirel.Birlan@obspm.fr

[2] *Astronomical Institute of the Romanian Academy*
Str. Cuțitul de Argint, RO-75212 Bucharest 28, Romania

Abstract. High-resolution spectra of the impact sites and impact of the comet Shoemaker-Levy 9 with Jupiter have been performed at the Pic-du-Midi Observatory. The excitation of several chemical elements (Fe, Ca, Ba, Na, Mn, Mg, etc.) has been identified during the analysis of the L nucleus impact spectra obtained in visible and near-IR. The article presents the atomic lines and the time evolution of nine of them.

Key words: spectroscopy – comets – atomic lines.

1. INTRODUCTION

One of the major astronomical events of 1994 was the impact of the comet Shoemaker-Levy 9 with Jupiter. The astronomical community observed this event within the framework of the coordinated program; several ground-based and space instruments have been involved. SL9/Jupiter impact was a unique event (until now); before the show "live" of the impact SL9 comes inside Jupiter's Roche limit which broken the nucleus in 22 fragments.

The first impact for each nucleus occured on an unfavourable geometry, on the hidden part of Jupiter, not far from the limb. However, relevant data concerning the impacts were collected as soon the impact effects become visible.

2. OBSERVATIONS

The paper presents the spectroscopy in the wavelength range of visible and near-IR (5460-8750 Å) performed for the L impact site. The observations were performed with the 2-meter Bernard Lyot telescope from the Pic du Midi Observatory. The spectra were recorded by a 1024 × 1024 Thomson CCD chip, and

Rom. Astron. J., Vol. 10, No. 2, p. 137–144, Bucharest, 2000

the spectral resolution was 36 000. The fibber of the spectrograph has 50 microns, which corresponds to a field of view of 2.2". This field of view is small enough to obtain high quality spectra only from the impact site (the apparent diameter of Jupiter is about 38"). The guidance software of the telescope allows both automatic/manual tracking during the exposure.

3. DATA REDUCTION

The pre-treatment of the observed data was performed using MUSICOS software. MUSICOS makes the calibration pixel-wavelength for the intensities spectra. Each spectrum was split in several wavelength intervals (named "orders") which little overlap between the adjacent orders. For the analysis in the absorption line we choose as target on Jupiter the L impact site for July 19/20 at 22:30:55 UT (referred to as S167), and July 20/21(referred to as S213), 1994. As reference, the Jupiter spectrum was taken on July 20/21 (referred to as R216). The spectrum S167 emission lines have already been analysed in several papers (Roos-Serote et al. 1995a,b; Barucci et al. 1995).

The MIDAS software procedures for spectroscopy were employed. The goal of this work was to check the atomic absorption line depth one day after the impact moment and to see the excitation of different atoms of Jupiter-SL9 L impact plume. To reach this goal, all the orders of both spectra of impact site were compared with the reference spectrum R216. Then the results S213/R216 and S167/R216 in each order were compared.

In this treatment, the major problem of the differential rotation of the atmosphere of Jupiter occured. From an order to another, in different spectra, the same atomic line presents a slight shift in wavelength, following the expression:

$$\frac{\Delta\lambda}{\lambda} = \frac{v_{diff}}{c},$$

where v_{diff} denotes the differential speed of Jupiter and c stands for the speed of light.

Thus, an automatic procedure of shift cannot be taken into account. For a good preliminary result in some orders the spectra were rebined. Then, shifting the lines in such a way made the subtraction or division between spectra, so that the minima of the lines are at the same wavelength.

The cosmic ray signatures represented another problem that occured during the treatment. This was skipped manually, each time when the spectrum of Jupiter had no lines in this region, and one given atomic line had an abnormal profile.

At least, we cannot omit the presence of the terrestrial lines, even after a major part of them where eliminated by an automatic procedure. Their presence could alter our qualitative analysis and they were carefully analysed and skipped.

4. RESULTS

The comparison of the L impact site spectra with the unperturbed Jupiter's atmosphere spectrum was made in order to minimize any ambiguity. Then the shifted spectra S167 and S213 were compared in each order. To obtain a good signature for each excited atomic line, the ratio S167/S213 has been analysed. As presented in Fig. 1, only the signatures of atomic lines with amplitude larger than three times the noise amplitude were considered (three sigma relevance).

The analysis reveals orders on which the spectral lines were not perturbed by the impact of the comet (as seen on Fig. 2). At the opposite, there are spectral intervals where almost all of the atomic lines were perturbed.

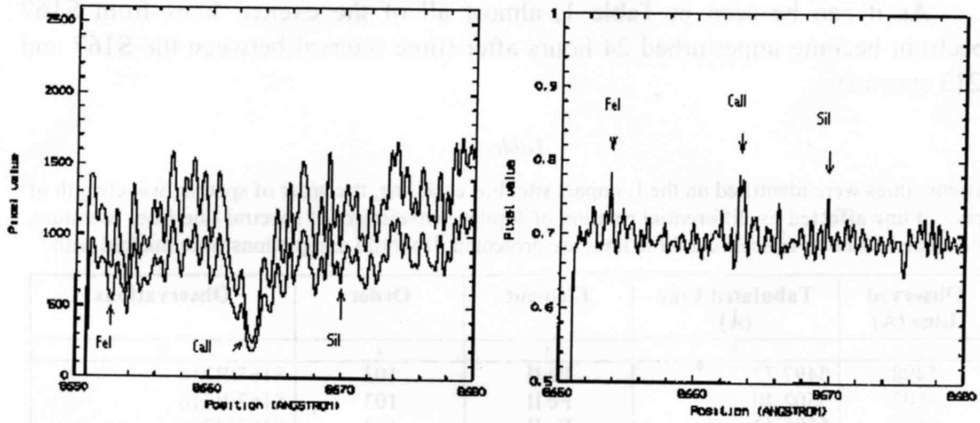

Fig. 1 – Left: Spectra of the 65-th order of R216, and S213 (upper and lower spectrum, respectively). On the center of this order the Paschen $n = 13$ absorption line of Ca II ion. Right: Signatures of Ca II, Fe I, and Si I after the S213/R216 computation.

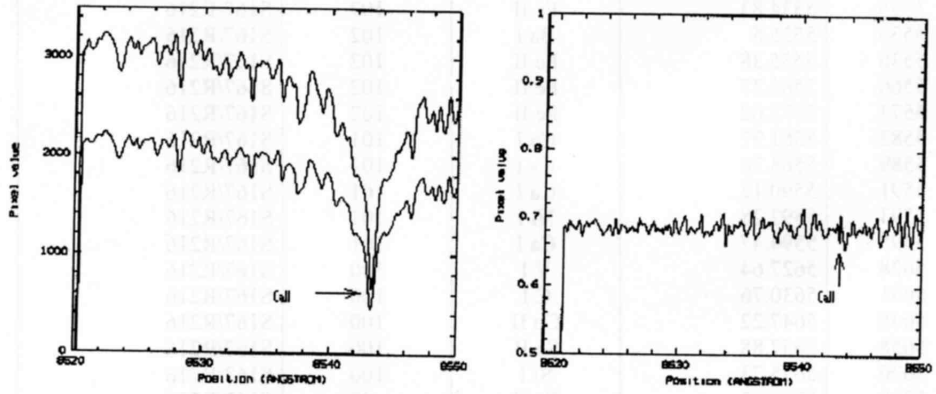

Fig. 2 – "Quiet" order. Spectra of the 66-th order of R216, and S213 (upper and lower spectrum, respectively) containing Paschen line $n = 15$ of Ca II ion (left plot). The result of the S213/R216 computation (right plot).

For the S213, almost of the orders are "quiet". At the opposite, the S167 spectrum presents high differences for several atomic lines (Fig. 3). Thus, the Fe I, II, and III lines are excited on almost all of orders as well as the representative lines of Ca I, and II ions.

Table 1 lists the excited lines. In a first time the line identification was made taking as origin the profile of spectral lines from *The High Resolution Spectral Atlas of the Solar Irradiance* by Beckers, Bridges and Gilliam (1976), and *The Solar Spectrum from λ 6000 to λ 13495* by Babcock and Moore (1947). Then our identification was refined using the articles of Morton (1991, 2000), Morton and Noreau (1994), and the VizieR database of atomic lines (http://vizier.u-strasbg.fr), Reader and Corliss, and Hirata catalogues.

As it can be seen in Table 1, almost all of the excited lines from S167 spectrum become unperturbed 24 hours after (time interval between the S167 and S213 spectra).

Table 1

Atomic lines were identified on the L impact site. For each line, the order of spectra, wavelength of spectral line affected by differential rotation of Jupiter, wavelength of spectral line from literature, element, and notes concerning these lines are presented. Doubtful assignations were marked with *

Observed Line (Å)	Tabulated Line (Å)	Element	Order	Observations
1	2	3	4	5
5498	5497.77	Fe II	103	S167/R216
5502	5502.30	Fe II	103	S167/R216
5507	5506.44	Fe II	103	S167/R216
5511	5512.98	Ca I	103	S167/R216
5511	5510.61	Cr I	103	S167/R216
5527	5526.8	Sc II	102	S167/R216
5533	5535.05	Mo I	102	S167/R216
5535	5534.83	Fe II	102	S167/R216
5536	5535.5	Ba I	102	S167/R216
5536	5535.38	Fe II	102	S167/R216
5566	5565.37	Fe II	102	S167/R216
5573	5572.62	Fe II	102	S167/R216
5582	5581.97	Ca I	101	S167/R216
5589	5588.76	Ca I	101	S167/R216
5591	5590.12	Ca I	101	S167/R216
5593	5592.28	Ni I	101	S167/R216
5595	5594.47	Ca I	101	S167/R216
5628	5627.64	V I	100	S167/R216
5631	5630.76	C I	100	S167/R216
5648	5647.22	Co II	100	S167/R216
5658	5657.88	Sc II	100	S167/R216
5676	5675.73	Si I	100	S167/R216
5710	5708.93	Fe II	99	S167/R216
5737	5736.75	Ca I	99	S167/R216
5788	5787.9	Cr I*	98	S167/R216

Table 1 (continued)

Observed Line (Å)	Tabulated Line (Å)	Element	Order	Observations
1	2	3	4	5
5853	5853.45	Fe II	97	S167/R216
5858	5857.45	Ca I	97	S167/R216
5863	5862.89	Fe I	97	S167/R216
5890	5889.95	Na I	96	S167/R216
5896	5895.92	Na I	96	S167/R216
5915	5914.97	Fe II	96	S167/R216, S213/R216
5984	5983.86	Fe II	95	S167/R216
6014	6013.5	Mn I	94	S167/R216
6017	6016.6	Mn I	94	S167/R216
6066	6065.83	Fe II	93	S167/R216
6123	6122.22	Ca I	92	S167/R216
6142	6141.72	Ba II	92	S167/R216
6163	6162.17	Ca I	92	S167/R216
6176	6176.05	N II	92	S167/R216
6210	6209.73	Fe I	91	S167/R216
6226	6225.92	Cr II*	91	S167/R216
6243	6242.87; 6242.9	Ca I*; Mn I*	91	S167/R216
6245	6244.47	Si I	91	S167/R216
6319	6318.66	Fe II	90	S167/R216
6359	6358.76	Fe II	89	S167/R216
6439	6439.07	Ca I	88	S167/R216
6451	6449.81; 6450.24	Ca I+Co I	88	S167/R216
6472	6471.66	Ca I	87	S167/R216, S213/R216
6494	6493.78	Ca I	87	S167/R216
6496	6495.78	Fe I	87	S167/R216, S213/R216
6498	6498.75	Ba I	87	S167/R216, S213/R216
6501	6499.65	Ca I	87	S167/R216, S213/R216
6563	6562.85	H I	86	S167/R216
6574	6572.78	Ca I	86	S167/R216
6679	6678.9	Fe II	85	S167/R216
6708	6707.91; 6707.76	Li I	84	S167/R216 (double)
6978	6978.48	Cr I	81	S167/R216
7289	7288.88	Fe II	78	S167/R216
7290	7290.26	Si I	78	S167/R216
7326	7326.15	Ca I	77	S167/R216, S213/R216
7327	7325.51	Mn I	77	S167/R216, S213/R216
7853	7852.86	C I*	72	S167/R216
7858	7858.09	Fe III	72	S167/R216
7938	7938.06	Fe II	71	S167/R216
8095	8094.93	Fe I	70	S167/R216
8187	8186.97; 8186.99	F III*, Mn II*	69	S167/R216
8195	8194.70	Fe I	69	S167/R216
8405	8404.77; 8404.84	Mn III*, Fe II*	66	S167/R216
8415	8414.89; 8414.95	Fe II*, F I*	66	S167/R216, S213/R216
8664	8662.14	Ca II	65	S167/R216, S213/R216
8683	8683.4	N I	65	S167/R216, S213/R216
8710	8710.03	Fe I	65	S167/R216, S213/R216
8737	8736.02; 8736.48	Mg I, Mn I	65	S167/R216
8790	8789.34	Fe I	65	S167/R216

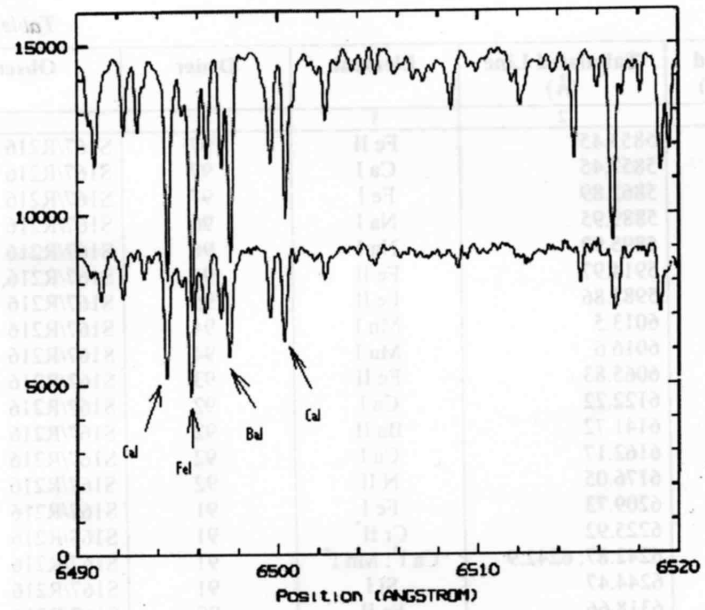

Fig. 3 – Order 87 on S167 (top), and R216 (bottom) spectra. We can distinguish the perturbed lines of Fe I, Ca I, and Ba I lines (marked by arrows).

However, some excited lines are present in both spectra (S167 and S213). In order to have their temporal evolution, casually the orders of a third spectrum were analysed. This spectrum (S166) was taken on July 19/20, 1994, just at the moment that L impact site and plume appeared on the Jupiter visible hemisphere. Table 2 presents such an evolution in the case of some important lines. The percentage values given by the last three columns of Table 2 are computed only from the geometrical consideration, taking into account the depth of the line in the R216 spectrum.

Table 2

The evolution of some spectral lines in three analysed spectra. The spectral line contains the differential rotation shift imposed by Jupiter's rotation.

Element	Wavelength (Å)	S166/R216	S167/R216	S213/R216
Ca I	6472	26%	25%	7%
Ca I	6494	13%	20%	–
Fe I	6496	26%	29%	13%
Ba I	6498	16%	20%	1%
Li I	6708	3%	24%	–
Ca II	8664	84%	70%	10%
N I	8683	15%	33%	13%
Fe I	8790	44%	35%	–
Mg I, Mn I	8737	16%	25%	–

We have paid a special attention to the hydrogen quadrupolar momentum lines. We have searched for the S(0) – S(3) H signatures (6270.24 Å, 7959.77 Å, 8150.67 Å, and 8272.67 Å, respectively), but our search has not provided positive results.

5. DISCUSSION

The greatest part of the absorption atomic lines of the solar spectrum (of our spectral interval) remained unperturbed after the reflection on Jupiter. The Jovian atmosphere does not present metallic compounds on the analysed spectral interval, the profile of Jupiter's spectrum reproduces the solar spectrum. The perturbed spectra come from the L impact site. Therefore, we can formulate the conclusion that the most significant part of this excitation was released by the cometary material.

Various mechanisms could be responsible of the presence of the atom excitation. The perturbation of atomic lines could be explained as the effect of such a mechanism (or several such mechanisms). As long as the goal of this article is to present the qualitative results of spectra analysis, these mechanisms will be only remembered. However, the author intimate conviction is that different excited lines could be explained only by individual theories.

The main known mechanisms are: the resonant fluorescence, the thermal collision (if we consider the temperature on the impact site and plume greater than 1000 K), and the electronic recombination. The resonant fluorescence mechanism is unanimously accepted as the responsible of the presence of metallic lines on the cometary's spectra as well as for the presence of molecular bands. The thermal collisions could contribute to atomic lines only if the collision rate of atoms is high enough to produce transitions between the corresponding energy levels, and the electronic recombination could be efficient for the excitation of atoms in metastable states.

6. CONCLUSIONS

The analysis of the L impact spectra reveals several excited atomic lines. Alkaline lines (Li, Na, Ba, Ca, Mg) as well as line of transition metals (Fe, Cr, Ni, Co, Mn) are listed in Table 1. Nitrogen (N) and maybe flour (F) and carbon (C) lines are presented and rest to be confirmed by further analysis and astronomical observations. The major part of the atomic lines disappear 24 hours after the impact instant, which shows the efficiency of the de-excitation mechanism and energy dissipation on Jupiter's atmosphere.

REFERENCES

Babcock, H. D., Moore, C. E.: 1947, *The Solar Spectrum from λ 6000 to λ 13495*, Carnegie Inst. Washington Publ., No. 579.

Barucci, M. A., Roos-Serote, M., Fulchignoni, M., Lecacheux, J., Crovisier, J., Drossart, P., Roques, F.: 1994, *ASP Conf. Series*, **81**, 404.

Beckers, J. M., Bridges, C. A., Gilliam, L. B.: 1976, *The High Resolution Spectral Atlas of the Solar Irradiance*, Sacramento Peak Observatory, Env. Res. Papers, No. 565.

Morton, D.: 1991, *Astrophys. J. Suppl. Ser.*, **77**, 119.

Morton, D.: 2000, *Astrophys. J. Suppl. Ser.*, **130**, 403.

Morton, D., Noreau, L.: 1994, *Astrophys. J. Suppl. Ser.*, **95**, 301.

Roos-Serote, M., Barucci, M. A., Crovisier, J., Drossart, P., Fulchignoni, M., Lecacheux, J., Roques, F.: 1995, in R. West and H. Bohnhardt (eds), *European SL-9/Jupiter Workshop*, Garching-bei-Munchen.

Roos-Serote, M., Barucci, M. A., Crovisier, J., Drossart, P., Fulchignoni, M., Lecacheux J., Roques, F.: 1995, *Geophys. Res. Lett.*, **22**, 1621.

Received on 12 December 2000

I.4. Astrométrie et systèmes de références.

Le terme générique d'astrométrie définit toute démarche d'observations permettant d'obtenir des positions instantanées précises d'un objet sur la voûte céleste. Dans le cas des objets du système solaire, ce type d'observation mène finalement à l'amélioration des paramètres orbitaux (ou des éléments osculateurs définissant l'orbite de l'objet) et à l'obtention d'une meilleure prédiction de son mouvement (défini par le calcul d'éphémérides). Grâce à de nouvelles technologies (CCD, algorithmes de réduction, programmes de réduction en chaîne), l'aspect astrométrique des divers programmes d'observations en astronomie est dans la plus part des cas adapté à des automatisations importantes.

Deux aspects importants concourent à l'obtention d'une bonne précision sur les positions des objets du système solaire : la qualité du système de référence pris en compte et la qualité des méthodes d'analyse et de réduction des données.

La qualité du système de référence est liée à l'approche qu'il présente par rapport à un système inertiel parfait. Durant l'histoire de l'astronomie, les premiers catalogues d'étoiles ont représenté cette approche : la position des étoiles sur le ciel donnent une origine et une orientation du système. Tout objet nouveau était déterminé par rapport à ce système. Régulièrement, la position de l'origine ainsi que l'orientation des axes ont été remises en cause. La plupart des refontes des systèmes de référence s'est avérée nécessaire suite à une amélioration des observations et à la possibilité de mesure du temps beaucoup plus exacte.

Nous partons du constat qu'il n'y a pas de point fixe défini dans l'Univers. En ce cas, les objets (en mouvement eux aussi) qui peuvent nous donner un système de référence fiable sur une longue période, sont ceux obtenus en mesurant les positions des objets lointains. Actuellement c'est le cas du système de référence lié aux sources radio (noyaux actifs des galaxies et quelques quasars). L'établissement de ce système nouveau, pose des problèmes de

lien (rattachement) avec les anciens systèmes de référence, la plupart établis à base d'étoiles de notre galaxie observées dans la région visible du spectre.

Une partie de mes travaux s'inscrivent dans les efforts de rattachement entre des systèmes de référence optique et le système de référence des radiosources. Pendant plusieurs années nous avons observé des régions (1 degré carré) autour des radiosources afin d'obtenir des positions astrométriques précises des étoiles faibles (14-17 de magnitude), non-cataloguées, de ces régions (Bocsa & Birlan, RAJ, 2001).

L'astrométrie précise de ces régions permet, en seconde approche, l'astrométrie précise dans la région du visible des radiosources avec, finalement, la déduction des règles de rattachement du système de référence radio avec ceux réalisés dans le domaine du visible.

Je me suis aussi intéressé à l'astrométrie des petits corps du système solaire. Le programme CERES est un programme international ayant pour but l'établissement d'un système de référence à partir de mesures astrométriques sur quelques dizaines d'astéroïdes de grande taille. Les observations des astéroïdes de grande taille (tels que (1) Céres, (2) Pallas, (3) Juno, (4) Vesta, (7) Iris,…) se sont poursuivies pendant environ 20 ans. Les observations astrométriques (sur des plaques photographiques) ainsi que la réduction des données ont été effectuées à Bucarest (Birlan & Bocsa, RAJ, 1994). La centralisation des données a été effectuée à l'Institut d'Astronomie Théorique de Saint Petersbourg (coordonnateur du programme en Roumanie G. Bocsa). J'ai participé à l'observation et à la réduction des données. Un autre volet de mes activités astrométriques est constitué par les observations des objets « target of opportunity » comme les comètes Hale-Bopp et Hyakutake (Bocsa & Birlan, RAJ, 1997).

La préparation des observations et la réduction des données d'observations ont permis aussi l'automatisation et l'optimisation des processus. Ovidiu Vaduvescu, ancien collègue de l'Observatoire de Bucarest et moi-même avons conçu le logiciel Celestial Maps, aide pour des recherches en astrométrie (Vaduvescu & Birlan, RAJ, 1996).

Références :

Birlan M., Bocsa G. - *Observations of minor planets in 1990-1994 at the Bucharest Astronomical Observatory*, **Romanian Astronomical Journal**, vol. **5**, n. **2**, 185-191, 1995.
Bocsa G., **Birlan M.** - *Astrometric precise positions of the comet Hale-Bopp at Bucharest Observatory* **Romanian Astronomical Journal**, vol. **7**, 199-200, 1997.
Thuillot W., Arlot J-E., Stavinschi M., **Birlan M.**, Lainey V. - *Ground-based astrometry at the time of the GAIA mission* **Romanian Astron. J.** (in press)

Thuilllot, W., Vaubaillon, J., Scholl, H, Colas, F., Rocher, P., **Birlan, M.**, Arlot, J-E. - *Relevance of the NEO dedicated observing programs* – Comptes-Rendu de l'Académie des Sciences, vol **6** n **3**. 2005.
Bocsa G., **Birlan, M.** - *Intermediate stars in extragalactic radiosource fields* **Romanian Astronomical Journal**, vol **11**, n. **2**, 181-186, 2001.
Vaduvescu O., **Birlan M.** - *Software package for preparing and processing of an astronomical observation*, **Romanian Astronomical Journal** vol. **6**, n. **1**, 97-99, 1996.

OBSERVATIONS OF MINOR PLANETS IN 1991–1994 AT THE BUCHAREST ASTRONOMICAL OBSERVATORY

MIREL BÎRLAN and GHEORGHE BOCŞA

Astronomical Institute of the Romanian Academy
5, Cuţitul de Argint str., 75212 Bucharest 28, Romania

Abstract. The precise positions of asteroids observed at Bucharest Observatory in 1991–1994 period are presented.

Key words. Astrometry, minor planets.

This paper presents the observations of minor planets, obtained in 1991– 1994 with a 380/6000 mm astrograph. Astrophotographic plates with a 2° × 2° field were used. The measurements were carried out by means of an ASCORECORD measuring machine. Both Turner's constants and Schlesinger's dependence methods were used for the computation of the normal coordinates of the object.

In Table 1 the observations of minor planets are presented: the date of the observation and the UT values, the right ascension and the declination, the (O–C) values on the ascension respectively the declination and the observer's initials.

Table 2 presents the reference stars used to compute the values for the 1 Ceres, 2 Pallas, 4 Vesta, 6 Hebe, 7 Iris, 11 Parthenope, 39 Laetitia, 148 Gallia, 389 Industria, 532 Herculina asteroids which are selected in the "Establish the fundamental plane of an inertial reference system" program. Table 2 contains the index number (the same as that in Table 1), the BD number from the catalogue for reference stars, the ascension (s), the declination (′′) and the dependences.

Rom. Astron. J. Vol. 5, No 2, p. 185–191, Bucharest, 1995

Table 1

No	Date and UT		$\alpha_{1950.0}$			$\delta_{1950.0}$			$(O-C)_\alpha$	$(O-C)_\delta$	O.C.
			h	m	s	°	′	″	s	″	
					1991						
					3 JUNO						
1	9.76072	Sep.	19	00	31.67	–10	27	52.6	–0.062	+0.64	GB
2	9.77457	„	19	00	31.72	10	27	57.7	–0.068	+0.69	GB
3	12.77408	„	19	00	52.74	10	46	23.9	–0.040	+0.45	MB
4	12.77784	„	19	00	52.85	–10	46	28.7	–0.042	+0.58	MB
					6 HEBE						
5	9.84659	Sep.	22	21	21.52	–20	48	37.2	–0.039	–0.50	MB
6	9.85491	„	22	21	21.20	20	48	44.3	–0.009	–0.91	MB
7	10.81858	„	22	20	43.99	21	01	20.6	–0.058	–0.11	MB
8	10.82689	„	22	20	43.66	–21	01	26.8	–0.050	+0.27	MB
					7 IRIS						
9	26.76347	Sep.	22	33	56.01	+2	29	36.0	–0.079	–0.75	GB
10	26.769	„	22	33	55.74	2	29	33.6	–0.095	–0.82	GB
11	27.78740	„	22	33	16.47	2	23	09.6	–0.061	–0.60	GB
12	27.79295	„	22	33	16.24	2	23	07.1	–0.071	–0.45	GB
13	30.81141	„	22	31	29.80	2	04	13.1	–0.045	–0.50	GB
14	30.81834	„	22	31	29.53	2	04	10.7	–0.065	–0.35	GB
15	7.82727	„	22	28	27.07	1	22	13.8	+0.022	+0.18	MB
16	7.83628	„	22	28	26.88	+1	22	10.5	+0.024	–0.13	MB
					39 LAETITIA						
17	9.73786	Sep.	18	24	26.58	–15	02	31.3	+0.023	–0.40	GB
18	9.74895	„	18	24	26.86	15	02	34.6	+0.010	–0.30	GB
19	10.74205	„	18	24	55.98	15	07	31.6	+0.026	+0.17	GB
20	10.75314	„	18	24	56.30	–15	07	35.2	+0.028	–0.11	GB
					1992						
					532 HERCULINA						
21	24.82830	Jun.	16	11	35.32	–6	32	37.7	–0.023	–0.03	GB
22	24.83869	„	16	11	34.93	–6	32	42.3	—0.015	+0.14	GB

Table 1 (continued)

1993

No	Date and UT		$\alpha_{2000.0}$			$\delta_{2000.0}$			$(O-C)_\alpha$	$(O-C)_\delta$	O.C.
			h	m	s	°	′	″	s	″	
					1 CERES						
23	11.85165	Oct.	2	16	44.40	+0	00	19.7	–0.068	+0.33	GB
24	11.86065	„	2	16	44.00	+0	00	18.8	–0.026	+0.14	GB
					2 PALLAS						
25	3.76738	Sep.	21	40	12.08	+6	15	07.5	–0.008	+0.15	GB
26	3.77915	„	21	40	11.56	6	14	58.9	–0.028	+0.23	GB
27	10.75450	„	21	35	37.41	4	47	59.4	–0.041	–0.68	GB
28	10.76835	„	21	35	36.88	4	47	48.9	–0.052	–0.73	GB
29	13.73385	„	21	33	51.86	4	10	15.2	–0.065	–0.65	GB
30	13.74770	„	21	33	51.38	+4	10	5.6	–0.061	–0.28	GB
					4 VESTA						
31	7.82329	Sep.	22	32	37.56	–20	00	39.4	+0.058	–0.64	GB
32	7.83022	„	22	32	37.20	20	00	40.7	+0.074	+0.44	GB
33	10.83310	„	22	30	3.79	20	16	32.8	+0.014	–0.30	GB
34	10.84003	„	22	30	3.50	20	16	34.1	+0.080	+0.53	GB
35	13.81280	„	22	27	39.41	20	30	16.1	+0.058	–0.94	GB
36	13.82388	„	22	27	38.82	20	30	18.4	+0.010	–0.42	GB
37	11.79071	„	22	15	20.08	20	56	42.5	+0.044	–0.34	GB
38	11.80040	„	22	15	20.02	20	56	41.0	+0.025	–0.13	GB
39	13.73227	„	22	15	17.97	20	52	13.3	+0.050	–0.63	GB
40	14.74196	„	22	15	17.97	–20	52	11.9	+0.032	–0.71	GB
					11 PARTHENOPE						
41	11.80906	Oct.	1	1	47.47	–1	42	23.9	–0.049	–0.13	GB
42	11.82083	„	1	1	46.83	–1	42	27.6	–0.040	+0.20	GB

Table 1 (continued)

No	Date and UT				$\alpha_{2000.0}$			$\delta_{2000.0}$	$(O-C)_\alpha$	$(O-C)_\delta$	O.C.
					80 SAPPHO						
43	26.80669	Jul.	18	33	56.84	–7	39	46.2	–0.070	–0.40	GB
44	26.81708	„	18	33	56.36	–7	39	47.4	–0.070	–0.40	GB
					148 GALLIA						
45	27.76779	Apr.	11	56	10.15	+23	40	22.3	–0.045	+0.15	GB
46	27.77957	„	11	56	9.91	+23	40	23.0	–0.014	+0.20	GB
					389 INDUSTRIA						
47	11.83087	Oct.	1	32	42.19	+22	53	36.5	+0.037	–0.30	GB
48	11.84126	„	1	32	41.61	22	53	33.5	+0.032	–0.43	GB
49	13.75270	„	1	30	57.41	22	44	23.8	–0.004	–0.09	GB
50	13.75962	„	1	30	57.07	+22	44	21.6	+0.042	–0.27	GB
					409 ASPASIA						
51	26.83474	Jul.	19	43	34.67	–5	13	34.7	–0.070	+0.00	GB
52	26.84617	„	19	43	34.02	–5	13	35.3	–0.070	+0.00	GB
					1994						
					48 DORIS						
53	1.77282	Sep.	20	56	55.65	–10	44	7.1	+0.040	+0.10	GB
54	1.78667	„	20	56	55.16	–10	44	11.2	+0.040	–0.10	GB
					179 KLYTAEMNESTRA						
55	1.80329	Sep.	21	24	19.03	–2	38	50.4	–0.010	+0.60	GB
56	1.81714	„	21	24	18.39	–2	38	54.1	–0.010	+0.60	GB
					216 KLEOPATRA						
57	1.83376	Sep.	23	20	37.52	+14	23	46.4	+0.190	+0.00	GB
58	1.84484	„	23	20	37.13	+14	23	41.7	+0.170	+0.10	GB

Table 2

No	BD	$(\alpha_i)^s$	$(\delta_i)''$	Dependences	
1–2	–10–4904	22.629	44.35	0.010349	0.010110
	–10–4912	20.512	36.44	.186698	.185447
	–10–4918	49.884	34.91	.043847	.045221
	–10–4930	52.496	34.59	.271566	.272689
	–10–4934	23.503	12.25	.487540	.486534
3–4	–10–4918	49.968	33.99	0.283145	0.282661
	–11–4849	19.500	62.81	.236471	.237827
	–10–4931	14.138	17.74	.200104	.198219
	–11–4869	4.865	55.11	.143360	.144196
	–10–4946	14.344	37.91	.136919	.137099
5–6	–22–5897	50.581	61.78	–0.196843	–0.194913
	–21–6207	12.816	52.11	+.057731	+.058379
	–21–6213	48.267	0.59	.454236	.453187
	–21–6214	1.017	14.05	.421114	.419989
	–2215881	31.378	3.91	.263761	.263359
7–8	–22–5897	50.581	51.78	0.187275	0.188238
	–21–6207	12.816	52.11	.281005	.281265
	–21–6213	46.267	0.59	.300064	.299629
	–2215889	52.994	11.33	.053406	.053671
	–21–6226	23.206	25.32	.178250	.177197
9–10	2 4520	23.721	10.93	0.196177	0.196768
	1 4629	36.930	6.09	.051275	.052065
	2 4528	20.439	14.09	.383204	.382658
	1 4634	43.549	55.11	.072350	.072533
	1 4637	24.537	42.35	.296993	.295977
11–12	2 4520	23.721	10.93	0.279808	0.280326
	1 4629	36.930	6.09	.169692	.170267
	2 4528	20.439	14.09	.297213	.296874
	1 4634	43.549	55.11	.104583	.104658
	1 4637	24.537	42.5	.148703	.147875
13–14	1 4623	49.130	43.84	0.220136	0.221198
	1 4626	14.520	4.89	.250585	.251687
	2 4520	23.721	10.93	.172965	.172518
	1 4629	36.930	6.09	.201374	.301047
	1 4631	57.031	9.28	.154939	.153551
15–16	0 4884	47.386	38.82	0.256246	0.258078
	1 4620	48.130	6.67	.472409	.471684
	0 4891	6.204	57.41	.171442	.170693
	0 4892	8.054	46.22	.075199	.075462
	0 4894	7.811	4.71	.024704	.024084

Table 2 (continued)

No	BD	$(\alpha_i)^s$	$(\delta_i)''$	Dependences	
17–18	–15–4965	45.795	55.77	0.157403	0.156880
	–14–5044	16.029	25.32	.274611	.273365
	–15–4972	39.240	19.78	.114593	.115391
	–14–5065	15.320	11.26	.287454	.287138
	–15–4982	25.879	59.14	.165938	.167226
19–20	–15–4965	45.795	55.77	0.098672	0.098071
	–14–5044	16.029	25.32	.155637	.154273
	–15–4972	39.240	19.79	.187286	.188182
	–14–5065	15.320	11.26	.264060	.263700
	–15–4982	25.879	59.14	.294345	.295774
21–22	–6–4377	20.089	4.11	0.213139	0.213789
	–5–4254	15.359	56.64	.239434	.239337
	–7–4230	32.437	53.85	.162543	.163534
	–6–4393	47.032	20.50	.168198	.167909
	–5–4267	21.444	1.00	.216686	.215431
23–23	–0–0336	43.050	35.55	0.152210	0.153101
	–1–0307	13.152	52.85	.128012	.128848
	–0–0338	38.335	40.87	.222278	.222466
	–1–0311	19.190	31.11	.163099	.162848
	–0–0345	41.514	54.02	.334401	.332737
25–26	5 4831	48.182	10.95	0.106449	0.108678
	6 4868	58.932	25.96	.077545	.077900
	6 4878	48.969	13.71	.197881	.196569
	5 4841	5.705	5.66	.269397	.270066
	5 4847	43.702	15.08	.348729	.346786
27–28	3 4575	11.067	47.37	0.168670	0.170501
	4 4701	35.900	5.01	.172569	.171682
	3 4581	47.409	29.97	.205539	.207403
	4 4705	18.515	36.77	.202240	.200457
	3 4588	5.909	59.06	.250982	.249958
29–30	3 4570	38.579	6.23	0.039674	0.040874
	3 4572	8.549	3.37	.050991	.053487
	3 4577	22.048	13.94	.287993	.285402
	3 4578	36.746	10.05	.217563	.218668
	3 4581	47.409	29.97	.403779	.401569
31–32	–20–6439	42.516	4.40	0.098737	0.099416
	–20–6441	36.985	21.80	.244490	.245254
	–20–6442	11.737	8.22	.082042	.081994
	–21–6248	58.268	40.15	.361169	.360881
	–20–6453	33.015	56.72	.213561	.212455

Table 2 (continued)

No	BD	$(\alpha_i)^s$	$(\delta_i)''$	Dependences	
33–34	–21–6221	0.931	40.25	0.211939	0.212382
	–20–6431	20.222	43.69	.167310	.167487
	–21–6241	22.974	13.13	.260651	.260842
	–20–6445	46.430	6.17	.147861	.147865
	–21–6248	58.268	40.15	.212239	.211865
35–36	–21–6221	0.931	40.25	0.349610	0.351567
	–20–6431	20.222	43.69	.214223	.214659
	–21–6230	30.650	51.30	.274254	.274819
	–20–6439	42.516	4.40	.046092	.044422
	–21–6241	22.974	13.13	.115820	.114532
37–38	–21–6175	46.699	25.41	0.004560	0.004746
	–21–6178	38.952	19.72	.096919	.097141
	–22–5867	56.126	18.06	.250922	.250593
	–21–6185	11.976	28.78	.265527	.265809
	–21–6188	9.021	18.42	.382072	.381712
39–40	–21–6175	46.699	25.41	–0.005056	–0.005045
	–21–6178	38.952	19.72	+0.128226	+0.128444
	–22–5867	56.126	18.06	.185342	.185013
	–21–6185	11.976	28.78	.337970	.338266
	–21–6188	9.021	18.42	.353519	.353322
41–42	–2–0136	3.672	8.43	0.160997	0.163225
	–2–0137	5.470	29.44	.315737	.316281
	–2–0148	25.442	28.05	.111079	.111662
	–2–0154	25.756	43.18	.271700	.269537
	–2–0155	55.475	16.35	.140486	.139294
45–46	24 2405	34.277	39.60	0.349011	0.349742
	24 2407	2.883	24.80	.287224	.287466
	25 2439	54.988	9.86	.153410	.153520
	24 2414	16.544	19.21	.169672	.169207
	24 2416	5.939	21.56	.040684	.040064
47–48	22 0236	41.178	34.06	+0.099327	+0.100311
	22 0238	48.684	26.09	–0.011457	–0.010875
	21 0200	6.816	53.63	+0.198115	+0.199065
	22 0246	28.705	25.80	.276933	.275641
	21 0211	0.128	1.76	.437082	.435858
49–50	22 0236	41.178	34.06	0.277585	0.278170
	22 0238	48.684	26.09	.089981	.090235
	21 0200	6.816	53.63	.372071	.372704
	22 0246	28.705	25.80	.043505	.042735
	21 0211	0.128	1.76	.216859	.216155

Received on 10 April, 1995

ASTROMETRIC POSITIONS OF THE COMET 1995/O1 (HALE-BOPP)

GHEORGHE BOCŞA, MIREL BÎRLAN

Astronomical Institute of the Romanian Academy,
Str. Cuţitul de Argint, 5, 75212 Bucharest 28,
Romania

Abstract. Precise positions of the comet 1995/O1 (Hale-Bopp) observed in Bucharest are presented. These observations were made with a 380/6000 mm astrograph. We used astrophotographic plates and an Ascorecord measuring machine.

Key words: comet, astrometry.

The comet 1995/O1, very well known by the astronomers (professionals and amateurs) as the comet *Hale-Bopp*, offered us a brilliant cosmic show. The computed preliminary orbit reveals that the comet 1995/O1 is for the first time when it passes across the Sun. Systematic observations of its "atmosphere" allow the identification of new chemical compounds (Circular 6568, 6573, 6614, 6625, 6631) never before reported for any other comet.

During autumn 1996, several nights of observation allowed us to perform precise astrometric positions of the comet. The observations were made with the *Mertz-Prin* astrograph (380/6000 mm) from Bucharest.

These positions were calculated using 5–10 PPM reference stars, chosen around the comet, not farther than 1° from the center of the plates. From the α_i, δ_i coordinates (corrected with the proper motions) of the reference stars, and α_0, δ_0 of the center of the plate, the normal coordinates X_i, Y_i were computed. Both Turner's (constants) and Schlesinger's (dependences) methods (Brouwer & Clemence 1961) were used to compute the normal coordinates of the comet. Then, starting with the normal coordinates X, Y, the topocentric coordinates α, δ, of the comet were determined.

The results are presented in Table 1. The first column contains the date of the observations (year, month, day with fraction of day); the topocentric right ascension and the declination of the comet for the 2000.0 epoch are presented in the second

Rom. Astron. J., Vol. 7, No. 2, p. 199–200, Bucharest, 1997

and the third column, respectively; the last column contains the number of the reference stars used for computing.

Table 1

Astrometric positions of the comet 1995/O1 (Hale-Bopp)

DATE UT	$\alpha_{2000.0}$	$\delta_{2000.0}$	N
1996 09 10.76657	$17^h33^m34^s.69$	$-6°00'26''.0$	5
" 09 10.77453	17 33 34 .45	−6 00 24 .3	5
" 09 10.73788	17 33 10 .43	−5 57 19 .0	10
" 09 11.75034	17 33 10 .10	−5 57 16 .7	10
" 10 03.71416	17 29 51 .17	−4 52 15 .2	8
" 10 15.69075	17 32 18 .87	−4 16 34 .4	9
" 10 15.69802	17 32 18 .99	−4 16 33 .3	9
" 11 04.67492	17 42 05 .11	−3 04 25 .2	10
" 11 04.68219	17 42 05 .34	−3 04 22 .6	10
" 11 12.66901	17 47 44 .94	−2 27 43 .1	7
" 11 12.67697	17 47 45 .29	−2 27 42 .8	7

These astrometric observations were already reported to the Central Bureau for Telegrams of the International Astronomical Union and used to improve the orbital elements of the comet.

REFERENCES

Brouwer, D., Clemence, G.: 1961, *Methods of Celestial Mechanics*, Academic Press, New York & London.

⁂ *Circula Nos. 6568, 6573, 6614, 6625, 6631*, Central Bureau for Astronomical Telegrams of the International Astronomical Union.

Received on 8 July, 1997

GROUND-BASED ASTROMETRY AT THE TIME OF THE GAIA SPACE MISSION

WILLIAM THUILLOT[(1)], JEAN-EUDES ARLOT[(1)], MAGDALENA STAVINSCHI[(2)], MIREL BIRLAN [(1,2)], VALERY LAINEY [(1,3)]

[(1)] Institut de mécanique céleste et de calcul des éphémérides
IMCCE/Paris Observatory
77 av. Denfert Rochereau 75014 Paris, France)
[(2)]Astronomical Institute of the Romanian Academy
str Cutitul de Argint – 5, 040557, Bucharest, Romania
[(3)]Royal Observatory of Belgium,
Av. Circulaire, 3 - Ringlaan 3
1180 BRUXELLES - BRUSSEL (Belgium)

Abstract. The next space astrometry mission GAIA will be launched before 2012 with the purpose to perform a wide 3-D cartography of the Galaxy. During this 5 years long mission many Solar System objects will be scanned and measured. Each object will be observed about one hundred times and a very accurate astrometry, down to 10 μas, will be carried out. Furthermore, since the limiting magnitude will be 21 and observations could be made rather close to the Solar direction, many new Solar System objects will certainly be discovered. Therefore this mission will be a milestone in particular for astrometry of the Solar System. Several ground-based programs of observation of Solar System objects will probably have to be stopped or reoriented in order to remain relevant. Our paper intends to discuss these circumstances and the relevance of selected observations. Several proposals are made for coordinating efforts in order to get a better knowledge of these objects. Either autonomous programs or programs complementary to the GAIA mission are proposed. Small telescopes will be still very useful for these programs.

Key words: space mission – astrometry – catalogue – follow-up.

1. INTRODUCTION

Several astrometric programs can be undertaken in order to get a better knowledge of the dynamics of several objects of the Solar System. These observations help us to get improved the dynamical models, to make better predictions of some phenomena (such as stellar occultations) or to find better interpretation of observations and the astrophysical measurements.

But the GAIA astrometric mission scheduled in 2011 for mapping the Galaxy, will certainly question a part of our knowledge of the objects of the Solar System. In

Rom. Astron. J., Vol. XXX, No. XXXX, p. XXX–XXX, Bucharest, 2005

particular the motions and some physical parameters of many small objects will be studied by GAIA and this will decrease the interest of several ground-based programs.

Nevertheless several programs could still remain relevant due to specific aspects of the phenomena implied, or to the range of magnitude of the objects concerned. Our interest is mainly oriented to the following topics:

- Ground based observations of Near Earth Asteroids and main belt asteroids for a GAIA Follow-up
- Astrometry of the new faint planetary satellites
- Mutual events of natural satellites for the improvement of the dynamical models
- Astrometry of the Martian satellites in support to the Mars Express mission
- Stellar occultation by asteroids and satellites for the morphology and the atmosphere probing
- Determination of masses of asteroids by observation of asteroids encounters

2. **THE GAIA MISSION.**

After the successful Hipparcos mission, the space astrometric GAIA ESA mission (http://astro.esa.int/gaia/) intends to make a wide cartography of the Galaxy with a never reached accuracy (Fig. 1). It will probably take place from 2011 to 2015 and will provide a huge amount of data with a high accuracy (down to 10 μas). GAIA will provide positions, parallaxes, proper motions, multicolour photometry and radial velocities. Several hundred of thousands Solar System objects will be detected and measured and our knowledge of these objects will be drastically improved. The main characteristics of this mission are given in the Tab. 1.

Fig.1 – Illustration of GAIA design and artist picture of the spacecraft (from ESA)

Table 1

Several characteristics of the GAIA mission

Launch	~2011
Duration	5 years
Limiting magnitude	21
Number of stars	1.3 billion
Accuracy	10 μas
Number of asteroids	10^5 to 10^6
Accuracy	100 μas

3. A PROJECT FOR A FOLLOW-UP PROGRAM

Actually, GAIA will perform a wide scan of the sky and will have generally not the possibility to immediately re observe an event or an object just detected. Therefore a follow-up program for the GAIA mission will be a useful complementary program. Observations on alert will be a requirement in order to catch more data on these targets, or even to avoid for losing them.

It will be the case for possible Gamma Ray Bursts, microlensing events, novae or other transient events. But it will be certainly the case for fast moving objects and it will be very interesting to use ground based telescopes. Fast moving objects such as Near-Earth Asteroids will require fast reactions to operate several telescopes after receiving an alert from the GAIA control centre.

Limiting magnitude down to 21 and Solar elongation close to 35 degrees will have to be reached. Such specifications may correspond to what a small telescope (50cm) is able to do in an appropriate location. A follow-up network of 0.5m to 1.5m telescopes seems to be well suitable for this task. Robotic and automatic telescopes would obviously be very more efficient in order to shorten the reaction time and we hope that more such instruments will be installed in the next years.

4. CALL FOR A FOLLOW-UP NETWORK

Thanks to a call (http://aira.astro.ro/wg/) through the IAU commission 8 and its Working Group “The Future Development of the Ground-Based Astrometry “ led by M. Stavinschi and J. Kovalevsky, we have already identified several stations which are interested by this program (Fig. 2). The extension of this network and the increasing of the efficiency for the asteroid follow-ups will be studied: identification of each limiting magnitude, determination of the individual astrometric accuracy, rules to apply for a fast reaction on alert.

On this map several stations directly answered to our call for this network : 1: Brooks observatory (USA), 2: Pic-du-Midi and 3: Haute-Provence observatory (France), 4: Uppsala (Sweden), 5: Pulkovo observatory (Russia), 6: NAO Nikolaev Observatory (Ukraine), 13: Valhinos station (Brazil), 15: Sheshan station (China)

Other stations are possible and contacts are in progress for 7: AOE Kazan state univ. (Russia), 8: TUG observatory (Turkey), 9, 10, 11, 12, 14 in Brazil where are robotics telescopes of a Brazilian education program. Any other observers interested by these observations on alert are welcome.

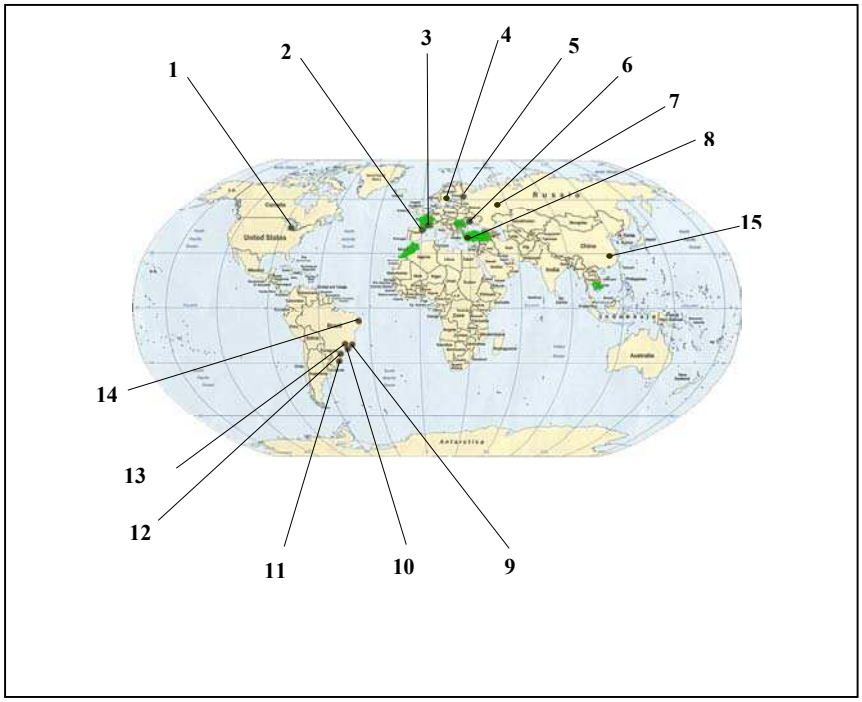

5. NATURAL SATELLITES; PHENOMENA APPLIED TO THE IMPROVEMENT OF THE DYNAMICAL MODELS

Several natural satellites will be observable by GAIA but not all the satellites. Several ones will require special method of observations to be determined due to their brightness and the induced saturation. But on one hand, the new faint satellites, generally irregular satellites, will not be observable at all by GAIA and remain an interesting field for dynamical researches. Nevertheless their faint magnitudes generally require the use of large telescopes. On the other hand, several large and bright satellites will probably be observed but with less accuracy by GAIA. These satellites still require accurate observational data since new and improved dynamical models have recently

been developed (Lainey et al. 2004a, 2004b) and that some physical effects (tidal effects) can be explored with them. Mutual phenomena are this kind of observations.

5.1. MUTUAL PHENOMENA: CALL FOR OBSERVERS

Mutual phenomena (eclipses and occultations of satellites by each other) occur in several satellites system. These events were first observed among the Galilean satellites, but they also occur in the Saturnian system and in the Uranian system. This is the opportunity to get very accurate data from the ground since no atmosphere is generally involved. 15 to 30 mas of astrometric accuracy can be obtained with these photometric observations. Campaigns are organized by IMCCE (Institut de Mécanique Céleste et de Calcul des Ephémérides) for the Galilean system (Arlot 2002, Vasundhara et al. 2003) every six years, and for the Saturnian one (Thuillot et al. 2001) every 15 years.

During these campaigns, photometric measurements lead to lightcurves such as the curve given in Fig. 3 from which astrometry of high precision (5 to 10 mas) can be deduced. Such an accuracy obtained on observations spread out over several decades will help to quantify the tidal effects on the Galilean satellites.

A new program for mutual phenomena of the Uranian satellites will be organised for the period 2006-2007. Later a new campaign of observation of the mutual phenomena of the Galilean satellites will be also organized in 2009. During several months, about 400 phenomena could be observed and a network of observers is necessary in order to catch a maximum of phenomena thanks to a large longitude coverage. Observers are invited to contact IMCCE.

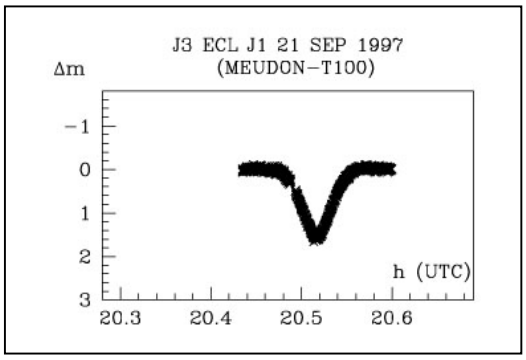

Fig.3 – Lightcurve obtained during the eclipse of Io by Ganymede, observed from the Meudon observatory in 1997

5.2. DETERMINATION OF PHOBOS MASS USING MARS EXPRESS CLOSE FLYBYS VS PHOBOS EPHEMERIS

The first determinations of Phobos mass have been obtained using Viking-1 spacecraft flybys in the year 1977. Since that day, many efforts have been made to improve these determinations. Several combinations of each flyby have been used, involving mainly Viking 1, and Phobos 2 missions. Although many studies converged on an unexpected low value of Phobos mass, no real agreement has been found yet, as seen from the comparison of the values and the error bars. A better determination of Phobos mass (and so its density) would be of great importance regarding the still puzzling origin of the Martian satellites.

Several close encounters between Mars Express and Phobos are scheduled for 2005. These flybys will be the opportunity to reconsider the previous determination of Phobos mass using radio-science.

In particular, the shift between the center of mass and the center of figure (J_1 coefficient) shall be determined. The knowledge of a mass anomaly inside the satellite (especially following the Stickney impact) would be the witness of internal stress. The interpretation of such data will enlighten the key-point of an assumed (but still not demonstrated) homogeneous density. Furthermore, the determination of the higher harmonics coefficients of the gravity field like the J_2 and C_{22} coefficients will also allow us to have additional information on the interior of Phobos.

In order to achieve these goals, a high accurate ephemeris of Phobos in 2005 is required. Tides raised among the Martian surface by Phobos induce a secular acceleration on its motion. This implies to fit Phobos dynamical motion model regularly.

As a consequence, new ground-based observations of Phobos are welcomed and if provided to us, will be used in a very short time. A new dynamical model of the motion of the Martian satellites is currently developed jointly at ROB (Royal Observatory of Belgium) and IMCCE.

6. STELLAR OCCULTATIONS BY ASTEROIDS AND SATELLITES

Stellar occultations by objects of the Solar System (Fig. 4) allow a network of observers to acquire very accurate data on the size, the morphology, the binarity of asteroids. Furthermore it allows us also to explore atmospheres when they exist. Last minute astrometry is a very important task in order to improve the predictions of such events. Succeeding in these observation depends both on improved orbital models of the objects and on high accuracy of the stellar positions (and therefore of the proper motions). This is a complex problem, in particular for the natural satellites, and even if

in the future we get new accurate stellar catalogues, the need of high accuracy of the relative positions (better than 1 mas) required in order to have observers well disseminated on the track of the umbra will certainly imply to continue these last minute observations even after the GAIA mission.

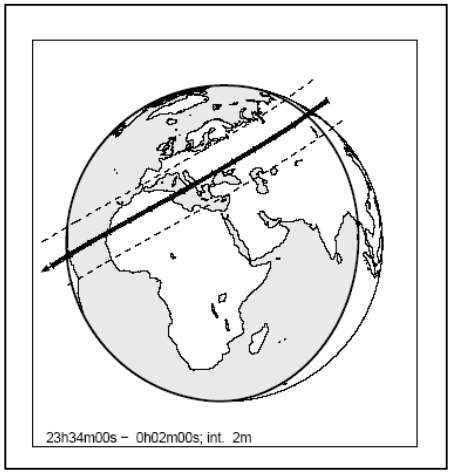

Fig.4 – Path of the umbra of 230 Athamantis during a stellar occultation on 18 November 2004 (from L. Vasta and I. Manek website http://mpocc.astro.cz/2004/)

7. **ASTEROID MASS DETERMINATION BY CLOSE ENCOUNTERS**

Only a few masses of some asteroids are well known with enough accuracy to be efficiency included in the planetary solutions. At this time several space missions are planned toward Mars, but the theory of its motion, which is of interest for the interpretation of their data, is limited by this problem. One of the methods successfully applied for determining asteroids masses is the observation of encounters and measurement of gravitational deflections of the perturbed asteroid (Fig. 5).

We have predicted these phenomena (Fienga et al. 2003) on a period of time spanning the GAIA mission (2003-2022). We found that the GAIA mission will allow us to determine one hundred masses thanks to observation of close encounters down to 1 mas. But we also predicted than a few masses can be determined before the GAIA mission from ground based observations. We have computed several encounters at the level of 50 mas (CCD astrometry can reach this accuracy) of changes in the angular positions by comparison of perturbed and unperturbed orbits around the date of encounters. Among the asteroids concerned, 10 Hygiea, 16 Psyche, 31 Euphrosyne, 704 Interamnia, 87 Sylvia will be good candidates to have their masses accurately determined before the GAIA mission.

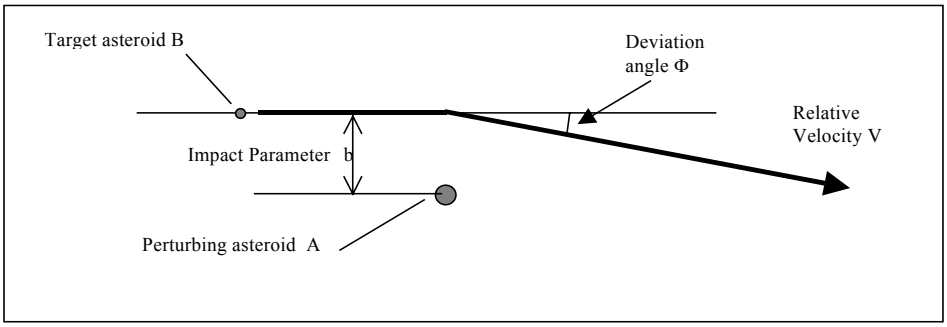

Fig.5 – Gravitational deflection of a small asteroid during an encounter

4. CONCLUSION

By mapping the sky, the next GAIA astrometric space mission will drastically improve in particular our knowledge of the Solar System objects. Numerous new asteroids will be detected and their orbital elements determined. Several natural satellites will also be observed. Nevertheless it appears than ground-based programs for astrometric observations remain of interest for several purposes. A ground-based follow-up program has to be developed in order to avoid for losing the fast moving objects by GAIA and to improve the orbital elements of new objects which will be detected by the space probe. Several natural satellites will not be accurately observed or even not included in the GAIA program. Astrometry of the new faint satellites, or campaign of observation of the mutual phenomena are to be carried out. Starting from now, observations of the Martian satellites would be very useful in support to the Mars Express mission, in order to deal with the mass determination of Phobos. Furthermore several specific ground based observations can lead to original results or to information helpful for the GAIA mission: stellar occultations for the accurate morphological studies, measurement of gravitational deflections during asteroids encounters are such programs.

REFERENCES

Arlot, J.-E.: 2002, *Astron. Astrophys*. **383**, 719
Fienga, A. et al: 2003, *Astron. Astrophys*. **406**, 751
Lainey, V., Vienne, A., Duriez, L.: 2004a, Astron. Astrophys. **420**, 1171
Lainey, V., Arlot, J.-E., Vienne, A..: 2004b, Astron. Astrophys. **427**, 371
Thuillot, W. et al.: 2001, *Astron. Astrophys*. **371**, 343
Vasundhara,R. et al: 2003, *Astron. Astrophys*. **410**,.

Received on XXXXX

Title: Relevance of the NEO dedicated observing programs

Titre: Importance des programmes d'observation des objets géocroiseurs

Authors: William Thuilllot [a], Jérémie Vaubaillon [a], Hans Scholl [b], François Colas [a], P. Rocher [a], Mirel Birlan [a], Jean-Eudes Arlot [a]

Laboratories:

[a] *Institut de mécanique céleste et de calcul des éphémérides, IMCCE/Observatoire de Paris, 77 av. Denfert-Rochereau 75014 Paris, France*

[b] *Observatoire de la Côte d'Azur, BP 4229, 06304 Nice cedex 04, France*

Proofs should be sent to :

William Thuillot,
Institut de mécanique céleste et de calcul des éphémérides,
IMCCE/Observatoire de Paris, 77 av. Denfert-Rochereau 75014 Paris, France
Phone 33 1 40 51 22 62
Fax 33 1 46 33 28 34

Abstract

The study of NEOs (Near Earth Objects) has considerably been developed in several ways under the huge impulse of the researches on the risks of an hazardous collision with the Earth. In this context the observations play a very important role. This article attempts to underline their importance to improve our knowledge of these objects and the necessity of organizing dedicated programs. It develops the objectives of these observations, describes methods to perform the detection of new objects, discuss their follow-up and the necessity to find and to use archives. It also gives information about the fit of the observations in order to improve the knowledge of the orbits of NEO and about the effect of the planetary theories taken into account in the model.

Résumé

L'étude des objets géocroiseurs (NEO ou Near Earth Objects) s'est considérablement développée sous de multiples aspects sous l'impulsion notable des recherches concernant les risques de collision avec la Terre. Les observations jouent dans ce contexte un rôle primordial. Cet article s'attache à souligner leur importance pour accroître notre connaissance de ces objets et la nécessité d'en organiser des coordinations spécifiques. Il développe les objectifs de ces observations, explicite des méthodes pour réaliser la détection de nouveaux objets, discute de leur suivi et de l'archivage des données, donne des informations sur leur utilisation pour améliorer la connaissance de leurs orbites et sur l'influence du choix des théories planétaires prises en compte dans le modèle.

Keywords: asteroids; NEO; detection surveys; follow up; observations
Mots-clefs: astéroïdes; NEO ; objets géocroiseurs; surveillance; suivi ; observations

1. Introduction

The study of the NEOs (Near Earth Objects) is a very active domain of research nowadays and the observational data are obviously very appropriate to perform improvements in this domain. We need to increase the amount of these data and their quality for different purposes. The detection of new objects is obviously the first task to be carried out in order not only to identify the potentially hazardous objects, but also in order to get a better knowledge of their dynamical behavior. A second and very important task is the follow-up observation. This task only will lead to the improvement of the orbital elements of the detected objects and to the physical characterization by measuring several parameters. It requires dedicated astrometric, photometric and spectroscopic measurements through a network of stations of observation. Finally, the best determination of orbital elements requires the search in archived observations where the objects could have already been observed.

If all these steps have been done, the collected data can allow to compute a realistic orbit of a NEO and to assess the risk of collision or, at least, to estimate the uncertainty of the least distance to the Earth and of its epoch. In the following sections we develop these topics and we describe some numerical experiments done to evaluate several effects which may act on this uncertainty: influence of the density of observations, of the spanning time span of observations and of the effect of the planetary ephemerids that are used in the gravitational perturbations.

2. Surveys and detection programs

The current observational programs set to catalogue NEOs (NEAs, Near Earth Asteroids and NECs, Near Earth Comets) use dedicated ground-based telescopes equipped with CCD detectors. Possible NEOs are identified by automated computer software packages. Not surprisingly, those detection programs which search the largest amount of sky each month have most success in finding new NEOs. Since more than ten years, the large majority of NEOs has been discovered by search programs based in the United States. Table 1 shows the corresponding statistics.

The yearly discovery rate of the American programs increased strongly from 26 in 1995 to 421 in 2003 while the other programs never exceeded 20 discoveries per year. LINEAR contributed mainly to the success of the American programs. The other American programs NEAT, Spacewatch, LONEOS and Catalina had sometimes strongly variable discovery rates. The variations were due to technical changes concerning the telescope, the CCD camera used, the automatic detection software and sometime the obligation to share observation time with other programs. The American survey programs are coordinated through the NASA NEO program Office at the Jet Propulsion Laboratory (JPL) [1]. NASA's search program is designed to discover 90 percent of the NEO population (1 km in diameter or larger) within 10 years. There were never comparable national search programs in other countries which is one of the major reasons for the few detections outside the United States.

Most American search programs changed or upgraded their telescopes since 1995 and added a separate telescope for follow-up of NEOs which allows also to determine more precisely their astrometric positions. We give a very brief description of the presently used telescopes for detection

The by far most successful detection program LINEAR (Lincoln Near-Earth Asteroid Research) [2] is run by the Lincoln Laboratory of the Massachusetts Institute of Technology (MIT) in cooperation with the U.S. Air Force. The observing site is Socorro, New Mexico.

Two one-meter aperture wide field Air Force telescopes (GEODSS) specially designed to optically observe Earth satellites are used. The field of view is 2 square degrees. The NEAT (Near-Earth Asteroid Tracking) team [3-4] uses an AMOS (Air Force Maui Optical and Supercomputing) 1.2-meter telescope in Haleakala, Maui, Hawaii and the 1.2-meter Oschin telescope at Mt. Palomar, California which previously performed the two Palomar Sky Surveys. The telescope in Hawai has a field of view of 1.4 square degrees. Spacewatch is the oldest NEO detection program started in 1984 by T. Gehrels at Kittpeak, Arizona. At present, a 0.9-meter telescope is used with a field of view of 2.9 square degrees [5]. The telescope is used also for detecting objects in the outer solar system. LONEOS (Lowell Observatory Near-Earth Object Search) [6] uses a 0.6-meter Schmidt telescope in Flagstaff, Arizona. It covers a field of view of 2.9 square degrees [6]. The Catalina Sky survey operates a 0.7-meter Schmidt telescope at Mt. Bigelow near Tucson, Arizona. Its field of view is 2.9 square degrees [7].

Year	Li	N	S	Lo	C	Other	≥1km	Total NEA	Total NEO
1995	0	0	26	-	-	6	196	347	385
1996	1	10	28	-	-	6	202	392	430
1997	17	11	14	-	-	11	217	445	483
1998	135	11	36	7	3	13	269	650	688
1999	161	0	19	13	30	5	336	879	918
2000	258	15	26	38	13	12	440	1241	1281
2001	277	92	22	42	0	4	531	1678	1724
2002	286	145	22	21	1	11	627	2163	2211
2003	235	68	56	54	8	17	694	2601	2650
2004*	277	25	62	35	65	7	748	3130	3179

Table 1. Number of NEAs discoveries by detection programs, total number of NEAs and NEOs (from A. Chamberlin, NASA). We note Li for Linear, N for NEAT, S for Spacewatch, Lo for LONEOS, C for Catalina (*: incomplete)

Currently, there are three somewhat regular NEO detection programs outside the United States, the Asiago DLR Asteroid Survey ADAS [8], the Campo Imperatore Near-Earth Objects Survey CINEOS [9] and the Japanese Spaceguard Association (JSGA) survey [10]. The telescopes of the three detection programs are not fully dedicated for NEO search. CINEOS observations are performed by a Schmidt telescope (60/90/183 cm) at Campo Imperatore Observatory on Gran Sasso Mountain, 130 km from Roma (Italy). The field of view is 52' x 52'. ADAS uses the 60-cm Schmidt telescope in Asiago near Padova (Italy), with a field of view of 49'x 49'. The two European telescopes for NEO search have much smaller field of views and apertures as compared to the American telescopes. Therefore, even the full dedication of the European telescopes for NEO detection would not significantly increase the European contribution. The Japanese Spaceguard Association uses a 1-meter Cassegrain telescope with a field of view of 2.5 x 3.0 degrees partially for NEO detection [10] at the Bisei Spaceguard Center in the Okayama region. In France a Schmidt telescope which is located near Caussols (Observatoire de la Côte d'Azur) searched for NEOs until 1999. It was not built for NEO detection purposes, however the famous 4179 Toutatis was discovered in one of its photographic plate. During the last 5 years a CCD camera was used but it was covering only a small part of the field. Twelve NEOs were discovered with this telescope

which is no longer operating. However, using a mosaic of CCDs it may be possible at this time to reach an efficiency similar to the NEAT program.

Why is LINEAR so successful in discovering NEOs? A priori, the observing site, the aperture and field of view of the telescopes do not appear to give a significant advantage for the LINEAR search program. The number of NEO detections depends on the area of the sky scanned during a given time and on the limiting magnitude reachable by the instrument. Dynamical models for assumed NEO populations do not indicate regions of the sky where a significantly higher density of NEOs can be expected.

According to the above technical data of the different search telescopes, the limiting magnitudes of the LINEAR telescopes do not give a decisive advantage for this search program. Other telescopes reach even fainter magnitudes. The success must be, therefore, due to an optimized sky coverage and also to an efficient software which finds and extracts a maximum number of NEOs from CCD images.

While the detection rate of NEOs between 1995 and 2001 strongly increased, it seems to become constant now. New generations of telescopes reaching much lower magnitudes may change this situation in the future. The goal to detect all 1 km sized or larger NEOs is not yet reached. Since 2000, year of a maximum of 104 discoveries, the rate decreases slightly on the mean, but is far from being exponentially decreasing.

3. Follow up programs for the dynamics

Once the objects are detected, follow-up observations are required and this hard to organize. Nevertheless all the objects need further astrometric and photometric measurements in order to be fully characterized and to be identified on several oppositions. Unfortunately many objects are even lost after their detections. One of the reasons is that a detection by a survey program will only lead to few measurements; therefore a short orbital arc is not sufficient to get accurate enough ephemerides. Another reason may be due to the faint magnitude of some NEO detected by the surveys which remain beyond the limiting magnitude of the instruments available for their follow-up observations.

In October 2004 for example, the orbits of more than 263 000 objects have been computed by T. Bowell; his database (ftp://ftp.lowell.edu/pub/elgb/astorb.txt) indicates that more than 400 have been poorly observed, and many are even certainly lost. This situation is particularly uncomfortable if the object is a NEO.

We can estimate the effect of the degradation of the precision in the determination of an orbit due to the lack of observations. Considering for example the NEO object 4179 Toutatis, we have first computed a nominal orbit by using a fit of all the available observations extracted from the MPC database [11] and a numerical integration using 2004 as the year of the initial conditions.

In order to test the influence of the availability of observations we did compute several orbits of 4179 Toutatis with different sets of observations. This NEA passed close to the Earth in 2004 (perihelion), and thus led to series of observations all around the world. We have simulated the lack of observations, or the influence of bias such as the limiting magnitude in the calculation of the position of the object. Then by fitting the remaining set of observation, we obtain another orbit to be compared to the nominal one.

Therefore, several fits of the orbit have been carried out, taking into account:

- all the available observations (marked as “All” in the figures below, hereafter called the “nominal solution”)
- all observations until year 2000 (marked as “without 2000+”)
- all observations until year 2002 (marked as “without 2002+”)
- only those observations providing the magnitude of the object (“All Mag”)

- among these above observations, only those with a limiting magnitude of 17.

Then the propagation of the orbit is performed, and the differences of orbital elements as well as Cartesian coordinates are plotted in Fig.1 to 3. The maximum differences to the nominal solution are found close to perihelion (1996, 2000, 2008, 2012, except 2004), where the heliocentric velocity of the body is maximum. Therefore a small error in the observations (or a lack of observation) implies a large error on the position of the body itself which in fact is mainly an error of longitude. The difference between two solutions is maximum because of the time lag between two perihelion returns. The asteroid is found to be in advance or late compared with the nominal solution (Fig. 1). This has to be compared to the motion of the Earth on its orbit. A delay of 0.005 day of the return of Toutatis corresponds to a planet displacement of 13 000 km, therefore far more than one planet radius. This value is reached in 16 years, but this is not a realistic case as it is done only with the 2004 data. A more realistic test is to use all the data except 2004 ones, which simulates the recent discover of the asteroid and the use of its observation during a few previous oppositions to predict an impact. In this case, the error is still of the order of 2000 km, which is still rather big. It is clear that if we want to predict something useful we have to use the 2004 observations. It is important to stress that using classical astrometry makes impossible to predict with a high accuracy an impact on Earth. It is fundamental for that goal to use radar data with a meter level accuracy.

The difference of orbital elements can seem to be low (Fig.2), but by converting them into Cartesian coordinates, one found a few thousands of kilometres of difference (Fig.3), at least. This is far from being negligible, especially in the case of an impact calculation, where the position of the impact has to be accurately found.

We can see that the highest differences to the nominal solution are found for the calculations that take into account the most recent observations only. This stresses the need to have as many available past observations as possible . The error of the position of the object almost doubles between the solution including observations up to 2000 and the one involving all the observations up to 2002. Interestingly the number of observations done between 2000 and 2002 is the same as the number of observations done up to 2000. This does not mean that the accuracy is proportional to the number of observations, but only underlines the fact that, to derive a reliable orbit, lots of observations on a large time scale are necessary.

Considering only the brightest observations has only a minor effect, compared to the solution including all the available magnitudes estimates. A reason for that is that the faintest observations are done when the asteroid is far from perihelion. The distance between the Earth and the asteroid is then larger, and then astrometrical errors much more important. Many NEOs are discovered when they are as close as 0.1 AU to the Earth, but most of the time this asteroid stay as far as 1 to 3 AU. Therefore the observations made during Earth close encounter are at least 10 times more important.

At aphelion the heliocentric velocity is minimum, the position of the NEO changes slowly compared to the situation at perihelion. The positional errors are then less relevant than at any other point of the orbit.

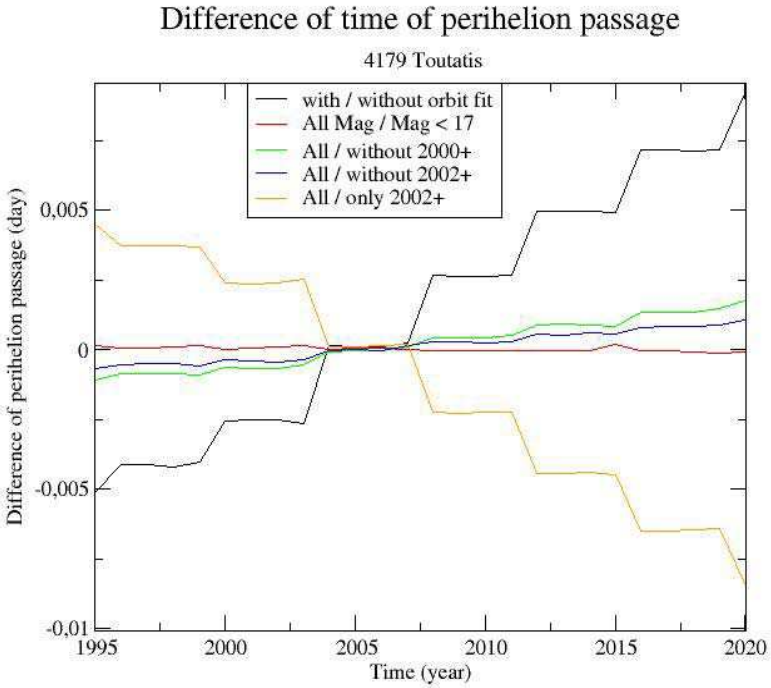

Fig 1. Computed orbits of 4179 Toutatis: differences of time of perihelion passage obtained by comparing several biased orbits with a nominal orbit

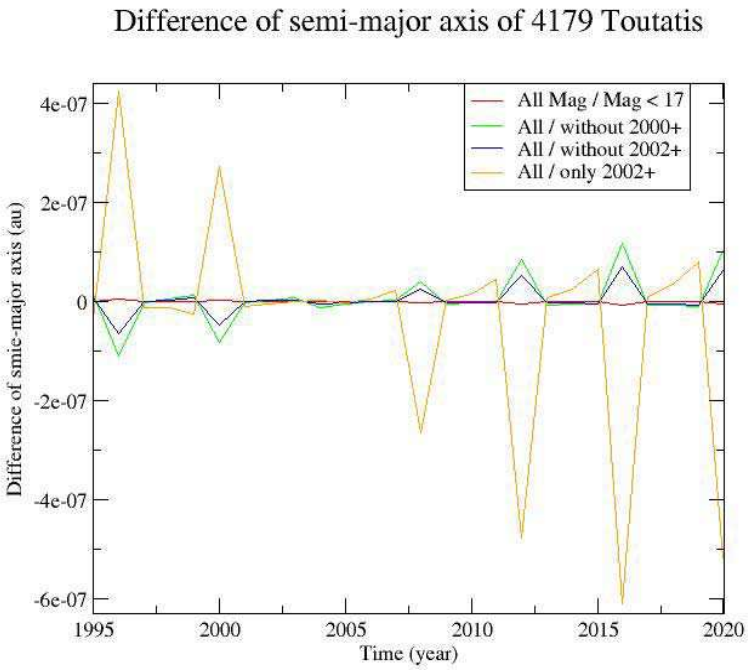

Fig 2. Computed orbits of 4179 Toutatis: differences of semi-major axis obtained by comparing several biased orbits with a nominal orbit

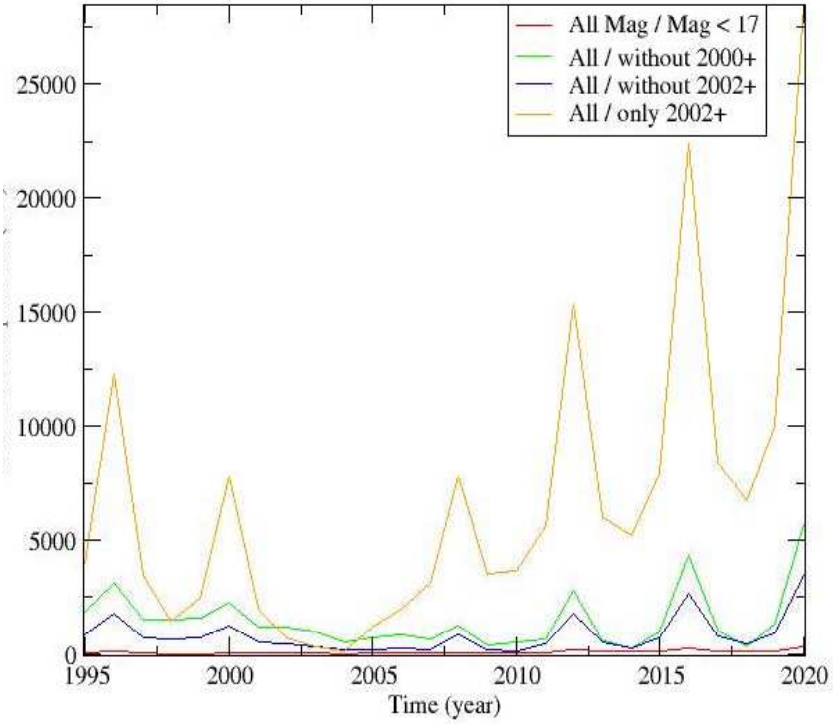

Fig 3. Computed orbits of 4179 Toutatis: differences of position in space obtained by comparing several biased orbits with a nominal orbit

The dedicated NEO programs of observations lead to discoveries of new objects which requires much more observations than what is done by the survey programs. The Minor Planet Center maintains Web pages mainly to stimulate observations just after discoveries to avoid the loss of these objects. This is also done by the Spaceguard Central Node in Italy. Lowell observatory makes also this kind of work by maintaining a critical list of asteroids. This list helps the observers to choose the asteroids to observe in order to maximize the orbit improvement. It is important to note that the observers are organised in a faint network compared to the huge resources of the detection programs. At this time, no really dangerous object was found, but in case we would have to carry out a fast follow-up program for such objects, all the work done by these centers will be a precious benefit to coordinate observers and to collect observations. As illustrated in the previous numerical experiment the orbital precision is improved by increasing the density and the spread of the astrometric observations. Therefore the accurate computation of close approaches to the Earth and the improvement of their prediction require also the search for past observations if they exist. Jointly with a follow-up program of observation, the “data mining” can then highly improve the quality of NEOs ephemerides by imposing some strong orbital constraints on a long time interval.

4. Astrometry and orbitography

The determination of accurate orbits of NEOs requires not only the use of accurate astrometric measurements but also their adjustment with a model involving all the forces acting on the objects: gravitational forces (central force, planetary perturbations) and non gravitational ones like the radiation pressure and the Poynting-Robertson drag. Among these

forces we wondered how large would be the effect of different choices of planetary ephemerides.

At the present time two main methods are used to compute planetary ephemerides: numerical integrations made at JPL by Standish [12] widely used and analytical theories developed at IMCCE by Bretagnon and his colleagues [13]. Both include now small effects such as for example some relativistic effects or effect of the Solar oblateness. But into these models, the perturbations by the largest main-belt asteroids remain hard to accurately assess since we have a very poor knowledge of their masses. Nearly 300 asteroids require to be included in the computation of the perturbations. Apart from the largest ones, their masses can only be estimated by taxonomic considerations and assumptions on the respective density of each class. But even the accuracy of the determination of the mass of the largest ones is not better than 10%. This lack of information led Standish and Fienga [14] to estimate the accuracy of the ephemerides of the four inner planets at a 2-3 km level over more than two decades. The theory of motion of Mars, which is the most sensitive to the gravitational action of asteroids, appears to be the less accurate of the planetary dynamical models. Therefore this feature may influence the computation of the orbit of Mars crosser objects and the modelling of their long term behaviour.

In order to estimate the maximum effect of such uncertainties in the computation of asteroids orbital motion, we made a selection of several Mars and Earth crosser asteroids and we carried out several numerical experiments. Two kinds of calculation were made.

The first experiment is a long term numerical integration of the orbit of 4179 Toutatis by using initial conditions extracted from a fit of the osculating elements given by the Minor Planet Center on the whole set of collected observations. The algorithm is a 15^{th} order Radau algorithm by Everhart [15]. Eight perturbing planets are considered as well as non-gravitational forces described previously.

Fig. 4 shows the differences of position of the asteroid from two different computations. Each one takes into account a different planetary theory from JPL, DE405 and DE406. Standish [12] gives details on their estimated precision. We can see that the shift between the two orbits increases with the time, the initial conditions taken in 2004. The time span of the DE405 theory did not allow to conduct the numerical integration further than the year 2199 AD. The comparison with DE406 is thus restricted to the period 1600-2199 AD. The difference of position of Toutatis begins to be significant (i.e.; larger than a few kilometres) after 200 years (backwards or forwards in time), and reaches a maximum around 300 years in the past, but no comparison with the future motion is available, because of the restriction of the DE405 theory.

The Fig. 5 shows the difference of position for several NEA that are also Mars crossers, for planetary ephemerides SLP96 from IMCCE and DE403 from JPL. We can see that the differences are much larger than when comparing DE405 and DE406, with a rapid increase to 50 km on the average after 10 years. Such differences are not that relevant in case of a 1 km diameter object or more, able to cause a global catastrophe. But it must be emphasized that even by using the best data, it is hard to reach an accuracy better than a few tens of kilometres. This could be important for a small size asteroid impact causing damage similar to the Tungunska event.

.

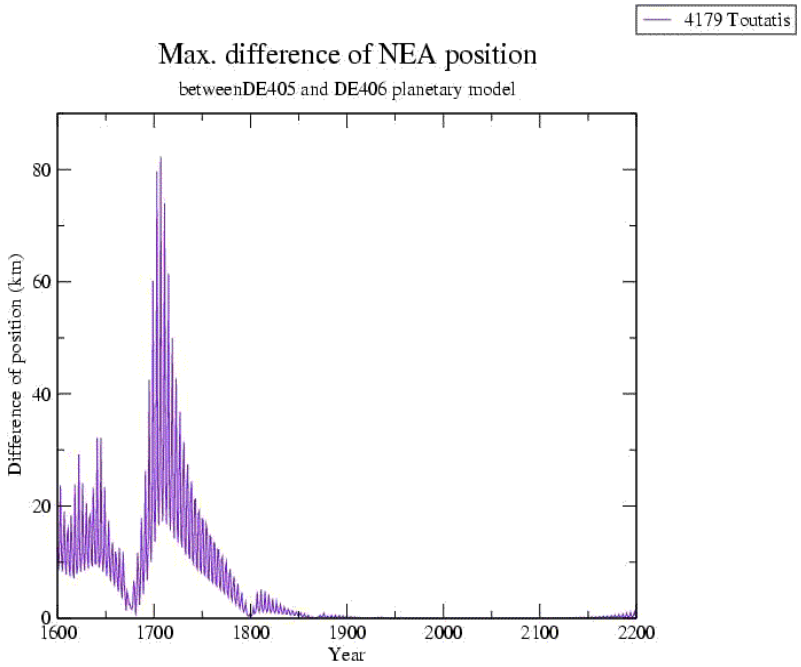

Fig 4. Shift of orbits of 4179 Toutatis due to the use of two different planetary ephemerides.

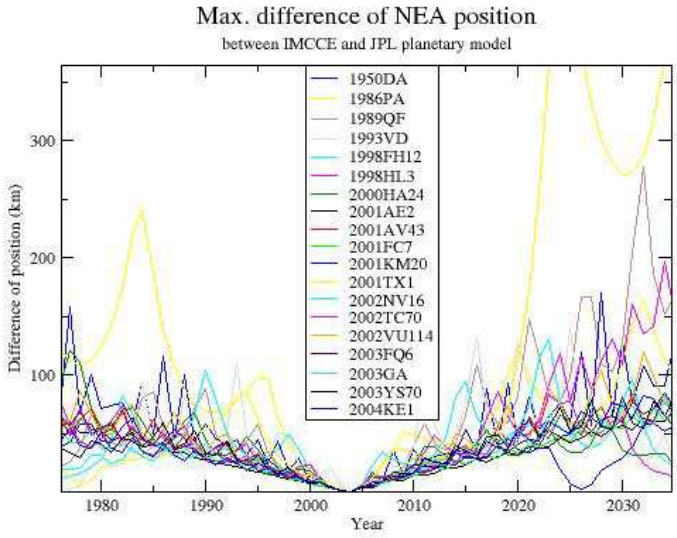

Fig 5. Shift of orbits of several Mars crossers due to the use of two different planetary ephemerides

5. Follow up programs for the physical characterization

By physical properties of a minor body we design the data obtained through observations and related to its intrinsic basic aspects such are colours, light curve, visible and near-IR spectra, thermal albedo, modelled shape and spin from radar measurements.

Continuous observational efforts must be done in order to improve both physics and internal structure of NEO population. Such programs have already been realised in the past, sporadically, for particular objects among NEOs [16,17]. Such programs provide interesting

results namely the complex rotation of 4179 Toutatis and the bi-lobed shape of 4769 Castalia from Hudson and Ostro [18]. Even if these results were presented as “unusual”, nowadays the astronomical community agrees with these conclusions (with a non-negligible importance) in the large picture featuring the minor bodies of the solar system.

Peculiar programs concerning NEOs are also offered as ground-based support of space missions, for example by Binzel et al. [19] or Sekeguchi et al. [20]. Comparative planetology and laboratory results allow to refine the knowledge of the NEO-targets, and to offer good models to explain both their physical and mineralogical feature.

Systematic spectroscopy programs of NEO population only started in the 21st century, and first outcomes of these efforts are reported by Binzel et al [21]. In terms of taxonomy, the results reveal that the NEO population is quite distinct from the Main-Belt one [22]. No systematic program concerning NEOs colors were reported, and only few ground-based instruments allow observations in thermal region (10-20 micron) [23]. NEOs light curve parameters are stored into an European database (http://earn.dlr.de/nea/database.htm), but this work is far from being achieved.

Technological acquirements in building detectors and instruments now allow ~~now~~ the observations and follow-up of faint fast-moving objects in the sky. Nevertheless, the absence of medium and large aperture telescopes devoted to NEOs physical observations makes hard the systematic studies, these programs must compete each semester with programs of various astronomical topics.

The remote observing technique could be the right choice to acquire the scientific information of a given NEO. In this sense, Paris Observatory has initiated the project of remote observing center CODAM [24], in order to offer alternatives and flexibility of scheduled observational programs. This project was started in 2002. Nowadays more than thirty nights of observations were reported. Part of the awarded time was devoted to NEO's near-IR spectroscopy. This work which is part of the remote project will continue by identifying the telescopes allowing remote observing, in order to offer a wide coverage in longitude for monitoring, in the case of this article, and clearly materialize defined NEO programs.

6. Conclusion

In this paper we give a short overview of several topics related to the observations of NEOs. Detections are mostly the task of large surveys and in these domains the American programs are obviously well in advance. But follow-up programs for dynamics as well as for physical characterization are very important. Such dedicated programs of observation, with large longitude coverage, are still necessary to make the observations more dense and continuous, namely when a NEO is just discovered or when such an object passes close to the Earth. We hope that in a next future more robotic telescopes could be used for these programs and will be able to make systematic follow-up observations. Furthermore supplementing a rich set of observations by extracting older ones from catalogues or archives will allow us also to refine the orbits, and the advent of the Virtual Observatory projects will be of great help for this purpose. Besides the increasing number and the higher quality of the observational data, the dynamical considerations are also important for the better understanding of the motion of the NEOs and we show here that the choice of a planetary theory can have a non negligible effect on the computed model to study the long term behaviour of a NEO.

References

[1] Yeomans D.K., Baalke R.C., Chamberlin A.B., Chesley S.R., Chodas P.W., Giorgini J D.; Keesey, M.S., Bulletin of the American Astronomical Society 33 (2001) 1116.

[2] Stokes G.H., Evans J.B., Shelly, F.C., Bulletin of the American Astronomical Society 34 (2002) 1315.

[3] Pravdo S.H., Hicks M., Helin E.F., Lawrence E.F., Bulletin of the American Astronomical Society 32 (2000) 1023.

[4] Talent D.L., Maeda R., Walton S.R., Sydney P.F., Hsu Y., Cameron B.A., Kervin P.W., Helin E.F., Pravdo S.H., Lawrence K., Rabinowitz D., in: Bilbro J.W., Breckinridge J.B., Carreras R.A., Czyzak S.R., Eckart M.J., Fiete R.F., Idell P.S. (Eds.), Imaging Technology and Telescopes, Proc. of SPIE 4091, 2000, p.225.

[5] McMillan R.S., Solar System Research with the Spacewatch 1.8-m Telescope, Lunar and Planetary Lab. Technical Report, Univ. of Arizona, Tucson, 2001.

[6] Koehn B.W., Bowell E.L.G., Bulletin of the American Astronomical Society 32 (2000) 1018.

[7] Larson S., Beshore E., Hill R., Christensen E., McLean D., Kolar S., McNaught R., Garradd, G., American Astronomical Society, DPS meeting 35 (2003) 36.04.

[8] Barbieri C., Calvani M., Hoffmann H.M., Mottola S., Pignata G., Salvadori L., Memorie della Societa' Astronomica Italiana 73 (2002) 636.

[9] Bernardi F., Boattini A., D'Abramo G., di Paola A., Masi G., Valsecchi G. B., in: Warmbein B. (Ed.), Proceedings of Asteroids, Comets, Meteors - ACM 2002, ESA SP-500, Noordwijk, 2002, p.801.

[10] Isobe S., Asami A., Asher D.J., Hashimoto T., Nakano S., Nishiyama K., Ohshima Y., Terazono J., Umehara H., Yoshikawa M., in: Tyson J.A., Wolff S. (Eds.), Survey and Other Telescope Technologies and Discoveries, Proceedings of SPIE Volume 4836, 2002, p.83.

[11] Marsden B., in S.Ferraz-Mello, B. Morando, and J.-E. Arlot Eds, Dynamics, ephemerides, and astrometry of the solar system: proc. of the 172nd Symposium of the International Astronomical Union, held in Paris, France, 38 July, 1995. p. 153, (1996).

[12] Standish E. M., A&A 417 (2004) 1165-1171.

[13] Moisson X., Bretagnon P., Celest. Mech. Dyn. Astron. 80 (2001) 205-213

[14] Standish E. M., Fienga A., A&A 384 (2002) 322-328.

[15] Everhart E., An efficient integrator that uses Gauss-Radau spacings, in Dynamical of comets: their origin and evolution, A. Carusi and G. Valsecchi Eds., (1985) 185-202, Reidel, Dordrecht

[16] Spencer J. R., Akimov L. A., Angeli C., Angelini P., Barucci M. A., Birch, P., Blanco C., Buie M. W., Caruso A., Chiornij V. G. and 38 coauthors, Icarus 117 (1995) 71-89.

[17] Magnusson P., Dahlgren M., Barucci M. A., Jorda L., Binzel R. P., Slivan S. M., Blanco C., Riccioli D., Buratti B. J., Colas F. and 37 coauthors, Icarus 123 (1996) 227-244.

[18] Hudson R. S., Ostro S. J., Science 263, 5149 (1994) 940-943.

[19] Binzel R. P., Harris A. W., Bus S. J., Burbine Th. H., Icarus 151, 2, (2001) 139-149.

[20] Sekiguchi T., Abe M., Boehnhardt H., Dermawan B., Hainaut O. R., Hasegawa S, A&A 397 (2003) 325-328.

[21] Binzel R. P., Rivkin A. S., Stuart J. S., Harris A. W., Bus S. J., Burbine Th. H., Icarus 170, 2 (2004) 259-294.

[22] Stuart J. S., Binzel R. P., Icarus 170, 2, (2004) 295-311

[23] Delbó M., Harris A.W., Icarus, 166, 1, (2003) 116-130

[24] Birlan M., Barucci A., Thuillot W., *Astron. Nachr*. **325** (2004) 6/7.

INTERMEDIATE STARS IN EXTRAGALACTIC RADIOSOURCE FIELDS

GHEORGHE BOCŞA [1], MIREL BÎRLAN [1,2]

[1] *Astronomical Institute of the Romanian Academy*
Str. Cuţitul de Argint 5, RO-75212 Bucharest, Romania
E-mail: gbocsa@aira.astro.ro

[2] *Observatoire de Paris-Meudon, DESPA*
5, Place Jules Janssen, F-92195 Meudon, France
E-mail: Mirel.Birlan@obspm.fr

Abstract. The present paper joins the astrometric efforts to determine the connection between the optical reference frame and the radio one. The final product of this survey will be the astrometric catalogue of the intermediate stars in the neighbourhood of extragalactic radiosources. The statistic analysis of the O–C for the RRS2 standard stars for 188 extragalactic radiosource fields situated between –20° and +70° declination are presented. These results were performed in Bucharest Observatory.

Key words: astrometry – reference frames – radiosources.

1. INTRODUCTION

During the last decade several optical astrometric surveys provided us their results. The observations are performed using either instruments on board of space missions (like Hipparcos satellite), or the ground-based ones. The products of such surveys consist of high-accuracy astrometric catalogues for a large number of stars, including faint stars. We talk frequently now about the astrometric sub-milliarcsecond era (see, e.g., Kovalevsky 1994).

The great importance of an ideal reference system in astronomy is very well known. A reference system better connected with the inertial reference system can be obtained if we take into account the farthest objects on the sky: extragalactic radiosources. Unfortunately, the extragalactic radiosources are very faint in the optical domain; the astrometric positions are based on the radiointerferometric observations for most of them. For this reason, we need to find the mathematical form of passing through the optical reference system(s) on the radio reference system.

Rom. Astron. J., Vol. 11, No. 2, p. 181–186, Bucharest, 2001

The astrometric survey from Bucharest Observatory was started within the framework of the former CONFOR program.

The CONFOR survey was an astrometric joint program of several institutes from the Eastern Europe. Acronym of Connection of Frames in Optical and Radio regions, its aim was to establish a link between the fundamental system FK5 and the radioastronomical coordinate system.

For this pourpose, the catalogue of extragalactic radiosources (Argue and de Vegt 1984), was taken into consideration. The main concept in the CONFOR program was to use the optical fixed system of reference stars in the vicinity of the extragalactic radiosources. Thus, a reliable basis for a good astrometric reduction of the extragalactic radiosources will be created. For a consistent presentation of the CONFOR program, see, for instance, Gubanov et al. (1990).

Two major steps of the program were considered:

- astrometric accuracy for the standard and intermediate neighbouring stars;
- astrometric final measurements for the extragalactic radiosource of each area in the optical domain.

For the first step, one of the instruments used for the observations was the Merz-Prin double astrograph (f = 6 m, D = 38 cm) from the Bucharest Observatory. The instrumental field of 2° × 2° allowed us to reach the stars of 13–14th magnitude on astrophotographic plates with the exposure time varying between 30 and 50 minutes.

A total number of 188 extragalactic radiosource fields were observed between 1992–1999 with this instrument.

2. OBSERVATIONS

The observations were carried out on 24 cm × 24 cm astrophotographic plates. The major parts of the observations were made when the stellar field crossed the meridian. The exposure time was established as function of the field position in the sky: up to 50 minutes for the fields of –20° to 0° declination, and 30 minutes for the fields around 45° in declination.

The observations were reduced taking into account two intermediate catalogues acronym RRS2 and PIRS.

2.1. RRS2-STARS

The RRS2 catalogue contains astrometric positions for 2575 stars lying in the region –20° to +90° declination. The average number of RRS2-stars one degree around the extragalactic radiosources is 10. Theirs coordinates are reported to the mean epoch 1990.5 in the FK5 system, and their proper motions are known.

2.2. PIRS-STARS

The Photographic Intermediate Reference Stars (PIRS) catalogue contains stars from 11th to 14th visual magnitude, located in the 30-arcminute area neighbouring the radiosources. The origin of the PIRS-stars astrometric positions was the GSC catalogue. Thus, an average number of 25 PIRS-stars for each extragalactic radiosource field is measured. The 30-arcminute area choice was decided taking into account the field of the Merz-Prin refractor. For the instrumental field of $2^{\circ} \times 2^{\circ}$, we consider that the light sources measured 30-arcmin around the center are not affected by aberrations due to the optical system.

The importance of the intermediate PIRS catalogue was emphasized at the 22nd IAU General Assembly, held in the Hague in 1994. On this occasion, the idea of a standard list of intermediate stars in the extragalactic radiosource fields was enounced. This aspect can be found also in the B6, and B7 resolutions adopted by the Working Group for the reference frames (Kovalevsky, 1994).

3. RESULTS

Both RRS2 and PIRS measurements were performed with an ASCORECORD measuring machine. Then, the measurements were reduced using several catalogues: PPM, TYCHO, CAMC for the RRS2-stars astrometry, and GSC for the PIRS-stars. A total number of 1943 PPM stars and 1295 TYCHO stars were measured for the 188 considered areas. The presence of the proper motions in the reference catalogues stars, allowed us the determination of the standard errors in right ascension and declination, as well as the (O–C) analysis.

In Figs. 1 and 2, the ratio between the measured (O–C) and the latter's number is presented graphically for the PPM stars under the form of histograms for right ascension (Fig. 1) and declination (Fig. 2). In abscissa the (O–C) values are represented with the step of 0.001 time-second for ascension, and respectively 0.01 arc-second for declination; in the ordinate is represented the number of the values ranging between the respective intervals. In both graphics one can observe a good focusing in relation with the origin. In the ascension the Gaussian obtained is also symmetric, whereas in the declination the range of the negative values number is greater than that of the positive ones.

Fig. 3 presents for the TYCHO stars (in right ascension) the same ratio between the values O–C and their number. The Gaussian is centered in the origin and is also relatively symmetric. Fig. 4 presents, also for the TYCHO stars, the same ratio in declination. One can observe a slight shift of the top of Gauss' bell towards negative values and also a stranger range of the negative values of the (O–C)'s.

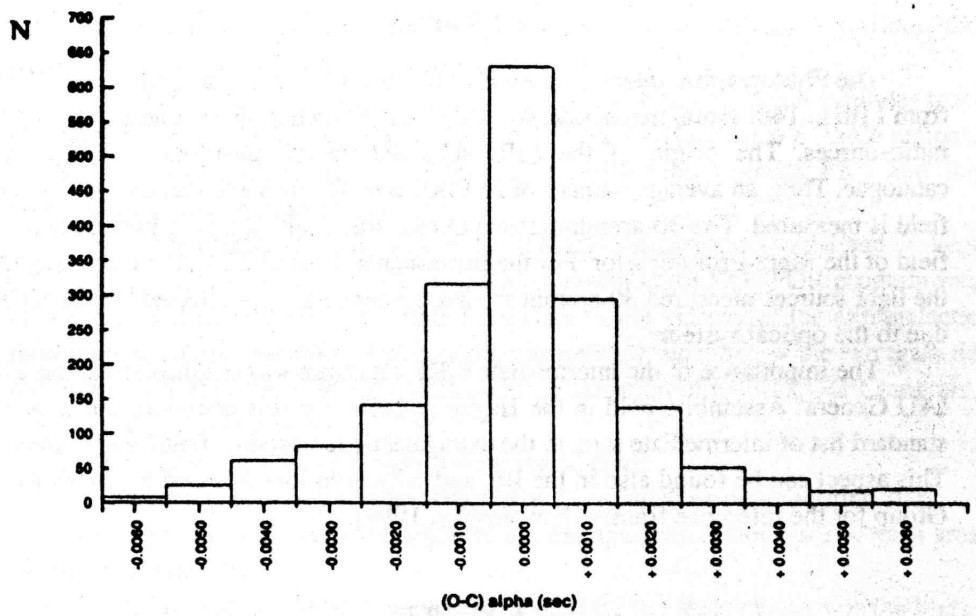

Fig. 1 – (O–C) in right ascension for the PPM stars measured on the 188 analyzed extrgalactic radiosource areas.

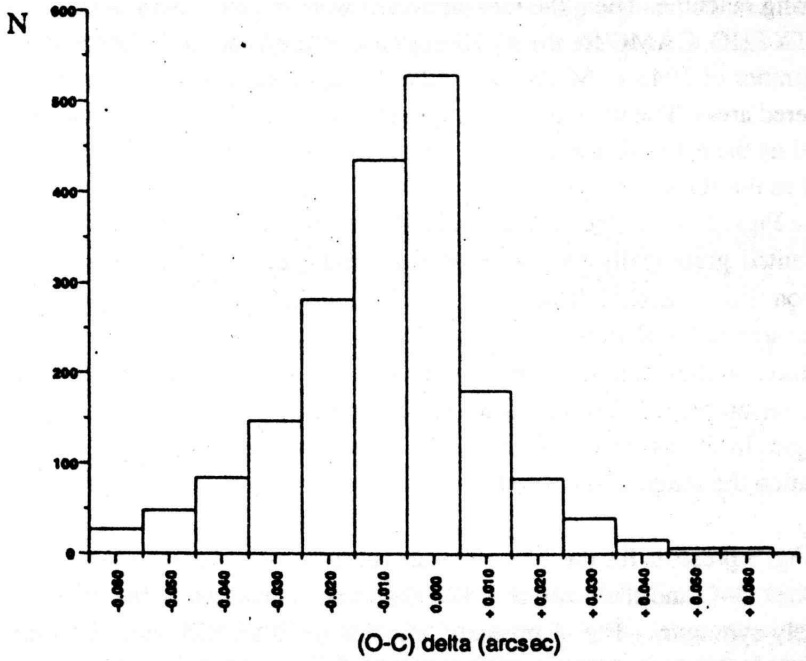

Fig. 2 – (O–C) in declination for the PPM stars measured on the 188 analyzed extragalactic radiosource areas.

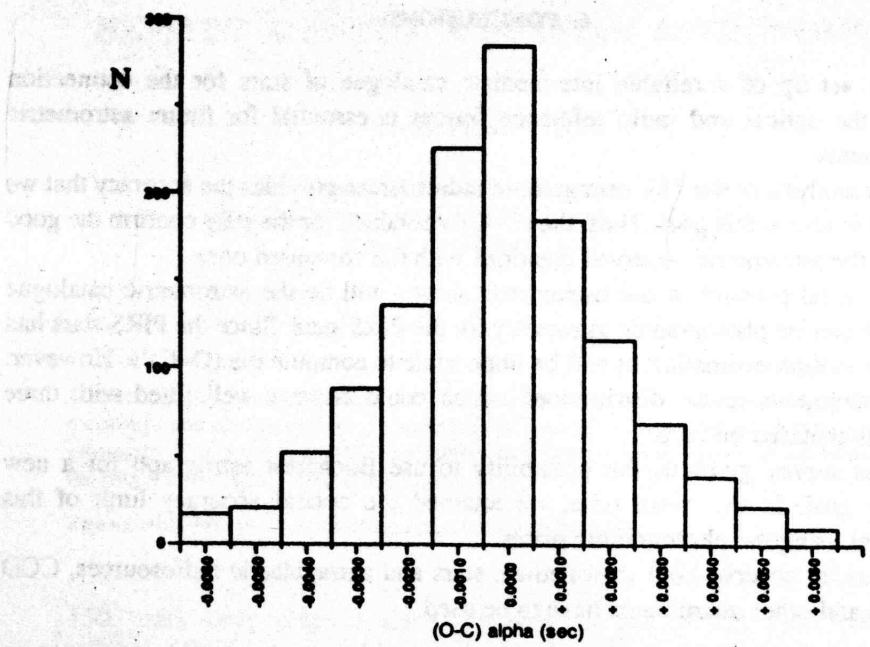

Fig. 3 – (O–C) in right ascension for the TYCHO stars measured on the 188 analyzed extragalactic radiosource areas.

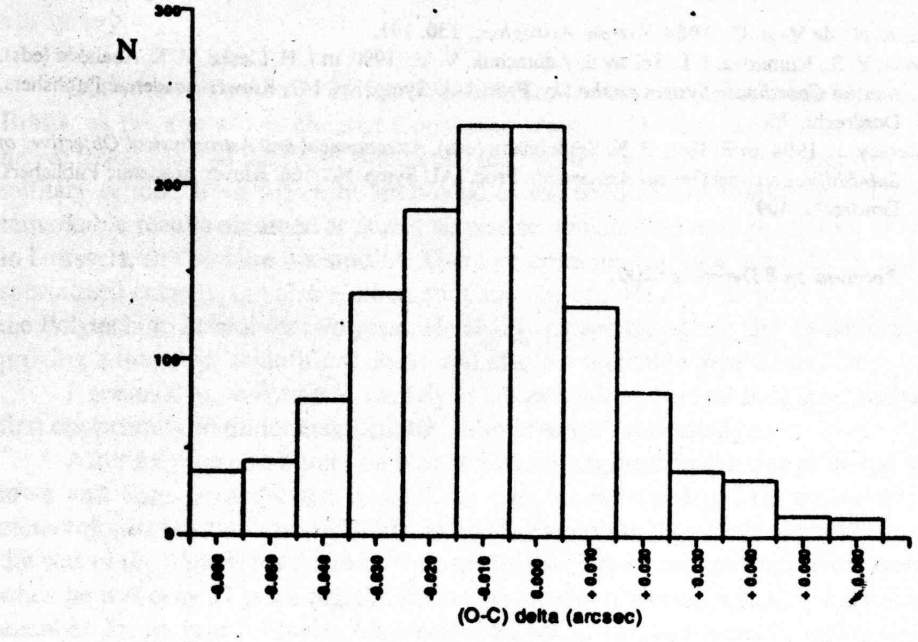

Fig. 4 – (O–C) in declination for the TYCHO stars measured on the 188 analyzed extragalactic radiosource areas.

6. CONCLUSIONS

The set up of a reliable intermediate catalogue of stars for the connection between the optical and radio reference frames is essential for future astrometric developments.

Our analysis of the 188 extragalactic radiosources provides the accuracy that we can reach to obtain this goal. Thus, the (O–C)'s obtained for the stars confirm the good match of the astrometric observed positions with the computed ones.

The final product of our astrometric survey will be the astrometric catalogue giving the precise photographic astrometry for the PIRS stars. Since the PIRS stars had no proper motion estimation, it will be impossible to compute the (O–C)'s. However, our measurements reveal distributions which could be very well fitted with three Gaussians centered on zero.

This survey gives us the possibility to use Bucharest astrograph for a new scientific goal. In the mean time, we attained the optical accuracy limit of this instrument using the photographic plates.

Thus, to observe both intermediate stars and extragalactic radiosources, CCD detectors and other instruments have to be used.

REFERENCES

Argue, A. N., de Vegt, C.: 1984, *Astron. Astrophys.*, 130, 191.

Gubanov, V. S., Kumkova, I. I., Tel'nyuk-Adamchuk, V. V.: 1990, in J. H. Lieske, V. K. Abalakin (eds), *Inertial Coordinate System on the Sky*, Proc. IAU Symp. No. 141, Kluwer Academic Publishers, Dordrecht, 75.

Kovalevsky, J.: 1994, in E. Hog, P. K. Seidelmann (eds), *Astronomical and Astrophysical Objectives of Sub-Milliarcsecond Optical Astrometry*, Proc. IAU Symp. No. 166, Kluver Academic Publishers, Dordrecht, 409.

Received on 8 December 2001

SOFTWARE PACKAGE FOR PREPARING AND PROCESSING OF AN ASTRONOMICAL OBSERVATION

OVIDIU VĂDUVESCU, MIREL BÎRLAN
Astronomical Institute of the Romanian Academy,
Str. Cuţitul de Argint 5, 75212 Bucureşti 28, Romania

Abstract. This paper presents an astronomical software package which draws celestial charts. It was conceived taking into account the technical possibilities available for the Romanian astronomers and the actual trend of the observational astronomy. The software package, now to its third version, comes to decrease the time to prepare an observation and to perform accurate charts for searching and identification.

Key words: software, astrometry, star database, celestial maps.

1. GLOBAL PRESENTATION

The name of this program is "CELESTIAL MAPS". It was written in Turbo Pascal medium, under the MS-DOS operating system (Makkai et al., 1991; Bălănescu et al., 1992; Cristea et al., 1992). Previous oral papers have announced both old version (Văduvescu and Bîrlan, 1992) and the recent version (Văduvescu and Bîrlan, 1994). This version (4.5) was conceived with about 10,000 instructions in five distinct unities. The menu-bar system makes the program very easy to use. The program can print the display. The technical needs are: PC (IBM or compatible, recommended up from 386), display (CGA, EGA, VGA, SVGA) and printer.

2. PROGRAM DESCRIPTION

The software package can be used for photometrical observations, photographical astrometry or CCD astrometry. The program gives accurate charts for searching a certain zone of the sky. The dimension of this zone can be established by the user. These charts can be evolved in three topographical types of projection, on a surface tangent to the celestial sphere in a common chosen point (the center of the chart).

The stars are plotted depending on their spectral class and magnitude. The spectral class dependence is noted on a color display and allows an optimal choice in photometry for the comparison star. For a realistic image of the projected zone, the dimensions of the stars are plotted in terms of stellar magnitudes.

Rom. Astron. J., Vol. 6, No. 1, p. 97–99, Bucharest, 1996

The dimensions of the sky zone have a minimum of 0.0001 degrees. So, in comparison with other softwares, one can plot small field charts. For instance, the dimension of the field for the refractor in Bucharest is 2° × 2°. The program is used to make charts for astrometrical measurements, which use astrophotographical plates.

The charts have a good accuracy, because there are procedures for reducing the epoch of the star catalogues to the observation epoch. These procedures include the corrections for precession, nutation, aberration, parallax and proper motions (Meeus, 1986; Oproiu et al., 1989).

From its second version, the program produces files containing information about the stars which appear in the field. These files are used for the reduction of the observations.

To simulate general conditions for an observation, the program also provides a global image of the sky for a given date and site on the Earth surface. Thus, the program projects the celestial sphere on the tangent plane in zenithal point. This branch offers the position of the planets, Sun and Moon (Văduvescu, 1991).

Another branch of the program shows the sky projection on a tangent plane to the celestial sphere in the North or South equatorial pole. This branch feigns the apparent motions of the planets. Optionally, it is also possible to plot the constellation lines and their name.

This software is endowed with a search procedure; optionally it also displays some nonstellar objects contained in a database.

3. DATABASE

The first version of our program used FK5 catalogue (1535 stars).

Celestial Maps 4.5 uses two 2000-epoch catalogues of the stars: "Catalogue of Positions and Proper Motions" (319494 stars) and "Smithsonian Astrophysical Observatory Catalogue" (258996 stars), selected from a CD-ROM (NASA, 1990). This selection increases the speed of execution and decreases the disk space. The choice of one of these catalogues is made in the second branch of the program, by selecting the option "large data base". The files containing the stars (type files) represent stripes of 10° of declination. Thus, the user can install partial database, in conformity with the disk space and the field of interest. The simple data base file is also a type file. These files contain four denominations of the stars (PPM, SAO, HD, DM). Also, there is another file (text) which contains additional stars, that can be modified by the user. The package requires min 1 Mb (simple database), 16 Mb (SAO large database) and/or 20 Mb (PPM large database).

4. CONCLUSIONS

Celestial Maps is useful for both professional and amateur astronomers, by using it for the scientific research and didactical activity.

If this program is used for preparing an observation night, the time will be shortened roughly with 15 minutes for each chosen object. In this way, the routine will be reduced.

Acknowledgement. The authors thank to the Informatics Department of the University of Craiova and especially Mr. Sorin Pescăruş for their scientifical and technical support. Special thanks are extended to Dr. Gheorghe Vass and Dr. Vasile Mioc from the Astronomical Institute of the Romanian Academy for their ideas, suggestions and observations as to the program.

REFERENCES

Bălănescu T., Gavril S., Georgescu H., Gheorghe M., Sofonea L., Văduva I.: 1992, *Pascal şi Turbo Pascal*, Ed. Tehnică, Bucureşti.

Cristea V., Kalisz E., Athanasiu I., Pănoiu A.: 1992, *Turbo Pascal 6.0*, Ed. Teora, Bucureşti.

Makkai A., Andras M., Crişan C., Şandor K.: 1991, *Ghid de utilizare Turbo Pascal 5.0-5.5*, Romanian Software Company, Cluj-Napoca.

Meeus J.: 1986, *Calculs Astronomiques à l'usage des amateurs*, Société Astronomique de France, Paris.

Oproiu T., Pál A., Pop V., Ureche V.: 1989, *Astronomie. Culegere de exerciţii, probleme şi programe de calcul*, Universitatea din Cluj-Napoca.

Văduvescu O.: 1991, *M. Sc. Thesis*, University of Craiova.

Văduvescu O., Bîrlan M.: 1992, Communication held at "Cluj Academic Days", Cluj-Napoca, October, 1992.

Văduvescu O., Bîrlan M.: 1994, Poster at The 2nd International School in Astronomy and Astrophysics, Rozhen, Bulgaria, April 1994.

* * * *Selected Astronomical Catalogue*, 1, Astronomical Data Center, NASA 1990.

Received on 26 November, 1995

II. Modélisation de la population de petits corps à partir des observations.

II.1. Etudes statistiques, taxonomies.

II.2. Modélisation des spectres des objets sans atmosphère.

II.3. Considérations sur la masse des astéroïdes.

Une analyse des données est incomplète sans une représentation sur la base d'un modèle physique. En fonction de l'approche choisie, les premiers modèles sont issus directement de l'observation. On parle d'un modèle empirique. On observe ainsi (par l'analyse statistique des données par exemple !) que les données obéissent à une ou plusieurs lois, sans que soit atteint le degré d'abstraction et de généralisation (axiomatisation !) d'un modèle physique. Si les données d'observations peuvent être partiellement confirmées par des raisonnement analytiques, alors on obtient la définition d'un modèle semi-empirique. Si l'axiomatisation des données est possible, alors nous parlons d'un modèle analytique, permettant également le caractère prévisionnel de la théorie.

II.1. Etudes statistiques, taxonomies.

Lorsque l'on analyse de nouvelles données et que l'on veut en tirer des conclusions globales sur la population étudiée, on passe forcément par une étape d'analyse statistique. Souvent décriée, cette étape est nécessaire et bien souvent fondamentale pour tout développement ultérieur dans le but d'obtenir un modèle physique crédible. L'analyse statistique nous permet de définir des classes d'équivalence qui caractérisent la similitude existant entre les différents objets. On peut parler par exemple de la classe des objets rouges ou de la classe des objets sphériques. Dans ces cas simples, l'attribut définit l'appartenance de l'objet à la classe.

Pour une classification plus complexe, le résultat est aussi plus complexe, les attributs sont remplacés par des « notions » et des « concepts».

Une analyse « sans a priori » donne lieu à une *classification non-supervisée* et elle joue un rôle très important dans tous les domaines scientifiques. On obtient ainsi ce que l'on appelle dans la littérature une *taxonomie*.

L'étude d'un ensemble d'objets est habituellement faite sur un ensemble de données décrivant une ou plusieurs caractéristiques de la population choisie. Si le nombre d'objets de la population étudiée est suffisamment grand, on peut arriver à distinguer des groupes d'objets dont les caractéristiques sont très proches . Ainsi on peut obtenir un *système taxonomique*.

Par exemple, les types spectraux des étoiles ainsi que leurs classes de luminosité sont des systèmes taxonomiques, il en est de même de la classification en galaxies elliptiques, spirales, spirales barrées et irrégulières. Plus les paramètres entrant dans l'analyse couvrent des aspects physiques de la population d'objets considérés, plus le système taxonomique est intéressant; plus il y a un nombre important d'objets, plus est renforcée notre confiance dans les groupes délimités par le système taxonomique en question.

Sous plusieurs aspects, la taxonomie des astéroïdes a beaucoup de similitudes avec le système de classification spectrale des étoiles. Au fur et à mesure que nos connaissances sur la population astéroïdale se sont affinées, différents systèmes de classification se sont succédés. Traditionnellement, les taxonomies d'astéroïdes se sont basées sur l'analyse de couleurs des objets ; ultérieurement de nouvelles taxonomies ont inclus des variables (couleurs et albédo thermique) couvrant aussi une partie du domaine de l'infrarouge proche.

Pour parler vraiment d'un système taxonomique, il faut effectuer la correspondance entre les caractéristiques de chaque classe et la composition chimique qui permet de le délimiter dans l'échantillon. Concrètement, il faut mettre en correspondance les caractéristiques moyennes des spectres de chaque classe taxonomique et les minéraux les plus probables qui sont à l'origine des signatures dans le spectre (exemple en Tableau 1).

Deux directions principales sont abordées :

i) des études directes par comparaison avec des résultats obtenus sur d'autres corps du système solaire ;
ii) des études indirectes, par comparaison avec les résultats obtenus en laboratoire sur des échantillons de météorites.

De nos jours, les systèmes taxonomiques se sont affinés et les nombre des classes et sous-classes d'astéroïdes ont augmenté. La diversification a été dictée par la densification des données d'observations sur le domaine spectral du visible, mais aussi par l'utilisation d'observations de l'intervalle spectral dans l'infrarouge proche.

Mes travaux portent sur l'analyse des données obtenues par la spectrophotométrie dans l'intervalle de longueur d'onde de 0,35µm à 2,5µm en combinaison avec l'albédo thermique obtenu par plusieurs programmes d'observations. L'analyse statistique a été faite à l'aide d'un algorithme de classification automatique d'analyse d'un facteur, connu dans la littérature scientifique sous le nom *G-mode*. J'ai pu ainsi montrer des structures fines à l'intérieur des classes taxonomiques « standard », qui sont mises en valeur essentiellement par la présence des nouvelles données, comme le présente l'article publié dans Astronomy & Astrophysics vol 305, 1996.

Une composante importante dans l'évolution d'un système taxonomique est la possibilité de l'étendre à de nouveaux objets (données d'observations obtenues ultérieurement par rapport à la réalisation du système), ou à des objets qui n'ont pas un jeu complet de variables (couleurs ou albédo manquantes).

Tableau 1. Exemple d'un système taxonomique pour les astéroïdes. Les classes taxonomiques sont décrites par une lettre, l'albédo thermique est estimé qualitativement, le spectre moyen de chaque classe est brièvement expliqué et les caractéristiques les plus prononcés/discriminatoires sont mises en évidence. Pour que le système taxonomique soit suffisamment important, une interprétation de la minéralogie de la surface des objets a été faite en termes des divers minéraux existant dans les météorites

Classe	albédo	Spectre	Minéralogie supposée de la surface	Météorites correspondantes
A	modéré grand	très rouge après 0,7 μm ; une bande d'absorption très prononcée avant 0,7 μm et une autre centrée à 1,05 μm	olivine ou olivine+métaux	olivine achondritique ou pallasite
B	modéré petit	le spectre à tendance décroissante vers les longueurs d'onde de l'infrarouge proche	silicates hydratés+carbone (ou substances organiques) - (ou matériaux opaques)	assemblages *CI1*-*CM2* produits soit par altération aqueuse, soit par métamorphisme des matériaux précurseurs de *CI/CM*
C	Petit	une bande d'absorption vers 0,4 μm et un spectre plat du visible à l'infrarouge	silicates hydratés + carbone (ou substances organiques) - (ou matériaux opaques)	assemblages *CI1*-*CM2* produits soit par altération aqueuse, soit par métamorphisme des matériaux précurseurs de *CI/CM*
D	très petit	un spectre sans bande d'absorption prononcée ; les valeurs de la réflectance spectrale augmentent rapidement et régulièrement vers l'infrarouge	carbone ou silicates riches en matériaux organiques (?)	poussières organiques (?) ou météorites CI1-CM2 et matériaux organique (?)
E	très grand	spectre monotone avec une tendance à l'augmentation de la réflectance spectrale vers l'infrarouge	enstatite ; d'autres silicates avec atomes de fer sont aussi possibles	enstatite achondritique
G	Petit	une bande d'absorption centrée vers 0,4 μm, plus prononcée que celle de la classe C; le reste du spectre est plat	silicates hydratés+carbone (ou substances organiques) - (ou matériaux opaques)	assemblages *CI1*-*CM2* produits soit par altération aqueuse, soit par métamorphisme des matériaux précurseurs de *CI/CM*
M	modéré	Un spectre monotone où la réflectance spectrale augmente très peu vers l'infrarouge	métaux (trace possible de silicates) ou métaux + enstatite	ferreux (avec des inclusions possible de silicates); enstatite chondritique(?)
S	modéré	une bande d'absorption avant 0,7 μm et une bande d'absorption modérée ou petite après 0,7 μm	métaux + olivine + pyroxène	pallasites dominés par des roches riches en pyroxène ou olivine et CV/CO chondrules
V	modéré grand	une forte bande d'absorption avant 0,7 μm et une autre bande d'absorption forte centrée sur 0,95 μm	pyroxène ± feldspath	basalte achondritique

Il est également important de noter que cette opération reste toujours dans le domaine du raisonnable tant que les résultats d'une telle classification « a posteriori » ne présentent pas trop « d'exceptions » (objets qui, par la procédure de classement, ne peuvent pas former une classe parmi les classes existantes). Dans ce cas, une nouvelle refonte du système taxonomique s'impose.

Une partie des mes travaux de recherche porte également sur l'analyse des paramètres physiques des astéroïdes ayant un jeu incomplet de variables. Pour cette analyse, une mise en œuvre d'un logiciel de décision a été réalisée, à partir d'un algorithme basé sur les travaux théoriques de A. I. Gavrishin, en extension de la méthode du paramètre G (*G-mode method*). L'extension de la méthode G-mode permet l'évaluation de la probabilité qu'un objet avec un nouveau jeu de données appartienne à une classe. Même si dans certains cas, l'analyse laisse une ambiguïté dans cette estimation (par exemple l'objet est estimé avec des probabilités voisines pour deux classes) elle offre un point de départ pour des investigations plus poussées de l'objet (à voir les articles d'Icarus vol. 124, 1996 et Icarus vol 146, 2000).

L'autre volet des activités scientifiques visant également les objets sans atmosphère du système solaire a été la réalisation des premières classifications pour les objets trans-neptuniens. L'expérience d'analyse statistique sur les astéroïdes nous ont permis l'adaptation des outils pour l'analyse des couleurs de ces objets par deux méthodes : la méthode du paramètre G (G-mode) et la méthode des composantes principaux (PCA method). L'analyse effectuée sur des collectifs statistiques des objets type Centaures avec des objets trans-neptuniens nous a révélé la structure bien distincte de quelques classes. Par conséquent, un système taxonomique simple a été mis en place (à voir les articles A&A vol 371, 2001 et EMP vol 92, 2003)

La réalisation d'un système taxonomique fait partie de l'approche générale de modélisation avec un fort degré d'empirisme. Nous sommes encore loin d'un modèle physique/analytique permettant l'explication d'une manière générale des différentes populations d'objets existant parmi les astéroïdes ou les objets trans-neptuniens. Une autre approche nous permettant des études plus poussées sur le sujet est l'analyse spectrale de ces objets en vue d'avoir plus d'informations sur les processus physiques permettant de résoudre la minéralogie de ces objets (et dans les cas des objets trans-neptuniens la composition et le circuit des glaces).

Références :

Birlan M., Barucci M.A., Fulchignoni M. - *G-mode analysis of reflection spectra for 84 asteroids* **Astronomy and Astrophysics** vol **305** n. **2**, 984-988, 1996.
Birlan M., Fulchignoni M., Barucci M.A. - *Effects of IRAS albedo corrections on Barucci's asteroid taxonomy*, **Icarus**, **124**, 352-354, 1996.
Fulchignoni M., **Birlan M.**, Barucci M.A. - *The extension of the G-mode asteroid taxonomy* **Icarus**, n. **146**, 204-212, 2000.
Birlan M. - *On the physical and dynamics properties of asteroids*, **Romanian Astronomical Journal** vol. **3**, n. **2**, 123-126, 1993.
Barucci M.A., Fulchignoni, M., **Birlan M.**, Doressoundiram A., Romon J., Boehnhardt H, - *Analysis of Trans-Neptunian and Centaur colours: continuous trend or grouping?*, **Astronomy and Astrophysics**, n **371**, 1150-1154, 2001.
Fulchignoni, M, Delsanti, A., Barucci, M.A., **Birlan, M.** - *Toward a Taxonomy of the Edgeworth-Kuiper Objects: A Multivariate Approach* - **Earth, Moon, and Planets**, vol. **92**:1-4, 2003.